ISSN 0021-9673

VOL. 684 NO. 2 4 NOVEMBER 1994

THIS ISSUE COMPLETES VOL. 684

JOURNAL OF CHROMATOGRAPHY A

INCLUDING ELECTROPHORESIS AND OTHER SEPARATION METHODS

ELSEVIER

JOURNAL OF CHROMATOGRAPHY A

INCLUDING ELECTROPHORESIS AND OTHER SEPARATION METHODS

Scope. The *Journal of Chromatography A* publishes papers on all aspects of **chromatography, electrophoresis** and related methods. Contributions consist mainly of research papers dealing with chromatographic theory, instrumental developments and their applications. In the *Symposium volumes*, which are under separate editorship, proceedings of symposia on chromatography, electrophoresis and related methods are published. *Journal of Chromatography B: Biomedical Applications* —This journal, which is under separate editorship, deals with the following aspects: developments in and applications of chromatographic and electrophoretic techniques related to clinical diagnosis or alterations during medical treatment; screening and profiling of body fluids or tissues related to the analysis of active substances and to metabolic disorders; drug level monitoring and pharmacokinetic studies; clinical toxicology; forensic medicine; veterinary medicine; occupational medicine; results from basic medical research with direct consequences in clinical practice.

Submission of Papers. The preferred medium of submission is on disk with accompanying manuscript (see *Electronic manuscripts* in the Instructions to Authors, which can be obtained from the publisher, Elsevier Science B.V., P.O. Box 330, 1000 AH Amsterdam, Netherlands). Manuscripts (in English; *four* copies are required) should be submitted to: Editorial Office of *Journal of Chromatography A*, P.O. Box 681, 1000 AR Amsterdam, Netherlands, Telefax (+31-20) 5862 304, or to: The Editor of *Journal of Chromatography B: Biomedical Applications*, P.O. Box 681, 1000 AR Amsterdam, Netherlands. Review articles are invited or proposed in writing to the Editors who welcome suggestions for subjects. An outline of the proposed review should first be forwarded to the Editors for preliminary discussion prior to preparation. Submission of an article is understood to imply that the article is original and unpublished and is not being considered for publication elsewhere. For copyright regulations, see below.

Publication information. *Journal of Chromatography A* (ISSN 0021-9673): for 1995 Vols. 683–714 are scheduled for publication. *Journal of Chromatography B: Biomedical Applications* (ISSN 0378-4347): for 1995 Vols. 663–674 are scheduled for publication. Subscription prices for *Journal of Chromatography A*, *Journal of Chromatography B: Biomedical Applications* or a combined subscription are available upon request from the publisher. Subscriptions are accepted on a prepaid basis only and are entered on a calendar year basis. Issues are sent by surface mail except to the following countries where air delivery via SAL is ensured: Argentina, Australia, Brazil, Canada, China, Hong Kong, India, Israel, Japan, Malaysia, Mexico, New Zealand, Pakistan, Singapore, South Africa, South Korea, Taiwan, Thailand, USA. For all other countries airmail rates are available upon request. Claims for missing issues must be made within six months of our publication (mailing) date. Please address all your requests regarding orders and subscription queries to: Elsevier Science B.V., Journal Department, P.O. Box 211, 1000 AE Amsterdam, Netherlands. Tel.: (+31-20) 5803 642; Fax: (+31-20) 5803 598. Customers in the USA and Canada wishing information on this and other Elsevier journals, please contact Journal Information Center, Elsevier Science Inc., 655 Avenue of the Americas, New York, NY 10010, USA, Tel. (+1-212) 633 3750, Telefax (+1-212) 633 3764.

Abstracts/Contents Lists published in Analytical Abstracts, Biochemical Abstracts, Biological Abstracts, Chemical Abstracts, Chemical Titles, Chromatography Abstracts, Current Awareness in Biological Sciences (CABS), Current Contents/Life Sciences, Current Contents/Physical, Chemical & Earth Sciences, Deep-Sea Research/Part B: Oceanographic Literature Review, Excerpta Medica, Index Medicus, Mass Spectrometry Bulletin, PASCAL-CNRS, Referativnyi Zhurnal, Research Alert and Science Citation Index.

US Mailing Notice. *Journal of Chromatography A* (ISSN 0021-9673) is published weekly (total 52 issues) by Elsevier Science B.V., (Sara Burgerhartstraat 25, P.O. Box 211, 1000 AE Amsterdam, Netherlands). Annual subscription price in the USA US$ 5389.00 (US$ price valid in North, Central and South America only) including air speed delivery. Second class postage paid at Jamaica, NY 11431. **USA POSTMASTERS**: Send address changes to *Journal of Chromatography A*, Publications Expediting, Inc., 200 Meacham Avenue, Elmont, NY 11003. Airfreight and mailing in the USA by Publications Expediting.

See inside back cover for Publication Schedule, Information for Authors and information on Advertisements.

0021-9673/94/$07.00

Printed in the Netherlands

CONTENTS

(Abstracts/Contents Lists published in Analytical Abstracts, Biochemical Abstracts, Biological Abstracts, Chemical Abstracts, Chemical Titles, Chromatography Abstracts, Current Awareness in Biological Sciences (CABS), Current Contents/Life Sciences, Current Contents/Physical, Chemical & Earth Sciences, Deep-Sea Research/Part B: Oceanographic Literature Review, Excerpta Medica, Index Medicus, Mass Spectrometry Bulletin, PASCAL-CNRS, Referativnyi Zhurnal, Research Alert and Science Citation Index)

REGULAR PAPERS

Column Liquid Chromatography

Gas Chromatography

Supercritical Fluid Chromatography

(Continued overleaf)

Contents (continued)

ELSEVIER

Journal of Chromatography A, 684 (1994) 175–188

JOURNAL OF CHROMATOGRAPHY A

Property–structure relationship of solute–stationary phase complexes occurring in a molecular mechanism by penetration of eluite in bonded alkyl chains in reversed-phase liquid chromatography

A. Tchapla*, S. Héron

LETIAM, IUT d'Orsay, Plateau du Moulon, B.P. 127, F-91403 Orsay Cedex, France

First received 9 November 1993; revised manuscript received 24 June 1994

Abstract

The analysis of the chromatographic behaviour of homologous series with a large range of chain lengths, $1 \leqslant n_c \leqslant 32$, allowed a second break in the curves of log k' vs. n_c to be observed. This occurs independently of the nature of the series, the length of bonded chain ($6 \leqslant n_{bp} \leqslant 22$), the analysis temperature (when it is higher than the temperature of phase transition); also, the qualitative mobile phase composition does not affect the phenomenon in partially aqueous reversed-phase liquid chromatography or in the non-aqueous reversed-phase mode (for mixtures $CHCl_3$–MeOH, $CHCl_3$–MeCN, H_2O–MeOH or H_2O–MeCN rich in MeOH or MeCN). The two breaks in the curves mark the limits of three zones which are characterized by two different values of n_c: $n_{crit.}$ and $n_{sat.}$. The first describes the phenomenon for values of $n_c \leqslant n_{crit.}$. In this range $n_{crit.}$ is independent of the homologous series but varies with the bonded chain length, n_{bp}. The methylene selectivity α is different for each series and a correlation with the increment of molecular volume of a methylene group, ΔV_{CH_2}, for each of them is established. The second break appears for values of $n_{crit.} \leqslant n_c \leqslant n_{sat.}$. In this case, the value of the methylene selectivity is the same regardless of the series. The same evolution can be demonstrated by examination of the increment of molecular volume of a methylene group. The third zone such as $n_c \geqslant n_{sat.}$ shows a behaviour identical with that of the second zone but with lower values of α and ΔV_{CH_2}. The value of $n_{sat.}$ is independent of the nature of the homologous series but is related to the bonding density of alkyl chains on silica. The results obtained are consistent with a molecular mechanism of interaction by insertion of the solute inside the bonded phase. The contacts are more or less tight depending on the space available between the chains of the stationary phase. This leads to three geometries of contact whose energetic phenomena are different.

1. Introduction

In an effort to verify the prediction of the solvophobic theory in reversed-phase liquid chromatography (RPLC) [1–4], many workers have shown that the logarithms of the capacity factors vary linearly with the number of carbon atoms n_c in constituents of homologous series [5–10]. These results were obtained with different alkyl-bonded silicas and different aqueous–organic mobile phases. However, this linearity is not always rigorously observed: we can obtain

* Corresponding author.

0021-9673/94/$07.00
SSDI 0021-9673(94)00596-2

sigmoidal plots of log k' vs. n_c, according to the nature of the silane used for the graft, and/or the temperature of the analysis, or the nature of the solvent of the mobile phase [11]. A second case of non-linearity appears when one works with a large number of homologues: there is a discontinuity in the plots of the logarithm of capacity factor versus n_c which is observed in the PARP (partially aqueous reversed phase) as well as in the NARP (non-aqueous reversed phase) mode. It has been explained by a molecular mechanism of interaction in which the solute interacts with the bonded chains by vertical penetration [4,12–14]. Such a molecular view of the phenomenon was verified experimentally by measuring the variations of transfer enthalpies and entropies vs. n_c [15].

To validate these mechanisms further, we decided to perform some complementary experiments. A linear increase in the cavity size in the mobile phase with the number of carbon atoms is not thermodynamically established. Hence we have to understand how such long-chain solutes behave when they are 10–20 carbon atoms longer than the length of the alkyl chain bonded to silica. Lundanes and Greybrokk [16] have previously published a similar study limited to a single homologous series and only one type of mobile phase (tetrahydrofuran–water). However, this solvent leads to a conformational modification of the grafted alkyl chains and a different chromatographic behaviour than those observed in methanol or acetonitrile [17].

We also investigated the behaviour of solutes containing saturated carbon rings or straight chains with the same number of carbon atoms. Finally, the role of free silanols was investigated. In the case of a polar head of solute which could interact with residual silanols, is there penetration of the polar part of the solute into the carbon chains of the support, to create supplementary interaction with silanols?

The purpose of this study was to answer these questions. To achieve this goal, the influence of the nature of and variations in the molecular volume of homologous series was studied. The influence of bonding ratio and alkyl chain length was also addressed.

2. Experimental

The equipment used and precautions taken to ensure the precision of the measurements of capacity factors were reported elsewhere [5,15]. The phenomenon is independent of the value of the dead time in the range of column porosities tested, as demonstrated earlier [5]. To permit comparison of the results collected at different temperatures, all the reported values were obtained with k' calculated with a dead time corresponding to the maximum column porosity. This is valid considering that there is no significant modification of the void volume with temperature [18]. This value was calculated by using the weighing method [19]. For calculation we have taken into account the true dead volume in the column compared with the total dead volume of the equipment [15].

Homologues ($C_nH_{2n+1}Z$) with Z = H, Cl, Br, OH, COPh, COOMe, Ph, CN, COOH, CH = CH_2, OCOMe, COMe, OCOPh, OCOPhCOO (*para*), COC_nH_{2n+1} ($1 \leq n_c \leq 32$) and liquid crystals [$OCO(C_6H_4)$-*p*-N = N (C_6H_4)-*p*-OC_2H_5] were used ($3 \leq n_c \leq 6$). In addition, cycloalkanones ($4 \leq n_c \leq 12$), 2,2,6,6-tetramethyl-4-piperidinyloxyl diesters of dicarboxylic acids (NO) ($3 \leq n_c \leq 10$) and symmetrical dialkyl ketones ($3 \leq n_c \leq 13$) were studied.

All the compounds were injected at least four times, at 25, 30.5, 36.2, 41.3, 45 and 50°C and sometimes at 60°C. For the analysis in NARP three experiments were carried out at 5, 10 and 25°C.

The analysis temperature on the monomeric C_{22} bonded phase was chosen in order to be above the phase transition temperature. Below this temperature the grafted chains are less mobile [12] and the retention mechanism is different [11].

The precolumn, column and injection valve were all thermostated using either a laboratory-made water jacket or a Crocosil oven (Cluzeau, Sainte-Foy-la-Grande, France). The bath temperature was controlled by a Huber HS 40 cryostat (Offenburg, Elgersweier, Germany) with a precision of ±0.1°C.

Nine columns were used: an Ultrasphere ODS

(Altex, CA, USA), 5 μm, 150 × 4.6 mm I.D. supplied by Beckman (Gagny, France); a LiChrospher RP-18 and a LiChrosorb RP Select B (Merck, Darmstadt, Germany), 5 μm, 240 × 4.0 mm I.D.; a C_8 high-density (Shandon SFCC, Eragny, France), 5 μm, 150 × 4.6 mm I.D.; LiChrosorb RP-18 (5 μm), LiChrosorb RP-8 (5 μm) (Merck) and Spherisorb C_6 (5 μm) (Phase Separations, Queensferry, UK), 150 × 4.6 mm I.D., laboratory packed. Experiments were also carried out with LiChrosorb RP-14, 10 μm, 300 × 4.6 mm I.D., and Spherosil XOB 075 C_{22}, 5 μm, 150 × 4.6 mm I.D., kindly supplied by L. de Galan (University of Delft, Netherlands) and J. Serpinet (LSA, University Claude Bernard Lyon I, France), respectively.

3. Theoretical

According to the thermodynamic approach [1] to solute interactions with non-polar alkyl chains of stationary phases, the capacity factor of a given eluite at fixed eluent properties and temperature can be approximated by the relationship [4]

$$\log k' = a\,\Delta A + f(V_{SP}) + C \qquad (1)$$

where ΔA is the contact area between the eluite molecule and the hydrocarbonaceous chains at the stationary phase surface, V_{SP} corresponds to the molecular size of the bonded chain and a and C depend on the solute and mobile phase properties and include the logarithm of the phase ratio for the C term.

Consequently, not only the size and the shape of the stationary phase but also its position at the surface in contact with a given eluent will have an effect on the chromatographic equilibrium constant [4]. In other words, the capacity factor of a substance is related to the change in partial molar free energy associated with the transfer of the solute (in the standard state at infinite dilution) from the mobile phase to the stationary phase, $\Delta G°$, according to Martin [20]:

$$\log k' = -\Delta G°/2.3\,RT + \log \phi \qquad (2)$$

As reported in a recent review [21], the knowledge of the retention process consists in determining how $\Delta G°$ and ΔA vary with the structure of the eluites. To answer to this problem, one approach is to use homologous series as probe compounds. There have been many studies that have demonstrated a linear relationship between log k' and the number of carbon atoms of homologues n_c in these series [21]:

$$\log k' = pn_c + q \qquad (3)$$

However, there are various ways to analyse retention data. As reported elsewhere, among them the use of methylene group selectivity for each pair of successive homologues, α_n, allows one to quantify the magnitude of the interactions involved.

Consequently, with the aim of elucidating the intermolecular mechanism of retention, we used this last chromatographic parameter calculated in two different ways, α_n and $\tilde{\alpha}$ [21]. Moreover, for each of them we calculated their mean values ($\bar{\alpha}_n$ and $\bar{\tilde{\alpha}}$, respectively).

First, because of the levelling effect of the logarithm function, the linearity of the log k' vs. n_c plots was investigated in terms of quadratic methylene selectivity α_n values [5]. For a given homologue, it was calculated for each studied homologous series using the equation

$$\alpha_n = (k'_{n_c+1}/k'_{n_c-1})^{1/2} \qquad (4)$$

As demonstrated previously, the α_n vs. n_c plots permit subtle details to be revealed that cannot appear on a logarithmic scale.

Considering that the curves α_n vs. n_c were similar independently of the nature of the tested series, we calculated the global methylene selectivity for a given chain length corresponding to n_c carbon atoms independently of the nature of the head of the homologue, $\bar{\alpha}_n$. This is the average value of α_n for all the solutes investigated possessing the same chain length:

$$\bar{\alpha}_n = \sum_1^x \frac{\alpha_n}{x} \qquad (5)$$

where x is the number of eluites tested. It has been reported that $\bar{\alpha}_n$ could be used to investi-

gate the influence of the bonded chain length [21].

The curves of $\bar{\alpha}_n$ vs. n_c gave us the opportunity to discriminate between four possibilities: a perfectly linear log k' vs. n_c plot corresponds to horizontal α_n vs. n_c plots (never observed experimentally), a curve with a sigmoidal shape corresponds to a curve with an apex [11], a smooth curve of log k' vs. n_c corresponds in terms of α_n vs. n_c to a straight line with a negative slope and a curve with break points corresponds to a curve with jumps or changes in slope [5]. Each of the last three have already been interpreted in terms of different mechanisms of interaction [11]. Among them, the last merits to be examined in another way, as follows.

In the range of n_c values where plots of α_n vs. n_c are straight lines with a negative slope, the average methylene selectivity $\tilde{\alpha}$ can be determined to correlate the molecular properties of the homologues of different polarity with their retention.

The value of $\tilde{\alpha}$ was calculated for each homologous series from the equation

$$\tilde{\alpha} = 10^p \tag{6}$$

where p is the slope of the experimental curves of Eq. (3). In terms of a thermodynamic approach, the combination of Eqs. 2 and 3 leads to

$$\log \tilde{\alpha} = -\Delta\Delta G^\circ/2.3\,RT = -\Delta G^\circ_{CH_2}/2.3\,RT \tag{7}$$

which accounts for the increment of change in partial molar free energy associated with the transfer of a single methylene group. Now, considering the molecular signification of Eq. 1, $\tilde{\alpha}$ must permit a correlation of the retention data with the molecular volume increment ΔV_{CH_2} of a CH_2 group calculated for each investigated homologous series. This must be done to propose a molecular mechanism of interaction between homologous series and bonded alkyl chain.

Finally, it is possible to calculate the mean average methylene selectivity, $\bar{\tilde{\alpha}}$. This is the average value of $\tilde{\alpha}$ calculated for all the series investigated. It was calculated with the equation

$$\bar{\tilde{\alpha}} = \sum_1^N \frac{\tilde{\alpha}}{N} \tag{8}$$

where N is the number of series tested.

Finally, the mean average methylene selectivity $\bar{\tilde{\alpha}}$ permitted the retention between different grafted silicas to be compared and the eluent strength scale to be determined.

To be sure of the interpretation of our results, two strategies were adopted: the use of many homologous series to demonstrate the generality of the phenomenon reported below, and a mathematical treatment of our results. This strategy was previously used successfully to demonstrate independently of the homologues tested the existence of a break at a value of n_c that is characteristic of the length of the bonded chain [15]. This value is called $n_{crit.}$ in the following. It was also revealed at the value of n_c at which a jump occurs on the α_n vs. n_c plots.

In this work we used the same method to establish the veracity of a second break point which occurs on the curves of log k' vs. n_c. It is observed for homologues whose chain length is longer than $n_{crit.}$. It appears at a value of the chain length called $n_{sat.}$ in the following. It was determined considering the value of n_c at which the experimental value of log k' of the corresponding solute does not fall on a straight line on the curve of either log k' vs. n_c or α_n vs. n_c drawn from the highest values of n_c. Thus, in the range of n higher than $n_{crit.}$, we compared two different representations of α_n vs. n_c plots for each homologous series. One of them was a single straight line whose linear correlation was always higher than 0.99. The other was two convergent lines with a break point. In this case, for each of the linear parts the linear correlation was also above 0.99. We verified that there is a significant difference (95% confidence interval) between the slopes and the origins of these two representations (single line or broken line) by using the standard deviations comparison test with the same degrees of freedom [22]. This fact, and the values at which the second break points occur (n_{sat}), observed independently of the series investigated, involve the choice that the best representation of the phenomenon is given by a

linear segment, an abrupt shift and a broken linear segment.

The molar volumes were calculated from relative molecular masses and densities of the different solutes studied. The values of these parameters were obtained from a reference book [23].

4. Results and discussion

4.1. Preliminary results: characterization of the bonded silica used

As reported by Unger [24], "from a purely geometric point of view, bonded phases can be divided into two types: monolayer and polymer layer". A monolayer can be obtained by using a monofunctional silane as reactant on silica or di- and trifunctional silanes, provided that water is excluded. The surface reactions between silica and trifunctional silanes in the presence of water yield polymer layers through condensation. These two kinds of bonded silicas lead to two different chromatographic behaviours, as follows.

Previous results have shown that the alkyl-bonded silicas that were synthetized from monofunctional or difunctional silanes could lead to a mechanism of insertion [5,15]. Hence they will be considered to have a "monomeric-like" behaviour. The silica bonded with a polymeric layer could lead to a partition mechanism [11]. It was described elsewhere by a molecular mechanism such that there is total insertion of the solute in the stationary phase. To be distinguished from the mechanism of insertion, it was defined as "polymeric-like" behaviour. In fact, this difference between "monomeric-like" and "polymeric-like" behaviour refers to a change in the conformation of the bonded chain and how the eluite interacts with the stationary phase. This was described in detail in a recent review [21]. It was also demonstrated that there is a reversible solvent and temperature-induced "monomeric-like–polymeric-like" transition in alkyl-bonded silicas [11,21].

We first checked that the commercial stationary phases used under the experimental conditions described here were "monomeric-like" or "polymeric-like". We used the results in the literature or the test of Sander and Wise [25,26] which allow this differentiation. Unambiguously, the C_{18}-bonded silicas giving $\alpha_{TBN/BaP} > 1.7$ reflect "monomeric-like" phases. The terminology "polymeric-like" is used for all phases obtained with polyfunctional silanes on silica, giving $\alpha_{TBN/BaP} < 1$. The results are given in Table 1.

Table 1
Characteristics of bonded phases used: values at which the breaks occur in log k' vs. n_c (or α_n vs. n_c) plots

Column	Nature of the silane reagent used	Stationary phase density (μmol/m^2)	n_{bp}	$n_{crit.}$	$n_{sat.}$	Test of Sander and Wise [35]
Spherisorb C-6			6	6	12–13	1.57 [37]
LiChrosorb RP-8	Difunctional [30,31]	3.0	8	8	15	1.36 [37]
LiChrosorb RP-14	Monofunctional [27]	3.4	14	12	22	1.64 [37]
LiChrosorb RP-18	Difunctional [30,31]	3.5	18	14	21	–
Spherosil XOB C_{22}	Monofunctional [12,32]	4.0	22	14	24	1.76 [37]
C_8 HD	Monofunctional [33]	4.7–5.2	8	8	10	1.71 [37]
LiChrosorb RP Select B	Difunctional [30,31]	2.4	8	8	14	1.36 [36]
LiChrospher RP-18	Difunctional [30]	3.3	18	14	22–23	Intermediate [35] 1.11 [36], 1.44 [37]
Ultrasphere ODS	Monofunctional [34]	3.6	18	14	20	Monomeric [35], 1.98 [36], 1.89 [37]

The stationary phase densities were obtained either from L. de Galan (LiChrosorb RP-14), J. Serpinet (Spherosil XOB 075 C_{22}) or from the manufacturers. Only the LiChrospher RP-18 support is not classified clearly using this test. Its response is characteristic of either dense monomeric or not dense polymeric materials. Our studies on this column showed that with both methanol and acetonitrile, with 100:0, 90:10 or 95:5 organic solvent–water mixtures, the α_n vs. n_c plots showed a break similar to that observed with well known monomeric phases such as Zorbax ODS and Ultrasphere ODS. As a consequence, we assumed that this spherical silica behaved similarly to "monomeric-like" phases with regard to homologous series [21].

4.2. Studies of long carbon chain solutes on bonded silica allowing insertion

Effect of bonded phase length. Examination of α_n vs. n_c

This study was carried out with bonded silicas with different chain lengths ($n_{bp} = 6$, 8, 14, 18, 22). The results are shown in Fig. 1. Whatever the chain length of the bonded phase, the homologous series or the organic solvent used (methanol, acetonitrile pure or mixed with water

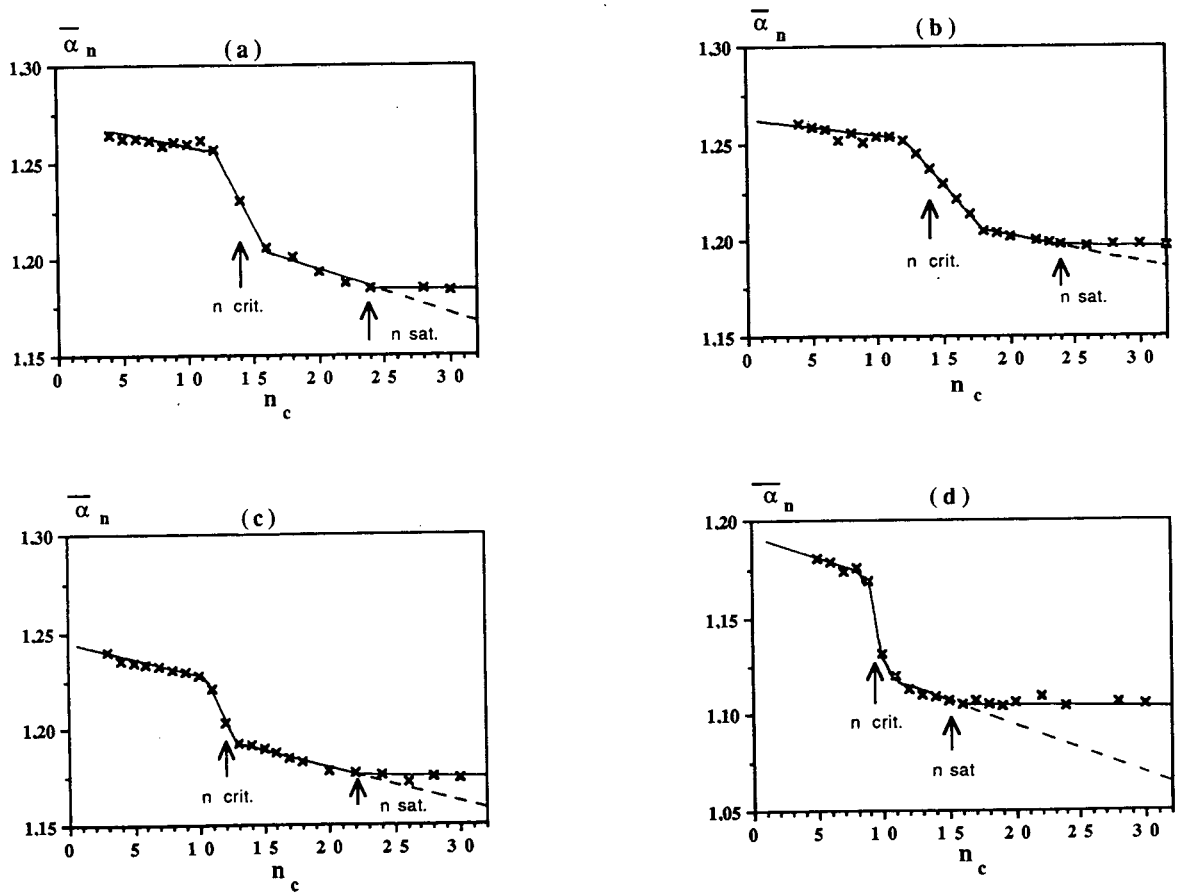

Fig. 1. Global methylene selectivity $\bar{\alpha}_n$ vs. n_c plots in pure methanol on various bonded phases: (a) monomeric C_{22}-bonded phase, 55°C; (b) monomeric C_{18}-bonded phase, 25°C; (c) monomeric C_{14}-bonded phase, 25°C; (d) monomeric C_8-bonded phase, 25°C.

but rich in organic modifier), the same plots were obtained.

The left part of the curves has already been described [5]. Surprisingly, the critical value ($n_{crit.}$) for docosyl-bonded silica is approximately the same as that for all the tested octadecyl phases. For long-chain solutes ($n_c > n_{crit.}$) the right-hand part of the curves display, for a given n value (called $n_{sat.}$), a change in the slope of methylene selectivity. After this $n_{sat.}$ value, $\bar{\alpha}_n$ remains relatively constant, or decreases slightly. This second break in α_n vs. n_c curves is independent of the series studied, but is dependent on the length of the bonded chains (Table 1). The shorter the bonded chains (with comparable ligand density), the lower the observed $n_{sat.}$ value. To specify the extent and limitations of this phenomenon, we studied columns with the same bonded alkyl chain length, but with different bonding ratios. In this case, $n_{crit.}$ remains constant but $n_{sat.}$ decreases with increase in the bonding ratio on silica. For example, for an n-octyl graft, $n_{sat} = 10$ for $\Gamma = 5.0$ μmol/m^2, $n_{sat} = 14$–15 for $2.4 < \Gamma < 3.0$ μmol/m^2.

The same plots have been obtained in various acetonitrile–chloroform mixtures [13]. Thus, these results seem to prove the generality of the phenomenon regardless of the monofunctional nature of the bonded phase and the NARP or PARP liquid chromatography modes.

Examination of average methylene selectivity $\tilde{\alpha}$

The value of the quadratic methylene selectivity α_n (Eq. 4) is not exactly constant in the range of n_c values for which the plateaux were observed [5]. Consequently, the calculation of the average methylene selectivity $\tilde{\alpha}$ was made for each investigated homologous series from Eq. 6. The selectivity is directly related to the variation of standard free energy at infinite dilution for the transfer from the mobile phase to the stationary phase, corresponding to a single methylene group of the solute.

In this way, $\tilde{\alpha}_{in}$ is the reflection of this energy change for a solute with $n_c < n_{crit.}$; $\tilde{\alpha}_{crit}$ characterizes the same phenomenon for $n_{crit} \leq n_c \leq n_{sat.}$ and $\tilde{\alpha}_{sat}$ for $n_c > n_{sat.}$. For the sake of example, we give in Table 2 the values of $\tilde{\alpha}_{in}$ and $\tilde{\alpha}_{crit}$ obtained with two different mobile phase compositions on a C_{14}-bonded silica. We observed that $\tilde{\alpha}_{crit}$ is approximately constant independently of the nature of the homologous

Table 2
Average methylene selectivity for $n < n_{crit.}$ ($\tilde{\alpha}_{in}$) and for $n_{crit.} \leq n \leq n_{sat.}$ ($\tilde{\alpha}_{crit.}$) versus the polar head of the homologous series, with a monomeric C_{14}-bonded phase

Z	MeCN–H_2O (95:05) at 30°C		Pure MeOH at 30°C	
	$\tilde{\alpha}_{in}$	$\tilde{\alpha}_{crit.}$	$\tilde{\alpha}_{in}$	$\tilde{\alpha}_{crit.}$
Cl	1.318	1.271		
COOMe	1.332	1.265		
COMe	1.362	1.283	1.333	1.181
OH	1.358	1.274		
OCOPh	1.302	1.265	1.222	1.170
COPh	1.351	–	1.323	–
OCOMe	1.329	1.268	1.239	1.175
Ph	1.319	1.272		
H	1.316	1.276		
Liquid crystals	1.261		1.160	
OCOPhCOO	1.300	1.259	1.254	1.171
CH=CH_2	1.306	1.273		
NO	1.281			
Br	1.324	1.274		

series for a given solvent and stationary phase. The values of $\bar{\alpha}_{in}$ are lower for non-polar homologous series ($Z = H$, $CH{=}CH_2$, Ph and surprisingly Cl and groups possessing a phenyl ring) than for polar series. We observed this effect for grafts of different lengths ($n_{bp} = 8$, 14, 18 and 22) percolated by mobile phases such as pure methanol, methanol–water (90:10, v/v), pure acetonitrile and acetonitrile–water (95:5, v/v). It must also be noted that a close re-examination of the results of Berendsen [27] and Berendsen and de Galan [28] leads to the same conclusion. This difference between polar and non-polar homologous series for $n_c < n_{crit.}$ can be related to the determination of two different values of compensation temperatures for these two classes of solutes [15]. Moreover, independently of the polar or non-polar nature of the solute, the value of the temperature of compensation becomes smaller for solutes such as $n_{crit} < n_c < n_{sat}$ than those such as $n_c < n_{crit.}$. It also appears that solutes with a chain length higher than 24 do not have exactly the same behaviour as the smaller ones ($15 < n_c < 22$) on a C_{14}-bonded silica [21]. They give a linear dependence of log k' vs. $1/T$ like the others, but the corresponding straight lines do not converge to a single point which is related to the temperature of compensation [15]. This last conclusion agrees with the fact that two breaks could be observed on the curves of log k' vs. n_c and that the corresponding values of the mean average methylene selectivity $\bar{\bar{\alpha}}_{sat}$ were smaller than $\bar{\bar{\alpha}}_{crit}$ independently of the nature of the series investigated (Table 3). The difference between $\bar{\bar{\alpha}}_{crit}$ and $\bar{\bar{\alpha}}_{sat}$ is approximately 0.02 methylene selectivity unit, independently of the chain density of the bonded phase, but their respective values are related to the chain length of the stationary phase.

Particular behaviour of μBondapak C_{18} and LiChrosorb RP-2 silicas

These two types of phases were not included in the results discussed previously because the α_n vs. n_c plots exhibit a regular decrease. This corroborates the fact that μBondapak C_{18} silicas are different from the others investigated here. Contrary to our first assertion, this stationary phase is not "polymeric-like" silica [15] but "monomeric-like" as reported by Sander and Wise [26]. For the sake of comparison, the reported value of the methylene selectivity in Table 3 was calculated as the global methylene selectivity $\bar{\alpha}_{14}$ at a value of n_c of 14. Surprisingly, the corresponding value for this particular C_{18}-bonded silica was close to the value of the mean average selectivity $\bar{\bar{\alpha}}_{sat}$ obtained for the other bonded silicas (C_{14}, C_{18}) (see Table 3). These experimental results were also observed in NARP liquid chromatography with various mobile phase compositions ($MeCN–CHCl_3$ or $MeOH–CHCl_3$) [13]. These results are not con-

Table 3
Mean average methylene selectivity for $n < n_{crit.}$ ($\bar{\bar{\alpha}}_{in}$), $n_{crit.} < n < n_{sat.}$ ($\bar{\bar{\alpha}}_{crit.}$) and $n > n_{sat.}$ ($\bar{\bar{\alpha}}_{sat.}$) versus the nature of the grafted silica

Mobile phase	Column	n_{bp}	$\bar{\bar{\alpha}}_{in}$	$\bar{\bar{\alpha}}_{crit.}$	$\bar{\bar{\alpha}}_{sat.}$	$\bar{\alpha}_{nc=14}$
Pure MeOH (25°C)	LiChrosorb RP-8	8	1.18	1.12	1.106	–
	LiChrosorb RP Select B	8	–	1.123	1.106	–
	LiChrosorb RP-14	14	1.23	1.185	1.172	–
	LiChrosorb RP-18	18	1.24	1.21	1.198	–
	μBondapak C_{18}	18				1.169
	LiChrosorb RP-2	1				1.15
$MeOH–H_2O$ (90:10) (25°C)	LiChrosorb RP-14	14	1.34	1.315	1.298	–
	LiChrosorb RP-18	18	1.39	1.36	–	–
	μBondapak C_{18}	18				1.27
	LiChrosorb RP-2	1				1.17

tradictory to those reported above. They suggest a loose contact between the bonded phase and the solute which is coherent with a monomeric stationary phase with a short chain length for which lying on the phase is the only possibility [21]. This is also valid for the octadecyl phase with a low bonding density for which a close insertion of solute in the phase cannot occur [21].

Correlation between average methylene selectivity $\tilde{\alpha}$ and molecular mechanism of retention

We have shown that $\tilde{\alpha}_{in}$ is not identical for all the homologues tested (cf., Table 2). The first hypothesis is to consider that the retention of the polar compounds (Z = COOMe, COMe, OH, COPh, OCOMe, Br) can be due to a mixed mechanism of retention as previously described by Nahum and Horváth [29]. The hydrocarbonaceous part of the solute interacts with the hydrocarbonaceous part of the bonded phase by dispersion interactions and the polar part of solute Z interacts with silanols located at the bottom of the chains of the stationary phase. In such a case, the polar head Z of the solute penetrates deeply inside the chains of the bonded phase. The influence of this contribution to the retention should decrease with increasing chain length of the solute owing to the increase in its size. This could explain why smaller alcohols ($n_c < 4$) are more retained than predicted by extrapolation from higher homologues of the straight lines of the log k' vs. n_c curves [5].

However, in this case the depth of penetration of a polar solute inside the bonded phase depends on the steric hindrance of the polar head. In order to verify this hypothesis, we tested the behaviour of alkyl acetates (Z = OCOMe). In this particular case, the polar head corresponds approximately to three methylene groups and should lead to a value of $n_{crit.}$ less than three carbon atoms than the other homologues tested. We have never observed this effect. The behaviour of alkyl acetates was identical with that of the other polar series. Such a mechanism of insertion of the head group of the homologues into the stationary phase was only observed for phenylalkanes and dialkyl *o*-phthalates [5,15].

The overall results are in favour of a mechanism of retention in which the polar head of solutes stays out of the chains of the stationary phase to maximize the polar interactions with the solvent [15]. For polar solutes the potential polar head–residual silanols interaction plays a role in the retention but it occurs just in the place of low-density of coverage of silica.

The second point to elucidate is the relationship between the London dispersive interactions and contacts between chains with increasing number of carbon atoms.

In the case of the penetration model, there is a close contact between the hydrocarbonaceous chain as described above. The regular increase in the values of k' is a consequence of the increase in molecular volume with n_c [1–4,11]. Thus, $\tilde{\alpha}_{in}$ must reflect the variation of the transfer energy related to the average molecular volume increment due to a single methylene group of the homologues. This aspect is discussed in the following section.

Correlation between average methylene selectivity $\tilde{\alpha}$ and molecular structure of the solute

For all the homologous tested, curves of variation of molecular volume V_M vs. n_c were plotted. Over a range of n_c values, the curves were not perfect straight lines. The values of the slope between two nearest homologues vs. n_c are not parallel to the n_c axis but decrease slowly. However, in the ranges $1 < n_c < 14$ and $14 < n_c < 24$ the linear regressions give a correlation coefficient always higher than 0.998, which shows that the curves can be treated as straight lines. Consequently, we considered for the following discussion that the average molecular volume of a methylene group, ΔV_{CH_2}, is given by the slope of the curves of V_M vs. n_c.

In general, we have observed that ΔV_{CH_2} is different for each homologous series tested. It is higher for the homologues with a polar head. The order is OCOPh > COMe > OCOPhCOO > COOMe > OCOMe > CHO > COOH > CN = OH > I > Br > Ph > CH=CH_2 = Cl > H > F.

For each series, and on different phases of various alkyl chain lengths, three values of the average molecular volume of a methylene group were calculated: the first, called ΔV_{in}, with $n_c < n_{crit.}$; the second, $\Delta V_{crit.}$, with $n_{crit.} < n_c < n_{sat.}$; and the third, $\Delta V_{sat.}$, with $n_c > n_{sat}$ (Table 4).

The values of $\Delta V_{crit.}$ are close together but those of ΔV_{in} are different for a given homologous series. Consequently, we tried to correlate the values of ΔV_{in} corresponding to each homologous series with the values of the average methylene selectivity $\tilde{\alpha}$ observed in RPLC with the graft of different investigated chain lengths. The results are shown in Fig. 2, where the linear regression coefficients are also reported. Their examination reveals that there is possibly a relationship between these two parameters in a range of n_c such that we think that the retention is described by a close contact between the hydrocarbonaceous parts of the solute and the bonded phase. This conclusion reported here with different bonded phases was also observed independently of the nature of the mobile phase (PARP and NARP modes).

The phenylalkanes are the only homologous series for which this correlation was not observed, but the fact that the phenyl ring penetrates into the bonded phase instead of the alkyl chain [5,15] leads to rationalization of this observation. The chain–chain contact must be weaker than for the other series owing to a more important steric hindrance of the aromatic ring.

Further, independently of the nature of the head Z of the homologue, it could be seen that the values of the average molecular volume of a methylene group, $\Delta V_{crit.}$ and $\Delta V_{sat.}$, are approximately constant in the ranges $n_{crit.} < n_c < n_{sat.}$ and $n_c > n_{sat.}$, respectively. These values decrease in the order $\Delta V_{in} > \Delta V_{crit.} > \Delta V_{sat.}$. This is consistent with the experimental observation that $\tilde{\alpha}_{in}$ values are higher than $\tilde{\alpha}_{crit}$ values (which are constant for all the homologues). The same conclusion could be drawn for the $\tilde{\alpha}_{sat.}$ values as for $\tilde{\alpha}_{crit.}$ values.

Particular behaviour of solutes with saturated cyclic structure

Independently of the nature of the mobile phase composition, the value of the average methylene selectivity $\tilde{\alpha}$ found for cycloalkanones with $n_c < n_{crit.}$ was equal to that obtained for linear chains in the range such that $n_{crit.} < n_c < n_{sat.}$. In the same way, we obtained for symmetrical aliphatic ketones ($3 < n_c < 11$) a value of this variable close to $\tilde{\alpha}_{in}$. This difference between alicyclic and linear ketones is not due to the carbonyl group. It could be attributed to the saturated cyclic configuration. In a penetration process it does not give a chain–cycle contact as close as two linear hydrocarbon chains.

Table 4
Values of the average methylene volume of different homologous series for $n_c < n_{crit.}$ (ΔV_{in}) and $n_{crit.} < n_c < n_{sat.}$ ($\Delta V_{crit.}$)

Z	ΔV_{in}			$\Delta V_{crit.}$	
	$n_{bp} = 8$	$n_{bp} = 14$	$n_{bp} = 18$	$n_{bp} = 8$	$n_{bp} = 14$ and 18
Cl	16.39	16.4	16.41	16.44	16.42
COOMe	16.91	16.76	16.70		
COMe	16.7	16.73	16.77		
OH	16.7	16.63	16.63	16.65	16.45
OCOMe	16.74				
Ph	16.58	16.49	16.53	16.50	16.30
$HC = CH_2$	15.28	15.80	15.89	16.32	16.42
Br	16.53	16.52	–	16.30	16.47
CN	16.87	–	–	16.48	16.51
H	15.57	15.95	15.85	16.45	16.34

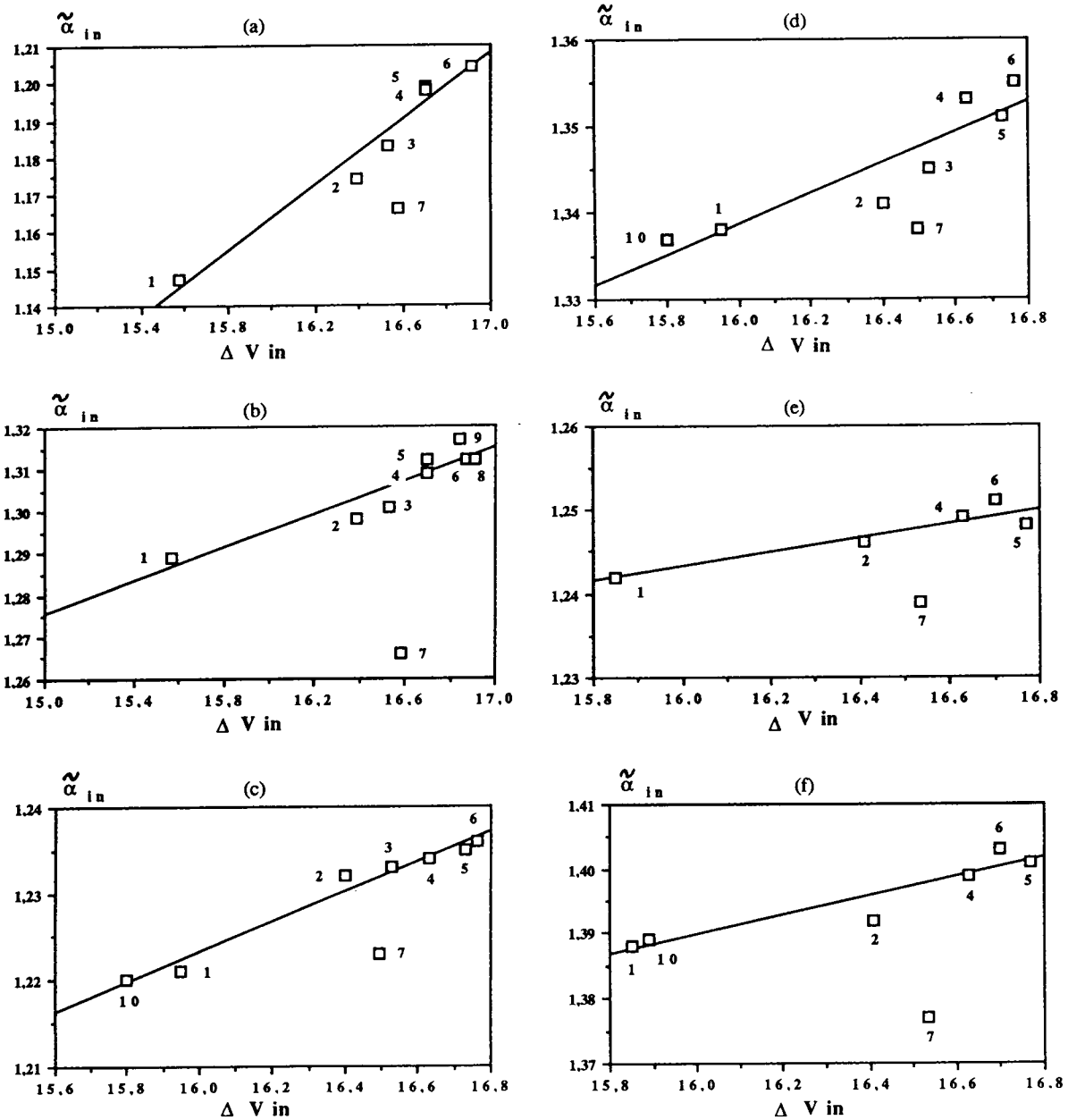

Fig. 2. Average methylene selectivity ($n_c \leq n_{crit.}$) $\tilde{\alpha}_{in}$ vs. average molecular volume of a methylene group ΔV_{in} ($n_c \leq n_{crit.}$) (a) C_8-bonded phase, pure methanol, $r = 0.978$; (b) C_8-bonded phase, methanol–water (90:10) $r = 0.925$; (c) C_{14}-bonded phase, pure methanol, $r = 0.987$; (d) C_{14}-bonded phase, methanol–water (90:10), $r = 0.914$; (e) C_{18}-bonded phase, pure methanol, $r = 0.92$; (f) C_{18}-bonded phase, methanol–water (90:10), $r = 0.941$. 1 = alkanes; 2 = alkyl chlorides; 3 = alkyl bromides; 4 = alkanols; 5 = 2-alkanones; 6 = methyl alkanoates; 7 = phenylalkanes; 8 = cyanoalkanes; 9 = carboxylic acids; 10 = alkenes.

Such a phenomenon was also observed with the 2,2,6,6-tetramethyl-4-piperidinoxyl diesters of dicarboxylic acids (reported as NO in Table 2) with $2 < n_c < 10$, which interact with the stationary phase even by an external chain–chain contact or by penetration with the very hindered ring. For these types of compounds we observed a value of methylene selectivity intermediate between $\tilde{\alpha}_{in}$ and $\tilde{\alpha}_{crit.}$ but close to the latter and not equal to $\tilde{\alpha}_{sat.}$ characteristic of an external contact [21]. Hence it is reasonable to think that this cyclic structure superficially penetrates the chains of bonded phase and their hydrocarbon chains interact more freely with the chains of the bonded phase.

We also report the results obtained with liquid crystals. Although the cyclic structures are aromatic, we observed a value of mean methylene selectivity close to $\tilde{\alpha}_{crit.}$ and not to $\tilde{\alpha}_{in}$. An examination of their structures leads to the conclusion that the aromatic part (EtOPhN = NPh) is equivalent to thirteen methylene groups. Consequently, the two aromatic rings penetrate the chain of the stationary phase. As their equivalent length is equal to the depth of penetration ($n_{crit.} = 14$) no break could be observed for these solutes on the bonded silicas investigated. The contact between saturated chains is less tight than in the case of direct penetration in the stationary phase. According to this last hypothesis, the average methylene selectivity would be equal to $\tilde{\alpha}_{in}$. Finally, this phenomenon is the same as that reported previously for phenylalkanes and dialkyl *o*-phthalates for which the penetration of the aromatic ring in the stationary phase was established without ambiguity [15].

5. Conclusions

Several conclusions can be drawn from the results presented above.

(1) The overall results permit us to propose a more complete model of molecular mechanism of interaction than that established previously for monomeric bonded silicas. Various criteria could be used to describe this mechanism: the plots of quadratic methylene selectivity α_n vs. n_c present two plateaux, the second of which is divided into two parts separated by a break. The drop between the two plateaux appears at a critical value of n_c, $n_{crit.}$, and the break at a value named the saturation value $n_{sat.}$. Three different values of mean average methylene selectivity can be calculated: $\bar{\tilde{\alpha}}_{in}$. which corresponds to the homologues such that $n_c < n_{crit.}$, $\bar{\tilde{\alpha}}_{crit}$ for $n_{crit.} < n_c < n_{sat.}$ and $\bar{\tilde{\alpha}}_{sat}$ for $n_c > n_{sat}$.

(2) The values of $n_{crit.}$ are independent of the nature of the homologous series and the mobile phase composition (PARP rich in organic modifier and NARP rich in methanol or acetonitrile); $n_{crit.}$ is directly connected to the length of the alkyl-bonded chain. Surprisingly, it is the same for octadecyl and docosyl chains. The value of $n_{sat.}$ is related to the density of the grafts. It decreases when the density increases. Conversely, for alkylsilicas with a low value of the carbon load the second break in the experimental curves cannot be observed. Finally, for a silica and a very low density no break appears.

(3) The average methylene selectivities $\tilde{\alpha}_{in}$ vary from one homologous series to another. The values of $\tilde{\alpha}_{crit.}$ and $\tilde{\alpha}_{sat.}$ are independent of the polar head.

(4) A correlation between the values of average methylene selectivity $\tilde{\alpha}$ and the average molecular volume of a methylene group ΔV_{CH_2} can be established. Thus, for values such that $n_c < n_{crit.}$, ΔV_{in} varies with the homologues. A linear relationship could be drawn between $\tilde{\alpha}_{in}$ and V_{in} for each tested series, independently of the nature of the length of monomeric bonded silica. For the homologues such that $n_{crit.} < n_c < n_{sat.}$ and $n_c > n_{sat}$, the corresponding values of $\tilde{\alpha}_{crit}$, $\Delta V_{crit.}$ and $\tilde{\alpha}_{sat}$ and $\Delta V_{sat.}$ are different but constant and independent of the nature of the homologous series.

(5) The precise determination of the value of the average methylene selectivity $\tilde{\alpha}$ of a particular series in a range of n_c such that $n_c < n_{crit.}$ permits the molecular mechanism of interaction with the stationary phase to be determined. Thus the liquid crystals interact with the alkyl-bonded chains by insertion of their aromatic rings. For the cycloalkanes their structures do not permit a

deep insertion with close contact. The interaction is more superficial exactly like aliphatic chains in a range of n_c such that $n_{crit.} < n_c < n_{sat.}$.

(6) These results suggest a molecular mechanism of retention for monofunctional bonded silicas with penetration and tight contact between the aliphatic chains of the bonded phase and the solute for $n_c < n_{crit.}$. This contact is responsible for the close correlation between ΔV_{in} and $\tilde{\alpha}_{in}$ and rationalizes the fact that $\tilde{\alpha}_{in}$ is different with regard to the nature of homologues. When there are supplementary methylene groups in the structure of the solute there is always penetration of the solute inside the alkyl chains of the bonded phase but the contact is less tight. It occurs with solute molecule in folded conformations such that all the available space between the chains of the bonded phase is engaged. There is no contact between each methylene group of the bonded phase and of the solute. The role of the polar head is levelled. ΔV_{CH_2} is independent of the polar or non-polar nature of the solute and also $\alpha_{crit.}$. When there is no additional space between the chains of the bonded phase their contact with the chain of a longer solute could be established by lying on the external methyl groups of the bonded phase. In this case no differentiation can be observed between the different homologous series. The corresponding $\Delta V_{sat.}$ and $\tilde{\alpha}_{sat.}$ are constant but smaller than $\Delta V_{crit.}$ and $\tilde{\alpha}_{crit.}$.

6. Symbols

a = Characteristic constant which depends on the solute and the mobile phase.

C = Characteristic constant which depends on the solute and the mobile phase.

k' = Capacity factor of solute.

$n_{crit.}$ = carbon number of homologue for which the first break is observed for log k' vs. n_c plots.

$n_{sat.}$ = carbon number of homologue for which the second break is observed for log k' vs. n_c plots.

p = Slope of the curve log k' vs. n_c.

q = Intercept with the y-axis of the curve log k' vs. n_c.

R = Gas constant.

T = Absolute temperature.

V_M = Molecular volume of solute.

V_{SP} = Molecular size of the bonded chain.

Z = Functional group of homologous series.

$\alpha_n = (k'_{n_c+1}/k'_{n_c-1})^{1/2}$: quadratic methylene selectivity.

$\overline{\alpha_n} = \sum_1^x \alpha_n/x$: global quadratic methylene selectivity where x is the number of tested eluites with a chain length of n carbon atoms.

$\tilde{\alpha}$ = average methylene selectivity calculated from the slope of log k' vs. n_c.

$\bar{\tilde{\alpha}} = \sum \alpha/N$: mean average methylene selectivity where N is the number of tested homologous series.

$\alpha_{TBN/BaP}$ = selectivity between tetrabenzonaphthalene and benzo[a]pyrene obtained with MeCN–H_2O (85:15) as mobile phase.

$\tilde{\alpha}_{in}$ = average methylene selectivity for homologues such that $n_c < n_{crit.}$.

$\tilde{\alpha}_{sat.}$ = average methylene selectivity for homologues such that $n_c > n_{sat.}$.

$\tilde{\alpha}_{crit.}$ = average methylene selectivity for homologues such that $n_{crit.} < n_c < n_{sat.}$.

Γ = Surface concentration of bonded organosilyl group.

ϕ = Phase ratio.

ΔA = Contact area between the solute and the stationary phase.

$\Delta G°$ = Partial molar free energy associated with the transfer of the solute and the stationary phase (assumed to be in the standard state at infinite dilution) from the mobile phase to the stationary phase.

$\Delta G°_{CH_2}$ = Partial molar free energy associated with the transfer of single methylene

group of solute from the mobile phase to the stationary phase.

ΔV_{CH_2} = average molecular volume of a methylene group.

ΔV_{in} = average molecular volume of a methylene group for $n_c < n_{crit.}$.

$\Delta V_{sat.}$ = average molecular volume of a methylene group for $n_c > n_{sat.}$.

$\Delta V_{crit.}$ = average molecular volume of a methylene group for $n_{crit.} < n_c < n_{sat.}$.

References

[1] O. Sinanoglu, in B. Pullman (Editor), *Molecular Associations in Biology*, Academic Press, New York, 1968, p. 427.

[2] Cs. Horváth, W. Melander and I. Molnár, *J. Chromatogr.*, 125 (1976) 129.

[3] Cs. Horváth and W. Melander, *Int. Lab.*, Nov./Dec. (1978) 11.

[4] W. Melander and Cs. Horváth, in Cs. Horváth (Editor), *High Performance Liquid Chromatography —Advances and Perspectives*, Vol. 2, Academic Press, New York, 1980, Ch. 2, p. 113.

[5] A. Tchapla, H. Colin and G. Guiochon, *Anal. Chem.*, 56 (1984) 621.

[6] M. Czok and H. Engelhardt, *Chromatographia*, 27 (1989) 5.

[7] P. Dufek, *J. Chromatogr.*, 299 (1984) 109.

[8] P. Jandera and J. Rozkosna, *J. Chromatogr.*, 556 (1991) 145.

[9] P. Jandera, *J. Chromatogr.*, 352 (1986) 91.

[10] P. Jandera, *J. Chromatogr.*, 449 (1988) 361.

[11] S. Héron and A. Tchapla, *Chromatographia*, 36 (1993) 11.

[12] D. Morel, J. Serpinet, J.F. Letoffe and P. Claudy, *Chromatographia*, 22 (1986) 103.

[13] G. Thevenon, *Ph.D. Dissertation*, Université Paris VI, Paris, 1985.

[14] M. Martin, G. Thevenon and A. Tchapla, *J. Chromatogr.*, 452 (1988) 157.

[15] A. Tchapla, S. Héron, H. Colin and G. Guiochon, *Anal. Chem.*, 60 (1988) 1443.

[16] E. Lundanes and T. Greybrokk, *J. Chromatogr.*, 322 (1985) 347.

[17] S. Héron and A. Tchapla, *J. Chromatogr.*, 556 (1991) 219.

[18] R.J. Laub and S.J. Madden, *J. Liq. Chromatogr.*, 8 (1985) 187.

[19] E.H. Slaats, J.C. Kraak, W.J.T. Brugman and H. Poppe, *J. Chromatogr.*, 149 (1978) 255.

[20] A.J.P. Martin, *Biochem. Soc. Symp.*, 3 (1949) 4.

[21] A. Tchapla, S. Héron, E. Lesellier and H. Colin, *J. Chromatogr. A*, 656 (1993) 81.

[22] C. Liteanu and I. Rice (Editors), *Statistical Theory and Methodology of Trace Analysis*, Ellis Horwood, Chichester, 1980, p. 156.

[23] R.C. Weast (Editor), *CRC Handbook of Chemistry and Physics*, CRC Press, Boca Raton, FL, 1984, p. C65.

[24] K.K. Unger, in K.K. Unger (Editor), *Packings and Stationary Phases in Chromatographic Techniques (Chromatographic Science Series*, Vol. 47), Marcel Dekker, New York, 1990, p. 364.

[25] S.A. Wise and L.C. Sander, *J. High Resolut. Chromatogr. Chromatogr. Commun.*, 8 (1985) 248.

[26] L.C. Sander and S.A. Wise, *CRT Crit. Rev. Anal. Chem.*, 18 (1987) 299.

[27] G.E. Berendsen, *Ph.D. Dissertation*, University of Delft, Delft, 1980.

[28] G.E. Berendsen and L.C. de Galan, *J. Chromatogr.*, 196 (1980) 21.

[29] A. Nahum and Cs. Horváth, *J. Chromatogr.*, 203 (1981) 53.

[30] C. Lullmann, H.G. Genieser and B. Jastorff, *J. Chromatogr.*, 323 (1985) 273.

[31] S.D. Fazio, S.A. Tomellini, H. Shih-Hsien, J.B. Crowther, T.V. Raglione, T.R. Floyd and R. Hartwick, *Anal. Chem.*, 57 (1985) 1559.

[32] Z. Sahraoui, *Ph.D. Dissertation*, Université Lyon I, Lyon, 1987.

[33] F. Meiouet, *Ph.D. Dissertation*, Université Bordeaux I, Bordeaux, 1989.

[34] N.H.C. Cooke and K. Olsen, *J. Chromatogr. Sci.*, 18 (1980) 1.

[35] L.C. Sander and S.A. Wise, *LC·GC Int.*, 3, No. 6 (1990) 24.

[36] L.C. Sander and S.A. Wise, *J. High Resolut. Chromatogr. Chromatogr. Commun.*, 11 (1988) 383.

[37] E. Lesellier and A. Tchapla, unpublished results.

ELSEVIER

Journal of Chromatography A, 684 (1994) 189–200

JOURNAL OF CHROMATOGRAPHY A

Mechanistic evaluation of the resolution of α-amino acids on dynamic chiral stationary phases derived from amino alcohols by ligand-exchange chromatography

Myung Ho Hyun*, Duk Ho Yang, Hyeon Ju Kim, Jae-Jeong Ryoo

Department of Chemistry, Pusan National University, Keumjeong-Ku, Pusan 609-735, South Korea

First received 6 April 1994; revised manuscript received 24 June 1994

Abstract

Two dynamic chiral stationary phases (CSP **7** and **12**) were prepared starting from (*R*)-2-amino-1-propanol and (*R*)-α-phenylethylamine. The resolution of racemic α-amino acids on the two dynamic CSPs thus prepared were compared with previously reported resolution data on a dynamic CSP (**2**) derived from (1*S*,2*R*)-norephedrine. The enantioselectivity for the two enantiomers of α-amino acids on CSP **7** was found to be comparable to or better than that on CSP **2** while the enantioselectivity for the two enantiomers of α-amino acids on CSP **12** was much worse than that on CSPs **2** or **7**. From these results, we concluded that the phenyl functionality at the first chiral center of CSP 2 is not essential in the chiral recognition. However, the hydroxy functionality of CSPs **2** or **7** does play a very important role in the chiral recognition.

1. Introduction

Chiral ligand-exchange chromatography has been widely employed in resolving racemic α-amino acids since the pioneering work of Davankov and co-workers in the late 1960s (see [1–3]). Copper(II) complexes of optically pure α-amino acids and their derivatives have been usually applied as chiral mobile phase additives [4,5] or chiral stationary phases (CSPs) after binding covalently [6,7] or hydrophobically [8–10] to solid column support. However, copper(II) complexes of other optically active materials have been rarely adopted as chiral selectors in chiral ligand-exchange chromatography [1,11,12].

Recently, we reported the use of the Cu(II) complex of a (1*S*,2*R*)-norephedrine derivative **1** mechanically adsorbed onto a commercial octadecyl-silica gel column as a dynamic chiral stationary phase (CSP **2**) in resolving underivatized racemic α-amino acids [13,14]. CSP **2** was very efficient in resolving various underivatized α-amino acids. Based on the resolution trends influenced by the organic modifier content, the Cu(II) concentration and the pH of the mobile phase, a chiral recognition model demonstrating the formation of the energetically different two diastereomeric ternary complexes shown in Fig. 1 from the fixed chiral ligand, racemic amino acid and Cu(II) was proposed [14]. In that model, chiral selector is bound to octadecyl-silica gel through the lipophilic interaction between the octadecyl chains of silica gel and the dodecyl alkyl chain of the chiral selector. The bounded

* Corresponding author.

0021-9673/94/$07.00
SSDI 0021-9673(94)00595-Z

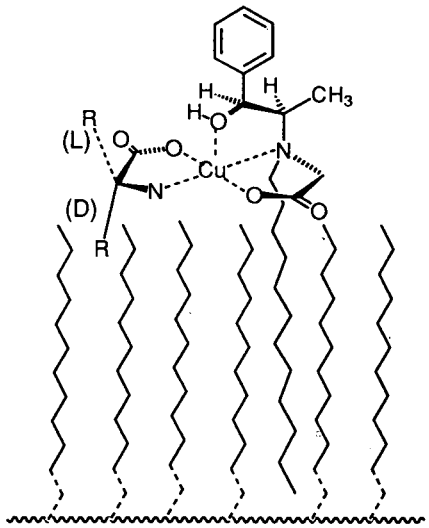

Fig. 1. The proposed structure of the ternary complex formed from the fixed ligand of CSP **2**, D- or L-amino acid and Cu(II).

chiral selector and an α-amino acid coordinate Cu(II), forming a ternary complex with *trans* (N,N) arrangement which is known to be energetically more favorable than that with *cis* (N,N) arrangement [8]. Simultaneously, the hydroxy oxygen of the chiral selector occupies the axial position in the coordination sphere of the Cu(II) of the square planar complex. However, based on the model shown in Fig. 1, the phenyl functionality at the first (1*S*)-chiral center of the chiral selector does not seem to have any role in the chiral recognition except hindering the axial coordination by the hydroxy oxygen because of the steric hindrance.

To explore the role of the phenyl functionality and the importance of the axial coordination by the hydroxy group in the chiral recognition model shown in Fig. 1, in the present study, we wish to prepare two new dynamic CSPs, one of which does not contain a phenyl functionality and the other of which does not have an axially coordinating hydroxy group. The resolution of α-amino acids on the two new dynamic CSPs may elucidate the role of the phenyl group and the importance of the axial coordination by the hydroxy group in the chiral recognition.

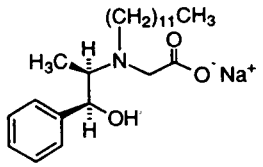

1

2. Experimental

2.1. Instrumentation

Melting points were determined by a Rigaku thermal analyzer TAS 100. ^{1}H NMR spectra were recorded on a Varian Gemini 300 or on a Varian Gemini 200 spectrometer using tetramethylsilane as an internal standard. IR spectra were recorded on a Mattson Polaris or Mattson Galaxy 2000 Fourier transform IR spectrometer.

Chromatography was performed with a Waters Model 510 pump, a Waters Model U6K universal chromatographic injector equipped with a 20-μl sample loop, a Waters Model 441 absorbance detector with 254-nm UV filter, and a Waters Model 740 data module recorder.

2.2. Preparation of dynamic CSP 7 from (R)-2-amino-1-propanol

Dynamic CSP **7** based on (*R*)-2-amino-1-propanol was prepared as shown in Fig. 2. The detailed procedures are as follows.

(R)-N-Lauroyl-2-amino-1-propanol **3**

In a 250-ml flask equipped with a magnetic stir bar were dissolved 15 ml (0.064 mol) of (*R*)-2-amino-1-propanol and 10 ml (0.072 mol) of triethylamine in 50 ml of methylene chloride. To the stirred mixture were slowly added 15 ml (0.064 mol) of lauroyl chloride dissolved in 20 ml of methylene chloride under nitrogen. The reaction mixture was stirred at room temperature for 2 h and then washed with saturated $NaHCO_3$ solution three times. The organic solution was dried over anhydrous $MgSO_4$ and the solvent was evaporated. The solid residue was crys-

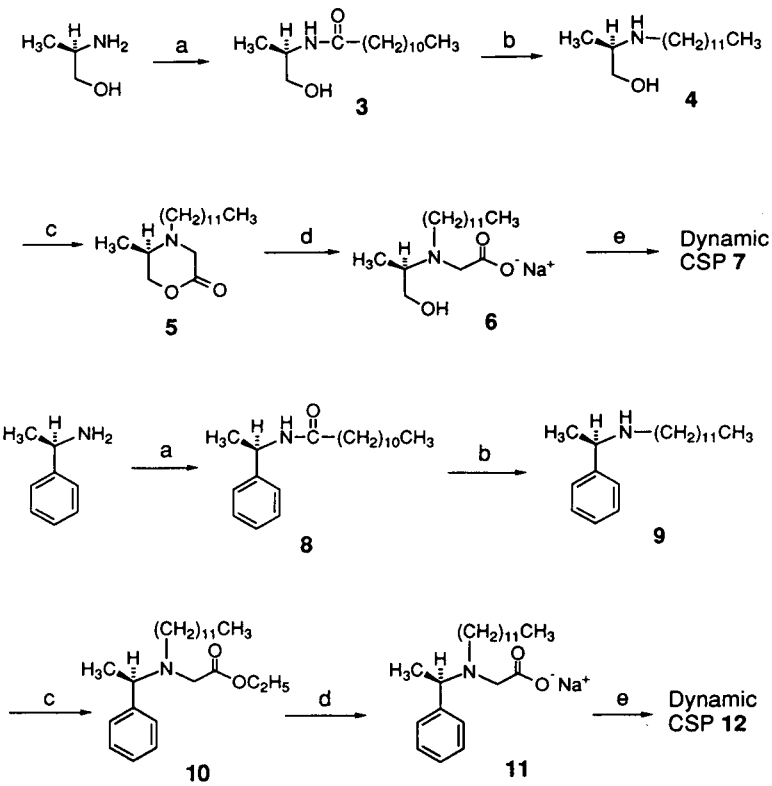

Fig. 2. Preparation of CSPs **7** and **12**. a = Lauroyl chloride, triethylamine, CH_2Cl_2, room temperature; b = $LiAlH_4$, THF, 0°C to reflux; c = ethylbromoacetate, propylene oxide, CH_2Cl_2, room temperature; d = 1 *M* NaOH in methanol; e = hydrophobic loading onto a commercial octadecyl-silica gel column.

tallized from the mixed solvent of acetone and hexane to afford compound **3** as a white crystalline solid (13.5 g, 80% yield). m.p. 70–72°C; ^{1}H NMR (C^2HCl_3) δ 0.87 (t, 3H), 1.16 (d, 3H), 1.25 (broad s, 16H), 1.55–1.70 (m, 2H), 2.18 (t, 2H), 3.08 (broad s, 1H), 3.48–3.69 (m, 2H), 4.00–4.12 (m, 1H), 5.68 (broad s, 1H). IR (KBr) cm^{-1} 3302, 2922, 2852, 1641, 1549, 1467.

(R)-N-Dodecyl-2-amino-1-propanol ***4***

In a 250-ml flask charged with 10 g (0.038 mol) of compound **3** and 6 g of $LiAlH_4$ were added 50 ml of dry tetrahydrofuran (THF) at 0°C under nitrogen. The mixture was heated to reflux for one day. The reaction mixture was cooled to 0°C and then the reaction was quenched by adding water. The whole mixture was filtered through a Celite pad and then THF was removed under reduced pressure. The aqueous solution was extracted with methylene chloride, and then the organic layer was dried over anhydrous $MgSO_4$ and concentrated. The resulting residue was crystallized from the mixed solvent of methylene chloride and hexane to afford compound **4** as a white crystalline solid (7.6 g, 83% yield). m.p. 63–65°C; ^{1}H NMR (C^2HCl_3) δ 0.88 (t, 3H), 1.10 (d, 3H), 1.25 (broad s, 18H), 1.47–1.56 (m, 2H), 2.49–2.62 (m, 1H), 2.68–2.88 (m, 4H; 2H with ^2H_2O), 3.32 (dd, 1H), 3.62 (dd, 1H). IR (KBr) cm^{-1} 2919, 2849, 1466.

(R)-4-Dodecyl-5-methyl-2,3,5,6-tetrahydro-4H-1,4-oxazin-2-one ***5***

In a 250-ml flask equipped with a magnetic stir bar were dissolved 6 g (0.025 mol) of compound

4 in 50 ml of methylene chloride. To the stirred solution were added 2.75 ml (0.025 mol) of ethylbromoacetate and 1 ml of propylene oxide at room temperature. The whole mixture was stirred for one day at room temperature and then washed with water. The organic solution was dried over anhydrous $MgSO_4$, filtered, concentrated and the resulting residue was purified by silica gel column chromatography to afford product **5** as a sticky solid (2.2 g, 27% yield). ^1H NMR (C^2HCl_3) δ 0.88 (t, 3H), 1.08 (d, 3H), 1.26 (broad s, 18H), 1.39–1.47 (m, 2H), 2.24–2.32 (m, 1H), 2.60–2.69 (m, 1H), 2.77–2.83 (m, 1H), 3.19 (d, 1H), 3.60 (d, 1H), 4.05 (dd, 1H), 4.30 (dd, 1H); IR (C^2HCl_3) cm^{-1} 2928, 2857, 1740.

(R)-N,N-Carboxymethyl dodecyl-2-amino-1-propanol monosodium salt ***6***

Compound 6 (2.0 g, 0.006 mol) was dissolved in 20 ml of methanol in a 50-ml flask. To the stirred solution were added 6.2 ml of 1 *M* NaOH solution in methanol. The whole mixture was stirred for 5 h and then evaporated. The residue was dried under high vacuum for 10 h to afford oily product **6** (1.8 g). ^1H NMR (^2H_2O) δ 0.80–0.98 (broad m, 6H), 1.27 (broad s, 18H), 1.48 (broad s, 2H), 2.39 (broad s, 1H), 2.54 (broad s, 1H), 2.92 (broad s, 1H), 3.00 (broad d, 1H), 3.27 (broad d, 1H), 3.40 (broad s, 2H); IR (KBr) cm^{-1} 2900, 1620, 1480, 1410.

Preparation of dynamic CSP ***7***

Dynamic CSP **7** was prepared by loading **6** onto a octadecyl-silica gel column. The loading of **6** onto a commercial octadecyl-silica gel column (Waters μBondapak C_{18}, 300 × 3.9 mm) was accomplished at room temperature by eluting a solution of **6** (1.8 g, 0.0054 mol) in 50 ml of methanol–water (1:2, v/v) through the column (flow-rate: 0.8 ml/min) followed by washing with mixture of methanol–water (1:2, v/v, flow-rate: 0.3 ml/min) for 7 h and then with water (flow-rate: 0.3 ml/min) for 5 h. The effort to figure out the loaded amount of **6** was not successful. However, the used amount of **6** (1.8 g) was assumed to be large enough for full loading because the bleeding of the excess of **6** from the column was detected by the UV monitor.

2.3. Preparation of dynamic CSP ***12*** *from (R)-α-phenylethylamine*

Dynamic CSP **12** based on (*R*)-α-phenylethylamine was prepared as shown in Fig. 2. The detailed procedures are as follows.

(R)-N-Lauroyl-α-phenylethylamine ***8***

This compound was prepared as a white solid material using 3.2 ml (0.025 mol) of (*R*)-(+)-α-phenylethylamine, 3.5 ml (0.025 mol) of triethylamine and 5.8 ml (0.025 mol) of lauroyl chloride by the same procedure as described in the preparation of compound **3** (7.13 g, 94% yield). m.p. 54.5–55.5°C; ^1H NMR (C^2HCl_3) δ 0.88 (t, 3H), 1.25 (broad s, 16H), 1.49 (d, 3H), 1.58–1.65 (m, 2H), 2.17 (t, 2H), 5.10–5.20 (m, 1H), 5.66 (d, 1H), 7.24–7.38 (m, 5H); IR (C^2HCl_3) cm^{-1} 3293, 3065, 2926, 2855, 1642.

(R)-N-Dodecyl-α-phenylethylamine ***9***

This compound was prepared as a yellowish liquid using 7.13 g (0.023 mol) of compound **8** and 1.78 g (0.05 mol) of $LiAlH_4$ by the same procedure as described in the preparation of compound **4** (5.77 g, 85% yield). ^1H NMR (C^2HCl_3) δ 0.88 (t, 3H), 1.18–1.30 (m, 19H), 1.37 (d, 3H), 1.42–1.52 (m, 2H), 2.37–2.54 (m, 2H), 3.77 (q, 1H), 7.27–7.36 (m, 5H); IR (C^2HCl_3) cm^{-1} 3065, 2926, 2855, 1466.

(R)-N-Ethoxycarbonylmethyl-N-dodecyl-α-phenylethylamine ***10***

This compound was prepared as an oily liquid using 5.79 g (0.02 mol) of compound **9**, 2.22 ml (0.02 mol) of ethylbromoacetate and 2.78 ml (0.02 mol) of triethylamine by the same procedure as described in the preparation of compound **5** (4.66 g, 62% yield). ^1H NMR (C^2HCl_3) δ 0.89 (t, 3H), 1.24–1.33 (m, 21H, triplet for 3H is imbedded), 1.35 (d, 3H), 1.40–1.47 (m, 2H), 2.54–2.60 (m, 2H), 3.27 (d, 1H), 3.43 (d, 1H), 4.04 (q, 1H), 4.14 (q, 2H), 7.20–7.40 (m, 5H); IR (C^2HCl_3) cm^{-1} 3065, 2926, 2855, 1740.

(R)-N-Carboxymethyl-N-dodecyl-α-phenylethylamine mono sodium salt ***11***

This salt was prepared as an oily product using 4.66 g (0.012 mol) of compound **10** by the same procedure as described in the preparation of salt **6** (4.4 g). ^{1}H NMR (^2H_2O) δ 0.87 (t, 3H), 1.10–1.40 (m, 23H), 2.12–2.38 (broad m, 2H), 2.88 (d, 1H), 3.19 (d, 1H), 3.82–3.90 (m, 1H), 6.98–7.30 (m, 5H); IR (KBr) cm^{-1} 3100, 2950, 2870, 1650.

Preparation of dynamic CSP ***12***

Dynamic CSP **12** was prepared by loading **11** onto a octadecyl-silica gel column. The loading of **11** onto a commercial octadecyl-silica gel column (Waters μBondapak C_{18}, 300 × 3.9 mm) was achieved at room temperature by passing a solution of **11** (2.1 g, 0.0054 mol) in 50 ml of methanol–water (1:2, v/v) through the column (flow-rate: 0.8 ml/min) followed by washing with mixture of methanol–water (1:2, v/v; flow-rate: 0.3 ml/min) for 7 h and then with water (flow-rate: 0.3 ml/min) for 5 h. The effort to figure out the loaded amount of **11** was not successful. However, the used amount of **11** (2.1 g) was assumed to be large enough for full loading because the bleeding of the excess of **11** from the column was detected by the UV monitor.

2.4. Chromatography

To resolve racemic α-amino acids on the two dynamic CSPs prepared as above, a mobile phase was passed through the column until the baseline (UV monitor, 254 nm) became stable to equilibrate the column and then, a methanolic solution (usually 5 μl) containing a racemic or optically enriched α-amino acid was injected with a flow-rate of 0.8 ml/min. Mobile phase was prepared by dissolving a specified amount of $CuSO_4$ in deionized water or in deionized water containing acetonitrile or methanol as an organic modifier. Column void volume (the elution time of an unretained solute) was measured by injecting aqueous $NaNO_3$ solution [15]. The dynamic CSPs used in this study were found to be equally effective for the chiral separation of α-amino acids after the use of three months.

3. Results and discussion

Dynamic CSP **7** based on (*R*)-2-amino-1-propanol was prepared by mechanically loading (*R*)-N,N-carboxymethyl dodecyl-2-amino-1-propanol mono sodium salt **6** onto a commercial reversed-phase octadecyl-silica gel column as shown in Fig. 2. The diastereomeric transient ternary complex expected to be formed during the resolution of α-amino acids on dynamic CSP **7** using Cu(II) as complexing metal ion is shown in Fig. 3. The structure of the ternary complex shown in Fig. 3 is very similar to that shown in Fig. 1 except the absence of the phenyl functionality in the axial position. Therefore, based on the model shown in Figs. 1 and 3, the resolution behaviors of racemic α-amino acids on dynamic CSP **2** and **7** are expected to be quite similar except the effect of the phenyl functionality upon the chiral recognition.

Table 1 summarizes the resolution of various racemic α-amino acids on dynamic CSP **7** at constant Cu(II) concentration ($2.5 \cdot 10^{-4}$ *M*) with the variation of the content of organic modifier in the aqueous mobile phase. Most of the tested α-amino acids were resolved with reasonable or good separation factors. The separation factors shown in Table 1 are comparable to or better than those on dynamic CSP **2**

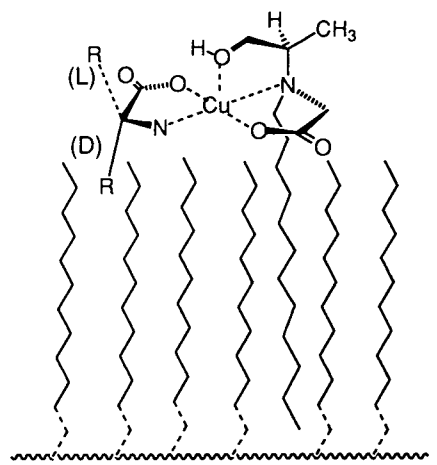

Fig. 3. The proposed structure of the ternary complex formed from the fixed ligand of CSP **7**, D- or L-amino acid and Cu(II).

Table 1
Resolution of racemic α-amino acids on dynamic CSP 7 with varying organic modifier content in the aqueous mobile phase at constant Cu(II) concentration ($2.5 \cdot 10^{-4}$ *M*)

Amino acid	20% MeOH		10% MeOH		100% Water		10% CH_3CN		20% CH_3CN	
	k' [a]	α [b]	k' [a]	α [b]	k' [a]	α [b]	k' [a]	α [b]	k' [a]	α [b]
Alanine	1.70 (L) 2.86 (D)	1.69	1.89 (L) 3.48 (D)	1.85	1.96 (L) 3.97 (D)	2.02	2.37 (L) 3.14 (D)	1.32	1.08 1.08	1.00
Valine	3.44 (L) 16.03 (D)	4.66	4.60 (L) 23.60 (D)	5.14			3.99 (L) 13.53 (D)	3.39	1.46 (L) 2.29 (D)	1.56
Leucine	8.33 (L) 30.89 (D)	3.71					10.14 (L) 28.74 (D)	2.83	2.25 (L) 3.36 (D)	1.52
Proline	3.86 (L) 11.41 (D)	2.95	4.76 (L) 20.50 (D)	4.30	5.49 (L) 32.14 (D)	5.85	4.24 (L) 9.45 (D)	2.23	1.37 (L) 1.75 (D)	1.28
Aspartic acid	1.18 (L) 1.52 (D)	1.28	1.92 (L) 2.69 (D)	1.40	3.54 (L) 5.21 (D)	1.47	1.28 (L) 1.51 (D)	1.18	0.03 0.03	1.00
Glutamic acid	2.47 (L) 5.10 (D)	2.06	4.04 (L) 9.54 (D)	2.36	8.27 (L) 22.07 (D)	2.67	2.57 (L) 4.77 (D)	1.86	0.17 0.17	1.00
Glutamine	1.67 (L) 2.38 (D)	1.42	2.21 (L) 3.63 (D)	1.64	2.83 (L) 5.52 (D)	1.95	2.23 (L) 2.73 (D)	1.22	0.89 0.89	1.00
Serine	1.20 (L) 1.71 (D)	1.42	1.48 (L) 2.15 (D)	1.45	1.78 (L) 2.64 (D)	1.49	1.93 (L) 2.26 (D)	1.17	1.02 1.02	1.00
Threonine	1.52 (L) 2.02 (D)	1.33	1.95 (L) 2.68 (D)	1.38	2.43 (L) 3.65 (D)	1.50	2.22 (L) 2.49 (D)	1.12	0.98 0.98	1.00
Methionine	5.83 (L) 13.55 (D)	2.32	9.06 (L) 22.81 (D)	2.52			7.02 (L) 13.68 (D)	1.95	1.71 (L) 2.21 (D)	1.29
Histidine	2.31 (D) 2.96 (L)	1.28	3.48 (D) 4.26 (L)	1.22	4.83 (D) 5.39 (L)	1.12	4.06 (D) 5.55 (L)	1.37	1.78 1.78	1.00
PheAla									3.25 (L) 5.25 (D)	1.61
PheGly									1.76 (L) 3.44 (D)	1.95
Tyrosine									1.32 (L) 1.82 (D)	1.37
Tryptophan									5.36 (L) 7.96 (D)	1.49

For chromatographic conditions, see Experimental section. For blanks, data could not be collected because of the long retention times (more than 3 h) of the two enantiomers on the column.
[a] Capacity factors for the first- and second-eluted enantiomers.
[b] Separation factors.

reported previously [14]. Particularly, the separation factors for α-amino acids containing a hydrophobic α-substituent are much greater on CSP **7** than on CSP **2** [14]. The retention times of the two enantiomers of several α-amino acids having a relatively large hydrophobic α-substituent were too long to be measured with certain mobile phases and so the resolution data for those are left blank in Table 1. An increase in the content of organic modifier in the aqueous mobile phase is found to diminish the retention of the two enantiomers on the column. Especially, the retention of D-enantiomers containing a hydrophobic α-substituent is diminished more significantly than that of L-enantiomers and, as a consequence, the separation factors decrease as the content of organic modifier in the aqueous mobile phase increases. The use of acetonitrile as an organic modifier decreases the retention of D-enantiomers much more drastically than the use of methanol as shown in Fig. 4 and, consequently, the separation factors decrease more drastically when acetonitrile is used as organic modifier. All of these trends are consistent with those on CSP **2** reported previously [14]. However, these trends are much more significant on CSP **7** than on CSP **2**.

The elution orders shown in Table 1 are quite consistent. The D-enantiomers are retained always longer than the L-enantiomers except for the resolution of histidine. These elution orders are somewhat different from those on CSP **2**. On CSP **2**, the D-enantiomers of α-amino acids having a simple hydrophobic α-substituent were retained longer than the L-enantiomers except phenylalanine [14]. However, for α-amino acids having a hydrophilic α-substituent (e.g. aspartic acid, serine, threonine, histidine and tyrosine), L-enantiomers eluted last except glutamine and glutamic acid on CSP **2** [14].

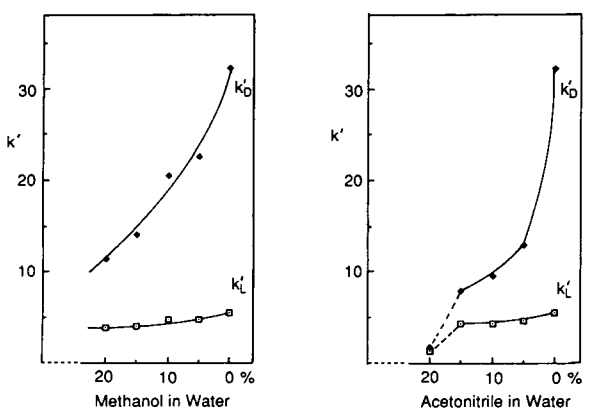

Fig. 4. Dependence of the retention (capacity factor, k') of D-proline and L-proline on the methanol and acetonitrile content in the aqueous mobile phase on CSP **7**. For chromatographic conditions, see Experimental section.

The chiral recognition model shown in Fig. 1 has been utilized to rationalize the resolution trends and the elution orders on CSP **2** [14]. As shown in Fig. 1, the α-alkyl substituent of a D-amino acid was proposed to be intercalated between the octadecyl chains of silica gel while that of a L-amino acid directed into the bulk of mobile phase. In consequence, the ternary complex formed from a D-amino acid with a simple hydrophobic α-alkyl substituent is presumed to be more stable than that from a L-amino acid because of the lipophilic interaction between the hydrophobic α-alkyl substituent of a D-amino acid and the octadecyl chains of silica gel and, in consequence, the D-enantiomers are retained longer on the column. However, the lipophilic interaction between the hydrophobic α-alkyl substituent of a D-amino acid and the octadecyl chains of silica gel decreases as the content of organic modifier in the mobile phase increases and, as a result, the separation factors decrease.

The exactly same rationale can be applied for explaining the elution orders and the trends of retention times and separation factors for the resolution of α-amino acids with a simple hydrophobic α-alkyl substituent on CSP **7**. However, it should be noted that, based on the chiral recognition model shown in Figs. 1 and 3, CSP **7** may form more stable and tighter ternary complex with Cu(II) and an α-amino acid having a simple hydrophobic α-alkyl substituent than CSP **2** because the hydroxy axial coordination is hindered by the phenyl functionality in the case of complexation with CSP **2**. The tightness of the ternary complex may be greater with D-enantiomers than with L-enantiomers because of the lipophilic interaction between the hydrophobic α-alkyl substituent of a D-amino acid and the

octadecyl chains of silica gel as mentioned above. In consequence, the retention times of D-enantiomers are much longer on CSP **7** than on CSP **2** for the resolution of α-amino acids having a simple hydrophobic α-alkyl substituent. The lipophilic interaction between the hydrophobic α-alkyl substituent of D-amino acids and the octadecyl chains of silica gel can be reduced quite much by the organic modifier in the aqueous mobile phase. The reduction of the lipophilic interaction between the hydrophobic α-alkyl substituent of D-amino acids and the octadecyl chains of silica gel seems to be greater with the use of less polar organic modifier in aqueous mobile phase and with tighter complexes. In this context, the use of acetonitrile as an organic modifier should decrease the retention of D-enantiomers and, as a result, the separation factors more drastically than the use of methanol. All of these trends should be more significant with tighter ternary complexes on CSP **7** than on CSP **2**. This is indeed the case as evidenced by the comparison of the resolution results on CSP **7** with those on CSP **2** [14] and by the example for the resolution trends shown in Fig. 4. Note that the high content (20%) of acetonitrile in the aqueous mobile phase reduces the retention of two enantiomers drastically as shown in Fig. 4.

In resolving the two enantiomers of α-amino acids having a hydrophilic α-alkyl substituent on CSP 2, in our previous study, the L-enantiomers were assumed to form more stable complexes than the D-enantiomers because the extra hydrophilic functionality of the α-alkyl substituent of the L-enantiomers may interact with the hydroxy group of the fixed ligand, for example, through the hydrogen bonding or may occupy the axial coordination sphere instead of the hydroxy group of the fixed ligand [14]. As a result, the L-enantiomers are retained longer on the column than the D-enantiomers. The occupation of the axial coordination site by the hydrophilic α-alkyl substituent of L-α-amino acids during the formation of the ternary complex from the fixed ligand constituting CSP **7**, α-amino acids and Cu(II), however, seems to be more difficult and, in consequence, not to occur because the axial coordination by the hydroxy group of the fixed ligand of CSP **7** is stronger than with CSP **2**. In this case, the stability of the ternary complex from L-enantiomers can not be greater than that from D-enantiomers. Accordingly, the elution orders on CSP **7** should be different from those on CSP **2** in resolving the two enantiomers of α-amino acids having a hydrophilic α-alkyl substituent.

However, the α-side chain of L-histidine seems to occupy the axial coordination site of the ternary complex formed with CSP **7** using the imidazole nitrogen as shown in Fig. 5a [9] possibly because of the relatively high basicity of imidazole ring [16]. It has also been reported that the α-amino group and the imidazole nitrogen of histidine may coordinate Cu(II) at the square planar coordination site to form ternary complex with another α-amino acid, with the carboxylic acid group of histidine placed in an axial position and with the two amino groups from histidine and the other amino acid in *cis*-positions of the Cu(II) coordination square [5] even though the *cis* orientation of the two amino groups is controversial [3,9]. In this context, the ternary complex formed from the fixed ligand constituting CSP **7**, L-histidine and Cu(II) has the structure shown in Fig. 5b. In both Fig. 5a and b, L-histidine is retained longer. However, it is hard to determine which mode among those shown in Fig. 5a, b and a combination of them may actually be responsible for the chiral recognition.

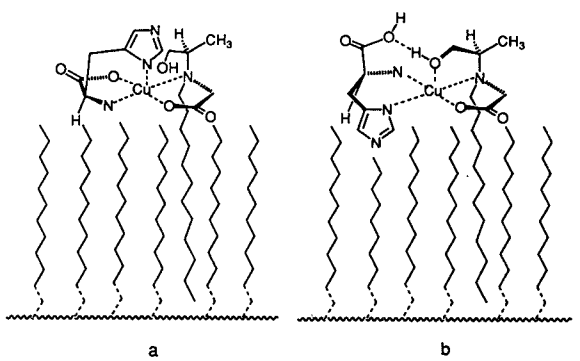

Fig. 5. The proposed structures of the ternary complex formed from the fixed ligand of CSP **7**, L-histidine and Cu(II). See text.

The variation of the Cu(II) concentration in the mobile phase of constant composition [methanol–water (20:80, v/v)] was found to affect the resolution trends for resolving the two enantiomers of α-amino acids on CSP **7** as shown in Table 2. The resolution data summarized in Table 2 indicates that the retention of the two enantiomers decreases appreciably as the Cu(II) concentration increases while the enantioselectivity denoted by the separation factors, α, does not show any noticeable trend. These tendencies are consistent with those on CSP **2** and may be

Table 2
Resolution of α-amino acids on dynamic CSP **7** with varying Cu(II) concentration in methanol–water (20:80, v/v)

Amino acid	0.10 m*M* Cu(II)		0.15 m*M* Cu(II)		0.20 m*M* Cu(II)		0.25 m*M* Cu(II)	
	k' [a]	α [b]	k' [a]	α [b]	k' [a]	α [b]	k' [a]	α [b]
Alanine	2.63 (L) 4.44 (D)	1.69	2.06 (L) 3.52 (D)	1.70	1.84 (L) 3.10 (D)	1.68	1.70 (L) 2.86 (D)	1.69
Valine	5.05 (L) 24.57 (D)	4.86	3.92 (L) 19.61 (D)	5.00	3.57 (L) 17.28 (D)	4.84	3.44 (L) 16.03 (D)	4.66
Leucine			10.08 (L) 39.56 (D)	3.93	8.88 (L) 34.32 (D)	3.86	8.33 (L) 30.89 (D)	3.71
Proline	6.05 (L) 17.43 (D)	2.88	4.79 (L) 14.14 (D)	2.95	4.16 (L) 12.49 (D)	3.00	3.86 (L) 11.41 (D)	2.95
Aspartic acid	1.52 (L) 1.93 (D)	1.27	1.55 (L) 1.98 (D)	1.28	1.42 (L) 1.84 (D)	1.30	1.18 (L) 1.52 (D)	1.28
Glutamic acid	3.31 (L) 6.77 (D)	2.04	3.43 (L) 7.04 (D)	2.05	3.08 (L) 6.39 (D)	2.07	2.47 (L) 5.10 (D)	2.06
Glutamine			1.95 (L) 2.75 (D)	1.41	1.74 (L) 2.44 (D)	1.40	1.67 (L) 2.38 (D)	1.42
Serine	1.85 (L) 2.61 (D)	1.41	1.56 (L) 2.21 (D)	1.42	1.30 (L) 1.84 (D)	1.42	1.20 (L) 1.71 (D)	1.42
Threonine	2.43 (L) 3.23 (D)	1.33	1.97 (L) 2.65 (D)	1.34	1.56 (L) 2.09 (D)	1.34	1.52 (L) 2.02 (D)	1.33
Methionine	9.32 (L) 22.10 (D)	2.37	7.63 (L) 18.14 (D)	2.38	6.28 (L) 14.97 (D)	2.39	5.88 (L) 13.55 (D)	2.32
Arginine	7.70 (L) 9.30 (D)	1.21	4.64 (L) 5.68 (D)	1.22	4.22 (L) 5.20 (D)	1.23	3.78 (L) 4.79 (D)	1.27
Histidine	3.88 (D) 4.94 (L)	1.27	2.78 (D) 3.69 (L)	1.33	2.59 (D) 3.32 (L)	1.28	2.31 (D) 2.96 (L)	1.28

For chromatographic conditions, see Experimental section. For blanks, data could not be collected because of the unreadability (glutamine at 0.10 m*M* $CuSO_4$) of the chromatogram or the long retention times (leucine at 0.10 m*M* $CuSO_4$) of the two enantiomers.

[a] Capacity factors for the first- and second-eluted enantiomers.

[b] Separation factors.

explained by the fact that the increase of the Cu(II) concentration in the mobile phase enhances the formation of the mobile binary complex from Cu(II) and resolving amino acid, and subsequently diminishes the retention of amino acids on the column as described previously in explaining the resolution trends on CSP **2** [14].

Dynamic CSP **12** based on (*R*)-α-phenylethylamine was prepared as shown in Fig. 2. Dynamic CSP **12** does not contain the hydroxy group which is utilized in the axial coordination shown in Figs. 1 and 3. In consequence, it is expected that comparison of the resolution behaviors of racemic α-amino acids on dynamic CSP **12** with those on dynamic CSP **2** or **7** may explore the importance of the hydroxy axial coordination in the chiral recognition.

The resolution of various α-amino acids on dynamic CSP **12** under various conditions is summarized in Table 3. The trends shown in Table 3 in the capacity factors with the variation of the organic modifier content and the Cu(II)

Table 3
Resolution of racemic α-amino acids on dynamic CSP **12** with varying organic modifier content in the aqueous mobile phase and with varying Cu(II) concentration

Amino acid	0.10 m*M* $CuSO_4$, 10% CH_3CN		0.10 m*M* $CuSO_4$, 7% CH_3CN		0.10 m*M* $CuSO_4$, 5% CH_3CN		0.15 m*M* $CuSO_4$, 5% CH_3CN		0.20 m*M* $CuSO_4$, 5% CH_3CN	
	k' [a]	α [b]	k' [a]	α [b]	k' [a]	α [b]	k' [a]	α [b]	k' [a]	α [b]
Alanine					4.27 4.27	1.00	3.16 3.16	1.00	2.25 2.25	1.00
Valine	1.50 1.50	1.00	2.78 (D) 3.20 (L)	1.15	7.12 (D) 7.64 (L)	1.07	4.76 (D) 5.15 (L)	1.08	3.25 (D) 3.64 (L)	1.12
Leucine	2.02 (D) 2.38 (L)	1.18	4.36 (D) 5.14 (L)	1.18	9.37 (D) 10.67 (L)	1.14	6.65 (D) 7.64 (L)	1.28	4.51 (D) 5.73 (L)	1.27
Proline	1.18 1.18	1.00	2.53 (D) 2.91 (L)	1.15	5.65 (D) 6.15 (L)	1.11	4.29 (D) 4.79 (L)	1.12	2.82 (D) 3.21 (L)	1.14
Aspartic acid	0.19 0.19	1.00	0.39 0.39	1.00	1.23 1.23	1.00	1.07 1.07	1.00	0.92 0.92	1.00
Glutamine	1.10 1.10	1.00	2.39 2.39	1.00	4.40 4.40	1.00	3.00 3.00	1.00	2.38 2.38	1.00
Methionine	2.08 2.08	1.00	3.92 (D) 5.47 (L)	1.00	8.05 (D) 8.95 (L)	1.11	5.68 (D) 6.28 (L)	1.11	4.16 (D) 4.64 (L)	1.12
Histidine	1.95 1.95	1.00	3.63 3.63	1.00	8.23 8.23	1.00	5.74 5.74	1.00	3.60 3.60	1.00
PheGly	1.91 (D) 2.33 (L)	1.22	3.95 (D) 4.85 (L)	1.23	8.53 (D) 10.04 (L)	1.18	5.92 (D) 6.99 (L)	1.18	4.23 (D) 5.19 (L)	1.20
Tyrosine	2.15 2.15	1.00	3.94 (D) 4.30 (L)	1.09	9.23 9.23	1.00	6.52 6.52	1.00	5.22 5.22	1.00

For chromatographic conditions, see Experimental section. For blanks, data were not collected.
[a] Capacity factors for the first- and second-eluted enantiomers.
[b] Separation factors.

concentration in the aqueous mobile phase are consistent with those on CSP **2** or CSP **7** and can be rationalized as described above or previously [14]. However, the degree of enantioselectivity denoted by the separation factors, α, on CSP **12** is much worse than that on CSPs **2** or **7**. The elution orders on CSP **12** are totally different from those on CSPs **2** or **7**. These results indicate that the axial coordination by the hydroxy group shown in Figs. 1 and 3 is very important in the chiral recognition.

The chiral recognition model for resolving α-amino acids on CSP **12** is proposed as shown in Fig. 6. To minimize the disturbance of steric hindrance in forming the ternary complex, the least bulky hydrogen at the chiral center of the fixed ligand is assumed to be positioned above the metal ion in Fig. 6. In this instance, the phenyl and methyl groups at the chiral center of the fixed ligand are placed as shown in Fig. 6a or b. The complex shown in Fig. 6a is quite similar to that shown in Figs. 1 and 3 except the absence of the hydroxy axial coordination and the D-enantiomers are selectively retained because of the lipophilic interaction between the side α-alkyl chains of D-enantiomers and the octadecyl chains of silica gel as noted in Figs. 1 and 3. In Fig. 6a, however, the most bulky phenyl group is eclipsed with the N-carboxymethyl unit of the fixed ligand and some steric hindrance is expected. To lessen the steric hindrance between the phenyl group and the N-carboxymethyl unit of the fixed ligand during the formation of the ternary complex, the bonding direction of the N-carboxymethyl unit of the fixed ligand is reversed as shown in Fig. 6b and, in consequence, the phenyl group is positioned out of the N-carboxymethyl sphere of the fixed ligand. On this occasion, the L-enantiomers are selectively retained because of the lipophilic interaction between the side α-alkyl chains of L-enantiomers and the octadecyl chains of silica gel. Based on the structure of the two complexes shown in Fig. 6, it is concluded that the complex which selectively retains the L-enantiomers is more stable than that which selectively retains the D-enantiomers. Consequently, the L-enantiomers are retained longer on dynamic CSP **12** than the D-enantiomers. However, the stability difference between the two complexes shown in Fig. 5 is presumed to be quite small based on the degree of enantioselectivity shown in Table 3.

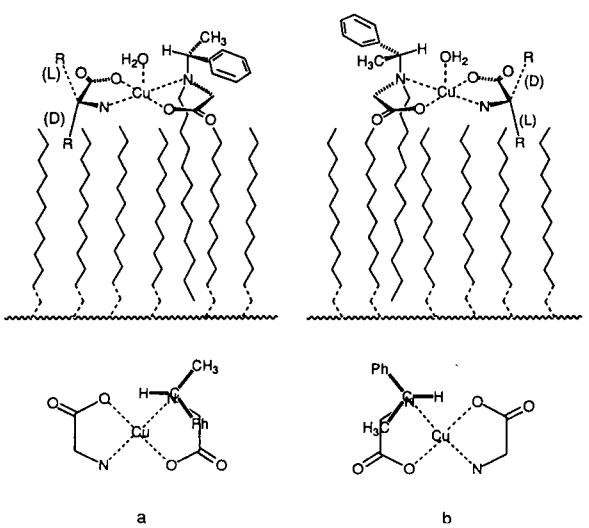

Fig. 6. Top: the proposed structures of the ternary complex formed from the fixed ligand of CSP **12**, D- or L-amino acid and Cu(II). Bottom: schematic representation of the top ternary complexes viewed from above. See text.

In summary, in the present study, we prepared dynamic CSP **7** from (*R*)-2-amino-1-propanol and dynamic CSP **12** from (*R*)-α-phenylethylamine and resolved the two enantiomers of various α-amino acids on the two new CSPs. CSP **7** does not contain any phenyl functionality which is present at the first chiral center of CSP **2** and CSP **12** does not contain any hydroxy functional group which occupies the axial coordination site in the ternary complex formed from CSP **2** or **7**. Based on the trends for resolving α-amino acids on CSP **7** and the comparison of these trends with those on CSP **2**, we concluded that the phenyl functionality at the first chiral center of CSP **2** is not essential in the chiral recognition and simply disturbs the axial coordination of the hydroxy group of the fixed ligand in the square planar coordination sphere of the ternary complex. In consequence, CSP **7** with its lack of the phenyl functionality forms a more stable and tighter complex and, as a result, shows higher enantioselectivity for the two en-

antiomers of α-amino acids having a simple hydrophobic α-alkyl substituent than CSP **2** and different elution orders from CSP **2** in resolving α-amino acids having a hydrophilic α-alkyl substituent. On the other hand, the enantioselectivity for the two enantiomers of α-amino acids on CSP **12** was much worse than that on CSPs **2** or **7** and the elution orders were totally different from those on CSPs **2** or **7**. From these results, the hydroxy group of CSPs **2** and **7** is concluded to play a very important role in the chiral recognition.

Acknowledgement

This work was supported by the grants from the Organic Chemistry Research Center sponsored by the Korea Science and Engineering Foundation and from the Basic Science Research Program, Ministry of Education, Korea (BSRI-94-3410).

References

[1] V.A. Davankov, J.D. Navratil and H.F. Walton, *Ligand Exchange Chromatography*, CRC Press, Boca Raton, FL, 1988.

[2] S. Lam, in W.J. Lough (Editor), *Chiral Liquid Chromatography*, Blackie, Glasgow, London, 1989, Ch. 5, p. 83.

[3] V.A. Davankov, A.A. Kurganov and A.S. Bochkov, *Adv. Chromatogr.*, 22 (1983) 71.

[4] P.E. Hare and E. Gil-Av, *Science*, 204 (1979) 1226.

[5] E. Gil-Av, A. Tishbee and P.E. Hare, *J. Am. Chem. Soc.*, 102 (1980) 5115.

[6] V.A. Davankov and Yu A. Zolotarev, *J. Chromatogr.*, 155 (1978) 303.

[7] G. Gubitz, F. Juffmann and W. Jellenz, *Chromatographia*, 16 (1982) 103.

[8] V.A. Davankov, A.S. Bochkov, A.A. Kurganov, P. Roumeliotis and K.K. Unger, *Chromatographia*, 13 (1980) 677.

[9] V.A. Davankov, A.S. Bochkov and Yu.P. Belov, *J. Chromatogr.*, 218 (1981) 547.

[10] H. Kiniwa, Y. Baba, T. Ishida and H. Katoh, *J. Chromatogr.*, 461 (1989) 397.

[11] V.A. Davankov, in A.M. Krstulovic (Editor), *Chiral Separations by HPLC : Applications to Pharmaceutical Compounds*, Ellis Horwood, Chichester, 1989, Ch. 15, p. 446.

[12] Y. Yuki, K. Saigo, H. Kimoto, K. Tachibana and M. Hasegawa, *J. Chromatogr.*, 400 (1987) 65.

[13] M.H. Hyun, N.-E. Lim and S.-N. Choi, *Bull. Kor. Chem. Soc.*, 12 (1991) 594.

[14] M.H. Hyun, J.-J. Ryoo and N.-E. Lim, *J. Liq. Chromatogr.*, 16 (1993) 3249.

[15] M.J.M. Wells and C.R. Clark, *Anal. Chem.*, 53 (1981) 1341.

[16] A. Streitwieser, C.H. Heathcock and E.M. Kosower, *Introduction to Organic Chemistry*, Macmillan, New York, 4th ed., 1992, p. 1102.

ELSEVIER

Journal of Chromatography A, 684 (1994) 201–211

JOURNAL OF CHROMATOGRAPHY A

High-performance anion exchange of small anions with polyethyleneimine-coated porous zirconia

Clayton McNeff, Qianhua Zhao, Peter W. Carr*

Department of Chemistry, University of Minnesota, 207 Pleasant Street S.E., Minneapolis, MN 55455, USA

First received 18 April 1994; revised manuscript received 12 July 1994

Abstract

The preparation and chromatographic characterization of an ion-exchange high-performance liquid chromatographic support by deposition and crosslinking of polyethyleneimine (PEI) on the surface of porous zirconia is described. Adsorption and evaporation methods were used for coating PEI onto the zirconia particles. These two stationary phases were compared by elemental analysis, ion-exchange capacity and by chromatography. High efficiency and good selectivity were observed for inorganic and organic anions. The addition of a strong, hard Lewis base to the mobile phase dramatically improved the peak shape and efficiency of *para* benzoic acid derivatives. PEI-coated zirconia showed a distinct elution sequence for organic anions when compared to *bare* zirconia or silica-based phases. The polyamine coated zirconia was stable over a pH range from 2.75 to 9. Flow studies, using nitrite as a probe solute, showed that both coating procedures produced packed columns with good mass-transfer properties.

1. Introduction

Ion-exchange chromatography is a powerful technique for the separation of both inorganic and organic charged molecules [1–4]. Zirconium oxide (ZrO_2, zirconia) has been shown to be a useful alternative to silica as a stationary phase in reversed-phase high-performance liquid chromatography [5–7], as an adsorbent [8] and for ligand-exchange chromatography of carboxylates [9,10]. The shortcomings of silica and derivatized bonded phases in aqueous mobile phases have been well documented [11–14]. Most significantly, silica is soluble in aqueous alkali and siloxane bonds are unstable in acidic media. In general, it lacks tolerance to harsh chemical or thermal treatment. Above pH 8 the Si–O–Si bonds in silica hydrolyze resulting in dissolution of the phase. Zirconia exhibits good mechanical and thermal stability, and is chemically stable over the entire pH range [5,15]. Zirconia can be coated with various polymers to modify its surface interactions with solutes. Zirconia coated with polybutadiene (PBD 7) produces a stationary phase that is useful in reversed-phase separations. Polyethyleneimine (PEI) modified silica is widely used as anion exchanger [16–18]. Polymer-based stationary phases are generally stable to a wide range of mobile phase pHs. PEI-coated polystyrene–divinylbenzene (PS–DVB) supports are reported to withstand pHs in the range of 4–12 [19]. However, polymer supports are not fully mechanically stable due to swelling or shrinking in organic solvents and at extreme pHs

* Corresponding author.

0021-9673/94/$07.00
SSDI 0021-9673(94)00651-2

and ionic strength [20]. We report here the synthesis of PEI-coated zirconia supports that are useful as stationary phases in high-performance anion-exchange chromatography (HPAEC). Two coating methods, namely adsorption and evaporation, were used to deposit PEI onto zirconia particles.

2. Experimental

All chemicals were reagent grade or better. Polyethyleneimine (PEI), average molecular mass 1800, was obtained from Polysciences (Warrington, PA, USA). 50% sodium hydroxide solution, 3,5 dinitrobenzoic acid, sodium acetate, and HPLC-grade isopropanol were obtained from Fisher Scientific (Fairlawn, NJ, USA). Aniline, *p*-nitrotoluene, *p*-cyanobenzoic acid, *p*-iodobenzoic acid, *p*-hydroxybenzoic acid, and *p*-ethylbenzoic acid, were obtained from Aldrich (Milwaukee, WI, USA). *p*-Toluenesulfonic acid, *p*-aminobenzoic acid, and *p*-nitrobenzoic acid were obtained from Eastman (Rochester, NY, USA). Sodium bromate and concentrated phosphoric acid were purchased from J.T. Baker (Phillipsburg, NJ, USA). Sodium nitrite, benzoic acid, sodium nitrate, potassium iodide, potassium phosphate dibasic, and sodium fluoride were from Mallinckrodt (St. Louis, MO, USA). Piperazine-N, N'-bis-[2-ethanesulfonic acid] (Pipes) and tris(hydroxymethyl)aminomethane (Tris) buffers were obtained from Sigma (St. Louis, MO, USA).

All chromatograms were collected on a Hewlett-Packard 1090 (Palo Alto, CA, USA) chromatograph with a photodiode-array detector (PDA), and a Hewlett-Packard ChemStation for data collection. PEI-coated particles were packed into 5 cm × 4.6 mm I.D. stainless steel columns by the stirred upward slurry method at 5000 p.s.i. (1 p.s.i. = 6894.76 Pa) in HPLC-grade isopropanol. Water was obtained from a Barnstead Nano-Pure system, with an Organic-Free final cartridge, and boiled to remove dissolved carbon dioxide. All buffer solutions were filtered using Millipore (type HA) 0.45-μm membrane filters prior to use.

The dead volume marker used for all experiments was the negative peak obtained upon injection of pure water. The dead volume was checked for each new mobile phase used and was found to deviate less that 3% over the course of the work.

2.1. Zirconia substrate particles

Porous zirconia particles (batch Coac-15) produced by the polymerization induced colloid aggregation [21,22] method were used as the substrate material for this work. The particles have an average diameter of 6 μm, a surface area of 29 m^2/g and an average pore size of 220 Å, as analyzed by BET nitrogen adsorption. An energetically more homogeneous surface was obtained by washing in acid and base: 85 grams of zirconia were suspended in 300 ml of 0.5 *M* HCl and sonicated under vacuum for 5 min. The slurry was further sonicated for 45 min and then allowed to stand for four h with occasional mixing. The particles were allowed to settle, and the liquid was decanted. The particles were collected on a sintered glass funnel and rinsed with 500 ml of water until neutral. This procedure was repeated using 0.5 *M* NaOH and then the particles were dried at 150°C overnight.

2.2. The coating of zirconia with PEI by adsorption

Adsorptive coating was carried out by a modification of the procedure developed by Kennedy et al. [23]. A 6-g amount of dry zirconia was placed in 30 ml of 2% (w/v) polyethyleneimine (PEI) in methanol. The mixture was then sonicated under vacuum for 1 h and swirled many times. It was then allowed to sit at room temperature for 3 h. The product was isolated on a sintered glass funnel and dried under vacuum for 30 min. The PEI was then crosslinked with 30 ml of 5% (v/v) 1,4 butanedioldiglycidylether (BUDGE) in methanol and allowed to react overnight. At the end of this period, 2 ml of triethylamine was added, and the mixture was refluxed at 70°C for 30 min. The coated and crosslinked particles were collected, washed with

100 ml of triethylamine and 300 ml of methanol, and stored in a vacuum desiccator.

2.3. The coating of zirconia with PEI by evaporation

The evaporation coating method differed from the adsorption method in that after the particles were coated with PEI, the methanol was slowly removed (over 2 h) with a rotary evaporator, using a baffled flask, at 60°C while periodically pulling a vacuum. The particles were recovered and washed as above.

2.4. Physical characterization procedures

The two PEI-coated zirconia phases were characterized by elemental analysis (C, H and N), and ion-exchange capacity. The elemental composition of the coatings was determined by M–H–W laboratories (Phoenix, AZ, USA). The anion-exchange capacity was determined by a small molecule binding assay [16]. 0.1 grams of PEI-coated zirconia were sonicated in 4 ml of methylene chloride and then centrifuged. The supernatant was decanted and replaced by 4 ml of 200 m*M* picric acid. After mixing, centrifugation, and decanting, unbound picric acid was washed out with four 4-ml portions of methylene chloride. Bound picric acid was released using a 5% (v/v) solution of triethylamine in methylene chloride with repeated washings and centrifugation until the supernatant was colorless. Each washing with triethylamine was collected in a single volumetric flask. These combined washings were brought to volume with methylene chloride and assayed spectrophotometrically; the extinction coefficient of triethylamine picrate is 14 500 at 358 nm. Each sample was analyzed in duplicate and the average taken. Duplicate analyses differed by less than 5%.

3. Results and discussion

3.1. Stationary phase characterization

The two stationary phases were characterized by elemental analysis and by picric acid assay. The picric acid assay is sensitive to non-ionized primary, secondary and tertiary amines. The results of the chemical characterization are given in Table 1. As expected, the loading of PEI on the zirconia surface was higher when deposited by evaporation. The elemental analysis showed consistently higher results than the picric acid assay. The picric acid assay results are within the range of Regnier et al.'s work with polyethyleneimine (average molecular mass of 600) on silica [23]. They reported from 2.1–26 μmol/m^2 of nitrogen for eight different silicas, three aluminas, and one titania substrates. PEI-coated zirconia showed 7.2 and 10.8 μmol/m^2 of nitrogen for the adsorptive and evaporative coatings respectively. Since the theoretical molar ratio of carbon to nitrogen (C/N) for PEI is 2.0, values

Table 1
Composition of stationary phases

Phase	Elemental analysis			Picric acid assay, nitrogen[a]	PEI[d]	C/N ratio[e]
	Carbon[a]	Hydrogen[a]	Nitrogen[a]			
Adsorption[b]	50.3	113	11.0	7.2	0.23	4.52
Evaporation[c]	67.0	427	18.3	10.8	0.44	4.48

[a] All results are in μmoles/m^2 of zirconia surface.
[b] Prepared by the adsorption method as described in text.
[c] Prepared by the evaporation method as described in text.
[d] Micromoles of PEI per square meter on the zirconia surface by elemental analysis, assuming 42 nitrogen per PEI molecule.
[e] Carbon to nitrogen mole ratio by elemental analysis.

greater than 2.0 provide information about the amount of crosslinking. The results of the carbon to nitrogen ratio indicated that both methods produced phases with similar extents of crosslinking. BUDGE has an elemental formula of $C_{10}H_{18}O_4$. If we assume that PEI has a formula $(C_2H_5N)_n$ and both ends of BUDGE are linked with PEI, then ca. 50% of the amine groups on the surface of both phases are crosslinked.

3.2. Chromatographic characterization

The two stationary phases showed high efficiency for the chromatography of small anions. An example separation of nitrite and nitrate (reduced plate height of 2.8 for each solute) on the adsorptively coated column is shown in Fig. 1. The separation of a mixture of organic acids on the same column is shown in Fig. 2. Results for the chromatography of a number of small anions on both columns and a measure of the reduced plate height, are given in Table 2. The evaporatively coated phase showed more retention towards anions than the adsorptively coated phase, but generally had lower efficiency. The height-over-area method was used to calculate the number of theoretical plates and reduced plate height:

$$N = 2\pi\,(H\,t_R/A)^2 \quad (1)$$

$$h = L/(N\,d_p) \quad (2)$$

where N is the number of theoretical plates, H is the height of the peak, t_R is the retention time, A is the area of the peak, h is the reduced plate height, and d_p is the average diameter of the particles. The height-over-area method typically gives more conservative estimates than the inflection-point or half-width methods, especially for skewed peaks [24].

The elution order of solutes contained in Table 2 was as expected. Aniline, which is cationic at pH 7.0, eluted before any of the other solutes. 4-Nitrotoluene, which has no net charge, eluted slightly after aniline but before any of the anionic solutes. The fact that both aniline and 4-nitrotoluene were retained at all indicates there must be some hydrophobic interaction of the solutes with the stationary phase. The inorganic anions listed in Table 2 eluted in the same order (bromate < nitrite < nitrate < iodide) as on a typical silica-based anion exchanger [25]. However, nitrite, nitrate and iodide exhibited a distinctly different elution order on *bare* zirconia [9]. This suggests that the PEI coating at least partially blocks interactions with the bare zirconia substrate. Both benzoic acid and 3,5-dinitrobenzoic acid showed poor efficiency compared to the inorganic anions.

The capacity factors of anions on both the adsorptively and evaporatively coated columns followed the loading of stationary phase on the substrate zirconia. The increase in capacity factor was more accurately predicted by the elemental analysis results than the anion-exchange capacity. The picric acid assay showed that the evaporatively coated particles had 49% more PEI, while elemental analysis indicated a 66% higher loading. The average increase in capacity factor for the anionic solutes listed in Table 2 was 82% with a standard deviation of 5%. If we assume that both columns are identical except for the phase ratio then the capacity factor on the evaporatively coated column (k'_e) and the adsorptively coated column (k'_a) should be related as:

$$k'_e = (\phi_e/\phi_a)\,k'_a \quad (3)$$

where ϕ is the phase ratio. As shown in Fig. 3, Eq. 3 is followed very nicely for the anionic solutes. Least-squares analysis of the anionic solutes gives $n = 6$, $(\phi_e/\phi_a) = 1.72$, S.D. $= 0.17$, and intercept $= 0.16 \pm 0.25$. We note that the intercept is statistically zero as predicted by Eq. 3, and the slope is in fairly good agreement with elemental analysis (72% versus 66%, respectively). We also note that the cationic solute, aniline, is less retained on the more heavily loaded evaporatively coated column. Donan exclusion from the more positively charged surface is stronger on the more heavily coated particles resulting in a lower capacity factor for the cationic solute.

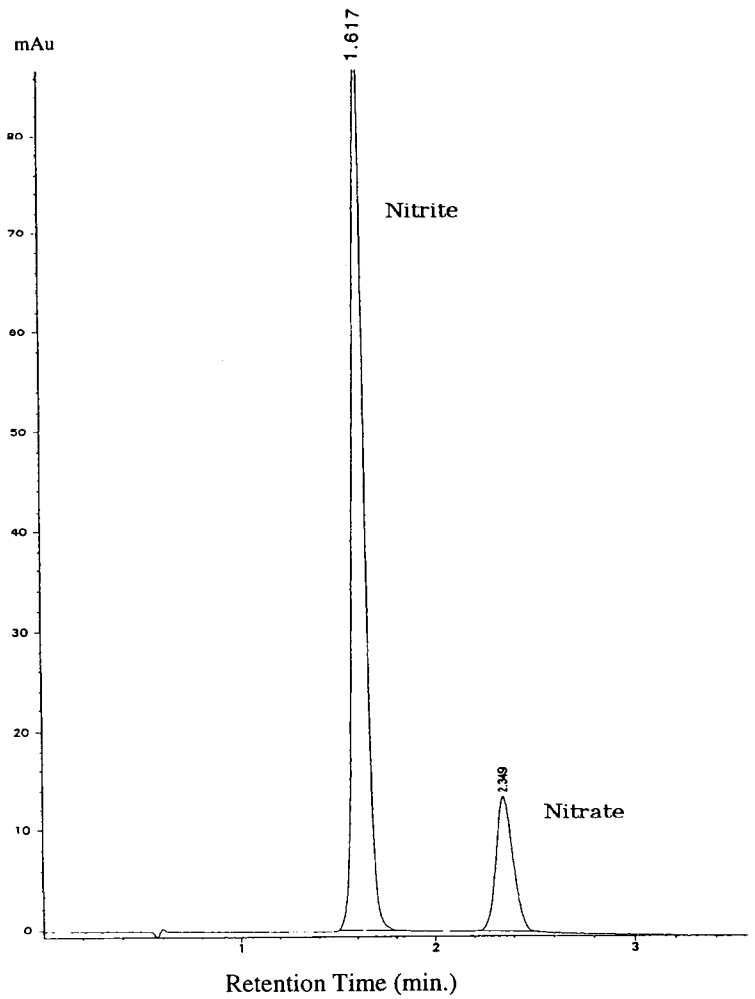

Fig. 1. The separation of nitrite and nitrate on adsorptively coated PEI-zirconia. Column, 5 cm × 0.46 cm I.D.; mobile phase, 500 m*M* sodium acetate at pH 7.0; flow rate, 1.0 ml/min; column temperature, 35°C; injection volume, 5 μl; solute concentration, 10 m*M*; detection at 240 nm.

3.3. The effect of adding fluoride to the mobile phase

The surface chemistry of zirconia is very complex [22]. It has been demonstrated that zirconia interacts strongly with hard Lewis bases [25,26]. Without additives in the mobile phase, strong hard Lewis bases, like benzoates, elute with poor peak shapes. This is primarily due to interactions between the carboxylate group (Lewis base) and bare zirconia (Lewis acid), leading to a mixed mode retention [27]. The addition of fluoride, a very strong, hard Lewis Base, to the mobile phase helps control Lewis acid–base interactions of solutes and peak shape often improves dramatically (see Table 3). To investigate Lewis acid–base interactions with the bare zirconia surface in the PEI-coated zirconia,

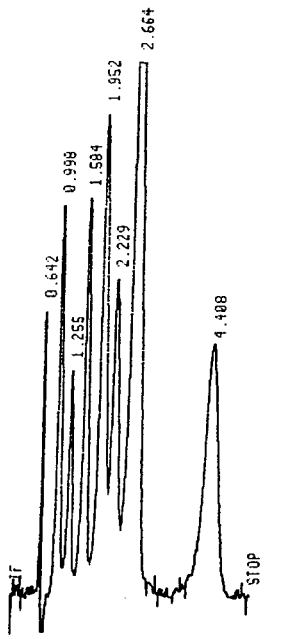

Fig. 2. The separation of organic acids on evaporatively coated PEI-zirconia. Column, 5 cm × 0.46 cm I.D.; mobile phase, 100 m*M* sodium acetate at pH 7.0; flow rate, 1.0 ml/min; column temperature, 35°C; injection volume, 5 μl; solute concentration, 10 m*M*; detection at 240 nm. Solutes and their retention times in minutes: Phenylphosphonic acid (0.998), benzoic acid (1.255), *p*-nitrobenzoic acid (1.584), diphenylphosphate (1.952), *p*-chlorobenzoic acid (2.229), *p*-hydroxybenzoic acid (2.664), *p*-iodobenzoic acid (4.408), dead-volume peak (0.642).

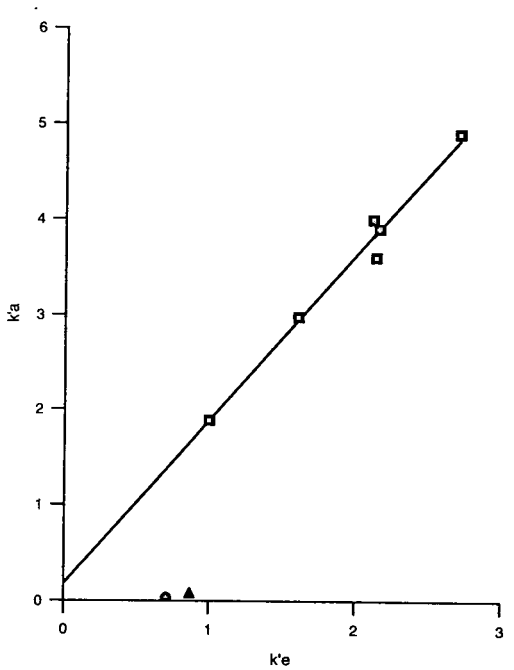

Fig. 3. Plot of capacity factors for the evaporatively and adsorptively coated columns for solutes contained in Table 2. □ = Anions, ○ = cation, ▲ = neutral.

six different *p*-benzoic acid derivatives were examined with and without fluoride in the mobile phase. The addition of fluoride to the mobile phase produced a dramatic improvement in the

Table 2
Comparison of adsorptively and evaporatively coated columns

Solute	$k'_{adsorption}$	$k'_{evaporation}$	Reduced plate height ($h_{ads.}$)	Ratio $h_{ads.}/h_{evap.}$
Aniline	0.70	0.03	3.9	0.6
4-Nitrotoluene	0.87	0.98	4.3	0.5
Potassium bromate	1.00	1.89	3.8	0.8
Sodium nitrite	1.61	2.97	2.8	0.8
3,5-Dinitrobenzoic acid	2.12	3.99	7.9	0.8
Benzoic acid	2.15	3.59	10.4	1.1
p-Toluenesulfonic acid	2.17	3.90	4.4	0.6
Sodium nitrate	2.72	4.90	2.8	0.9
Potassium iodide	5.26	–	3.8	–

Mobile phase for both columns, 0.5 *M* sodium acetate at pH 7.0; column temperature, 35°C; flow rate, 1.0 ml/min; solutes concentration 10 m*M*; injections, 5 ml; detection, 240 nm.

Table 3
Effect of fluoride in the mobile phase

Solute	k'		Reduced plate height [b]	Ratio h^{b}/h^{a}
	Fluoride [a]	No fluoride [b]		
p-Cyanobenzoic acid	2.12	3.52	27.7	4.1
p-Aminobenzoic acid	2.75	13.6	83.3	11.6
p-Nitrobenzoic acid	2.87	5.74	23.8	4.0
p-Ethylbenzoic acid	3.39	6.59	55.6	6.7
p-Hydroxybenzoic acid	6.52	15.2	83.3	11.6
p-Iodobenzoic acid	10.8	19.2	36.2	4.4

[a] Mobile phase, 0.5 *M* sodium acetate, 100 m*M* sodium fluoride at pH 7.0; column temperature, 35°C; flow rate, 1.0 ml/min; solute concentration, 10 m*M*; injections, 5 μl; detection, 240 nm.
[b] Same as footnote a, but no fluoride in the mobile phase.

peak shape and efficiency for all solutes. Fluoride addition also had an effect on the selectivity towards *p*-aminobenzoic acid. The capacity factor changed from 13.6 with no fluoride in the mobile phase to 2.75 with fluoride. A chromatogram of *p*-hydroxybenzoic acid with and without fluoride in the mobile phase is shown in Figs. 4 and 5. A comparison of the two chromatograms shows an 11-fold improvement in efficiency and no peak tailing when fluoride was present in the mobile phase.

3.4. A comparison of a strong silica-based, bare zirconia, and PEI-coated zirconia ion exchangers

The differences in retention under similar mobile phase conditions between PEI-zirconia, silica-based and *bare* zirconia ion exchangers is shown in Table 4. There was very little retention and no discernible dependence of retention on pK_a for the silica-based system. The para benzoic acids were strongly retained on *bare* zirconia

Table 4
Comparison of silica-based, *bare* zirconia and PEI-coated zirconia anion exchangers

Para benzoic acid	pK_a	Capacity factor (k')		
		Spherisorb 5 SAX [a]	Bare zirconia [b]	PEI-coated zirconia [c]
Nitro	3.44	0.2	4.6	5.7
Cyano	3.55	0.2	4.3	3.5
Iodo	4.00	0.3	13.7	19.2
Ethyl	4.35	0.4	18.1	6.6
Hydroxy	4.58	0.2	24.7	15.2
Amino	4.85	0.3	50.5	13.6

Para benzoic acid derivatives on silica-based, *bare* zirconia, and PEI-coated zirconia columns. column temperature, 35°C; flow rate, 1.0 ml/min; solute concentration, 10 m*M*; injections, 5 μl; detection, 254 nm.
[a] Mobile phase, 100 m*M* Pipes at pH 6.8 [9].
[b] Mobile phase, same as footnote a [9].
[c] Mobile phase, 100 m*M* Pipes at pH 7.0;

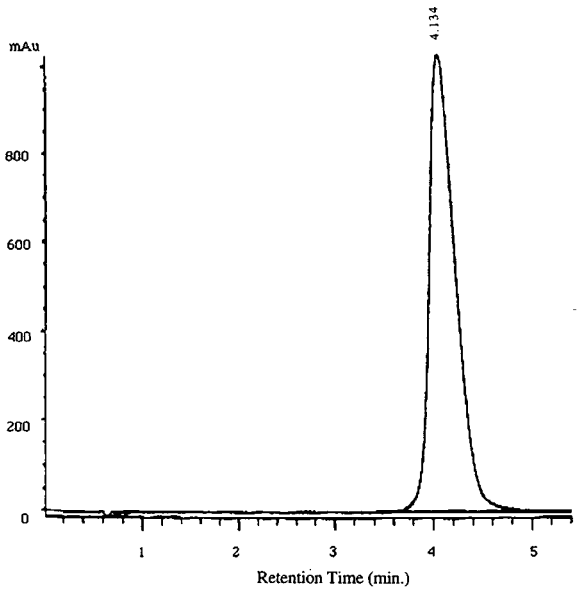

Fig. 4. The elution of *p*-hydroxybenzoic acids on adsorptively coated PEI-zirconia. Column, 5 cm × 0.46 cm I.D.; mobile phases, 100 m*M* Pipes buffer at pH 7.0 containing 100 m*M* sodium fluoride; flow rate, 1.0 ml/min; column temperature, 35°C; injection volume, 5 μl; solute concentration, 10 m*M*; detection at 254 nm.

with capacity factors ranging from 4 to 50. The elution order for the *bare* zirconia column showed a strong correlation between pK_a and capacity factor. This is primarily due to the strength of the Lewis acid–base interactions between the carboxylate groups and the zirconia surface. In general, the higher the pK_a value the stronger the Lewis acid–base interaction and the greater the capacity factor. The PEI-coated zirconia also showed a wide range in capacity factors for the *para* benzoic acids, but there was no apparent correlation with pK_a. The PEI-coated zirconia exhibited an elution order for *para* benzoic acids different from either the silica-based or *bare* zirconia columns.

3.5. Flow study of PEI-zirconia columns

A flow study was done to evaluate the coefficients of the Knox–Bristow [28] equation:

$$h = A\nu^{0.33} + B/\nu + C\nu \quad (4)$$

where h is the reduced plate height, ν is the reduced velocity and A, B, and C are the fitting

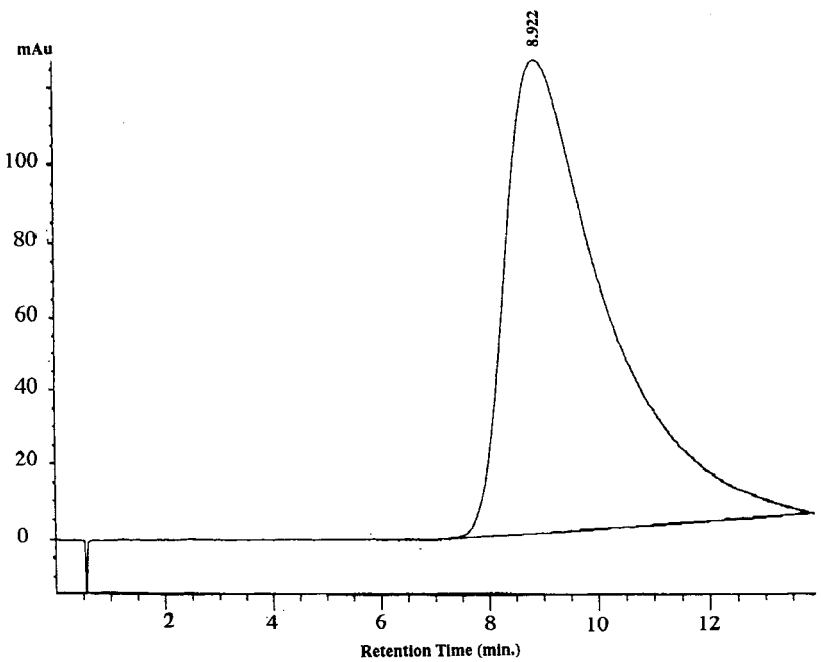

Fig. 5. The elution of *p*-hydroxybenzoic acids on adsorptively coated PEI-zirconia. All conditions as in Fig. 4, except for absence of 100 m*M* fluoride.

coefficients. Typical coefficient values for a good column are $A < 1$, $B \approx 2$ and $C < 0.2$. A diffusion coefficient (D_m) of 2×10^{-5} cm^2/s [29] was used for the calculation of reduced velocity. This coefficient was estimated by analogy to the observed diffusion coefficient of potassium nitrate at room temperature. This value gave a reasonable estimate of the B coefficient, which is related to longitudinal diffusion within the column, and should have a value of about 2 [30]. Nitrite was used as the probe solute for the study and the results, along with the fit line, are shown in Figs. 6 and 7. The coefficients were evaluated using multi-variate regression and are given in Table 5. Coefficient A is related to the column packing, and C is related to the mass transfer within the column [24]. The results indicate that both columns exhibit good mass-transfer characteristics.

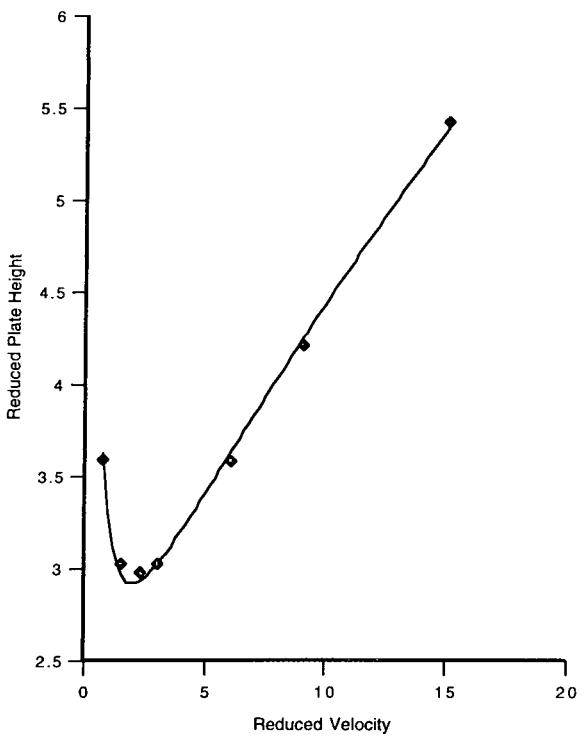

Fig. 6. Flow study on adsorptively coated PEI-zirconia. Column, 5 cm × 0.46 cm I.D.; mobile phase, 100 mM sodium acetate at pH 7.0; flow rate, 1.0 ml/min; column temperature, 35°C; injection volume, 5 μl; solute concentration, 10 mM; detection at 240 nm. ◆ = Nitrite probe solute.

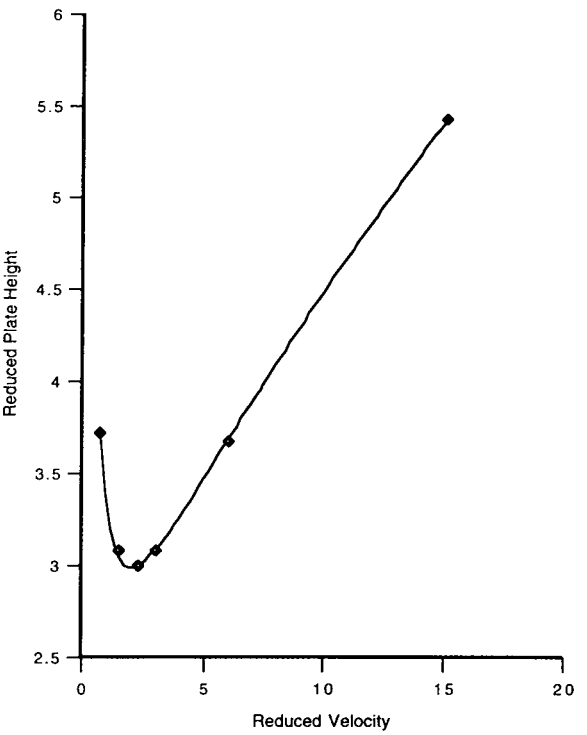

Fig. 7. Flow study on evaporatively coated PEI-zirconia. All conditions as in Fig. 6.

3.6. Acid and base stability

The acid and base stability of the PEI-coated zirconia was tested for each column. Stability studies did not use pHs above 9 as PEI becomes deprotonated, resulting in a loss of retention of anions. Future work using quaternized PEI coating will investigate the stability over a wider range of pHs. The evaporatively coated column was tested at pH 2.75 and pH 9.00 using potassium iodide as the probe solute with a phosphate buffer mobile phase. At each pH the ionic strength was kept constant at 0.20. The evaporatively coated phase proved to be stable under both acidic and basic conditions. The results are shown in Fig. 8. The iodide anion is very polarizable and is well retained at pH 2.75 with a k' around 7, while at pH 9.00 the k' dropped to slightly above 2. This large decrease in retention at pH 9.00 suggests that the PEI is becoming deprotonated. A chromatogram of iodide at pH

Table 5
Knox–Bristow coefficients

Column	A	B	C
Adsorptive	1.5 ± 0.05	1.6 ± 0.06	0.10 ± 0.01
Evaporative	1.5 ± 0.02	1.7 ± 0.02	0.10 ± 0.004

Mobile phase, 100 m*M* Pipes buffer, 100 m*M* NaF at pH 7.0; column temperature, 35°C; flow rate, 1.0 ml/min; solute concentration, 10 m*M*; injections, 5 μl; detection, 254 nm.

9.00 using the evaporatively coated column is shown in Fig. 9. The adsorptively coated column was initially tested at pH 5 using nitrite as a probe and then exposed to phosphate buffer mobile phases in the pH range of 3 to 9 in 1 pH increments. 500 ml of each pH was run through

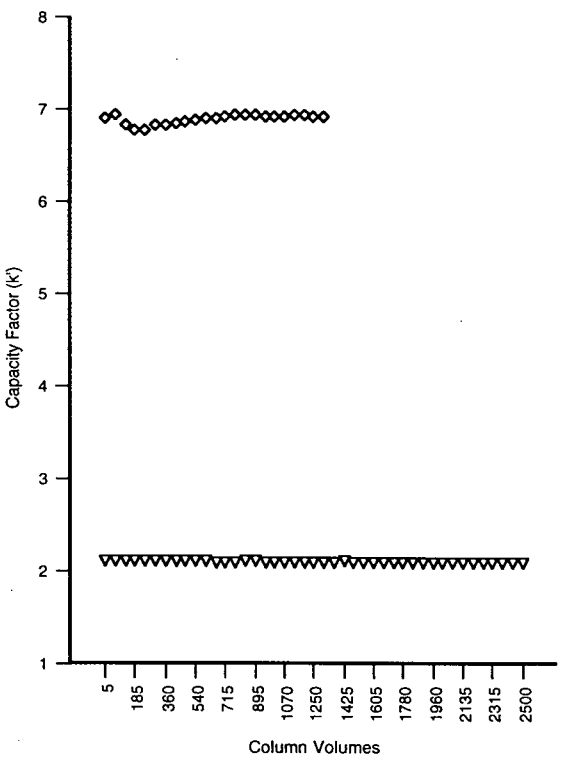

Fig. 8. Acid and base stability study on evaporatively coated PEI-zirconia. Column, 5 cm × 0.46 cm I.D.; mobile phases, 200 m*M* potassium phosphate dibasic at pH 2.75 (▽), 67 m*M* potassium phosphate dibasic at pH 9.0 (◇); flow rate, 1.0 ml/min; column temperature, 35°C; injection volume, 5 μl; solute concentration, 10 m*M*; detection at 240 nm.

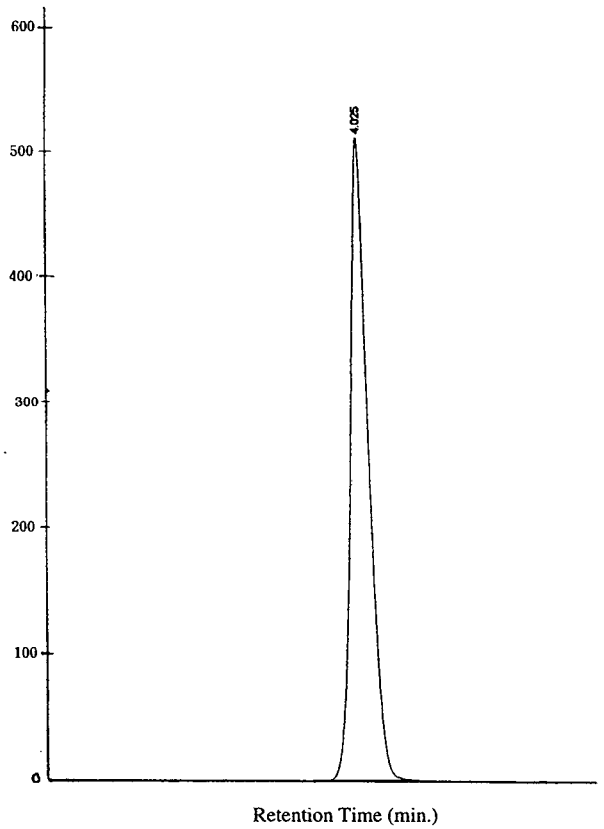

Fig. 9. The elution of potassium iodide on the evaporatively coated PEI-zirconia. Column, 5 cm × 0.46 cm I.D.; mobile phases, 10 m*M* Tris buffer, 500 m*M* sodium acetate at pH 9.0; flow rate, 1.0 ml/min; column temperature, 35°C; injection volume, 5 μl; solute concentration, 10 m*M*; detection at 240 nm.

the column for a total of 3.5 l. Nitrite was then tested again at pH 5 with a less than 1% change in the capacity factor.

4. Conclusions

Zirconia may be coated with polyethyleneimine by both adsorptive or evaporative methods to produce efficient anion-exchange stationary phases for use in high-performance liquid chromatography. The evaporative coating method allows for higher loading of PEI onto the zirconia surface. Both columns were efficient in

the separation of small inorganic and organic anions. Due to the Lewis acid–base chemistry of zirconia, the addition of fluoride to the mobile phase produced as much as an 11-fold increase in chromatographic efficiency for benzoic acid derivatives. PEI-coated zirconia showed a distinct elution order of *para* benzoic acids from *bare* zirconia or silica-based columns. Inorganic anions such as nitrite, nitrate and iodide had the same elution order as on a silica-based anion exchanger, but was opposite to that of *bare* zirconia. A flow study to evaluate the coefficients of the Knox–Bristow equation showed that both PEI-zirconia columns had good mass-transfer characteristics. Both columns were chemically stable from pH 2.75 to 9.

Acknowledgments

We would like to thank SarTec Corporation (Anoka, MN, USA.), the National Science Foundation (NSF), and the National Institutes of Health (NIH) for their support of this work.

References

[1] F.E. Regnier, *Methods Enzymol.*, 104 (1984) 170–189.
[2] H. Small, *J. Chromatogr.*, 546 (1991) 3–15.
[3] H.F. Walton, *Anal Chem.*, 52 (1980) 15R–27R.
[4] R. Wood, L. Cummings and T. Jupille, *J. Chromatogr. Sci.*, 18 (1980) 551–558.
[5] M.P. Rigney, T.P. Weber and P.W. Carr, *J. Chromatogr.*, 484 (1989) 273–91.
[6] W.A. Schafer and P.W. Carr, *J. Chromatogr.*, 587 (1991) 149–160.
[7] L. Sun and P.W. Carr, *Anal. Chem.*, (1994) submitted for publication.
[8] J.A. Blackwell and P.W. Carr, *J. Chromatogr.*, 549 (1991) 43–57.
[9] J.A. Blackwell, *Ph.D. Thesis*, University of Minnesota, Minneapolis, MN, 1991.
[10] J.A. Blackwell and P.W. Carr, *J. Chromatogr.*, 549 (1991) 59–75.
[11] K.K. Unger, *J. Chromatogr.*, 16 (1979).
[12] A. Wehrli, J.C. Hildenbrand, H.P. Keller, R. Stampeli and R.W. Frei, *J. Chromatogr.*, 149 (1978) 199.
[13] Cs. Horváth, W. Melander and I. Molnar, *Anal. Chem.*, 49 (1967) 142.
[14] G. Schomburg, J. Kohler, U. BienVogelsang, H. Czisch, A. Deege, G. Heinemann and P. Kolla, *LC·GC*, 6 No. 1 (19XX) 36–44.
[15] T.P. Weber, E.F. Funkenbusch and P.W. Carr, *J. Chromatogr.*, 519 (1990) 31–52.
[16] L.A. Kennedy, W. Kopaciewicz and F.E. Regnier, *J. Chromatogr.*, 359 (1986) 73–84.
[17] J.D. Pearson and F.E. Regnier, *J. Chromatogr.*, 255 (1983) 137–149.
[18] N. Kitagawa, *LC·GC*, 6 No. 3 (19YY) 260–262..
[19] M.A. Rounds, W.D. Rounds and F.E. Regnier, *J. Chromatogr.*, 397 (1987) 25–38.
[20] R. Arshady, *J. Chromatogr.*, 586 (1991) 199–219.
[21] L. Sun, M.J. Annen, C.F. Lorenzano-Porras, P.W. Carr and A.V. McCormick, *J. Colloid Interface Sci.*, 1994, in press.
[22] J. Nawrocki, M.P. Rigney, A. McCormick and P.W. Carr, *J. Chromatogr.*, 657 (1993) 229–282.
[23] A.J. Alpert and F.E. Regnier, *J. Chromatogr.*, 185 (1979) 375–392.
[24] A. Berthod, *J. Liq. Chromatogr.*, 12(7) (1989) 1169–1185.
[25] J.A. Blackwell and P.W. Carr, *J. Liq. Chromatogr.*, 14(15) (1991) 2875–89.
[26] J.A. Blackwell and P.W. Carr, *J. Chromatogr.*, 549 (1991) 59–75.
[27] G.D. Christian (Editor), *Peptides and Polynucleotides*, VCH Publishers, NY, 1991.
[28] P.A. Bristow and J.H. Knox, *Chromatographia*, 10 No. 6 (1977) 279–298.
[29] H.S. Harned and R.M. Hudson, *J. Am. Chem. Soc.*, 73 (1951) 652.
[30] J.H. Knox, *High Performance Liquid Chromatography*, Edinburgh University Press, 1982.

ELSEVIER

Journal of Chromatography A, 684 (1994) 213–219

JOURNAL OF CHROMATOGRAPHY A

Liquid chromatographic determination of ethylenediaminetetraacetic acid as metal complexes on a porous graphitic carbon column

Olle Stålberg[a], Torbjörn Arvidsson[b,*]

[a]*Analytical Pharmaceutical Chemistry, Uppsala University Biomedical Centre, P.O. Box 574, S-751 23 Uppsala, Sweden*
[b]*Bioanalysis, Pharmaceutical and Analytical R & D, Astra Pain Control AB, S-151 85 Södertälje, Sweden*

First received 17 January 1994; revised manuscript received 4 July 1994

Abstract

A novel liquid chromatographic system for determination of ethylenediaminetetraacetic acid (EDTA), using a complex-forming metal ion [Fe(III)] in the eluent was developed. Optimisation of the system was obtained after a careful choice of complex-forming metal and pH of the eluent. The porous graphitic carbon column permits use of a wide pH range and due to its high hydrophobicity it is possible to determine EDTA without addition of ion-pair reagents to the eluent. The chromatographic behaviour of the Fe(III) complex, the free EDTA and Fe(III) ions were considered and possible pitfalls due to equilibrium disturbances are shown and discussed. Applications to analysis of EDTA in local anaesthetic parental solutions and determination of nitrilotriacetic acid as an impurity in EDTA substance are given.

1. Introduction

Ethylenediaminetetraacetic acid (EDTA) is a strong complex-forming agent widely used as a metal-masking additive in e.g. the pharmaceutical and the food industries. EDTA forms complexes with several metals and is suitable as an additive where metal ions may cause problems like e.g. metal-catalysed degradation and occurrence of coloured metal complexes. In the pharmaceutical industry there is a need for determination of EDTA both as a quality control test on the substance itself and as an assay of EDTA in different formulations.

EDTA has been determined with different techniques, e.g. titrimetric analysis [1,2], gas chromatography [3], UV spectrophotometry [4], flame atomic absorption spectrometry [5], isotachophoresis [6] and electroanalytical methods [7]. During the last decade several ion chromatographic and reversed-phase liquid chromatographic methods were presented [8–21].

In the LC methods the content of EDTA is often determined as metal complexes. In some cases occurrence of "ghost peaks" and peak splitting is reported [9,11,12,19]. The cause of these effects has been briefly discussed, but seems to be due to equilibrium disturbances.

This study is an effort to describe and explain the causes of such disturbances, in order to optimise the chromatographic system. A method was developed using a system involving one

* Corresponding author.

0021-9673/94/$07.00
SSDI 0021-9673(94)00622-9

dominating metal complex. To avoid disturbances the metal ion was added to the eluent.

The method described has been applied to the determination of EDTA and nitrilotriacetic acid (NTA) in pharmaceutical samples.

2. Experimental

2.1. Reagents and chemicals

EDTA and NTA were obtained as disodium salts, Titriplex III and Titriplex I, from E. Merck, Darmstadt, Germany. A Carbocaine adrenaline formulation containing EDTA was obtained from Astra Pain Control, Södertälje, Sweden. All other chemicals were of analytical-reagent quality or better.

2.2. Chromatographic system

The liquid chromatographic system consisted of parts obtained from Spectra-Physics (San José, CA, USA). The pump was a Model 8800. The autosampler, 8880, was modified with a Valco CV6H injector. The UV detector was a Spectra 200. A Chrom-Jet integrator connected to a Chromstation computing system was used to collect and interpret data. The column was a Hypercarb 100 × 4.6 mm I.D., 10-μm particles from Shandon (Cheshire, UK).

2.3. Procedures

The eluents used were aqueous solutions containing 2% ethylene glycol. Different buffering additives were used, at pH 1.5 a sulphuric acid buffer and at pH 5.0 an acetate buffer. The eluents containing metal ions were obtained by adding iron(III) sulphate or copper(II) acetate. The sample solutions were prepared by adding a 2–3-fold molar excess of the metal salt compared to EDTA. All solutions were prepared from doubly distilled water.

The injected sample volume was 20 μl. The flow-rate was set at 1.0 ml/min and detection was by UV. EDTA as acid was detected at 220 and 240 nm, the copper complex at 254 nm and the iron complex at 270 nm, due to differences in absorption maxima for free EDTA and the two complexes.

3. Results and discussion

3.1. EDTA

EDTA is a multidentate agent which is able to form very strong complexes with various metal ions [22]. The complex-forming ability of EDTA increases with increasing pH since the $EDTA^{4-}$ ion forms the complex [22]. However, at high pH, undissolved metal hydroxides may decrease the complex formation. The influence of pH on the complex formation for several metal ions is shown in Fig. 1 (cf. Ref. [22]). The conditional complex-forming constant is plotted against the pH. As shown, e.g. at pH 7 the conditional constant of Cu(II) is higher then that of Fe(III), about 2 log units. Thus Cu(II) is preferably chosen as complex-forming metal ion in this pH region. However, interference from Ni(II) may occur (cf. Fig. 1). At pH 5 the ratio of the conditional constant of Fe(III) and Cu(II) is reversed. If Cu(II) is chosen as complexing

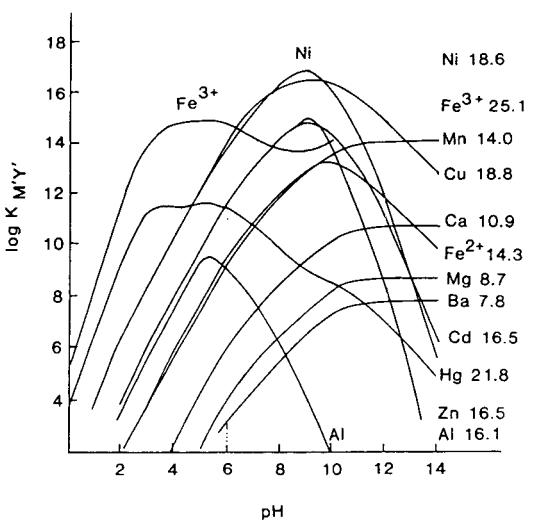

Fig. 1. Complex-binding constants of EDTA with various metal ions: influence of pH. From Ref. [22]. Stability constants are given in the margin.

metal ion strong interference will appear in the presence of Fe(III). Also Ni(II), Hg(II), Cd(II) and Zn(II) may cause interference.

The ability of Fe(III) to form strong complexes at low pH can be used to increase the selectivity. Ringbom [1] showed that Fe(III) can be used in quantitative titrimetric determination of EDTA at pH 1. In this pH region other metal ions show low ability to form complexes with EDTA (Fig. 1).

3.2. Chromatographic system

In reversed-phase liquid chromatography, EDTA is mainly determined as metal complexes in systems where a counter-ion is added to the mobile phase [11–17,20,21]. The retention of the EDTA complexes will depend on the charge and type of metal complex, the surface concentration of the counter-ion, the ionic strength and the dielectric constant of the mobile phase [23].

In other systems EDTA itself is used as a complex-forming agent in the eluent to achieve separation between metal ions [10,24,25].

In the present study the main purpose was to interpret the complex-forming behaviour of EDTA in the chromatographic system. To simplify the LC system the counter ion was not included. This will remove potential disturbances which may occur if the EDTA peak is co-eluted in the counter-ion system peak [26,27].

To obtain a suitable retention of EDTA without addition of a ion-pair reagent, the column surface must be strongly hydrophobic. Furthermore, it would be desirable if the column is stable within a wide pH range.

The Hypercarb column (porous graphitic carbon) possesses the qualities mentioned. EDTA is retained in a buffer-containing eluent, but a low percentage of an organic additive, ethylene glycol, was added to stabilise the detection signal. Ethylene glycol has only a minor effect on the retention of EDTA.

3.3. Choice of complex-forming metal ion

In the literature the copper ion was used as complexing ion in some papers [8,9,11,12,15,19] and peak distortion was reported in some of them [9,11,12,19].

The Cu(II) ion is suitable for complex binding to EDTA in the pH range 7.5–12. At lower pH interference from other metal ions e.g. the Fe(III) ion will be pronounced and effects of such interferences have been observed in LC systems [11,19]. The choice of pH is crucial. Even though it has been known for some decades that the complex-forming ability of EDTA is strongly pH dependent, unfavourable pH conditions were used in several papers [8,9,11,15,19].

To study the effects of unfavourable conditions for complex formation in the LC system used in the present investigation, the Cu(II)–EDTA complex was chosen. Cu(II)–EDTA was injected in a LC system containing acetate buffer pH 5.0 with 1 m*M* Cu(II) ions in the eluent. An additional peak eluted before the Cu(II)–EDTA peak (Fig. 2A) and by adding Fe(III) ions to the sample, the peak increased significantly and we suggest its identity to be the Fe(III)–ETDA complex (Fig. 2B).

In spite of the fact that Cu(II) ions were

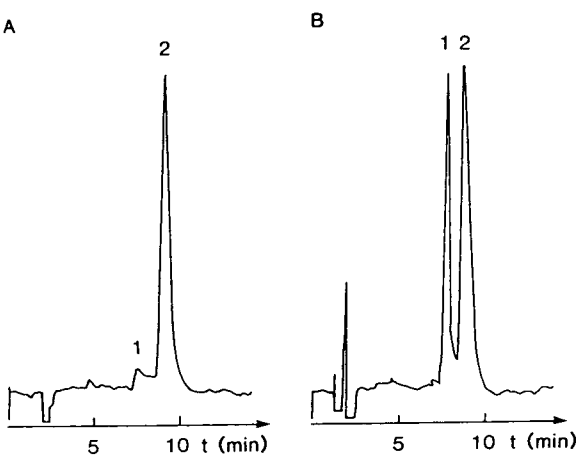

Fig. 2. Interference of Fe(III) ions in a system with an eluent containing Cu(II) ions at non-optimal conditions. Solutes: (A) EDTA 0.27 m*M* in mobile phase; (B) EDTA 0.27 m*M* + iron(III) sulphate 0.07 m*M*. Wavelength: 254 nm. Mobile phase: acetate buffer 0.05 *M*, pH 5.0 with 1 m*M* Cu(II) and 2% ethylene glycol. Peaks: (A) 1 = unknown, 2 = Cu(II)–EDTA; (B) 1 = Fe(III)–EDTA, 2 = Cu(II)–EDTA.

present in the eluent, they were exchanged for Fe(III) ions in the EDTA complex. This is due to the fact that the complex-forming constant of Fe(III) ions is higher compared to the Cu(II) ions, the logarithmic values of the conditional complex-forming constants are 14.9 and 12.3, respectively, at pH 5.0.

Fe(III) ions are always present as an impurity in the eluent in LC systems with stainless-steel parts, which was confirmed by an atomic absorption determination of Fe(III) ions.

The eluent contained a Fe(III) concentration of 90 μM.

Restrictions in choice of complex-forming metal will appear due to the high Fe(III) concentration in the background and the Fe(III) ions were chosen as complex-forming ions in further studies.

Fe(III) ions form a stable complex with EDTA at low pH values and a high selectivity in complex formation is obtained under these conditions (cf. Fig. 1).

The stability of the Fe(III) complex in the described LC system was further investigated by adding Ni, Cu, Cr and Zn ions to a Fe(III)–EDTA sample. No "ghost peaks" or peak distortions were obtained in the LC system with a sulphuric acid buffer pH 1.5 and 0.1 mM Fe(III) ions added to the eluent.

3.4. Chromatography of EDTA and Fe(III)–EDTA

Injection of the acid form of EDTA in a LC system with no metal ions added to the eluent, resulted in an EDTA peak with an anomalous band spreading (Fig. 3A).

The band spreading can be explained by secondary equilibria causing different distribution to the stationary phase. These secondary equilibria are most likely due to trace amounts of metal ions from the chemicals applied and the metal parts in the LC system. The band spreading can be suppressed either by removal of interfering metal ions or by addition of a metal which forms a strong complex with EDTA.

When a sample of Fe(III)–EDTA is injected into the system without addition of metal ions to the mobile phase, also a broad and anomalous band is obtained (Fig. 3B).

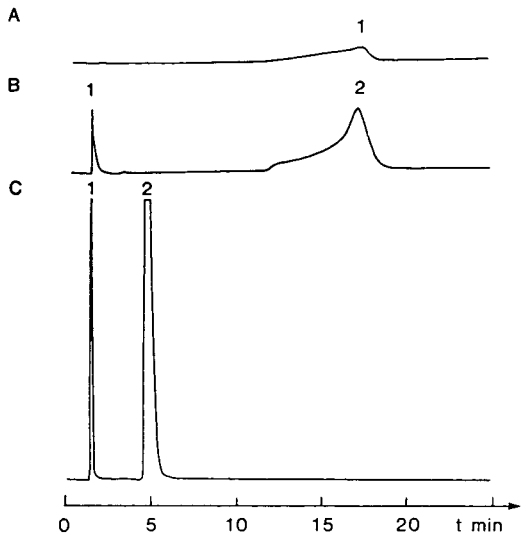

Fig. 3. Effect of addition of Fe(III) ions to the mobile phase. Solutes: (A) EDTA 2.70 mM; (B, C) EDTA 2.70 mM + 5.90 mM iron(III) sulphate. Wavelengths: (A, B) 220 nm; (C) 270 nm. Mobile phases: (A, B) sulphuric acid buffer 0.1 M, pH 1.5, 2% ethylene glycol; (C) as in A and B but 0.1 mM iron(III) sulphate is added. Peaks: (A) 1 = band of EDTA; (B) 1 = iron(III) sulphate, 2 = anomalous band of dissociated Fe(III)–EDTA; (C) 1 = iron(III) ions, 2 = Fe(III)–EDTA.

The result in Fig. 3B clearly shows that the complex between Fe(III) and EDTA dissociate during the elution, since no distinct peak is eluted at the retention time of the complex (cf. Fig. 3C). This is due to the fact that the retention of the free acid is much higher than the retention of the complex and that the Fe(III) ions are eluted close to the front. A similar observation was made when the complex of naproxen and albumin was chromatographed [28]. To avoid the disturbances described above the metal ion is added to the eluent.

A retention model for metal complexes in similar LC systems was proposed by Horváth et al. [29]. The retention was found to be affected by both the retention of the solute molecule, the

retention of the complex, the retention of the complex-forming agent as well as the size of the complex-forming constant,

$$k = \frac{k_0 + k_c K[\mathrm{H}]}{1 + K[\mathrm{H}]} \quad (1)$$

where k is the capacity factor (k_c being the capacity factor of the complex and k_0 that of the non-complexed solute), K is the complex-forming constant and [H] is the concentration of the complex-forming metal in the mobile phase.

Since the complex formation is a reversible equilibrium it is important to have an excess of the complex-forming agent in both the sample solution and in the chromatographic eluent.

From Eq. 1 derived by Horváth et al. it can be concluded that the retention of the complex is dependent on the concentration of the complexing agent in the eluent in a hyperbolic fashion. The retention is affected in a narrow concentration range in a order of +/− 2 log units in magnitude, where the concentration of the complex agent is $1/K$.

The complex-binding constants of EDTA with different metal ions are high, e.g. at pH 1.5 log K for Fe(III) is about 10, i.e. the retention of EDTA will be effected in the concentration range of 10 nM–1 pM for Fe(III). These concentrations are much lower compared to the normal sample concentration in LC. The fact is that the trace levels of Fe(III) from the chemicals applied and metal parts in the LC system are higher.

The conclusion is that the metal concentration will not affect the retention but the peak shapes.

Addition of Fe(III) to the eluent results in one sharp peak of Fe(III)–EDTA (Fig. 3C). The response of EDTA is also increased compared to Fig. 3A and B due to the increased molar absorptivity of the Fe(III)–EDTA complex compared to free EDTA. The concentration of Fe(III) ions in the eluent should be chosen sufficiently high to suppress the dissociation of the complex. However, the choice of the concentration in the eluent is limited, due to background absorbance. Our investigations showed that addition of 0.1 mM Fe(III) to the eluent resulted in an acceptable absorbance background level (0.21 AU) and a excellent peak performance.

4. Applications

4.1. Determination of EDTA in a local anaesthetic solution

Carbocaine adrenaline is a local anaesthetic formulation containing several components. EDTA is added to control the influence of unwanted contamination of trace metals which may promote degradation. Inman et al. [14] managed to determine EDTA in a complex pharmaceutical mixture with a gradient ion-pair RPLC system.

The methodology described in this paper was applied and a chromatogram of a diluted sample (1:1) from the Carbocaine adrenaline solution showed high selectivity and no interferences appeared (Fig. 4). An excellent linearity was obtained in the concentration range 0.01–0.21 mg/ml ($r^2 = 0.9999$). The quantification was per-

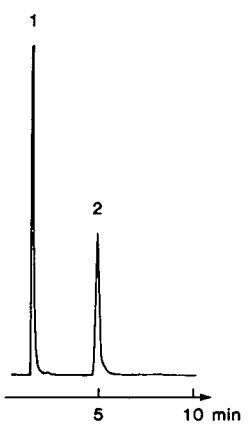

Fig. 4. EDTA in a local anaesthetic solution. Solute: Carbocaine adrenaline 20 mg/ml containing 0.25 mg/ml EDTA and a molar excess of iron(III) sulphate. Wavelength: 270 nm. Mobile phase: sulphuric acid buffer 0.1 M, pH 1.5, containing 0.1 mM iron(III) sulphate and 2% ethylene glycol. Peaks: 1 = iron(III) ions; 2 = Fe(III)–EDTA.

formed with a single-point calibration. Determination of an added amount of 0.250 mg/ml EDTA in a Carbocaine adrenaline solution resulted in a recovery of 0.248 mg/ml with a relative standard deviation of 0.8% ($n = 6$). The limit of detection was about 1 μM (0.4 μg/ml), which is similar compared to methods described in the literature [14].

4.2. Determination of NTA

NTA is determined as an impurity in EDTA, described in the US Pharmacopeia [30]. The specification limit for NTA in USP-grade disodium EDTA is maximum 0.1% (w/w). The US Pharmacopeial method developed by Parkes et al. [12] is an ion-pair RPLC method where NTA and EDTA form complexes with copper. The quantification of NTA is performed with a 10.0 mg/ml solution of EDTA and the content of NTA is determined with a standard-addition method. Determination of NTA complexes with Fe(III) in the system described in this paper is possible due to a UV response of the same order as Fe(III)–EDTA [16] and a sufficiently high complex-forming constant for NTA and Fe(III).

Fig. 5 shows a typical chromatogram. The detection limit of NTA is 0.4 μg/ml and when a 1.0 mg/ml EDTA sample was injected a detection limit of 0.05% (w/w) was easily obtained.

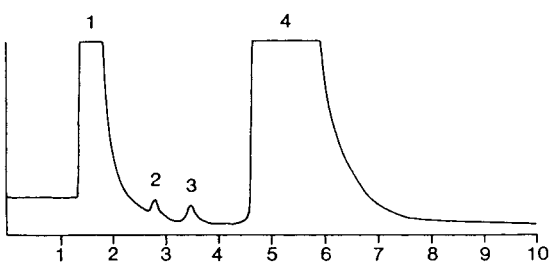

Fig. 5. Determination of NTA in EDTA. Solute: EDTA 2.70 mM (1 mg/ml) and a 3-fold molar excess of iron(III) sulphate. Wavelength: 270 nm. Mobile phase: sulphuric acid buffer 0.1 M, pH 1.5, containing 0.1 mM iron(III) sulphate and 2% ethylene glycol. Peaks: 1 = iron(III) ions; 2 = unknown; 3 = NTA; 4 = EDTA.

Acknowledgements

We thank Dr. Kerstin Gröningsson and Professor Douglas Westerlund for valuable comments on the manuscript.

References

[1] A. Ringbom, *Sv. Kem. Tidskr.*, 66 (1954) 159.
[2] G. Schwarzenbach, *Anal. Chim. Acta*, 7 (1952) 141.
[3] J. Gardiner, *Analyst*, 102 (1977) 120.
[4] *Annual Book of ASTM Standards*, Part 31, American Society for Testing and Materials, Philadelphia, PA, 1982, method ASTM D3113-80, p. 727.
[5] E.B. Milosavljević, L. Solujić, J.L. Hendrix and J.H. Nelson, *Analyst*, 114 (1989) 805.
[6] Y. Ito, M Toyoda, H. Susuki an M. Iwaida, *J. Assoc. Off. Anal. Chem.*, 63 (1980) 1219.
[7] Z. Stojek and J. Osteryoung, *Anal. Chem.*, 53 (1981) 847.
[8] W. Bucherberger, P.R. Haddad and P.W. Alexander, *J. Chromatogr.*, 558 (1991) 181.
[9] M. Unger, E. Mainka and W. König, *Z. Anal. Chem.*, 329 (1987) 50.
[10] W.F. Lien and B.K. Boerner, *J. Liq. Chromatogr.*, 10 (1987) 3213.
[11] D.L. Venezky and W.E Rudzinski, *Anal. Chem.*, 56 (1984) 315.
[12] D.G. Parkes, M.G. Caruso and J.E. Spradling III, *Anal. Chem.*, 53 (1981) 2154.
[13] J.H. Knox and M. Shibukawa, *J. Chromatogr.*, 545 (1991) 123.
[14] E.L. Inman, R.L Clemens and B.A. Olsen, *J. Pharm. Biomed. Anal.*, 8 (1990) 513.
[15] L. Hall and L. Takahashi, *J. Pharm. Sci.*, 77 (1988) 247.
[16] A. Yamaguchi, A.R. Rajput, K. Ohzeki and T. Kambara, *Bull. Chem. Soc. Jpn.*, 56 (1983) 2621.
[17] A. Yamaguchi, A. Toda, K. Ohzeki and T. Kambara, *Bull. Chem. Soc. Jpn.*, 56 (1983) 2949.
[18] J. Harmsen and A. van der Toorn, *J. Chromatogr.*, 249 (1982) 379.
[19] J. Dai and G.R. Helz, *Anal. Chem.*, 60 (1988) 301.
[20] G.A. Perfetti and C.R. Warner, *J. Assoc. Off. Anal. Chem.*, 62 (1979) 1092.
[21] H.-J. Götze and D. Bialkowski, *Z. Anal. Chem.*, 323 (1986) 350.
[22] A. Ringbom, *Treatise Anal. Chem.*, 1 (1959) 545–629.
[23] J. Ståhlberg and I. Hägglund, *Anal. Chem.*, 60 (1988) 1958.
[24] G. Saccero, O. Abollino, V. Porta, C. Sarzanini and E. Mentasti, *Chromatographia*, 31 (1991) 539.

[25] M.L. Marina, J.C. Diez-Masa and M.V. Dabrio, *J. High Resolut. Chromatogr. Chromatogr. Commun.*, 9 (1986) 300.
[26] T. Fornstedt, *J. Chromatogr.*, 612 (1993) 137.
[27] R.M Cassidy and M. Fraser, *Chromatographia*, 18 (1984) 369.
[28] K.G. Wahlund and T. Arvidsson, *J. Chromatogr.*, 282 (1983) 527.
[29] Cs. Horváth, W. Melander and A. Nahum, *J. Chromatogr.*, 186 (1979) 371.
[30] *US Pharmacopeia* National Formulary, USP XXII, NF XVII, The United States Pharmacopeial Convention, Rockville, MD, 1989, p. 492.

ELSEVIER

Journal of Chromatography A, 684 (1994) 221–234

JOURNAL OF CHROMATOGRAPHY A

Studies on the retention behaviour of a group of organic anions of biochemical interest on quaternary bonded silica columns equilibrated with a functionally coherent series of counterions

Use of 2-(N-morpholino)ethanesulphonate as a counterion and N-tris(hydroxymethyl)methyl-3-aminopropanesulphonate as an eluent

R.H.P. Reid

Department of Biochemistry, Wrexham Maelor Hospital, Wrexham, Clwyd, Wales, UK

Abstract

The anions of a functionally coherent series of Good's buffers have been used to provide the counterions for quaternary bonded silica and the mechanisms of exchange with a test sample of organic anions of biochemical interest studied with the objective of finding strategies which might be suitable for the extraction of organic anions from biological fluids. A dual retention mechanism involving the electrical double layer and the pH related ionisation of the counterion is proposed. The MES^- [MES = 2-(N-morpholino)ethanesulphonic acid] anion is shown to be a useful counterion and the $TAPS^-$ [TAPS = N-tris(hydroxymethyl)methyl-3-aminopropanesulphonic acid] anion a useful eluent in a series of compatible techniques which could be applicable in methods involving either solid-phase extraction or HPLC for separation purposes. An analytical protocol compatible with assay by capillary electrophoresis is described.

1. Introduction

The problems which may be encountered when attempting to apply capillary electrophoresis (CE) to the analysis of biological fluids have been summarised previously [1]. One of these problems is the high ionic strength of biological fluids relative to the ionic strengths of the buffers used in the electrophoresis. The high ionic strength of biological fluids is largely due to the presence of relatively large concentrations of strong electrolytes. When the ionic strength of the sample is higher than that of the running buffer peak spreading occurs because the electric field strength within the sample zone is less than in the running buffer and consequently electrophoretic velocities are less within the sample zone than in the running buffer. In these circumstances dilution of the sample or the use of a buffer with a higher ionic strength may be practical options but both are limited by other considerations. Dilution of the sample may compromise analytical sensitivity beyond a tolerable limit. Increasing the ionic strength of the running

0021-9673/94/$07.00
SSDI 0021-9673(94)00621-O

buffer will ultimately compromise the ability to maintain the capillary at a constant temperature. The ideal solution would be to isolate the analytes of interest in a solution of relatively low ionic strength thereby producing much greater flexibility in both the choice and strength of the buffer solutions available for the electrophoresis.

The technique of isolating analytes of interest from a biological fluid into a solid phase prior to subsequent chromatographic analysis was described in 1965 by Reid et al. [2,3] for the analysis of amino acids in human blood serum. A variety of commercially available kits and protocols now exist for the "solid-phase extraction" of analytes from fluids employing a range of bonded and unbonded chromatographic materials and some have found use in the extraction of analytes prior to analysis by CE or the related technique of micellar electrokinetic capillary chromatography [4–6]. Most workers have used octadecyl (C_{18})-bonded phases for the extraction of analytes which are essentially hydrophobic in character. As the majority of synthetic drugs which do not occur naturally are hydrophobic, extraction into a C_{18} phase has been particularly applicable to the analysis of drugs in biological fluids.

The principal objective of the present work was to establish techniques which might be generally applicable to the isolation of organic anions from the strong electrolyte environment in which they occur in biological fluids, to give extracts which were suitable for assay by CE. The techniques of ion-exchange chromatography appeared suitable for this purpose. The work presented here was aimed at achieving this solution for a test group of organic anions. The separation and assay of these organic anions by CE employing Good's buffers [7–9] has already been described [1]. Much of the data presented here would be equally relevant to the development of an HPLC system for the assay of some of these anions.

The solid adsorbent phase used consisted of macroporous silica particles covalently bonded to a strongly cationic quaternary amino nitrogen group giving a preparation which was a strong anion exchanger. Residual free silanol groups were largely eliminated by inert end-capping. This paper describes the results obtained when a functionally coherent series of the anions of a set of Good's buffers are used as counterions and exchange attempted with the anionic organic analytes. Good's buffers were chosen because their relatively low molar conductivities offered the hope of extracts with relatively low conductivities and because compatibility with existing methods of assay was assured [1]. The experimental observations are satisfactorily explained by an electrical double layer mechanism of the type proposed by Afrashtehfar and Cantwell [10] for styrene–divinylbenzene copolymer bonded to quaternary ammonium groups together with a counterion determined displacement mechanism. The proposed mechanism allows a number of experimentally verifiable predictions to be made which include a highly satisfactory method for the elution of retained analytes as an alternative to elution by acidification. Experimental conditions were found in which elution from the diffuse part of the electrical double layer can be distinguished from elution from the compact layer.

2. Experimental

2.1. Reagents and chemicals

Reference analyte solution

Reference preparations of creatinine, free base, anhydrous, crystalline; *trans*-urocanic acid [4-imidazoleacrylic acid; uric acid (2,6,8-trihydroxypurine)], monosodium salt; vanillylmandelic acid (VMA, *dl*-4-hydroxy-3-methoxymandelic acid); hippuric acid, (benzylaminoacetic acid), free acid; *trans*-cinnamic acid (3-phenylpropenoic acid); phenylacetic acid; orotic acid (6-carboxy-2,4-dihydroxypyrimidine), free acid, monohydrate; sodium benzoate; and sodium salicylate were obtained from Sigma, and used without further purification. Quantities of each of these analytes sufficient to give a 200 μM solution with respect to each analyte were transferred to a standard 500-ml volumetric flask

containing 200 ml water, 5 ml methanol, 2 ml 1 *M* sodium hydroxide solution and 1.0 ml 0.5 *M* disodium ethylenediaminetetraacetic acid and the mixture agitated until solution was complete. Water was added to the volumetric mark and the resulting reference solution divided into 20-ml aliquots in glass vials and stored at 4°C prior to use. Creatinine does not behave as a true analyte in the subsequent assay. It is included because it may occur in large quantities in urine and its behaviour needs to be followed. On assay by CE in the system employed here it migrates with the negative peak corresponding to the electroosmotic flow and accurate integration is impossible.

Solutions of Good's buffers

The free acid (zwitterionic) forms of 2-(N-morpholino)ethanesulphonic acid (MES), 3-(N-morpholino)-2- hydroxypropanesulphonic acid (MOPSO), 3-(N-morpholino)propanesulphonic acid (MOPS), N-(2-hydroxyethyl)piperazine-N″-(2-ethanesulphonic acid) (HEPES), N-tris(hydroxymethyl)methyl-3-aminopropanesulphonic acid (TAPS), 3-(cyclohexylamino)-2-hydroxypropanesulphonic acid (CAPSO) and the sodium salts of MES, MOPSO, MOPS, HEPES, TAPS and CAPSO were obtained from Sigma.

Buffers throughout this work were used at pH values at or close to their p*K* values with the exceptions of MES buffer at pH 7.30 and MOPS buffer at pH 6.07. These latter buffers, both at pH values approximately one unit from their respective p*K* values were made up as 50 m*M* solutions by dissolving the appropriate quantities of sodium salt and free acid in water. Stock solutions of other buffers were prepared by dissolving 50 mmol of the sodium salt and 50 mmol of the free acid in a small volume of water and making the solution volume up to 1 l. The working buffers of molarity 50 m*M* were prepared from the 100 m*M* stock solutions by the addition of an equal volume of water. The pH of a buffer was checked immediately before use at prevailing room temperature. Table 1 shows the essential parameters describing each of the buffers used in this study.

Table 1
Parameters describing the buffers used for establishing the counterion by equilibration with 1-g columns of quaternary bonded anion-exchange silica

50 m*M* Buffer	p*K*[a]	pH
MES	6.15	6.13
MOPSO	6.90	7.02
MOPS	7.15	7.23
HEPES	7.55	7.65
TAPS	8.55	8.65
CAPSO	9.60	10.1
MES[b]	6.15	7.30
MOPS[b]	7.15	6.07

[a] p*K* values are from Ref. [8].
[b] Buffers at pH values approximately one pH unit from their p*K* values used to provide data for the experiment illustrated in Fig. 4.

2.2. Adsorbent and preparation of chromatographic columns

The adsorbent used for these studies was quaternary amine bonded silica obtained from J.T. Baker UK, Hayes, UK (product No. 7043.00). The product is a strong anion exchanger and consists of irregular macroporous particles of average particle size 40 μm, average pore diameter 6 nm and with an exchange capacity of 0.7 mequiv./g and surface area of 500 m^2/g. As purchased the material is in the chloride state.

Aliquots (1 g) of the dry powdered adsorbent were poured into all glass columns (Bakerbond SPE glass columns, 8 ml capacity, 8 cm length, product No. 7328.06) containing approximately 5 ml chloroform. After removal of the residual chloroform from above the settled adsorbent, by suction from the bottom of the column, the column is washed with 2×5 ml chloroform followed by 2×5 ml methanol and finally 2×5 ml water or the appropriate buffer depending on whether the column is to be stored or used immediately. This washing protocol has been found to be essential for the successful subsequent analysis of eluates by capillary electrophoresis when monitoring in the UV region. It is of interest that the aqueous eluates which follow the chloroform and methanol washes of this

material have a pH of approximately 3! Columns prepared in this way have a void volume of 1 ml.

2.3. Equilibration with a new counterion

Columns were equilibrated and run by manual, stepwise application of 5-ml aliquots of eluent followed by manual removal of 5 ml eluate by suction from the bottom of the column at the approximate rate of 1 ml/min. Columns were equilibrated with counterion by repeated application of 5-ml aliquots of the appropriate buffer until the pH of two successive 5-ml aliquots of eluate was equal to the pH of the buffer. Before application of an analytical sample each column was washed once with 5 ml water.

When columns equilibrated with the MES^- anion came to be used frequently as analytical columns the equilibration process was greatly speeded up by employing MES buffers of strength 50 or 100 m*M* and with a pH approximately 1 unit above the p*K* of MES which is 6.15. Before application of sample the column was washed with 5 ml (5 void volumes) water.

2.4. Solid-phase extraction protocol

A common protocol was used for the chromatography of the test solution of organic anions irrespective of which buffer had provided the counterion for the quaternary bonded silica anion exchanger. The protocol was designed to be easily modified to provide a practical strategy for the solid-phase extraction of similar analytes from biological fluids. The reference analyte solution (5 ml) was applied to the top of the column and a corresponding 5 ml eluate removed from the bottom (E1). Two successive 5-ml aliquots of water were applied as eluents and the corresponding eluates collected (E2, E3). Elution was continued with four 5-ml aliquots 50 m*M* hydrochloric acid (E4–E7). Each of the successive eluent steps E1–E7 therefore comprised the equivalent of five void volumes giving a total eluent volume equivalent to 35 void volumes. In the later stages of this work 50 m*M* TAPS buffer, at a pH close to its p*K* of 8.55 replaced the hydrochloric acid as an eluent. Analysis of eluates by CE was carried out after transfer of each eluate step to a 5-ml glass sample phial and without any further treatment.

In the comparative studies in which different counterions were put in place by equilibration with the appropriate buffers hydrochloric acid was always employed in the elution stage as described above. In these latter studies each column was re-equilibrated with 50 m*M* MES buffer, pH 7.3 and re-run after loading the reference analyte solution in order to check that the ion-exchange properties of the bonded phase had not been degraded by either the equilibration or elution phases when using counterions other than MES^-.

2.5. Measurement of conductivities of buffers and eluates

These were done at a room temperature of 20°C using a Ciba-Corning portable M90 conductivity meter. All measurements were made in duplicate with frequent re-calibrations against a known commercial standard. The value for the cell constant was determined by measuring the conductance of a standard 100 m*M* solution of potassium chloride.

2.6. Analysis of eluates by CE

Eluates were analysed by CE in 50 m*M* MES buffer, pH 6.15 (or close to 6.15) at a temperature of 25°C with 25 kV applied across a capillary of 57 cm × 75 μm I.D. using Beckman P/ACE 2100 instrumentation as described previously [1].

3. Results and discussion

3.1. Quantitative and theoretical considerations

The buffering reaction for Good's buffers, using MES as an example is:

$$H^+ + MES^- = MES_{zwitterion}$$

and the pH in such a system is given by:

$$pH = pK + \log[MES^-/MES_{zwitterion}]$$

with the pK defined as the pH when the concentration of MES anion equals that of MES zwitterion.

The studies reported here employed 1-g columns of the quaternary bonded silica anion exchanger.These have an exchange capacity of 700 μmol/g for monovalent anions. The 50 mM buffers with pH values close to their pK values contain 125 μmol counter anion per 5-ml aliquot and therefore approximately six 5-ml aliquots of buffer contain sufficient anion to provide a complete counterion replacement on the 1-g columns. This is true in practice and after equilibration with six successive aliquots of buffer the eluate pH is equal to the pH of the eluent buffer.

The reference analyte solution is 200 μM with respect to each of ten analytes. Analytes are applied to the anion-exchange columns in a single 5-ml aliquot of the reference analyte solution which therefore contains 1 μmol each analyte per 5 ml or a total sample load 10 μmol anionic analyte (assuming monovalency which is approximately true). This is 1.43% of the total exchange capacity of 700 μmol and appears compatible with the trace conditions for both ion exchange and surface adsorption as defined by Afrashtehfar and Cantwell [10]. The anion-exchange activity of the quaternary bonded silica used in the present studies is assumed to occur at the surface of the bonded silica including the surface of the pore channels. There is no exchange within the material of the silica particles as occurs within the gel matrices of some ion-exchange resins.

3.2. The variation in the sorption and retention of analyte anions with the nature of the counterion at the bonded silica surface

The effect of the different counterions on the elution patterns of the reference analyte solution when the bonded silica columns are equilibrated, loaded and run as described in the experimental section is illustrated in Figs. 1 and 2. Recoveries refer to the summed recoveries of the analytes for each elution step (E1–E7). The data in Figs. 1 and 2 shows that as the pK of the buffer

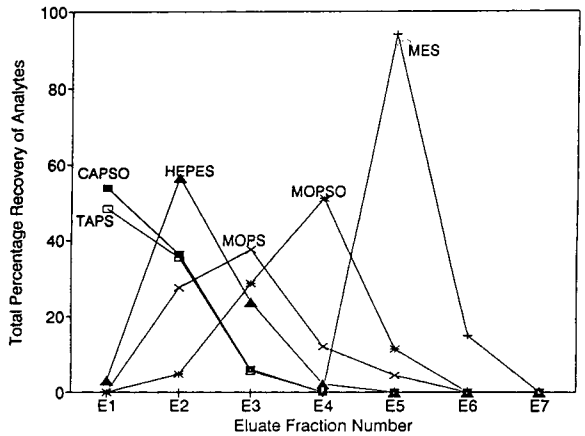

Fig. 1. Variation in the elution of the reference analytes from 1-g bonded silica anion exchange columns equilibrated with counterions from six different Good's buffers. The parameters describing the 50 mM buffers are given in Table I. Recoveries refer to the summed recoveries of analytes taken as a group in each eluate fraction. Seven 5-ml eluent steps E1–E7 were applied to each column giving seven 5-ml aliquots of eluent E1–E7. Key to eluents: E1 = 5 ml reference analyte solution (sample); E2, E3 = 5 ml water; E4–E7 = 5 ml 50 mM hydrochloric acid.

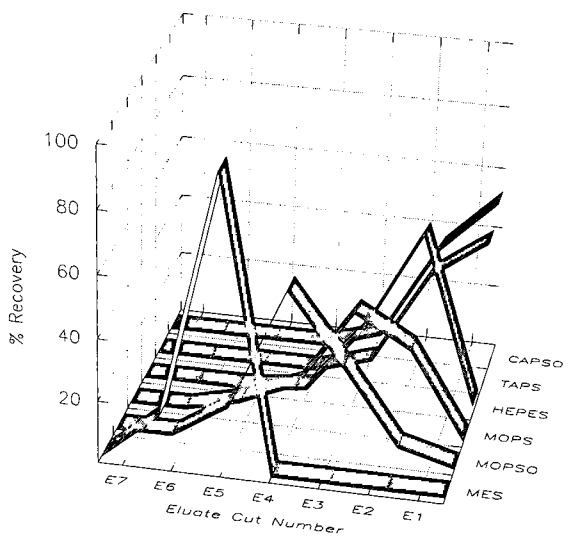

Fig. 2. The same data as in Fig. 1 presented as a pseudo-three-dimensional drawing emphasising the nature of the counterion as a determinant of the elution pattern. Note that to improve visibility E1–E7 are in reverse order. The counterions on the z-axis are arranged in order of increasing pK starting with MES. Elution details as in Fig. 1.

providing the counterion varies progressively from that of CAPSO at 9.6 to that of MES at 6.15 the retention of analytes by the bonded silica column increases. In all cases the total recovery of analytes by the elution procedure is approximately 100%. In the case of columns equilibrated with the MES counterion release of retained analytes does not occur until E5 after the column has been eluted with 50 m*M* hydrochloric acid at E4. By contrast, for columns equilibrated with the CAPSO counterion the elution of analytes is complete before the application of acid at E4. The counterions of TAPS, HEPES, MOPS and MOPSO, with progressively decreasing p*K* values, produce a continuum of elution patterns showing increasing retention of analytes between the limits exhibited by CAPSO and MES.

In Fig. 3 the pH profiles of eluate fractions E1–E7 corresponding to the six different counterions are shown. The eluate fractions E1–E3, corresponding to the loading and wash phases of the chromatographic protocol have pH values approximately equal to that of the buffer which provided the counterion while the post-acidification eluates E5–E7 have pH values of approximately 2. It is well known [11] that bonded silicas can behave unpredictably below an approximate pH of 3 when acidic degradation of the bonded phase occurs, and above an approximate pH of 8 when the alkaline dissolution of silica occurs. It was therefore important to be certain that the elution profiles illustrated in Figs. 1 and 2 were not, at least in part, pH-related artifacts. Each column was equilibrated with MES counterion after completion of its elution with 50 m*M* hydrochloric acid, re-loaded and re-run and the analyte elution pattern characteristic of the MES counterion obtained. This was considered to constitute adequate proof that under these experimental conditions the ion-exchange properties of the bonded phase remained essentially intact. This was a particularly relevant finding for the buffers TAPS and CAPSO with pH values over 8. No column in the above experiments was run more than twice as described, the second run always being to confirm the patency of the bonded phase. It appears that over periods of less than a few hours quaternary bonded silica can withstand exposure to solutions with pH values less than 3 or greater than 8 as determined by the exchange of trace amounts of analyte. It has been the subjective impression in the present studies that exposure to acidic conditions, for tens of hours, is more damaging to the bonded phase than similar exposure to relatively mild alkaline buffers.

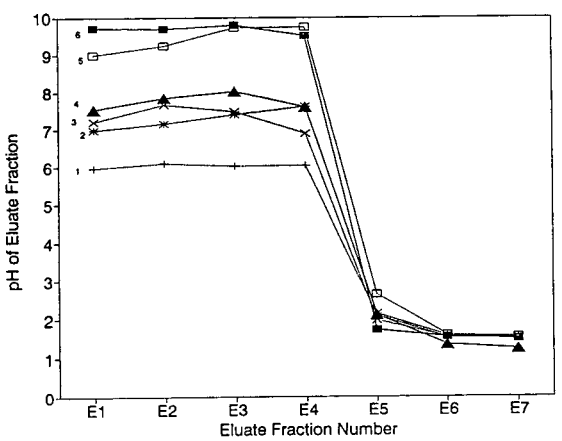

Fig. 3. The pH profiles of the eluate fractions from the columns whose analyte elution patterns are shown in Figs. 1 and 2. Key: 1 = 1 g quaternary bonded silica with MES^- counterion; 2 = $MOPSO^-$ counterion; 3 = $MOPS^-$ counterion; 4 = $HEPES^-$ counterion; 5 = $TAPS^-$ counterion; 6 = $CAPSO^-$ counterion. Elution details as in Fig. 1.

It may appear obvious that at least for monovalent buffers (like Good's buffers) where there is only a single anionic species and a single p*K*, the elution pattern of exchanged analytes should be independent of the pH of the buffer which provides the counterion at the bonded silica surface, provided that the counterion can exist at that pH. The retention patterns of organic analytes illustrated in Figs. 1 and 2 show clearly that the retention pattern of analytes for the series of counterions used in this study appears to be determined by the pH (or p*K*) of the buffers which provide the counterion. Because of its relevance to subsequent mechanistic considerations it was important to determine the variation in retention pattern with pH when the counterion was fixed. This was done by the experiment illustrated in Fig. 4 in which the elution patterns

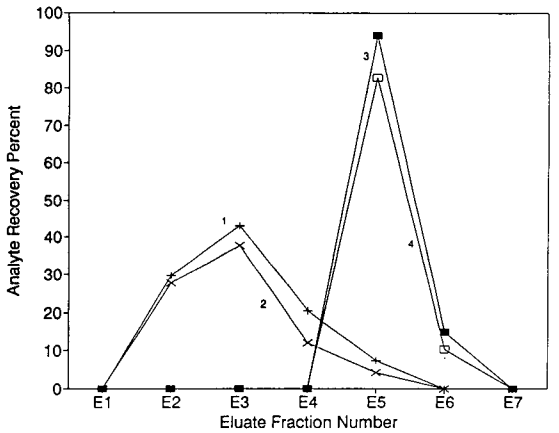

Fig. 4. Showing that when the counterion is fixed the elution pattern of the reference analytes is determined by the nature of the counterion and is, within limits, independent of the pH of the buffer used in placing the counterion. Curves: 1 = column equilibrated with 50 m*M* MOPS buffer, pH 6.07; 2 = column equilibrated with 50 m*M* MOPS buffer, pH 7.23; 3 = column equilibrated with 50 m*M* MES buffer, pH 7.30; 4 = column equilibrated with 50 m*M* MES buffer, pH 6.13. Eluents as in Fig. 1.

produced by equilibration of the quaternary bonded silica columns by MES and MOPS buffers, each at two different pH values, are compared. The data in Fig. 4 show that the elution pattern of the reference analytes is the same for MES anion irrespective of whether the counterion was achieved by equilibration with MES buffer at pH 6.13 (cf. a p*K* of 6.15) or at pH 7.30 (cf. a p*K* for MOPS of 7.15). Similarly, the elution pattern of the reference analytes was characteristic of the MOPS anion irrespective of whether the equilibrating buffer was at pH 6.07 (close to the p*K* of MES) or 7.23 (close to its own p*K*). These results suggest that for any given counterion the elution pattern of exchanged analytes is, at least over a limited pH range around the p*K*, independent of the pH of the buffer used to provide the counterion.

The fact that 50 m*M* MES buffer, pH 6.13 provides columns with elution patterns identical to 50 m*M* MES buffer, pH 7.30 has a useful analytical significance. The buffer with pH 7.30 has approximately ten times the anion concentration of the pH 6.13 buffer and will therefore bring a column to an equilibrated state much more rapidly than the buffer with the lower pH.

3.3. A hypothetical mechanism

The theoretical basis for the retention mechanism of organic anions on a low-capacity ion-exchange adsorbent was reported in 1982 by Afrashtehfar and Cantwell [10] using *p*-nitrobenzenesulphonate as a sample anion and a surface-quaternised macroporous styrene–divinylbenzene as the ion-exchange adsorbent ("QXAD"). These authors employed 1 m*M* aqueous ammonia containing concentrations of sodium chloride up to 1 *M* as mobile phases and studied the variation in the capacity factor for the anionic sample (k'_{s^-}) with the ionic strength of sodium chloride in the mobile phase. Afrashtehfar and Cantwell proposed a dual retention mechanism for the sorption of counterions by the exchange material in terms of the Stern–Gouy–Chapman model of the electrical double layer. The experimental results reported here are satisfactorily explained by this theory with minor modifications and in consequence the nomenclature used by these authors will be adopted. According to this theory sorption by the surface bonded anion-exchange material is determined by adsorption of counterion (including sample) by the charged surface and secondly by ion exchange of the sample ions for other counterions in the diffuse part of the electrical double layer. The compact region of the double layer according to these authors extends from the charged surface with its adsorbed counterions, up to but not including, the outer Helmholtz plane which is the start of the diffuse layer. Adsorption of counterion at the surface is dependent on the electrical potential at the surface while ion exchange between the bulk fluid and the diffuse layer is independent of the electrical potential at the surface. The authors emphasise that the structure of a sample molecule largely determines the relative extent of its partition between the compact and diffuse layers.

The results illustrated in Figs. 1 and 2 can be explained in terms of these concepts when the hydrogen ion concentrations of solutions of

Good's buffers in the region of their pK values are considered. All buffers for the experiment depicted in Figs. 1 and 2 were 25 mM with respect to the buffer anion and 25 mM with respect to the zwitterion (free acid) giving in each case a buffer with a pH close to or equal to the pK of the buffer. The hydrogen ion concentrations in the different buffer solutions varies widely however from 1000 nM at pH 6 (approximately that of MES) to 0.1 nM at pH 10 (approximately that of CAPSO). These pH values are only strictly applicable to the bulk buffer. All columns were equilibrated before use by exposure to approximately 30 column void volumes of each buffer until the eluate pH equalled the eluent pH. In the immediate vicinity of the adsorbed layer consisting of buffer anions, the adjacent diffuse layer will be enriched with buffer anions relative to the bulk buffer. There will also be a relative exclusion of hydrogen ions from this region (Donnan exclusion). These two effects would be expected to produce a pH in the region of the outer Helmholtz plane greater than that in the bulk buffer. It may be hypothesised that buffer anions are only displaced from the adsorbed layer after first accepting a proton thereby becoming zwitterions. Only then does a charged site become available for the adsorption of sample anions or indeed any anions. These arguments suggest that the rate at which charged sites become available for the re-adsorption of other anions is kinetically first order with respect to the hydrogen ion concentration. This means that an adsorption layer initially saturated with $CAPSO^-$ anions provides sites free for re-occupation by other anions at a rate approximately one thousandth of that for an adsorption layer initially saturated with MES^- anions. In both cases exchange occurs between analyte anions in the sample and buffer anions in the diffuse layer and in the case of MES equilibrated columns the analytes in the diffuse layer can enter and be retained by the adsorbed layer.

It seems that analytes retained in the adsorbed layer are not released by elution with 50 mM hydrochloric acid until the eluate is rendered acidic (at E5, cf. Figs. 1 and 2 with Fig. 3 for MES-equilibrated columns). There is no evidence for release by exchange with chloride ions in E4 when elution with hydrochloric acid is started. Acceptance of a proton may also be a pre-condition for the release of the reference organic anions from the adsorbed layer. It may be noted that all the analytes in the test solution have at least one pK value below the value of 6 and will be either ionised or strongly ionised under normal equilibrated column conditions.

The behaviour of the trace sample load of the reference analytes in bonded quaternised silica anion-exchange columns with the six counterions can now be explained. With CAPSO and TAPS equilibrated columns retention of analytes in the compact (adsorbed) layer is negligible but retention by ion exchange in the diffuse layer is evident (Fig. 1 and 2). At the lower limit of the pK range columns equilibrated with MES anion as the counterion exhibit strong retention of analytes predominantly in the adsorbed layer, from which they are released when the eluate pH approaches a value of 2. Columns equilibrated with the anions of HEPES, MOPS and MOPSO show progressively increasing retention of organic analytes with elution maxima at E2, E3 and E4 respectively. It seems reasonable to assume that the increased availability of hydrogen ions with decreasing pH in the vicinity of the compact layer is producing an increased proportion of sites in the adsorbed layer for occupancy by analyte ions.

The standard elution protocol in these studies employed water washes at E2 and E3. The purpose was twofold: firstly, to keep the chemistry simple and secondly to investigate the effect of washing on the retention of analytes prior to their deliberate elution at E4. The recoveries of analytes from the CAPSO and TAPS equilibrated columns are approximately 50, 35 and 5% in eluate cuts E1, E2 and E3, respectively, indicating weak retention in the diffuse layer in columns with void volumes of 1 ml. It is valid to ask what happens to the charged surfaces' requirement for counterion when some of that counterion is "leached" out by wash steps. The answer must be that more countercharge moves into the compact or adsorbed layer and more countercharge in the diffuse layer redistributes

closer to the compact layer. The diffuse layer becomes thinner according to the inverse square root of the ionic concentration in the bulk fluid as required by Debye–Huckel theory.

3.4. The use of TAPS buffer as an eluent

Inspection of the elution profiles in Figs. 1 and 2 and the matching eluate pH data in Fig. 3 show that columns with a MES counterion have qualities which are very suitable as the basis for a "solid-phase extraction" protocol for organic anions of the type present in the reference analyte solution. Columns equilibrated with the MES counterion can be rapidly prepared by elution with 50 or 100 m*M* buffer at a pH approximately 1 unit above the p*K* of 6.15. The organic analytes are quantitatively retained in the adsorbed layer, remain on the column after washing with 10 void volumes of water and can be rapidly recovered after acidification with 50 m*M* hydrochloric acid. This last step is unsatisfactory for several reasons. The acidic conditions limit the durability of the quaternary phase bonded to the silica surface. Secondly, if subsequent assay is to be by CE the presence of the chloride ion confers a relatively high conductivity on the sample. Thirdly, many biochemical substances might be labile in these acidic conditions.

The theoretical treatment outlined previously suggests that the anions of Good's buffers with a p*K* higher than that of MES should be successful as eluents for the removal of analytes. TAPS buffer (50 m*M*, pH 8.54) was tested and found to be much superior to acidification for this purpose. Apart from the avoidance of acidic eluates, elution with 50 m*M* TAPS at E4 results in the immediate elution of analytes at E4 with only a residual 10–20% eluting at E5. Table 2 shows in detail the recoveries of individual analytes at each of the steps in the elution procedure after analysis by CE. No data are available for creatinine which migrates with the electroosmotic flow. The negative solvent peak of the latter partly obscures the creatinine peak prohibiting its quantitation. The average recovery of the other analytes is approximately

Table 2
Recoveries of individual analytes from eluate fractions E1–E7 when sample is loaded onto 1-g quaternary bonded silica column equilibrated with MES counterion using 100 m*M* MES buffer, pH 7.2 followed by one 5-ml water wash and column run as described below

Analyte	Recovery (%)							
	E1	E2	E3	E4	E5	E6	E7	Total
Creatinine	–	–	–	–	–	–	–	–
Urocanic acid	0	0	0	73.7	15.9	0	0	89.6
Uric acid	0	0	0	89.1	8.4	0	0	97.5
VMA	0	0	0	75.9	28.3	0	0	104.2
Hippuric acid	0	0	0	87.5	15.5	0	0	103
Cinnamic acid	0	0	0	80.8	18.3	0	0	99.1
Phenylacetic acid	0	0	0	89.2	10.4	0	0	99.6
Orotic acid	0	0	0	93.8	7.1	0	0	100.9
Benzoic acid	0	0	0	82.7	15.3	0	0	98
Salicylic acid	0	0	0	79.2	15.0	0	0	94.2
Average total	0	0	0	83.5	14.9	0	0	98.4

Analytes loaded onto anion-exchange column in 5 ml reference solution containing 1 μmol of each analyte at E1. Elution continued with 2 × 5 ml aliquots water (E2, E3), 4 × 5 ml aliquots 50 m*M* TAPS buffer, pH 8.54 (E4–E7). Approximately 5 nl (5-s high-pressure injection) of each eluate analysed by CE at 25 kV in 50 m*M* MES buffer, pH 5.99 at 25°C with UV detection at 214 nm, capillary length 57 cm × 75 μm I.D. Conductivity and pH data for the eluates of the anion-exchange column and buffers involved in this experiment are given in Table 3.

98.5%. There are three recoveries, for VMA, hippuric and orotic acids which have values slightly over 100% and are easily accounted for by a computer integration strategy that was not entirely adequate.

3.5. Conductivity considerations in relation to analysis by CE

In 1991 Vinther and Soeberg [12] described a set of guidelines for determining the optimum relative conductivities of the sample and running buffer in CE. Their main recommendations were that the conductivity of the running buffer should be "low" to minimise Joule heating and that "moderate stacking" conditions should be employed in which the conductivity of the sample solution should be only slightly lower than that of the buffer solution. Good's buffers [7–9] were specifically designed to achieve buffering with the minimum of concurrent ionic strength and conductivity and were for that reason employed in both the present and previous studies [1] with the express intention of using CE as the final method of analysis. In the techniques described above analyte anions displace MES^- counterions on a quaternary bonded silica surface and both analyte anions and MES^- counterions are subsequently eluted by a TAPS buffer solution at a pH close to its pK of 8.55 in which half the TAPS molecules are anionic. It is to be expected that in the absence of a more complicated exchange mechanism $TAPS^-$ anions would displace MES^- anions on a one-for-one basis and in consequence the ionic strength of the eluates should not exceed that of the eluent TAPS buffer (the contribution from eluting analytes being minute in the present case). As the specific purpose of the techniques described in this work was to obtain conditions which closely resembled those suggested by Vinther and Soeberg [12] it was considered necessary to prove by appropriate conductivity measurements that this had in fact been achieved (prompted by referee).

Conductance (reciprocal resistance in units of μS) data together with other column and buffer parameters are summarised in Table 3 corresponding to the experiment described in Table 2 for 50 mM TAPS as the eluent buffer. The data in Table 3 show several interesting features. The first eluate (E1) has a conductance which obviously reflects the loss of cations from the 5-ml reference analyte solution with which the anion-exchange column was loaded. This analyte reference solution has a conductance of 645 μS. The next two eluates E2 and E3 have conductances that reflect the two 5-ml water washes which precede elution with TAPS buffer. The conductances and pH values of eluates E4–E7 show that

Table 3
Conductivity, pH and CE parameters for the eluates of the quaternary bonded silica anion-exchange column for which analyte recoveries were given in Table 2

Parameter	Eluate No.						
	E1	E2	E3	E4	E5	E6	E7
pH of eluate	6.23	5.95	5.62	7.78	8.49	8.54	8.53
Conductance (μS)	504	327	116	1036	1460	1479	1526
Recovery (%) of analyte after CE in 50 mM MES	0	0	0	83.5	14.9	0	0
Capillary current (μA) at 25 kV	34.0	34.0	34..0	34.2	34.2	34.2	34.2

Eluent was 50 mM TAPS, pH 8.54 from E4 to E7. Conductivities may be obtained in SI units (S m^{-1}) by multiplying conductances by the conductivity cell constant which is 83 in these studies. Conductance of 50 mM TAPS, pH 8.54 was 1553 μS. Conductance of the CE buffer, 50 mM MES, pH 5.99 was 1540 μS. Conductance of 100 mM MES buffer, pH 7.2, used for establishing the MES anion as the counteranion was 4510 μS.

the conductance and pH of the eluent TAPS buffer (1553 μS and pH 8.54, respectively) are not approached until the last eluate E7. The analytes are eluted sharply at E4–E5 when conductances have values relative to the CE buffer (50 m*M* MES, pH 5.99, conductance 1534 μS) which are as close to those required by the rules of Vinther and Soeberg as could reasonably be expected. The properties of MES buffer with respect to the CE of the analytes in this study has been fully described previously [1].

The data in Table 4 show the effect of changing the eluent buffer to 25 m*M* TAPS, pH 8.43. The conductance of the eluates is what might be predicted from the data for 50 m*M* TAPS and a lower molarity of MES buffer could be used for the CE which would be speeded up in consequence. There appears to be a delayed appearance of analytes in the eluates and this might not be considered a desirable feature.

It may be noted that the capillary currents during the CE of any of the eluates described in Tables 3 and 4 show little variation with conductance of the analysed eluate although these vary from 89 up to 1526 μS.

3.6. Experimental demonstration of retention in diffuse and compact layers

It is now generally accepted that when ion-exchange processes occur at surfaces as distinct from within microporous gel beds the mechanism of retention must be associated with the presence of the electrical double layer at the surface [10,11,13–15]. The theory of Afrashtehfar and Cantwell [10] requires two distinctly different retention modes when a sample anion is retained by a surface quaternised material: adsorption in a compact layer and ion exchange in a diffuse layer. The exact details of the behaviour of a sample molecule in this system depends critically on the nature of the sample and the nature of the electrolytes in the mobile phase [10]. The above authors did not demonstrate experimentally the separate elution of analyte or other ions from compact or diffuse layers, but showed that the theoretical total analyte capacity factor agreed with experiment and was equal to the sum of theoretically derived contributions from the compact and diffuse layers.

It was hypothesised that if retention of analyte or other counterion does occur by way of a dual mechanism, it should be possible to arrange conditions such that dual elution from the two retention sites could be demonstrated experimentally. The method chosen was to apply the sample analytes in a solution containing a relatively high concentration of other anions which would compete for available sites in the compact and diffuse layers. Columns equilibrated with the MES anion, in which the retention of analytes appears to be predominantly

Table 4
Analyte recovery, pH and conductivity data when the 1-g quaternary bonded silica anion-exchange column is eluted with 25 m*M* TAPS buffer, pH 8.43 at E4–E7 followed by analysis using CE

Parameter	Eluate No.						
	E1	E2	E3	E4	E5	E6	E7
pH of eluate	5.96	5.61	5.28	6.64	8.05	8.31	8.31
Conductance (μS)	406	198	89.2	579	807	886	882
Recovery (%) of analyte after CE in 50 m*M* MES	0	0	0	26.7	65.3	5.9	0
Capillary current (μA) at 25 kV	34.2	34.2	33.6	33.8	33.9	33.7	33.8

Column equilibrated, loaded and apart from the molarity and pH of the TAPS buffer, eluted and the eluates analysed as described in Tables 2 and 3. Conductivities may be obtained in SI units (S m^{-1}) by multiplying conductances by the conductivity cell constant which is 83 in these studies. Conductance of 25 m*M* TAPS, pH 8.43 was 851 μS.

by adsorption into the compact layer and in which competition with other ions might force retention of a proportion of sample anions in the diffuse layer, were chosen for this experiment. Fig. 5 shows the results of this experiment when the reference analytes are applied to the column in solution with 150 m*M* sodium chloride. The expected bimodal elution pattern corresponding to the bimodal retention mechanism is evident with analytes leaching out of the diffuse layer at E1–E3 with desorption from the compact layer in E4–E5 after elution with 50 m*M* TAPS is commenced at E4. Elution at E4 and onwards by 50 m*M* TAPS (pH 8.65) means that the sample analytes would be fully ionised throughout the entire elution protocol. Attempts to reduce the thickness of the double layer by washing the prepared column with 5 ml methanol [16] immediately prior to loading with sample and thereby varying the bimodal elution pattern gave an elution pattern not conclusively different from the untreated column (Fig. 5). It may be noted

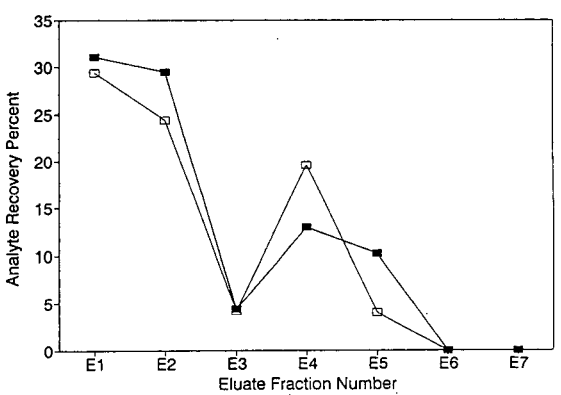

Fig. 5. Illustrating differential elution from the compact and diffuse regions of the electrical double layer when the reference analytes are applied to the 1-g bonded silica columns in solution with 150 m*M* sodium chloride. Columns equilibrated with MES counterion. Key: ◘ = normal column preparation and elution procedure as described in text and in caption to Fig. 1 except that 50 m*M* TAPS, pH 8.6 was the eluent at E4 and onwards; □ = column washed once with 5 ml methanol before application of sample at E1 then eluted as described for Fig. 1 until E4 when elution continued with 50 m*M* TAPS, pH 8.6.

that in these experiments it required a 75-fold excess of chloride ions to partially displace the analyte anions from the adsorption layer. The organic analytes appear to have a considerable competitive advantage in occupying sites in the compact layer.

3.7. Analytical implications

The experimental protocol described above in which MES-equilibrated columns are loaded with sample, washed with water and eluted with 50 m*M* TAPS buffer provides extracts suitable for analysis by CE when tested against an artificial reference sample of organic anions. The transcript of the recorder tracing of the electropherogram obtained from the analysis by CE of the eluate E4 corresponding to the experiment described by Tables 2 and 3 for elution by 50 m*M* TAPS, pH 8.54 is illustrated in Fig. 6. The essentials of this protocol are summarised in Fig. 7 in diagrammatic form. In accordance with the mechanism described above the buffers HEPES, MOPS and MOPSO would be expected to be effective as eluents although with progressively decreasing efficiency when compared with TAPS. If direct assay by HPLC were intended the buffers with the lower p*K* values would appear to be good candidates as eluents. Future work will be aimed at adapting the protocol to the analysis of biological fluids such as urine and blood. There are many substances in both these fluids which are structurally similar to the reference analytes chosen for the present work and there appears to be no reason why these techniques should not be applicable. The present work deliberately employed worst-scenario large sample volumes of 5 ml and relatively small amounts of exchange material. These proportions could be varied significantly together with other parameters in a protocol suitable for fluids such as urine or blood in which the challenge from strong electrolytes is both considerable and variable.

Despite their many admirable properties Good's buffers are not often the choice of many

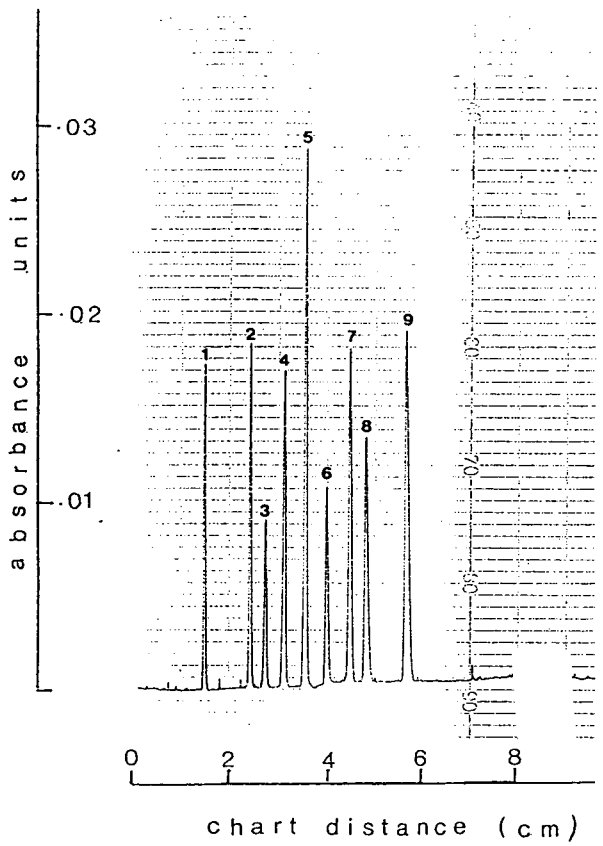

Fig. 6. The electropherogram obtained by the CE of eluate 4 (E4) of the experiment described in Tables 2 and 3 for elution of the anion exchange column with 50 m*M* TAPS buffer, pH 8.54. Peaks (retention times in minutes in brackets): 1 = urocanic acid (4.11); 2 = uric acid (4.55); 3 = VMA (4.72); 4 = hippuric acid (4.91); 5 = cinnamic acid (5.12); 6 = phenylacetic acid (5.35); 7 = orotic acid (5.59); 8 = benzoic acid (5.76); 9 = salicylic acid (6.17). Conditions for CE: capillary 57 cm × 75 μm, UV detection at 214 nm, high-pressure sampling for 5 s, running buffer 50 m*M* MES, pH 5.99, temperature 25°C, voltage 25 kV with 10-s ramp up time. Recorder chart speed 2 cm/min.

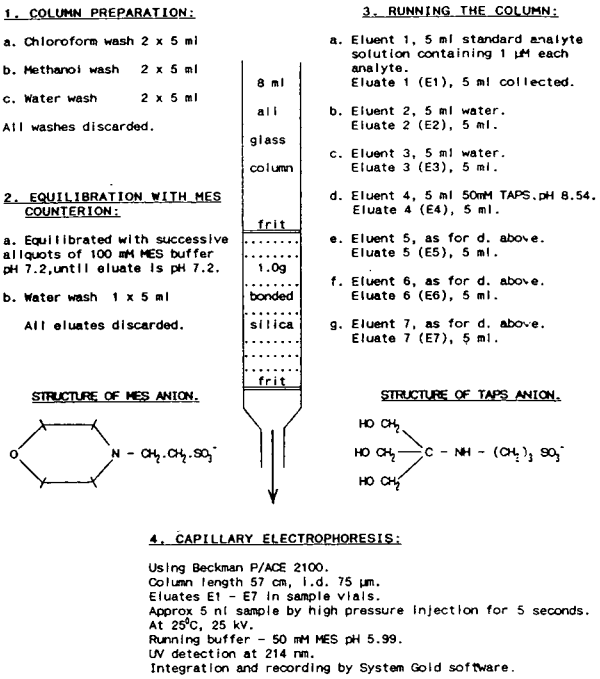

Fig. 7. Diagrammatic summary of the techniques described in the text when combined to give a method for the analysis of the organic anions present in a test solution at concentration 200 m*M*.

analysts for work in the pH range 6–10 and it is difficult to understand why this should be. In contrast a variety of other sulphonates such as hexyl-, heptyl- or octyl-sulphonate are widely used as anionic "pairing agents" in ion-pair chromatography [17]. Walton and Rocklin [18] in discussing eluents suitable for anion exchange, make no mention of the anions of Good's buffers as eluents.

Acknowledgements

The author thanks Mr. P. Hudson for help in file management in the course of the preparation of the manuscript using a word processing program. The assistance of Mr. R.I. Dodman in the preparation of Fig. 7 is acknowledged with gratitude.

References

[1] R.H.P. Reid, *J. Chromatogr. A*, 669 (1994) 151–183.

[2] R.H.P. Reid, M. Craft, L. Wise and E.C.G. Roberts, in H. Holy (Editor), *Automation in Analytical Chemistry*, Technicon Symposium, London, 1965, p. 671.
[3] R.H.P. Reid, M. Craft, L. Wise and E.C.G. Roberts, in D.I. Schmidt (Editor), *Automation in der Analytischen Chemie*, Internationalen Technicon Symposiums, Frankfurt am Main, 1965, p. 499.
[4] M.C. Roach, P. Gozel and R.N. Zare, *J. Chromatogr.*, 426 (1988) 129.
[5] W. Thorman, P. Meier, C. Marcolli and F. Binder, *J. Chromatogr.*, 545 (1991) 445.
[6] T. Nakagawa, Y. Oda, A. Shibukawa, H. Fukuda and H. Tanaka, *Chem. Pharm. Bull.*, 37 (1989) 707.
[7] N.E. Good, G.D. Winget, W. Winter, T.N. Connolly, S. Isawa and R.M.M. Singh, *Biochemistry*, 5 (1966) 467–477.
[8] N.E. Good and S. Isawa, *Methods Enzymol.*, 24B (1972) 53–68.
[9] W.J. Ferguson, K.I. Braunschweiger, W.R. Braunschweiger, J.R. Smith, J.J. McCormick, C.C. Wasman, N.P. Jarvis, D.H. Bell and N.E. Good, *Anal. Biochem.*, 104 (1980) 300–310.
[10] S. Afrashtehfar and F. Cantwell, *Anal. Chem.*, 54 (1982) 2422–2427.
[11] H.F. Walton and R.D. Rocklin, *Ion Exchange in Analytical Chemistry*, CRC Press, Boca Raton, FL, 1990, p. 19.
[12] A. Vinther and H. Soeberg, *J. Chromatogr.*, 559 (1991) 3–26.
[13] B.A. Bidlingmeyer, S.N. Deming, W.P. Price, B. Sachok and M. Petrusek, *J. Chromatogr.*, 186 (1979) 419.
[14] B.A. Bidlingmeyer, *J. Chromatogr. Sci.*, 18 (1980) 525.
[15] A. Iskanderani and D.J. Pietrzyk, *Anal. Chem.*, 54 (1982) 1065.
[16] K. Salomon, D.S. Burgi and J.C. Helmer, *J. Chromatogr.*, 559 (1991) 69.
[17] H.F. Walton and R.D. Rocklin, *Ion Exchange in Analytical Chemistry*, CRC Press, Boca Raton, FL, 1990, p. 117.
[18] H.F. Walton and R.D. Rocklin, *Ion Exchange in Analytical Chemistry*, CRC Press, Boca Raton, FL, 1990, pp. 59, 63.

ELSEVIER

Journal of Chromatography A, 684 (1994) 235–242

JOURNAL OF CHROMATOGRAPHY A

High-performance liquid chromatography of enantiomers of {2-[4-(3-ethoxy-2-hydroxypropoxy)phenylcarbamoyl]ethyl}-dimethylsulfonium *p*-toluenesulfonate (suplatast tosilate) on a cellulose tris-3,5-dimethylphenylcarbamate column

Takanori Ushio[a,*], Keiji Yamamoto[b]

[a]*Department of Analytical Research, Pharmaceutical Research Laboratory, Taiho Pharmaceutical Co., Ltd., 224-2, Ebisuno, Hiraishi, Kawauchi-cho, Tokushima 771-01, Japan*

[b]*Faculty of Pharmaceutical Sciences, Chiba University, 1-33 Yayoi-cho, Inage-ku, Chiba 263, Japan*

First received 29 March 1994; revised manuscript received 21 June 1994

Abstract

A high-performance liquid chromatographic method for the direct chiral resolution of suplatast tosilate (ST), {2-[4-(3-ethoxy-2-hydroxypropoxy)phenylcarbamoyl]ethyl}dimethylsulfonium *p*-toluenesulfonate and its decomposed products was developed using a cellulose tris-3,5-dimethylphenylcarbamate (Chiralcel OD-H) column eluted with a mixture of *n*-hexane, ethanol, trifluoroacetic acid and diethylamine. The method was applied to determination of the enantiomeric excess and chiral resolution of decomposed products of ST. The enantiomeric purity of the alternatively synthesized enantiomers was estimated to be 98.6% and 99.7% (enantiomeric excess) for (+)- and (−)-ST, respectively. No racemization of ST enantiomer was observed with decomposition at pH 6.8 and 37°C.

1. Introduction

Suplatast tosilate (ST), (±)-{2-[4-(3-ethoxy-2 hydroxypropoxy)phenylcarbamoyl]ethyl}dimethylsulfonium *p*-toluenesulfonate (under application for approval as a new anti-allergic drug by Taiho Pharmaceutical) shows effectiveness for the treatment of Type I allergy-related diseases such as bronchial asthma, allergic rhinitis, urticaria and similar maladies [1–6]. ST is a glycerol derivative containing a chiral centre and is available only as racemates in therapeutic formulations. In order to investigate the pharmacological, pharmacokinetic and toxicological properties of ST, enantiomers of ST were synthesized from enantiomers of 4-(3-ethoxy-2-hydroxypropoxy)aniline (D-2). Several physico-chemical properties of ST enantiomers were also examined. (+)-ST enantiomer showed a very small specific rotation, $[\alpha]_D^{25} = +1.7°$ (5% methanolic solution), which coincides well with the specific rotations of glycerol derivatives reported by Nelson et al. [7]. Although plasma levels of ST after oral administration in rats and dogs have been determined indirectly by measuring 4-(3-ethoxy-2-hydroxypropoxy)acrylanilide (D-1), a major metabolite which was produced quantita-

* Corresponding author.

0021-9673/94/$07.00
SSDI 0021-9673(94)00584-V

tively by alkaline hydrolysis of ST, the analytical method was complicated [8].

Chiral resolutions of β-brocking drugs [9] and many other drugs [10–21] have been successfully accomplished by using a cellulose derivative column. This paper describes the direct separation of ST enantiomers using a cellulose tris-3,5-dimethylphenylcarbamate column. Applications of the method to the determination of the optical purity of the alternatively synthesized ST enantiomers and to stability studies of enantiomers and racemates in solution are described.

2. Experimental

2.1. Chemicals

ST was synthesized in Taiho Fine Chemical (Saitama, Japan). (±)-4-(3-Ethoxy-2-hydroxypropoxy) - 3 - (methylthio)propionanilide (D-3), enantiomers of ST and enantiomers of D-3 were synthesized from racemic or optically resolved D-2 at Taiho Pharmaceutical (Tokushima, Japan).

Compounds **1–6** and D-1 shown in Fig. 1 were synthesized at Taiho Pharmaceutical.

n-Hexane and ethanol of HPLC-grade and diethylamine (DEA) and trifluoroacetic acid (TFA) of analytical-reagent grade were obtained from Wako (Osaka, Japan) and used as received.

2.2. HPLC apparatus and conditions

The HPLC system used consisted of an LC-6A pump, an SPD-6A detector operating at 254 nm, a CR 4A integrator (Shimadzu, Kyoto, Japan), a Rheodyne Model 7125 valve injector with a 20-μl sample loop (purchased from GL Sciences, Tokyo, Japan) or a WISP Model 710 autosampler (Waters Chromatography Division, Millipore, Milford, MA, USA), and a CS-300C column cabinet (Chromato Science, Osaka, Japan).

The following chiral HPLC columns were used: Chiralcel OD-H column, cellulose tris-3,5-dimethylphenylcarbamate coated on silica gel (25 cm × 0.46 cm I.D., particle size 5 μm); Chiralcel

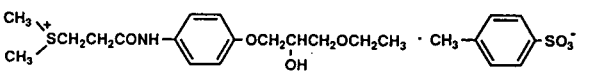

Suplatast tosilate

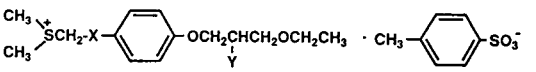

	X	Y
Compound 1 : CH_2CONH		OCH_3
Compound 2 : CONH		OH
Compound 3 : CH_2CH_2CONH		OH
Compound 4 : CH_2O		OH

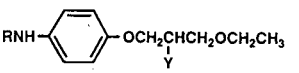

	R	Y
D-1	: CH_2=CHCO	OH
D-2	: H	OH
D-3	: $CH_3SCH_2CH_2CO$	OH
Compound 5 : CH_2=CHCO		OCH_3
Compound 6 : $CH_3SCH_2CH_2CO$		OCH_3

Fig. 1. Structures of suplatast tosilate and related compounds.

OG and Chiralcel OJ columns, cellulose tris-4-methylphenylcarbamate and cellulose tris-4-methylbenzoate, respectively, coated on silica gel (25 cm × 0.46 cm I.D., particle size 10 μm). All columns were obtained from Daicel Chemical Industries (Tokyo, Japan).

Racemic ST and related compounds were dissolved in methanol at concentrations of 1 mg/ml. ST enantiomers were dissolved in methanol at concentrations of 0.5 mg/ml. The volume injected was 10 μl and the flow-rate was 0.8 ml/min. The effects of mobile phase composition (ethanol, TFA and DEA contents), column temperature and sample size on the capacity factor (k'), enantioseparation factor (α), resolution (R_s) and tailing factor (T) were calculated from the recorded chromatograms as reported previously [22].

2.3. Decomposition of ST

About 0.20 g of ST or its enantiomers was weighed accurately, dissolved in 0.2 *M* phosphate buffer (pH 6.8) and kept at 37°C. A 3-ml volume of sample solution was withdrawn after 44 h and freeze-dried. The residue was dissolved in 3 ml of methanol and filtered. Each enantiomer of ST was determined by loading the filtrate under the optimized conditions.

3. Results and discussion

3.1. Optimization of chromatographic conditions

Preliminary studies showed that the presence of an amine in mobile phase was essential for the chiral separation of ST on a Chiralcel OD-H column. We found that the addition of an acid to the mobile phase was also necessary for the elution of ST from a silica gel column and that ST was extremely unstable in alkaline media. Thus, both TFA as an acid and DEA as an amine were added to mobile phase for the successful chiral separation of ST.

Effects of organic modifier

The influence of different types of alcohol in mobile phase on the enantioseparation factor, resolution, capacity factor and tailing factor of the second-eluted peak and peak-area ratios of enantiomers of ST is shown in Table 1 using a mixture of *n*-hexane and alcohol (75:25, v/v) containing 0.5% TFA and 0.1% DEA at 25°C as the eluent. With an increase in the alkyl chain length of the alcoholic modifier, longer retention times and greater peak broadening were observed. As the enantioseparation factor and resolution became smaller, the peak-area ratio of the enantiomers gradually deviated from 1.0, especially with *n*-butanol. In addition, the enantiomer peaks were not observed within 1 h when 2-propanol was used. When the concentration of 2-propanol was increased to 40%, however, the enantiomer peaks were observed, but all chromatographic parameters were unsatisfactory compared with the use of ethanol.

Effects of ethanol content in the mobile phase on the chromatographic parameters

The effects of ethanol content in the mobile phase were investigated at 25°C using a mixture of *n*-hexane and ethanol containing 0.5% TFA and 0.1% DEA. The results are summarized in Table 2. With an increase in ethanol content, the capacity factors of both isomers decreased. A favourable enantioseparation factor and resolution were obtained under all conditions, and (+)-ST was always eluted faster than (−)-ST. The optimum enantioseparation factor was determined at 25% or 30% ethanol content. The resolution became higher with a decrease in ethanol content. Because the second peak appeared 1 h after injection with a 15% of ethanol content, it was concluded that 25% ethanol was suitable.

Table 1
Effects of organic modifier in the mobile phase on the chromatographic parameters and peak-area ratio of (+)- and (−)-enantiomers of ST

Mobile phase	k'_2	α	R_S	T	r
n-Hexane–ethanol (75:25)	3.92	1.39	2.85	1.42	1.00
n-Hexane–*n*-propanol (75:25)	5.08	1.32	2.03	1.80	0.97
n-Hexane–*n*-butanol (75:25)	5.24	1.27	1.17	2.24	0.81
n-Hexane–2-propanol (60:40)	4.44	1.38	2.16	1.81	0.98

Chromatographic conditions: column, Chiralcel OD-H; mobile phase, as indicated, containing 0.5% TFA and 0.1% DEA; column temperature, 25°C; flow-rate, 0.8 ml/min; detection wavelength, 254 nm. k'_2 = Capacity factor of second-eluted peak; T = tailing factor of second-eluted peak; r = peak-area ratio of (+)- to (−)-enantiomer.

Table 2
Effects of ethanol on the retention and resolution of ST enantiomers

Ethanol (%)	k'_1	k'_2	α	R_S
15	8.42	11.39	1.35	3.71
20	4.70	6.37	1.36	3.06
25	2.89	3.95	1.37	2.63
30	1.96	2.70	1.37	2.39

Chromatographic conditions: column, Chiralcel OD-H; mobile phase, *n*-hexane–ethanol containing 0.5% TFA and 0.1% DEA; column temperature, 25°C; flow-rate, 0.8 ml/min; detection wavelength, 254 nm. k'_1 = Capacity factor of first-eluted peak; k'_2 = capacity factor of second eluted peak.

Effects of TFA content in the mobile phase on the chromatographic parameters

The effects of TFA content in the mobile phase were investigated by adding 0.125–0.75% TFA to *n*-hexane–ethanol (75:25, v/v) containing 0.1% DEA at 25°C. The results are shown in Table 3. The mobile phase is basic with a 0.125% TFA content and acidic with 0.25% or more. With an increase in TFA content in acidic media, the capacity factors decreased. This was expected as ST is a tautomeric compound having an amide group. Therefore, the structural change of ST seems to be responsible for the observed variation of the capacity factor. Both the enantioseparation factor and resolution were not affected by TFA content, and 0.5% TFA content was chosen.

Table 3
Effects of TFA on the retention and resolution of ST enantiomers

TFA (%)	k'_1	k'_2	α	R_S
0.75	4.53	6.19	1.36	3.11
0.5	4.70	6.37	1.36	3.06
0.25	4.77	6.44	1.35	3.17
0.125	4.50	6.02	1.34	3.11

Chromatographic conditions: column, Chiralcel OD-H; mobile phase, *n*-hexane–ethanol (75:25) containing 0.1% DEA and TFA (variable); column temperature, 25°C; flow-rate, 0.8 ml/min; detection wavelength, 254 nm. k'_1 = Capacity factor of first-eluted peak; k'_2 = capacity factor of second-eluted peak.

Effects of DEA content in the mobile phase on the chromatographic parameters

The effects of DEA content in the mobile phase were determined by adding 0–0.15% DEA to *n*-hexane–ethanol (75:25, v/v) containing 0.5% TFA at 25°C. The results are shown in Table 4. With an increase in DEA content, the capacity factors were decreased, and each enantiomer was incompletely resolved in the absence of DEA. The enantioseparation factor and resolution were not affected by the DEA content. Therefore, a 0.1% DEA content was selected.

Effects of column temperature

The effects of column temperature on the capacity factors, enantioseparation factor and resolution of ST were determined in the range 5–35°C using mobile phases A and B, which include 20 and 25% ethanol in *n*-hexane, respectively, and both containing 0.5% TFA and 0.1% DEA. The results are shown in Table 5. With an increase in the column temperature, the capacity factor, enantioseparation factor and resolution were decreased with both mobile phases, and a lower temperature resulted in good resolution. The resolution was almost the same when mobile phase A at 25°C (condition A) or mobile phase B at 15°C (condition B) were employed, but the enantioseparation factor was higher under the

Table 4
Effects of DEA on the retention and resolution of ST enantiomers

DEA (%)	k'_1	k'_2	α	R_S
0.15	4.39	5.97	1.36	2.98
0.1	4.70	6.37	1.36	3.06
0.075	4.89	6.66	1.36	3.07
0.05	4.98	6.78	1.36	3.14
0	6.07	7.95	1.31	1.18

Chromatographic conditions: column, Chiralcel OD-H; mobile phase, *n*-hexane–ethanol (75:25) containing 0.5% TFA and DEA (variable); column temperature, 25°C; flow-rate, 0.8 ml/min; detection wavelength, 254 nm. k'_1 = Capacity factor of first-eluted peak; k'_2 = capacity factor of second-eluted peak.

Table 5
Effects of column temperature on the retention and resolution of ST enantiomers

Temperature (°C)	Mobile phase A[a]				Mobile phase B[b]			
	k'_1	k'_2	α	R_S	k'_1	k'_2	α	R_S
35	3.62	4.66	1.29	2.47	2.41	3.13	1.30	2.02
30	4.16	5.49	1.32	2.76	2.74	3.65	1.33	2.38
25	4.70	6.37	1.36	3.06	2.89	3.95	1.37	2.63
20	5.59	7.89	1.41	3.49	3.19	4.48	1.40	2.93
15	6.32	9.13	1.44	3.60	3.62	5.25	1.45	3.10
10	–	–	–	–	4.07	6.04	1.48	3.40
5	–	–	–	–	4.92	7.43	1.51	3.39

Chromatographic conditions: column, Chiralcel OD-H; flow-rate, 0.8 ml/min; detection wavelength, 254 nm. k'_1 = Capacity factor of first-eluted peak; k'_2 = capacity factor of second eluted peak.
[a] *n*-Hexane–ethanol (80:20) containing 0.5% TFA and 0.1% DEA.
[b] *n*-Hexane–ethanol (75:25) containing 0.5% TFA and 0.1% DEA.

condition B than condition A. In addition, condition A needs a longer time for the analysis. Therefore, condition B is preferable for determination.

Effects of sample size

The effects of sample size on the capacity factors, enantioseparation factor, resolution, peak areas and peak-area ratios of the ST enantiomers were investigated using condition B. The results are shown in Table 6. With an increase in sample size, the capacity factors and resolution decreased, but the enantioseparation factor showed no dependence on the sample size.

Table 6
Effects of amount loaded on the retention and resolution of ST enantiomers

Amount loaded (μg)	k'_1	k'_2	α	R_S
10	3.92	5.67	1.45	3.11
7.5	3.93	5.69	1.45	3.29
5.0	3.97	5.75	1.45	3.55
2.5	4.01	5.77	1.44	3.88
1.25	4.13	5.92	1.43	3.85

Chromatographic conditions: column, Chiralcel OD-H; mobile phase, *n*-hexane–ethanol (75:25) containing 0.5% TFA and 0.1% DEA; column temperature, 15°C; flow-rate, 0.8 ml/min; detection wavelength, 254 nm. k'_1 = Capacity factor of first-eluted peak; k'_2 = capacity factor of second-eluted peak.

A chromatogram of ST under the optimized conditions is shown in Fig. 2. The plot of peak area against amount of ST loaded over the range 1.25–10 μg showed good linearity with correlation coefficients (r) of 0.9999 and 0.9998 for (+)- and (−)-ST, respectively. The peak-area ratios of two enantiomers were 1.00 for all sample sizes.

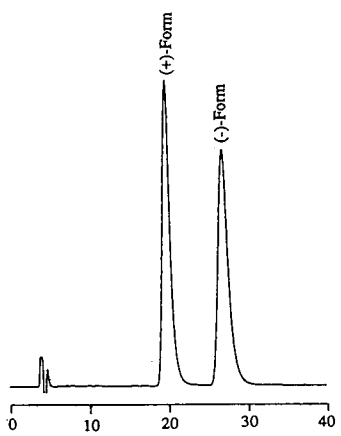

Fig. 2. Chromatogram of ST enantiomers on the Chiralcel OD-H column. Mobile phase, *n*-hexane–ethanol (75:25) containing 0.5% TFA and 0.1% DEA; flow-rate, 0.8 ml/min; detection wavelength, 254 nm; column temperature, 15°C; amount loaded, 5 μg.

This means that the optical purity of the enantiomer can be determined by the area percentage method.

3.2. Chiral resolution of ST and related compounds

The capacity factors and enantioseparation factor of ST and related compounds were determined using mobile phase B and Chiralcel OD-H, Chiralcel OG and Chiralcel OJ columns at 15°C. The results are summarized in Table 7. On the Chiralcel OD-H column, ST enantiomers were resolved with an enantioseparation factor of 1.40, while the methylation of the hydroxyl group of ST (compound **1**) resulted in poor retentivity and enantioselectivity. The same was observed with D-1 and **5** and with D-3 and **6**. It is interesting that **2** and **3**, having shorter and longer alkyl chains, were not resolved under condition B. It was impossible to resolve **4**, which has no amide or amine group on the side-chain, on the Chiralcel OD-H column. However, on the Chiralcel OG column, the enantiomers of **4** were resolved with an enantioseparation factor of 1.19. The enantiomers of **2** and **3** were successfully resolved by using the Chiralcel OG column. On the Chiralcel OJ column, the compounds except **4** and **6** were not resolved at all; **4** and **6** were partly resolved with enantioseparation factors of 1.09 and 1.06, respectively. The chiral recognition is assumed to be due to the formation of inclusion complexes [23] and binding to the polar carbamate groups. The racemates interact with the carbamate group via hydrogen bonding with the NH and C=O groups and dipole–dipole interaction with C=O group [11,24,25]. Further, the hydroxyl group of the amino alcohol seems to be of importance for the chiral recognition process [17]. The results for the chiral resolution of ST and related compounds on the cellulose trisphenylcarbamate derivative column coincided well with these results. It was also found that the length of the carbamoyl side-chain was the important factor for chiral recognition of ST.

It is noteworthy that the elution times of (−)-D-1 and (−)-D-3 was shorter than those of (+)-D-1 and (+)-D-3 on the Chiralcel OD-H column, while (+)-ST was eluted rapidly under the same condition. The dimethylsulfonium group of ST might greatly affect the elution order. The

Table 7
Capacity factors and enantioseparation factor of ST and related compounds on Chiralcel OD-H, Chiralcel OG and Chiralcel OJ columns

Substance	Chiralcel OD-H			Chiralcel OG			Chiralcel OJ		
	k'_1	k'_2	α	k'_1	k'_2	α	k'_1	k'_2	α
ST	3.99 (+)	5.59 (−)	1.40	20.1 (+)	28.1 (−)	1.40	2.32	2.32	1.00
1	1.58	1.86	1.18	11.5	11.5	1.00	2.17	2.17	1.00
2	2.29	2.29	1.00	11.9	15.1	1.26	2.53	2.53	1.00
3	1.73	1.73	1.00	9.40	11.8	1.25	1.50	1.50	1.00
4	1.22	1.22	1.00	9.69	11.5	1.19	1.95	2.12	1.09
D-1	0.94 (−)	1.14 (+)	1.20	1.94 (+)	2.23 (−)	1.15	1.10	1.10	1.00
D-2	0.18 (−)	0.21 (+)	1.16	0.72	0.72	1.00	0.21	0.21	1.00
D-3	1.24 (−)	1.44 (+)	1.17	3.85 (+)	4.54 (−)	1.18	2.28	2.28	1.00
5	0.76	0.76	1.00	3.05	3.05	1.00	1.41	1.41	1.00
6	0.88	0.88	1.00	3.36	3.36	1.00	2.16	2.28	1.06

Mobile phase, *n*-hexane–ethanol (75:25) containing 0.5% TFA and 0.1% DEA; column temperature, 15°C. k'_1 = Capacity factor of first-eluted peak; k'_2 = capacity factor of second-eluted peak; (+) and (−) mean (+)-enantiomer and (−)-enantiomer for each substance.

elution order of enantiomers of D-1 and D-3 on the Chiralcel OD-H column was opposite to that on the Chiralcel OG column. These results suggest that the substituent on the aromatic ring of the chiral stationary phase greatly affects the order of elution of enantiomers.

3.3. Determination of enantiomeric excess of ST

The enantiomeric excess (e.e.) of alternatively synthesized (+)- or (−)-ST was determined by the proposed method using *n*-hexane–ethanol (75:25, v/v) containing 0.5% TFA and 0.1% DEA as the eluent and a Chiralcel OD-H column at 15°C. The values obtained for (+)- and (−)-ST were 98.6 and 99.7% e.e., respectively.

3.4. Chiral resolution of decomposition products of ST

It has been reported that the decomposition of ST in acidic media results in the formation of D-2 together with a small amount of D-1 and D-3, and D-1 in alkaline media. The chromatogram of ST and its decomposed products is shown in Fig. 3. ST was separated completely from three decomposition products, and it was found that this HPLC condition could be used for the chiral resolution of the decomposition products of ST. For the complete separation of enantiomers of D-1, D-2 and D-3, we used a mobile phase with a low ethanol content (8.5%) and the chromatogram of the three decomposition products of ST is shown in Fig. 4. Although the resolution of D-2 enantiomers was incomplete under the conditions in Fig. 4, D-1 and D-3 enantiomers were completely resolved. For D-2, complete resolution was achieved when the mobile phase was changed to *n*-hexane–2-propanol (60:40, v/v) using the same column (Fig. 5). No racemization of ST enantiomer was observed with decomposition at pH 6.8 and at 37°C, and (+)- and (−)-STs yielded (+)- and (−)-decomposition products, respectively.

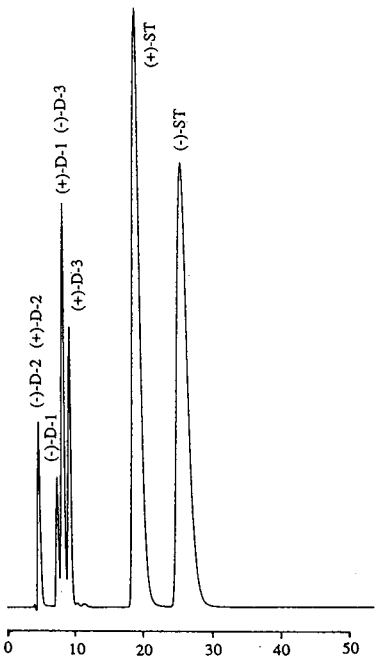

Fig. 3. Chiral resolution of ST and related compounds on the Chiralcel OD-H column. Mobile phase, *n*-hexane–ethanol (75:25) containing 0.5% TFA and 0.1% DEA; flow-rate, 0.8 ml/min; detection wavelength, 254 nm; column temperature, 15°C; amount loaded, 25 μg for ST and D-2 and 2.5 μg for D-1 and D-3.

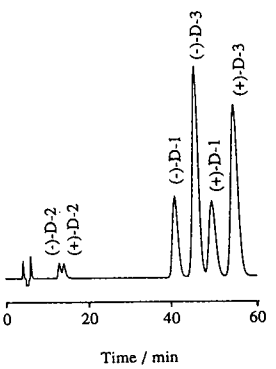

Fig. 4. Chromatogram of racemic D-1, D-2 and D-3 on the Chiralcel OD-H column. Mobile phase, *n*-hexane–ethanol (915:85) containing 0.5% TFA and 0.1% DEA; flow-rate, 0.8 ml/min; detection wavelength, 254 nm; column temperature, 15°C; amount loaded, 5 μg each.

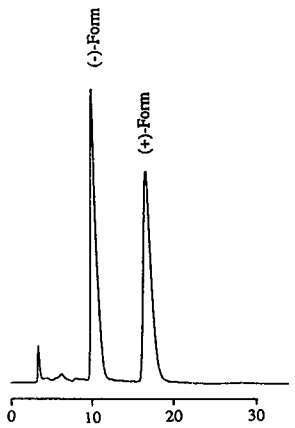

Fig. 5. Chromatogram of racemic D-2 on the Chiralcel OD-H column. Mobile phase, *n*-hexane–2-propanol (60:40); flow-rate, 0.8 ml/min; detection wavelength, 254 nm; column temperature, 15°C; amount loaded, 5 μg.

Acknowledgements

The authors are indebted to Dr. J. Haginaka, Mukogawa Women's University, for helpful comments on the manuscript and to Dr. Y. Tada, Mr. T. Hatayama and Mr. H. Nagasawa, Taiho Pharmaceutical, for supplying samples.

References

[1] E. Tsubura, S. Kobayashi, S. Makino, S. Takahashi, A. Miyamoto, T. Shida, M. Kawai, S. Kishimoto, S. Nakajima and N. Ogawa, Igaku No Ayumi, 162 (1992) 171.

[2] S. Baba, T. Takasaka, K. Baba, Y. Saito, Y. Sakakura, S. Iwata, T. Nishimura, T. Ishikawa and N. Ogawa, *Jpn. J. Inflamm.* 12 (1992) 379.

[3] A. Koda, Y. Yanagihara and N. Matsuura, *Agents Actions*, 34 (1991) 369.

[4] N. Matsuura, H. Mori, H. Nagai and A. Koda, *Folia Pharmacol. Jpn.*, 100 (1992) 485.

[5] Y. Yanagihara, M. Kiniwa, K. Ikizawa, H. Yamaya, T. Shida, N. Matsuura and A. Koda, *Jpn. J. Pharmacol.*, 61 (1993) 23.

[6] Y. Yanagihara, M. Kiniwa, K. Ikizawa, T. Shida, N. Matsuura and A. Koda, *Jpn. J. Pharmacol.*, 61 (1993) 31.

[7] W.L. Nelson, J.E. Wennerstrom and S.R. Sankar, *J. Org. Chem.*, 42 (1977) 1006.

[8] M. Tei, K. Kodama, A. Yafune, A. Muranushi, H. Takayanagi, M. Takebe, T. Shindoh, H. Masuda, K. Kuwata, E. Matsushima, K. Muramoto and Y. Umeno, *Clin. Rep.*, 26 (1992) 3199.

[9] Y. Okamoto, M. Kawashima, R. Aburatani, K. Hatada, T. Nishiyama and M. Nasoda, *Chem. Lett.*, (1986) 1237.

[10] Y. Okamoto, R. Aburatani, Y. Kaida and K. Hatada, *Chem. Lett.*, (1988) 1125.

[11] Y. Okamoto, M. Kawashima and K. Hatada, *J. Chromatogr.*, 363 (1986) 173.

[12] Y. Okamoto, M. Kawashima, R. Aburatani, K. Hatada, T. Nishiyama and M. Nasoda, *J. Chromatogr.*, 389 (1987) 95.

[13] Y. Okamoto, M. Kawashima, R. Aburatani, K. Hatada, T. Nishiyama and M. Nasoda, *J. Chromatogr.*, 448 (1988) 454.

[14] Y. Okamoto, Y. Kaida, R. Aburatani and K. Hatada, *J. Chromatogr.*, 477 (1989) 367.

[15] F.A. Maris, R.J.M. Vervoort and H. Hindriks, *J. Chromatogr.*, 547 (1991) 45.

[16] E. Francotte and R.M. Wolf, *J. Chromatogr.*, 595 (1992) 63.

[17] K. Balmér, P.O. Lagerstroem, B.A. Persson and G. Schill, *J. Chromatogr.*, 592 (1992) 331.

[18] R. Isaksson, P. Erlandsson, L. Hansson, A. Holmberg and S. Berner, *J. Chromatogr.*, 498 (1990) 257.

[19] T. Hollenhorst and G. Blaschke, *J. Chromatogr.*, 585 (1991) 329.

[20] S.L. Lin, S.T. Chen, S.H. Wu and K.T. Wang, *J. Chromatogr.*, 540 (1991) 392.

[21] K. Ikeda, T. Hamasaki, H. Kohno, T. Ogawa, T. Matsumoto and J. Sakai, *Chem. Lett.*, (1989) 1089.

[22] R. Rosset, M. Caude and A. Jardy, *Chromatographie en Phase Liquide*, Masson, Paris, 1982.

[23] I.W. Wainer, R.M. Stiffin and T. Shibata, *J. Chromatogr.*, 411 (1987) 139.

[24] M.H. Gaffney, R.M. Stiffin and I.W. Wainer, *Chromatographia*, 27 (1989) 15.

[25] Y. Fukui, A. Ichida, T. Shibata and K. Mori, *J. Chromatogr.*, 515 (1990) 85.

ELSEVIER

Journal of Chromatography A, 684 (1994) 243–249

JOURNAL OF CHROMATOGRAPHY A

High-performance liquid chromatographic reversed-phase and normal-phase separation of diastereomeric α-ketoamide calpain inhibitors

Chichih Wu, Alan Akiyama, Julie Ann Straub*

Alkermes, Inc., 64 Sidney Street, Cambridge, MA 02139, USA

First received 16 June 1994; revised manuscript received 4 July 1994

Abstract

α-Ketoamide calpain inhibitors contain a stereochemically labile chiral center adjacent to the keto moiety, which when epimerized results in diastereomers. High-temperature C_4 reversed-phase HPLC methods were developed for analysis of general purity of α-ketoamide calpain inhibitors and resulted in the separation of diastereomers of the positively charged inhibitor, AK295. Normal-phase methods that employed a Nucleosil Chiral-2 column were developed for separation of diastereomers of uncharged α-ketoamides. These methods used conditions in which the keto moiety of the inhibitors was minimally affected by the mobile phase.

1. Introduction

Calpain, a proteolytic enzyme, is activated in brain tissue through increased levels of intracellular calcium following a stroke. Calpain inhibitors are being evaluated as therapeutics for the treatment of neurodegeneration associated with ischemic events. The synthesis and biological activity of peptidyl α-ketoamide calpain inhibitors have been described [1–4]. These inhibitors were initially analyzed by ^{1}H NMR spectroscopy, which revealed that inhibitors produced using Dakin–West chemistry [1] were a mixture of stereoisomers, and that a key chiral center was subject to epimerization. Only one of the stereoisomers was active, therefore it was important to monitor lot-to-lot variations in diastereomeric ratio and the stability of the chiral center in potential dosing formulations. Application of NMR analysis for the formulations was impractical; therefore, identification of an HPLC method for the analysis of diastereomeric ratio was required.

A number of approaches to the HPLC characterization of stereoisomers exist, including the use of chiral mobile phase additives, ligand exchange, charge transfer complex formation, and a variety of chiral stationary phases [5–7]. The inhibitors of interest (Fig. 1) possess two chiral centers, the chiral center directly adjacent (α) to the keto group was the stereocenter of interest. Epimerization of this center (L configuration in the desired isomer) results in the production of a diastereomer that has been shown to be inactive in enzyme inhibition assays [2]. HPLC is one of the most powerful separation techniques; therefore, resolution of the diastereomers by HPLC was expected to be

* Corresponding author.

0021-9673/94/$07.00
SSDI 0021-9673(94)00623-7

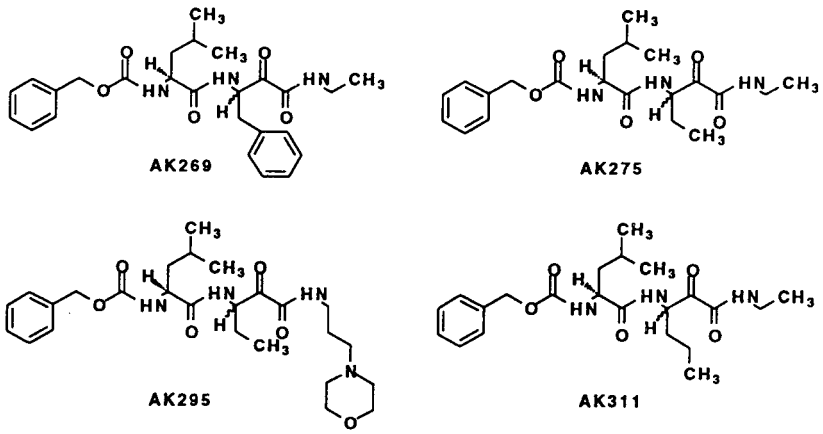

Fig. 1. Structures of calpain inhibitors. Chiral center of interest (α to ketone) has the hydrogen attached through a wavy bond.

relatively straightforward. However, the reactivity of the keto group present in the inhibitors was found to be a complicating factor. This paper describes the development of methods for such a separation.

2. Experimental

2.1. Materials

HPLC-grade acetonitrile, *n*-hexane, 1,4-dioxane, isopropanol and trifluoroacetic acid were obtained from Fisher Scientific. The calpain inhibitors were synthesized at Alkermes according to synthetic methods described in Refs. [1] and [2].

2.2. HPLC analysis

HPLC method A (general reversed-phase system)

The HPLC system consisted of a Hewlett-Packard 1050 HPLC system comprised of four reservoirs (only two used), a UV variable-wavelength absorbance detector, an autosampler equipped with a 100-μl loop and a HP 3396 series II integrator, and a Timberline Instruments column heater. The detector was set at 210 nm. The column used was a Vydac Protein C_4 column (5 μm particle size, 300 Å average pore diameter, 250 mm × 4.6 mm). The mobile phase consisted of a linear gradient system of 25% eluent B to 35% eluent B over 40 min (eluent A: 0.1% trifluoroacetic acid in water; eluent B: acetonitrile). The flow-rate was 1 ml/min. The column temperature was varied, with 60°C found to be the best temperature examined.

HPLC method B (reversed-phase system for AK295)

The HPLC system consisted of a Hewlett-Packard 1090M system Series II. The detector was set at 210 nm. The column used was a Vydac Protein C_4 column (5 μm particle size, 300 Å average pore diameter, 250 mm × 4.6 mm). The mobile phase consisted of a linear gradient system of 15% eluent B to 35% eluent B over 40 min (eluent A: 0.1% trifluoroacetic acid in water; eluent B: acetonitrile). The flow-rate was 1 ml/min. The column temperature was 60°C.

HPLC method C (Cyclobond column for analysis of AK269)

The HPLC system consisted of a Hewlett-Packard 1090M system. The detector was set at 210 nm. The column used as an ASTEC Cyclobond I (β-cyclodextrin) column. The mobile

phase consisted of a linear gradient from 27.5% eluent B to 37.5% eluent B over 30 min (eluent A: 0.1% triethylammonium phosphate, pH 4.0; eluent B: MeOH). The flow-rate was 1 ml/min. The column temperature was kept at 0°C by immersing the column in an ice bath.

HPLC method D (normal-phase analysis of AK275 on a Phenomenex column)

The HPLC system consisted of a Hewlett-Packard 1050 HPLC system comprised of four reservoirs (only one used), a UV variable-wavelength absorbance detector, an autosampler equipped with a 100-μl loop, and a HP 3396 series II integrator. The detector was set at 210 nm. The column was a Phenomenex Chirex (*S*)-Leu, (*R*)-1-(α-naphthyl)ethylamine (NEA) column (250 mm $\times$ 4.6 mm). According to the manufacturer, this column "consists of an optically pure amino acid derivative covalently bonded to δ-aminopropyl-silanized silica gel". The mobile phase consisted of an isocratic system of dioxane–hexane–acetonitrile (17:78:5). The flow-rate was 1 ml/min. The column temperature was ambient.

HPLC method E (normal-phase analysis of AK275 on a Nucleosil column)

The HPLC system consisted of a Hewlett-Packard 1050 series HPLC system comprised of four reservoirs (only one used), a UV variable-wavelength absorbance detector, an autosampler equipped with a 100-μl loop, and a HP 3396 series II integrator. The detector was set at 210 nm. The column was a Nucleosil Chiral-2 column (250 mm $\times$ 4 mm; Macherey–Nagel). The column has three chiral centers resulting from the bonding of L-tartaric acid and L-nitrobenzyl-phenylethylamine to Nucleosil silica via a propyl spacer. The mobile phase consisted of an isocratic system of hexane–1,4-dioxane–acetonitrile (86:11:3, v/v/v). The flow-rate was 1 ml/min. A new Nucleosil Chiral-2 column has to be preconditioned before use by washing the column with 30 ml methylene chloride, 30 ml isopropanol and 30 ml hexane at a flow-rate of 1 ml/min. The column temperature was ambient.

HPLC method F (normal-phase analysis of AK311 on a Nucleosil column)

The system is identical to method E except the mobile phase consisted of an isocratic system

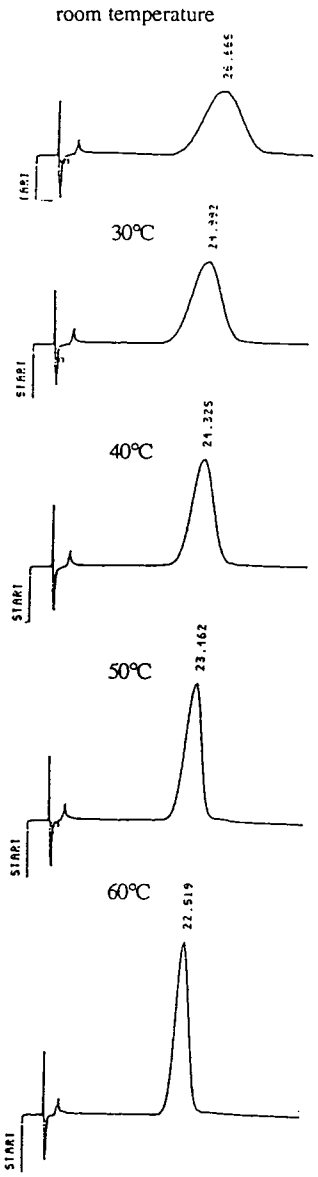

Fig. 2. Variable-temperature analysis (HPLC method A, reversed-phase) of AK275. Values at peaks are retention times in min.

of *n*-hexane–1,4-dioxane–acetonitrile (87:10:3, v/v/v).

HPLC method G (normal-phase analysis of AK269 on a Nucleosil column)

The system is identical to method E except the mobile phase consisted of an isocratic system of *n*-hexane–isopropanol–acetonitrile (94:4:2, v/v/v).

3. Results and discussion

The structures of the calpain inhibitors studied are shown in Fig. 1. The diastereomeric ratio of the calpain inhibitors could be evaluated by NMR techniques; however, this was time consuming and required significant sample quantity. Gas chromatography techniques were not an option, as the inhibitors were not sufficiently volatile. Therefore, an HPLC method for determining the diastereomeric ratio of inhibitor was needed.

A reversed-phase system (HPLC method A) was used for initial HPLC analyses. The effect of column temperature can be seen in Fig. 2. In the chromatograms of AK275 run near room temperature, the peak was broad. Increasing the column temperature improved the peak shape, increased the efficiency of the column and decreased the pressure drop. The best conditions were observed using a column temperature of 60°C. While high-temperature reversed-phase HPLC analysis has proven useful for general purity analysis, diastereomeric resolution was seen only for positively charged AK295 (Fig. 3, HPLC method B). Unfortunately, such high-temperature reversed-phase methods did not lead to separation of the diastereomers of the neutral compounds, AK275, AK311 and AK269.

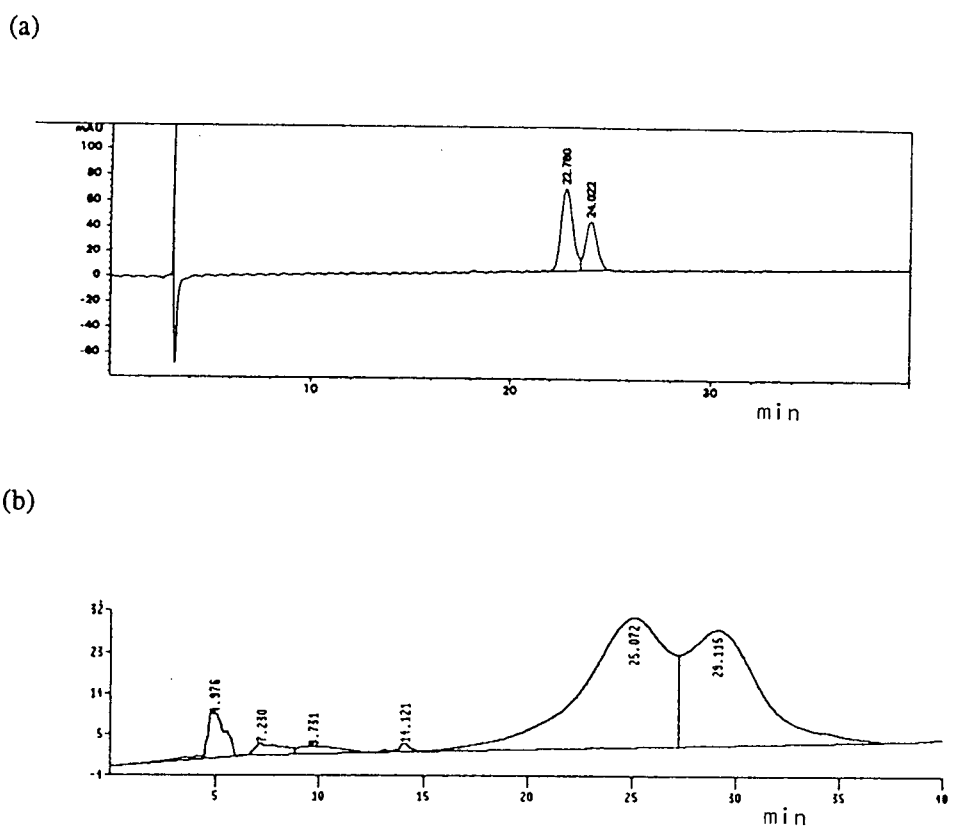

Fig. 3. Reversed-phase separation of calpain inhibitors: (a) AK295 (method B) and (b) AK269 (method C).

A large number of other aqueous-based HPLC systems were examined including Chiral Triacel, Chiralcel OD-R, cyclodextrin-based columns (Cyclobond I, II and III) and hydrophilic interaction (POROS OH/H from PerSeptive Biosystems). A system using Cyclobond II (HPLC method C) was found to give marginal separation of the diastereomers of AK269 (Fig. 3), which has the requisite aromatic group adjacent to the chiral center of interest. However, no separation of the diastereomers of AK275 and AK311 was seen in any reversed-phase system.

NMR studies indicated that the peak broadening seen in the chromatographic systems employing aqueous phases might have resulted from the reaction of the keto group of the inhibitors with water in mobile phase to form the hydrate. This ketone–hydrate equilibrium was affected by temperature, with the equilibrium shifted toward the ketone at higher temperatures (Fig. 4). Such a shift in the equilibrium might partially account for the improved peak shape in the high-temperature reversed-phase chromatography seen in Fig. 2. As the inclusion of water in the eluents appeared to be problematic, normal-phase HPLC methods were examined.

The neutral calpain inhibitors used in these studies were very hydrophobic molecules, which made them compatible with normal-phase HPLC analysis. Most of the inhibitors absorb strongly at 210 nm; therefore, we wanted to use 210 nm as the detection wavelength for maximum sensitivity. Unfortunately, the use of 210 nm limits the number of solvents that can be considered for the mobile phase. The solvents that were evaluated included *n*-hexane, *n*-heptane, dioxane, 1,2-dichloroethane, tetrahydrofuran and a few alcohols. Isocratic elution systems were used, which allowed the use of solvents such as 1,2-dichloroethane, which has a UV cut-off of 228 nm. The mobile phases containing hexane–dioxane or hexane–isopropanol mixtures were found to have the greatest promise for the diastereomeric separation. The addition of a small amount of acetonitrile sharpened the peaks and improved resolution.

The first observed chromatographic separation of the diastereomers of AK275 was performed

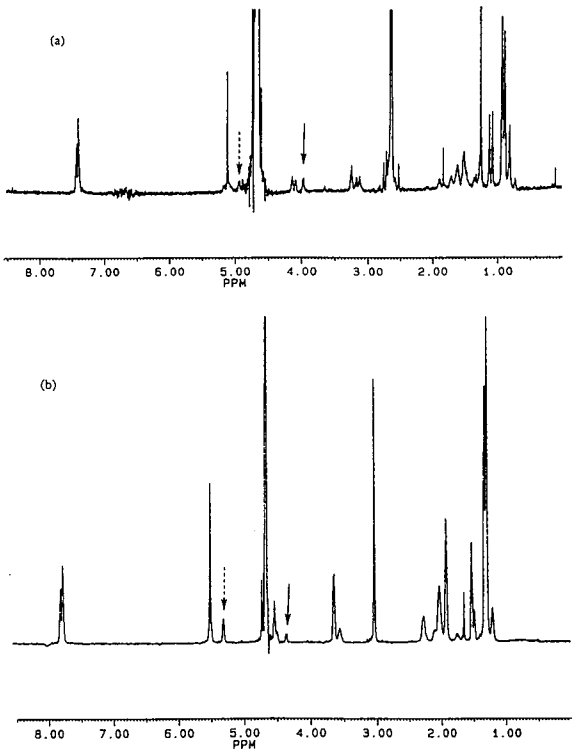

Fig. 4. Variable temperature ^1H NMR analysis of AK275 in ^2H_2O–[$^2H_6$]dimethyl sulfoxide (60:40): (a) room temperature; (b) 60°C. The dashed arrow indicates the position of the resonance of the hydrogen α to ketone. The solid arrow indicates the position of the resonance of the hydrogen α to the hydrated form of the ketone.

using a Phenomenex Chirex (*S*)-Leu and (*R*)-NEA column (Fig. 5a, method D). The mobile phase employed was hexane–1,4-dioxane–acetonitrile. It was subsequently found that a Nucleosil Chiral-2 column from Macherey–Nagel also resulted in separation of the diastereomers of AK275 (Fig. 5b, method E). New Nucleosil Chiral-2 columns had to be pretreated with methylene chloride, isopropanol and hexane before use, as the new column appeared to contain some storage solution with a high absorbance response at 210 nm. The inhibitor, AK311, was also successfully separated on a Chiral-2 column with a mobile phase of hexane–1,4-dioxane–acetonitrile (Fig. 5c, method F). AK269 required the use of a slightly different solvent system (hexane–isopropanol–acetoni-

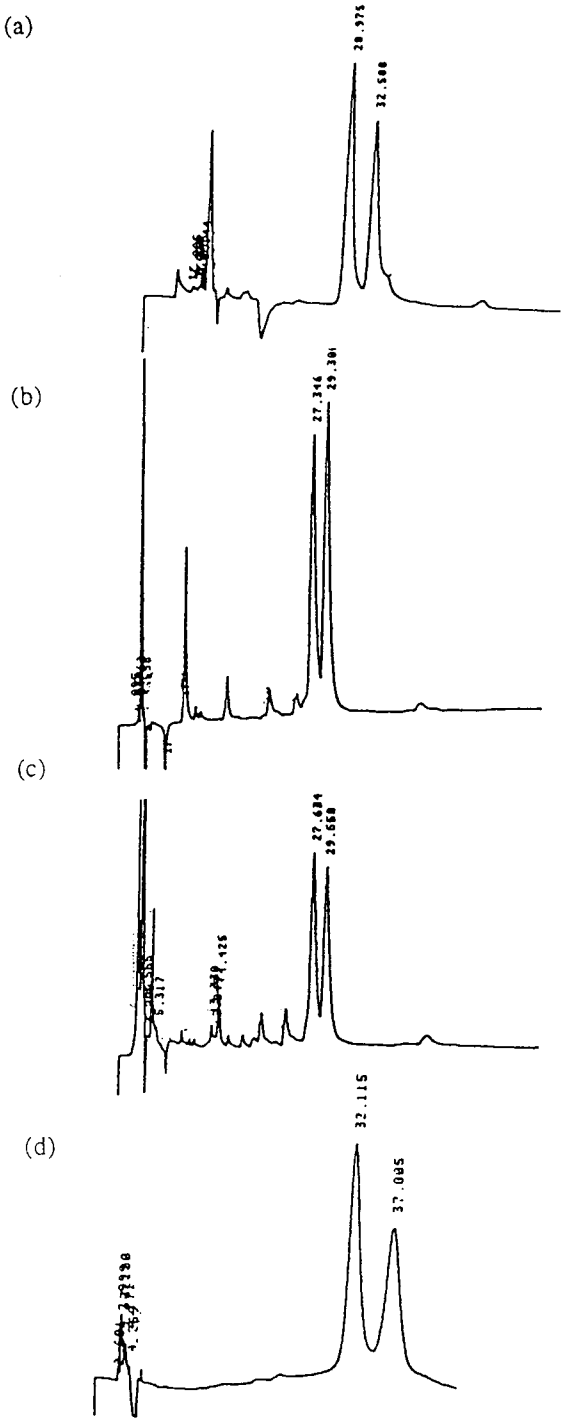

Fig. 5. Normal-phase separation of calpain inhibitors: (a) AK275 (method D), (b) AK275 (method E), (c) AK311 (method F) and (d) AK269 (method G).

trile, method G) with the Chiral-2 column for resolution of the diastereomers (Fig. 5d). While the isopropanol used in method G could potentially react with the keto group of AK269 to form hemi-ketals, previous ^1H NMR studies using methanol revealed that the rate of formation of such ketals at room temperature was slow relative to the rate of formation of a hydrate with water [2]. The isocratic elution system employed in the normal-phase methods minimized the background noise, allowing for detection at 210 nm. The relative and absolute retention times of the diastereomer peaks could be adjusted by small changes of the composition of mobile phase. Such adjustments have been required for analysis of diastereomeric ratio in various formulations (data not shown). Normal-phase separation of diastereomers of AK295 was not examined, since adequate separation was seen on the reversed-phase system (method B).

6. Conclusions

The high-temperature C_4 reversed-phase HPLC system could be used for analysis of general purity of the calpain inhibitors and allowed the separation of diastereomers of the positively charged inhibitor, AK295. This type of HPLC system has been used for supporting synthetic work, formulation evaluation, and pharmacokinetic studies. The normal-phase Nucleosil Chiral-2 stationary phase has been employed in the studies of epimerization rates and in formulation evaluation. The normal-phase methods have also been used for general purity assessment as a complement to the reversed-phase method. The two general methods (high-temperature reversed-phase analysis and normal-phase chiral analysis) that were found to be most useful for the analyses of calpain inhibitors were used in a manner in which the keto moiety of the inhibitors was minimally affected by the mobile phase. It is clearly important to take molecular reactivity into consideration when developing analytical assays.

Acknowledgements

The authors wish to thank Dr. Scott L. Harbeson and Robert Barrett for the syntheses of the inhibitors used in this study.

References

[1] Z. Li, G.S. Patil, Z.E. Golubski, H. Hor, K. Tehrani, J.E. Foreman, D.D. Eveleth, R.T. Bartus and J.C. Powers, *J. Med. Chem.*, 36 (1993) 3472.

[2] S.L. Harbeson, S.M. Abelleira, A. Akiyama, R. Barrett III, R.M. Carroll, J.A. Straub, J.N. Tkacz, C. Wu and G.F. Musso, *J. Med. Chem.*, in press.

[3] R.T. Bartus, K.L. Baker, A.D. Heiser, S.D. Sawyer, R.L. Dean, P.J. Elliott and J.A. Straub, *J. Cerebral Blood Flow Metab.*, 14 (1994) 537.

[4] R.T. Bartus, N.J. Hayward, P.J. Elliott, S.D. Sawyer, K.L. Baker, R.L. Dean, A. Akiyama, J.A. Straub, S.L. Harbeson, Z. Li and J. Powers, *Stroke*, in press.

[5] V.A. Davankov, *Adv. Chromatogr.*, 18 (1980) 139.

[6] V.A. Davanov, A.A. Kurganov, A.S. Bockkov, *Adv. Chromatogr.*, 22 (1983) 71.

[7] D.W. Armstrong, *J. Liq. Chromatogr.*, 7, Suppl. 2 (1984) 353.

ELSEVIER

Journal of Chromatography A, 684 (1994) 251–257

JOURNAL OF CHROMATOGRAPHY A

Determination of organic acids in cigarette smoke by high-performance liquid chromatography and capillary electrophoresis

D. Lagoutte*, G. Lombard, S. Nisseron, M.P. Papet, Y. Saint-Jalm

Research Department, SEITA, 4 Rue André Dessaux, 45401 Fleury-les-Aubrais Cedex, France

First received 13 April 1994; revised manuscript received 23 June 1994

Abstract

The most abundant low-molecular-mass organic acids in cigarette smoke are glycolic, lactic, formic and acetic acids. In this study, these substances were detected and determined by high-performance liquid chromatography (HPLC) and by capillary electrophoresis (CE). HPLC analysis used precolumn derivatization with the *p*-bromophenacyl bromide. The two methods were compared. The levels of each organic acid in a typical "European blend" cigarette smoke measured by HPLC and CE were comparable. The corresponding run-to-run relative standard deviations (R.S.D.s) ranged from 6 to 12.7% for HPLC and from 2.8 to 12.4% for CE. The smoking-to-smoking reproducibility (R.S.D.) was between 4.2 and 11.0% for HPLC and between 1.2 and 14.0% for CE. The limit of detection, calculated at a signal-to-noise ratio of 3 for each acid, was about 10^{-6} mol/l for the two methods, corresponding to 5 pmol of analyte injected for HPLC and 0.5 pmol for CE. CE was shown to be a good alternative to HPLC, requiring almost no sample preparation other than dilution, and giving a short analysis time (less than 15 min).

1. Introduction

The mainstream smoke aerosol phase produced by burning tobacco is a complex matrix composed predominantly of water, nicotine and organic molecules. Several organic acids have been identified in cigarette smoke: low-molecular-mass organic acids [1–5], mainly acetic, formic, lactic and glycolic [6]; aromatic acids [7,8]; and high-molecular-mass organic acids [9–11]. Analytical approaches adopted for the measurement of these compounds have been based on gas chromatographic (GC) methods with derivatization steps [6–13] or high-performance liquid chromatography (HPLC) [14,15].

GC methods used the conversion of organic acids into methyl [7,9,10], butyl [6] and pentafluorobenzyl [12,13] esters, or trimethylsilyl derivatives [2,6,8,9]. In all instances, complex extraction steps were necessary, because these methods were not specific for organic acids and the reagents used could interact with many compounds containing functional groups with an active hydrogen. Moreover, GC methods were difficult to use in a routine manner.

We have found no report on the use of high-performance ion-exclusion chromatography for the analysis of tobacco smoke and only two

* Corresponding author.

0021-9673/94/$07.00
SSDI 0021-9673(94)00593-X

references to anion-exchange chromatography. This is probably because smoke produced by burning tobacco is largely insoluble in water and most samples for ion chromatography are aqueous or are solubilized in an aqueous medium. As with GC methods, the HPLC methods also used complex extraction steps followed by separation on an anion-exchange column. Owing to the poor resolution of the analysis, only acetic and formic acids could be detected and determined [14].

Current HPLC or GC methods thus lack specificity and ruggedness for routine work. The aim of this work was to develop a routine method for the determination of the four most abundant low-molecular-mass organic acids (glycolic, lactic, formic, acetic) in cigarette smoke. We focused our attention on reversed-phase HPLC, including a derivatization step with *p*-bromophenacyl bromide, and capillary electrophoresis (CE). CE is a method with great potential for the high-resolution separation of various substances [16]. The detection and determination of organic acids by CE has been carried out in many raw materials such as wines [17], sugar refinery juices [18] and food samples [19]. To our knowledge, no report has been published concerning the CE separation of organic acids in cigarette smoke.

2. Experimental

2.1. Instrumentation

HPLC

The HPLC apparatus used in this study consisted of an LDC/Milton Roy Constametric I and II solvent-delivery system and an LDC/Milton Roy SM 4000 UV detector. The separation was carried out with a Nucleosil $5C_{18}$ column (12.5 cm × 3 mm I.D.) from Macherey–Nagel equipped with the corresponding precolumn (8 × 4 mm I.D.). Samples and standards were injected using a Rheodyne 5-μl loop. Data acquisition and treatment were accomplished by using a Minichrom data acquisition system (VG Data Systems).

CE

The CE instrument used was a Quanta 4000 (Waters Chromatography Division of Millipore) with a Maxima 820 data station (version 3.30). Conventional fused-silica capillaries (100 cm × 375 μm O.D. × 75 μm I.D.) were used. Detection was carried out by measuring the absorbance on the column at a position 10 cm from the end of the capillary tube. All pH values were measured with a Schott Geräte Model 6820 pH meter calibrated immediately prior to use.

2.2. Reagents

Deionized water (produced with a Millipore Milli-Q water-purification system) was used to prepare all solutions. Acetonitrile was obtained from Merck (LiChrosolv grade), methanol from Carlo Erba (for HPLC grade) and acetone from Merck (for analysis grade). All solvents were used as received. Sodium hydrogencarbonate was obtained from Fluka (Microselect grade). Sodium hydroxide (1 *M*) was purchased from Merck. The reagents used for HPLC were *p*-bromophenacyl bromide (Merck) and two crown ethers, dicyclohexane-18-crown-6 and 1,4,7,10, 13,16-hexaoxacyclooctadecane (Fluka). The internal standards were 2,5-dimethylacetophenone (ICN) for HPLC and methylsuccinic acid (Fluka) for CE. The electroosmotic flow modifier (OFM Anion-BT) was obtained from Millipore. It is composed mainly of tetradecyltrimethylammonium bromide (TTAB). The UV-active component used for CE, with the same charge as the analytes, was potassium hydrogenphthalate (Aldrich). The standard samples used for calibration were sodium L-lactate (Fluka, purum), potassium acetate (Prolabo, Normapur), potassium formate (Fluka, Microselect), glycolic acid (Merck, for analysis) and sodium succinate (Merck, for synthesis).

2.3. Mechanical smoking of cigarettes and trapping of smoke

Mechanical smoking of cigarettes was carried out under normal conditions [20]. A twenty-channel Filtrona 300 smoking machine was used.

The particulate phase of the smoke was trapped by filtration through a normalized Cambridge fibre-glass filter (Borgwaldt, Hamburg, Germany). Twenty-five cigarettes were smoked for each determination.

2.4. Procedures

HPLC

Immediately after smoking, five Cambridge filters (each corresponding to the smoke of five cigarettes) were placed in 25 ml of an acetone solution containing the internal standard (2,5-dimethylacetophenone, 0.5 μl/ml). After mixing, the filters were allowed to stand overnight in the acetone solution, which is the necessary duration to perform the extraction of the acid fraction of the smoke. The day after, the filters were crushed and the extract was filtered. The derivatization reaction was then performed following Durst et al.'s procedure [21]: 500 μl of the extract were added to 100 mg of sodium hydrogencarbonate, 100 μl of a solution of *p*-bromophenacyl bromide (80 mg/ml) in acetonitrile and 100 μl of a solution of dicyclohexane-18-crown-6 (8 mg/ml) and 1,4,7,10,13,16-hexaoxacyclooctadecane (8 mg/ml) in acetonitrile. The reaction was allowed to proceed at 80°C for 1 h, then the preparation was injected into the liquid chromatograph without further purification. The mobile phase consisted of a mixture of 39% acetonitrile–methanol (52:48) and 61% water between 0 and 20 min, then a linear gradient between 61 and 0% water was applied for 3 min. The flow-rate was 1 ml/min. All HPLC solvents were filtered and degassed prior to use. The absorption of the eluate was measured at 255 nm (direct UV detection). All experiments were performed at room temperature (22°C).

CE

Immediately after smoking, five Cambridge filters (each corresponding to the smoking of five cigarettes) were placed in 25 ml of acetone containing the internal standard (methylsuccinic acid, 50 μl of a 0.52 g/l aqueous solution). After overnight extraction, the filters were crushed and the extract was filtered. Sample solutions were placed in the CE apparatus after diluting each acetone solution with four volumes of deionized water. The background electrolyte was 5 m*M* potassium hydrogenphthalate + 1 m*M* OFM Anion-BT (TTAB) flow modifier. Its pH was adjusted to 5.6 with 10 m*M* NaOH. The indicated concentration of OFM Anion-BT refers to the concentration of the commercial solution; 5% (v/v) is equivalent to 1 m*M* active substance. Samples were introduced hydrostatically by elevation of the sample vials to 10 cm for 30 s. The migration voltage and the current were kept constant at 18 kV and 5.8 μA, respectively. Analyte zone were detected by indirect UV absorbance at 254 nm. The total analysis time was 15 min. The capillary was purged with 1 *M* NaOH for 10 min, followed by a 5-min purge with deionized water and a 5-min purge with the separation buffer, prior to the initial run. It was also purged with the separation buffer for 5 min between each run. All experiments were performed at 24°C (internal temperature of the CE apparatus).

3. Results and discussion

3.1. Identification of low-molecular-mass organic acids in cigarette smoke by HPLC and CE

The samples of smoke treated as described above were analysed by HPLC and CE and compared with a mixture of synthetic products. The corresponding chromatogram and electropherogram obtained from a typical "European blend" cigarette smoke are shown in Figs. 1 and 2, and those corresponding to the synthetic products are shown in Figs. 3 and 4. Peak confirmation was achieved by comparison of migration times and co-injections of authentic standards with the smoke samples. Four organic acids were detected by HPLC, glycolic, lactic, formic and acetic acids, and five were detected by CE, formic, succinic, glycolic, acetic and lactic acids.

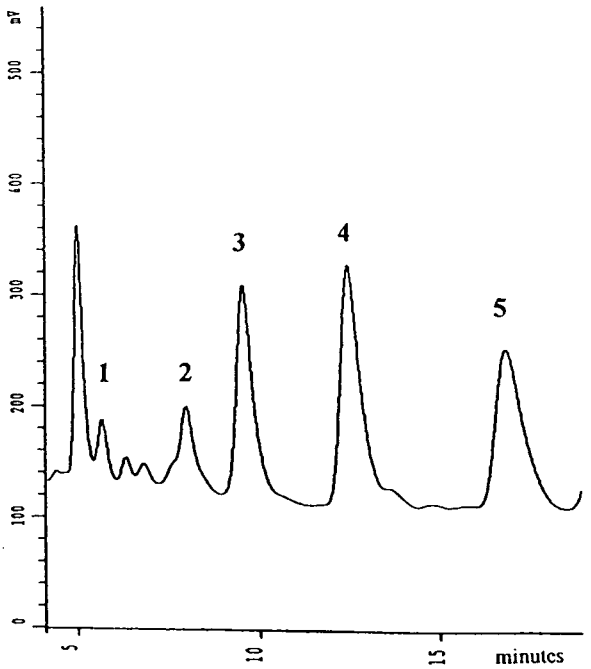

Fig. 1. Chromatogram of a European blend cigarette smoke. Peaks: 1 = glycolic acid; 2 = lactic acid; 3 = formic acid; 4 = acetic acid; 5 = internal standard.

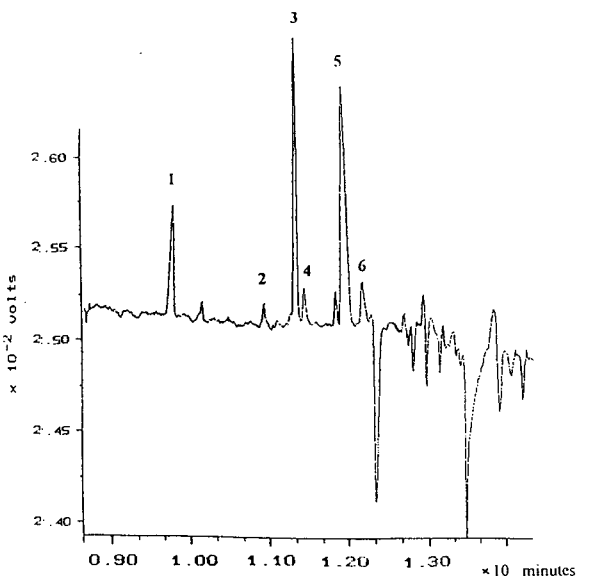

Fig. 2. Electropherogram of a European blend cigarette smoke. Peaks: 1 = formic acid; 2 = succinic acid; 3 = internal standard; 4 = glycolic acid; 5 = acetic acid; 6 = lactic acid.

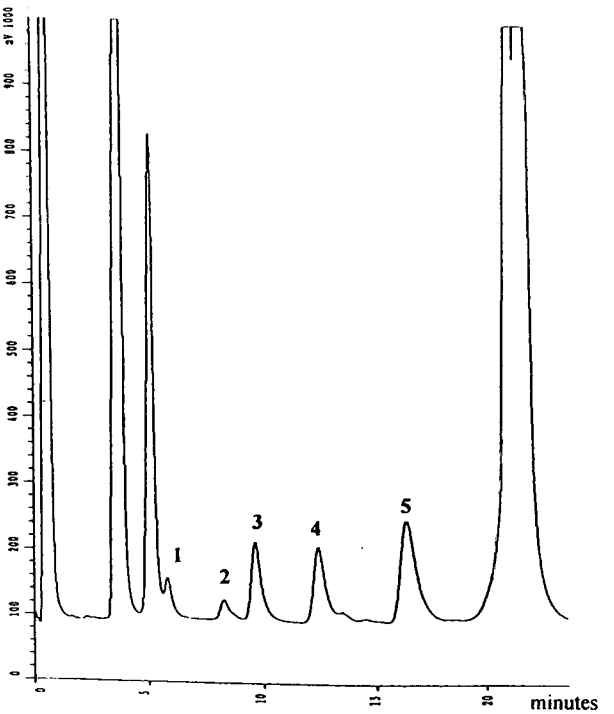

Fig. 3. Chromatogram of a standard mixture of four synthetic organic acids in acetone–water (9:1). Peaks: 1 = glycolic acid (52.6 μg/ml); 2 = lactic acid (57 μg/ml); 3 = formic acid (110 μg/ml); 4 = acetic acid (196 μg/ml); 5 = internal standard (0.5 μl/ml).

3.2. *Quantitative study of the three main organic acids (lactic, formic, acetic) in a "European blend" cigarette smoke*

Kinetics of the derivatization reaction (HPLC)

The kinetics of the reaction were studied directly on the smoke acetone solution. HPLC analyses of the reaction mixture were carried out at regular time intervals. The reaction was completed in 1 h (Fig. 5). A slower reaction rate was noted for acetic acid. The products formed were stable in the reaction mixture for at least 24 h.

Reproducibility and detection limit

A sample of the acetone smoke condensate was injected nine times into the HPLC apparatus and eight times into the CE apparatus. The reproducibility (R.S.D.) of the retention times was found to range from 1.4 to 1.7% for HPLC

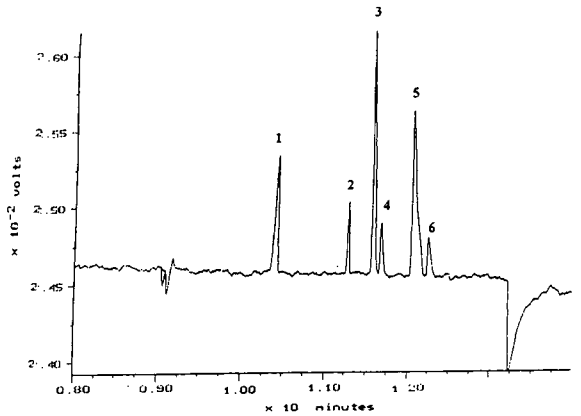

Fig. 4. Electropherogram of a standard mixture of five synthetic organic acids in acetone–water (9:1). Peaks: 1 = formic acid (27.3 μg/ml); 2 = succinic acid (26 μg/ml); 3 = internal standard (2 μl/ml); 4 = glycolic acid (28.3 μg/ml); 5 = acetic acid (97.5 μg/ml); 6 = lactic acid (30 μg/ml). Before injection into the CE apparatus, the standard solution was diluted with four volumes of deionized water.

and from 0.4 to 0.7% for CE (Table 1). The concentration reproducibility (R.S.D.) was 6–12.7% for HPLC and 2.8–10.5% for CE (Table 2). R.S.D.s obtained for retention time (Table 3) and concentration (Table 4) by repetition of the smoking were of the same magnitude: between 4.2 and 11.0% for HPLC, and between 1.2 and 14.0% for CE for concentration.

The detection limit, calculated at a signal-to-noise ratio 3 for each acid, was about 10^{-6} mol/l for both methods, corresponding to 5 pmol of analyte injected for HPLC and 0.5 pmol for CE.

Calibration

Standard samples were obtained by dissolving the acids, or their salts, in deionized water. Least-squares calibration graphs were constructed for lactic, formic and acetic acids (three concentration points). The HPLC calibration appeared to be linear in the concentration ranges 14–57 μg/ml for lactic acid ($R^2 = 1.00$), 27–110 μg/ml for formic acid ($R^2 = 1.00$) and 49–196 μg/ml for acetic acid ($R^2 = 1.00$) and CE calibration in the concentration ranges 7–30 μg/ml for lactic acid ($R^2 = 1.00$), 14–55 μg/ml for formic acid ($R^2 = 0.998$) and 25–100 μg/ml for acetic acid ($R^2 = 1.00$).

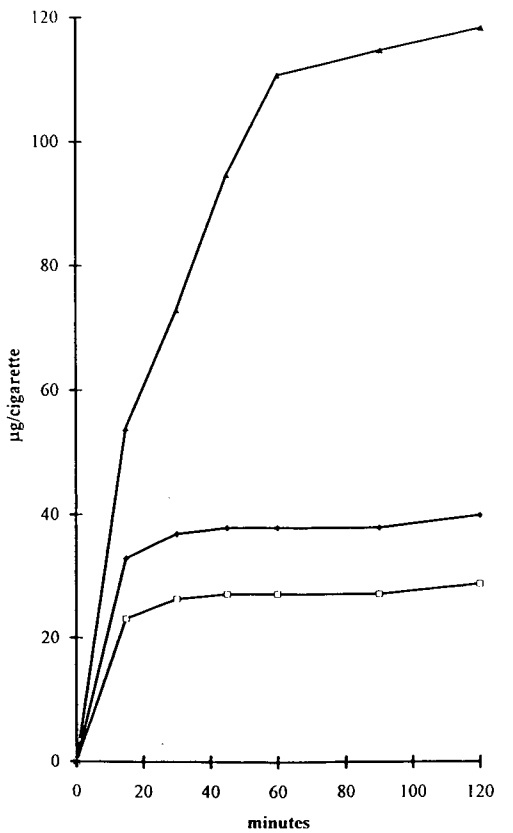

Fig. 5. Kinetics of the derivatization reaction with *p*-bromophenacyl bromide. Amount (μg per cigarette) of (▲) acetic acid, (□) lactic acid and (◆) formic acid derivatized versus the heating time (min).

Results of quantitative analysis of a "European blend" cigarette by both techniques

By repeating the smoking of 25 cigarettes, we carried out two series of measurements by both

Table 1
Run-to-run retention time (t_r) reproducibility of the HPLC and CE analyses

Compound	HPLC		CE	
	Mean t_r (min)	R.S.D. (%) ($n = 9$)	Mean t_r (min)	R.S.D. (%) ($n = 8$)
Lactic acid	7.9	1.7	12.21	0.7
Formic acid	9.5	1.5	9.66	0.5
Acetic acid	12.4	1.4	12.02	0.4

Table 2
Run-to-run concentration (c) reproducibility of the HPLC and CE analyses (μg per cigarette, obtained from the peak area by using the calibration graphs determined for each acid)

Compound	HPLC		CE	
	Mean c (μg/cig.)	R.S.D. (%) ($n = 9$)	Mean c (μg/cig.)	R.S.D. (%) ($n = 8$)
Lactic acid	32.9	6.0	22.8	10.5
Formic acid	41.7	12.7	41.6	2.8
Acetic acid	111.4	8.2	112.3	3.8

Table 3
Smoking-to-smoking retention time (t_r) reproducibility of the HPLC and CE analyses

Compound	HPLC		CE	
	Mean t_r (min)	R.S.D. (%) ($n = 5$)	Mean t_r (min)	R.S.D. (%) ($n = 3$)
Lactic acid	7.9	1.5	12.22	0.9
Formic acid	9.4	2.0	9.64	0.5
Acetic acid	12.2	1.5	12.00	0.3

Table 4
Smoking-to-smoking concentration (c) reproducibility of the HPLC and CE analyses (μg per cigarette, obtained from the peak area by using the calibration graphs determined for each acid)

Compound	HPLC		CE	
	Mean c (μg/cig.)	R.S.D. (%) ($n = 4$)	Mean c (μg/cig.)	R.S.D. (%) ($n = 3$)
Lactic acid	28.4	11.0	24.0	14.0
Formic acid	42.2	4.2	40.2	6.5
Acetic acid	120.5	8.5	113.9	1.2

HPLC and CE and the results are given in Table 5. The average results for both series are comparable. The calculation of the experimental F values between the two methods gives $F = 1.77$ for lactic acid, 1.58 for formic acid and 5.08 for acetic acid. The Snedecor table gives the critical F at 95% confidence level ($F = 18.51$ for acetic acid and 200 for lactic and formic acids). In all three instances, the calculated F value is less than the corresponding F value in the Snedecor table [22], so that one can conclude that the probability of the results obtained by the two methods for the three acids being the same is 95%.

Table 5
Comparison of HPLC and CE results (μg per cigarette) obtained for two smokings of 25 European blend cigarettes

Smoking	Lactic acid		Formic acid		Acetic acid	
	HPLC	CE	HPLC	CE	HPLC	CE
No. 1	24.3	23.4	41.1	42.1	118.6	110.7
No. 2	27.3	24.1	38.0	41.1	118.7	115.4

4. Conclusions

The two methods proposed for the determination of organic acids were sufficiently selective and sensitive to be applied directly to complex cigarette smoke mixtures. Both techniques provided rapid analyses, yielding quantitative information. They have distinct practical advantages over previous methods (GC or ion-exchange HPLC): they do not need complex extraction or prepurification steps, they are easy to use in a routine manner and they can detect and determine simultaneously the four most abundant low-molecular-mass organic acids in a cigarette smoke (glycolic, lactic, formic, acetic). Only two acids (acetic and formic) were determined using the ion-exchange HPLC method.

The agreement between the reversed-phase HPLC and CE methods was checked and it was concluded that the results provided by the two methods were the same. However, CE offers several features that make it more attractive than HPLC: (a) simplicity, as CE offers a rapid and simple means of identifying and analysing multicomponents mixtures such as cigarette smoke acid fraction without a derivatization step and sample preparation, other than dilution, and it is possible to inject dilute acetone smoke solutions

directly into the CE apparatus; (b) speed, as an analysis by HPLC takes 23 min (plus 1 h for derivatization) whereas CE takes only 15 min; (c) low costs and low solvent consumption (millilitres per day for CE versus centilitres per day for HPLC); and (d) the use of non-hazardous solvents (deionized water).

Acknowledgement

Financial support from the ARN (Association pour la Recherche sur les Nicotianées, Paris, France) is gratefully acknowledged.

References

[1] S. Ishiguro, S. Yano, S. Sugawara and Y. Kaburaki, *Agric. Biol. Chem.*, 40 (1976) 2005–2011.
[2] G.P. Morie, *Beitr. Tabakforsch.*, 6 (1972) 173–177.
[3] M.P. Newell, R.A. Heckman, R.F. Moates, C.R. Green, F.W. Best and J.N. Schumacher, *Tob. Sci.*, 22 (1978) 6–11.
[4] V. Norman, *Recent Adv. Tob. Sci.*, 3 (1977) 28–58.
[5] J.N. Schumacher, C.R. Green, F.W. Best and M.P. Newell, *J. Agric. food Chem.*, 25 (1977) 310–320.
[6] H. Sakuma, M. Kusama, S. Munakata, T. Oshumi and S. Sugawara, *Beitr. Tabkforsch. Int.*, 12 (1983) 63–71.
[7] J. Arnap, B.M. Dahlia, C.R. Enzell and T. Petterson, *Acta Chem. Scand.*, 43 (1989) 381–385.
[8] M.E. Snook, O.T. Chortyk and R.F. Arrendale, *Tob. Sci.*, 29 (1985) 25–31.
[9] R.F. Arrendale, R.F. Severson and O.T. Chortyk, *Beitr. Tabakforsch. Int.*, 12 (1984) 186–197.
[10] D. Hoffmann and H. Wodziwosdzki, *Beitr. Tabakforsch.*, 4 (1968) 167–175.
[11] D.B. Walters, W.J. Chamberlain and O.T. Chortyk, *Anal. Chim. Acta*, 77 (1975) 309–311.
[12] Y. Saint-Jalm, N. Beaulieu and G. Duval, *Ann. Tabac–Seita–Les Aubrais, Sect. 1*, 20 (1991) 7–16.
[13] Y. Saint-Jalm, N. Beaulieu and G. Duval, presented at *Symposium CORESTA, Jerez, Spain, 1992.*
[14] E.J. Nanni, M.E. Lovette, R.D. Hicks, K.W. Fowler and M.F. Borgerding, *J. Chromatogr. Sci.*, 28 (1990) 432–436.
[15] H. Yokota and M. Takegawa, presented at *Symposium CORESTA, Thessalonika, Greece, 1990.*
[16] B.L. Karger, A.S. Cohen and A. Guttman, *J. Chromatogr.*, 492 (1989) 584–614.
[17] V. Levi, T. Wehr, K. Talmadge and M. Zhu, *Int. Chromatogr. Lab.*, 15 (1993) 4–7.
[18] S.P.D. Lalljie, J. Vindevogel and P. Sandra, *J. Chromatogr. A*, 652 (1993) 563–569.
[19] W.R. Jones and P. Jandik, *Am. Lab.*, June (1990) 51–64.
[20] *CORESTA Inf. Bull.*, 3 (1991) 141–157.
[21] H.D. Durst, M. Milano, E.J. Kikta, S.A. Connelly and E. Grushka, *Anal. Chem.*, 47 (1975) 1797–1801.
[22] A. Hald, *Statistical Tables and Formulas*, Wiley, New York, 1975.

ELSEVIER

Journal of Chromatography A, 684 (1994) 259–268

JOURNAL OF CHROMATOGRAPHY A

Reactive-flow luminescence detector for gas chromatography☆

Kevin B. Thurbide, Walter A. Aue*

Department of Chemistry, Dalhousie University, Halifax, Nova Scotia B3H 4J3, Canada

First received 27 April 1994; revised manuscript received 20 June 1994

Abstract

A stable, several centimeters-long luminescent column is easily formed by a hydrogen–air mixture ascending through a glass capillary toward a glow-sustaining flame on top (which combusts the excess hydrogen with auxiliary air as a flame ionization detector). This encased glow can be used for the photometric determination of gas chromatographic effluents of sulfur and phosphorus, in what may be termed a "reactive-flow detector" (RFD). The RFD behaves in many —though not in all— respects similar to the well-known flame photometric detector (FPD). This manuscript reports analytical figures-of-merit for an RFD prototype that are as good as, or better than, those of a typical FPD.

1. Introduction

This study describes a new detector for gas chromatography (GC), which mimics some of the properties of much older and well-established GC detectors. Its concept hails from a general study [1,2] of the survival/transformation rates of organic molecules in a multi-capillary, high-capacity reactor. That reactor supported, enclosed, and compared low-temperature hydrogen–air flames of many varieties: fuel-rich and air-rich, diffusion and premixed, doped and undoped, etc. Effluents from the reactor were collected and analyzed by GC for intact molecules.

Two among the several processes this study attempted to explore were the formation and excitation of small molecules like S_2, HPO, SnH, etc.; and the peculiar type of quenching that befalls such emitters in the presence of hydrocarbonaceous materials. This quenching seriously hampers the use of the flame photometric detector (FPD) [3–9] and related analytical devices. Accordingly we often used gas streams doped with small amounts of sulfur compounds as probes of flame shape and conditions prevailing at the reactor's multicapillary burner head.

To gain further insight into the stability of flames at capillary orifices, single jets were also used. These jets were made of glass. Glass jets in open and encased versions could be produced fast, cheap, and in the laboratory; they were relatively inert; and they revealed the location of flames by the orange atomic emission of sodium traces emanating from their hot surfaces. Owing to the great general importance of combustion processes and various forms of spectroscopy, tomes are available on the physical behaviour, optical characterization, and analytical use of multifarious flames (cf. [9–17]).

While working with capillary glass jets, we

* Corresponding author.

☆ Part of doctoral thesis of K.B.T.

0021-9673/94/$07.00
SSDI 0021-9673(94)00581-S

noticed that premixed gases would often form elongated glows; glows that were situated beneath (and were dependent on the presence of) stable flames burning on top. Typically, such glows would extend over 1 to 4 cm in capillaries of 1.5 to 3 mm I.D., and would fill the available volume between the upper rim of the capillary and some lower restriction. If, however, a true flame (as judged by shape and heat, i.e. by the attendant sodium emission) would establish itself at the restriction, the glow above it would vanish.

The latter situation (though not used in, and of no direct relevance to, the current study) calls to mind the "separated" flame described by Smithells and Ingle [18] more than a century ago. A similarly configured hydrogen-flame burner, cooled to enhance the Salet effect of the divorced S_2 and HPO emissions, has in fact been put to good spectral and analytical use [9]. Tongue firmly in cheek, the by far most detailed, trustworthy and readable monograph on the flame spectroscopy of non-metals has even suggested that "the device would make a lovely ornament for restaurant tables in place of the usual candle" [9]. Present some stretch of imagination, its design might also have served as forerunner of today's dual flame photometric detector (FPD) flames [19,20]. Yet, to our knowledge, a "glow" (as we describe it here) was never found in such devices —not surprisingly so if one considers the *dual-flame* design, as well as the dimensions, materials and operating conditions— of the Smithells separator.

Our glow used a hydrogen-rich premixture, thereby raising the question whether it is the typical premixed flames that should be considered its forerunners or that could serve as its points of reference. Premixed low-temperature hydrogen flames have indeed been used for molecular luminescence, but they proved less efficient than diffusion flames [21]. In exploratory studies by our own group, premixed single flames (produced by fitting typical FPD jets with perforated hollow caps) performed sometimes similar to, but never better than, the original diffusion flames [22] —and they were harder to control. The only other device that to our knowledge used flame gases premixed (though not premixed with the column effluent), was the welder's torch FPD design of Moye [23].

Thus we are not aware of any case where glows similar to ours have been observed; much less where, containing analyte, they have been used to analytical ends. However, the range of interests that may have produced such glows is very large indeed, and we stand to be corrected on our presumption of absolute novelty. For instance, typical plasma afterglows and certain other low-pressure gas-phase chemiluminescences (cf. [24–28]) may be considered distant cousins to the ambient-pressure premixed hydrogen–air glows encountered here. Our glows may also be collateral relatives —in kinetic principles if not in initiation, composition and spectral performance— to the "pre-ignition glows" and "cool flames" {slow, luminescent oxidations of hydrocarbons to peroxides, aldehydes, etc. (e.g. [10,15,17])} of classical spectroscopy. Yet there does not appear to have existed any kindred (much less any legitimate next-of-kin) device to the glows described here.

2. Experimental

The metal jet of the flame ionization detector (FID) on an old Tracor Model 550 GC was replaced by a borosilicate capillary. The capillary had an inner diameter of 1.8 mm and a restriction of 1 mm I.D. about 3.5 cm down from the top. (These dimensions are typical and, for the most part, not crucial. Quartz capillaries also worked well.) When present in excess, background luminescence was suppressed with heavy injections of tetraethyllead [29]; deposits were removed with injections of Freon-113 ([cf. [30]). (Usually these tricks work, occasionally they do not).

For initial experiments, the outside of the capillary was painted with high-temperature black paint —of the type used on car exhausts— leaving a ca. 0.5 cm broad ring untouched (painting the capillary later turned out to be unnecessary). A 6 in. × 1/4 in. O.D. (1 in. = 2.54 cm) glass image conduit (No. 38307; Ed-

mund Scientific, 101 E. Gloucester Pike, Barrington, NJ 08007-1368, USA), shielded from light by a protective metal pipe, was inserted through the detector wall and moved against (the transparent section of) the capillary. The other end of this optical feed-through terminated vis-à-vis the photocathode of Hamamatsu 268 or 374 photomultiplier tubes (PMTs with nominal wavelength ranges of 300 to 650, and 300 to 850 nm, respectively), leaving a gap wide enough to insert an optical filter if desired. The PMT housing could be easily opened, giving the operator the chance to observe the reactive flow through the image conduit. The detector housing was reconstructed to prevent ambient light from entering, but no effort was made to change the Tracor detector base and FID-type design, or to minimize dead volume. Fig. 1 offers to-scale schematics of this first reactive-flow detector (RFD) version. (It does so mainly to placate an astute referee, provide an accurate record, and please the avid reader; however, an optimized RFD built from scratch would obviously have been different).

Test compounds were separated on an already installed, old 2 m × 1.8 mm I.D. borosilicate column, packed with 10% Apiezon L on Chromosorb W, 45–60 mesh (roughly 350–250 μm particle diameter), and purged by a nitrogen stream of ca. 12 ml/min. The signal from the Tracor electrometer was routed through a laboratory-made three-pole filter set at an resistance/capacitance (RC) = 0.5 s time constant, before being displayed on a strip-chart recorder. Other props and procedures were conventional as well; where important they will be described in the text or in the captions to the figures.

3. Results and discussion

Our glows, which developed easily inside the capillary carrying an FID-type flame on top, would turn brilliantly blue in the presence of small amounts of sulfur. Their visual appearance was certainly unlike that of any conventional flame —difficult, however, it may be to define what does and what does not constitute a "flame" [10]— but of something that we, for lack of a better term, like to refer to as "reactive flow".

This reactive flow is not self-sustaining: it

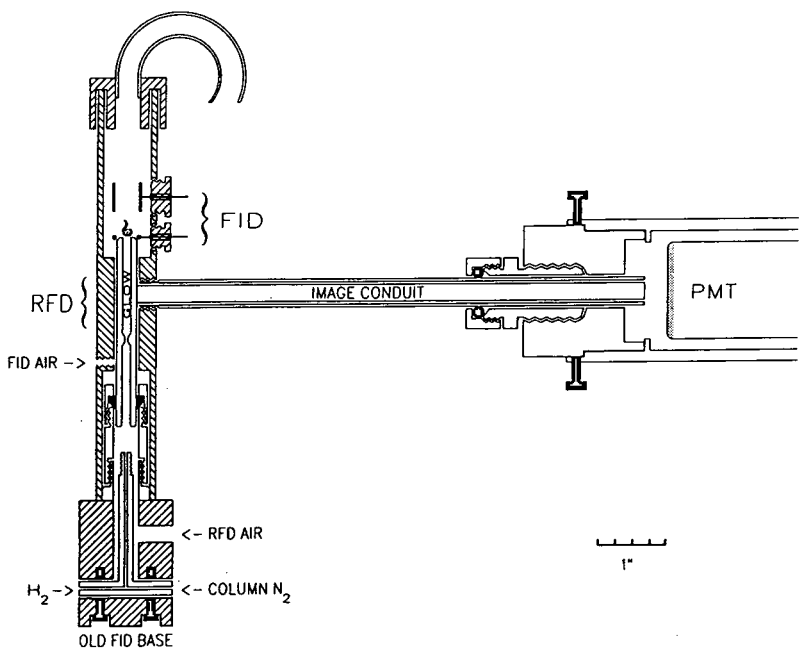

Fig. 1. Schematic of RFD prototype.

requires continuous access to a stable flame. A both tautological and talkative description of the phenomenon may assert that steady-state free-radical reactions are initiated and supported by the stable flame at the upper border of the reactive flow, and extend downward through the capillary to the lower border formed by the nearest stabilizing restriction; in a process that is sustained by the counter-reactionary mass movement of the premixed, excited gases.

As mentioned before, the reactive flow can give birth to a second flame at the restriction (present a suitable composition and supply rate of the hydrogen–air mixture). Yet if it does, it is quickly starved to death by its own offspring. Sans metaphor, the reactive flow is simply extinguished by a flame burning *below* it.

But still, the reactive flow needs a flame *above* it. If the flame atop the reactive flow is slowly suffocated —i.e. by carefully diminishing the auxiliary air supply— the reactive flow dies with it. The reactive flow may also succumb to, say, a sudden influx of solvent. But that is merely petit mort: As the injection solvent enters, the reactive flow appears to leap out of the capillary into the upper flame, which in turn becomes large and bright. Then, with the solvent gone, the flame shrinks and dulls again, sending the reactive flow back into the capillary. The extreme stages of this process are often accompanied by characteristic sounds.

Oscillations and singing flames are, of course, well-known phenomena, even in chromatographic detectors [31,32]. In the RFD, such events occur only under extreme, i.e. gas supply boundary or analyte overload conditions. Our typical reactive flow was silent and did not visibly fluctuate (as judged by the human ear, the human eye, and the oscilloscopic trace from a PMT); it was tolerant of considerable variation in flow conditions; and it was stable in time.

That a typical reactive flow is free of fluctuations (but that it can be easily made to fluctuate if so desired) is mechanistically interesting and analytically important. It is easy to calculate the minimum (i.e. the fundamental, quantum-related) noise from the photon flux [33]. A calculation of that kind showed that the RFD noise consisted, predominantly if not entirely, of photon shot noise. By definition, therefore, fluctuation noise was absent.

This, plus the unexpected brightness of the blue S_2 bands in the reactive flow (though in part due to visual compression by the capillary) suggested that we explore the RFD's analytical potential with organosulfur and, because of its striking similarity with the FPD, with organophosphorus compounds as well.

Fig. 2 shows the typical gas supply range for a reactive flow, as judged by the resulting signal-to-noise ratio (S/N) for test compounds of sulfur and phosphorus. Clearly, reactive flows could be established at quite a variety of conditions. In the upper portions of the curve, the hydrogen input was about two thirds in excess of stoichiometric. (Note that a certain excess of hydrogen was necessary to support the top flame and thereby provide radical sustenance to the reactive flow.) The thermocouple temperatures at four different flows of Fig. 1 were all in the 200 to 230°C range. (These measurements were done with the detector housing removed, the ther-

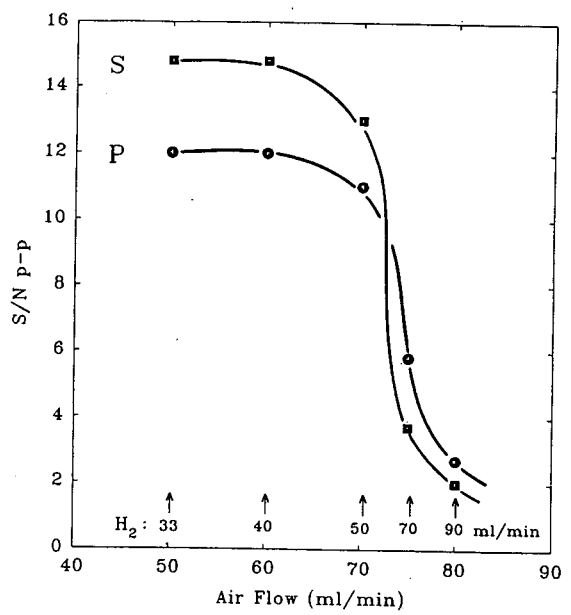

Fig. 2. Response of sulfur and phosphorus test analytes in reactive flows of different gas velocity and composition. No optical filter, R-268 PMT.

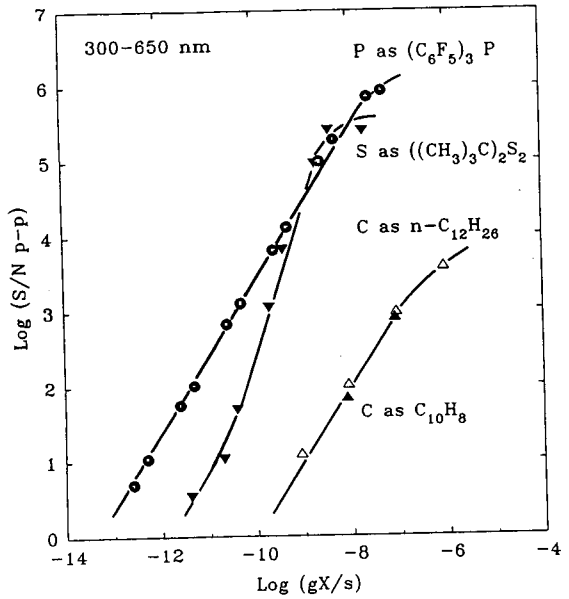

Fig. 3. Calibration curves of phosphorus (X = P), sulfur (X = S) and hydrocarbon (X = C) analytes without optical filter. Hamamatsu R-268 PMT. Gas supply rates: hydrogen 40, air 60, nitrogen (from column) 12 ml/min. Linear portions drawn at exactly slope 1 (for P and C) or exactly slope 2 (for S). $N_{p\text{-}p}$ is the peak-to-peak noise of the baseline, with drift and spikes excluded.

mocouple tip touching the reactive flow, and only minor heat emanating from the detector base.)

The most important criterion for setting gas supply rates was the creation of the reactive flow itself. Changing gas rates within its stability band (region of existence) contributed but little to its relative sensitivity for sulfur and phosphorus. If this should be confirmed as a characteristic trait of the RFD in broader-based future investigations, the detector could be used at one and the same condition for all elements to which it responds. That would greatly simplify analytical methodology, albeit at some cost in selectivity. (Note that, with the possible exception of Joonson and Loog's dual-chamber model [34], most FPDs use distinctively different gas supply rates for sulfur and phosphorus determinations [4].)

Fig. 3 shows calibration curves of sulfur and phosphorus analytes, and allows their comparison with aliphatic and aromatic hydrocarbons, in the "open", i.e. filterless mode. The straight-line portions of these log–log calibration curves are deliberately drawn at slopes of precisely 1 (for P and C) or 2 (for S). $N_{p\text{-}p}$ is the peak-to-peak noise of the baseline, with spikes and drift excluded (cf. [35,36]); S is the signal (peak height).

Graphically, the calibration curves end at the common chromatographic detection limit of $S/N_{p\text{-}p} = 2$. If the $S/\mathrm{RMS} = 3$ detection limit is preferred —where RMS (root mean square) denotes the standard deviation of the baseline noise— the plot should be extrapolated farther down to an ordinate value of about −0.3 [35]. Table 1 charts these limits and, of more original appeal, Fig. 4 pictures them as peaks of sulfur and phosphorus rising out of the baseline noise.

The most interesting aspect of the results shown in Fig. 3 and Table 1 emerges from their comparison with the characteristic performance

Table 1
RFD detection limits

Compound	X	At $S/N_{p\text{-}p} = 2$		At $S/\mathrm{RMS} = 3$	
		g Compound	gX/s	g Compound	gX/s
Di-*tert.*-butyl-disulfide	S	$7 \cdot 10^{-11}$	$2 \cdot 10^{-12}$	$2 \cdot 10^{-11}$	$5 \cdot 10^{-13}$
Tris(pentafluoro-phenyl)phosphine	P	$2 \cdot 10^{-11}$	$8 \cdot 10^{-14}$	$4 \cdot 10^{-12}$	$2 \cdot 10^{-14}$
Naphthalene	C	$3 \cdot 10^{-9}$	$2 \cdot 10^{-10}$	$8 \cdot 10^{-10}$	$5 \cdot 10^{-11}$

S = Signal (peak height); $N_{p\text{-}p}$ = peak-to-peak noise, with drift and spikes excluded; RMS = root mean square (the standard deviation in a Gaussian distribution).

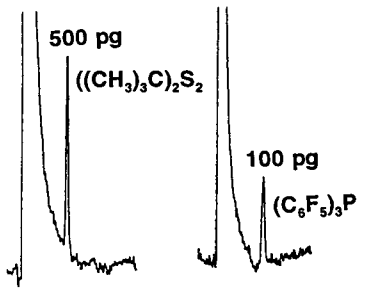

Fig. 4. Peaks of tris(pentafluorophenyl)phosphine and di-(*tert.*-butyl)disulfide near their detection limit. The RC filter time constant is 0.5 s. Conditions as in Fig. 3.

of the FPD. Dressler states in his monograph [4] that "the minimum detectable mass rate ranges from about $1 \cdot 10^{-13}$ g/s to $2 \cdot 10^{-12}$ g/s of P for phosphorus compounds and from about $2 \cdot 10^{-12}$ g/s to $5 \cdot 10^{-11}$ g/s of S for sulphur compounds" (his reference numbers deleted). In other words, the minimum detectable amounts in the RFD are equal to or better than those of the FPD. (They are, however, notably worse than those of the "pulsed-flame photometer", the "atomic emission detector", the "sulfur chemiluminescence detector", and various related detection devices [8,24,28,36–43]).

It may be noted that, at present, the RFD remains a simple prototype, designed to evaluate analytical potential in the shortest possible time and with the least instrumental effort. For instance, the type of inexpensive light conduit it uses restricts the optical range to the visible (whereas some of the strongest S_2 bands lie in the UV). It also samples only a fraction of the light generated by the reactive flow.

The shapes of the RFD phosphorus and sulfur calibration curves typically match those of the FPD. The bend-off to a first-order slope at the bottom of the sulfur curve is a common occurrence [44]; in fact, it can already be found in the seminal FPD paper by Brody and Chaney [45]. Also as in the FPD, temperature programming causes only minor, if indeed any, baseline drift.

The few data points for *n*-dodecane and naphthalene were added to Fig. 3 as an afterthought, just to indicate how strongly (or weakly) matrix hydrocarbons might show up in the RFD. As is well known, aromatics respond in the FPD stronger (and with a different spectrum [35]) than aliphatics. This seems not to be the case here. While that matter is of only minor interest under the present circumstances, it may well warrant careful study in a future context.

One (but not the only) reason for such future study is that our measurements of hydrocarbon survival in hydrogen-rich flames —using the "reactor" mentioned in the Introduction— showed considerable differences between diffusion and premixed systems. Whereas in diffusion flames compounds with high carbon numbers were less likely to survive intact than compounds with low carbon numbers, such discrimination was not found in premixed flames. Also, the overall survival rates of organics in premixed flames were generally much lower than those in diffusion flames of the same flow and overall stoichiometry [2] (this may, however, have been due to differences in local temperature as well as local gas-phase composition). Yet, much more work would need to be done on such systems before clear connections between the large-volume reactor experiments, the typical performance of the FPD, and the still largely unexplored behavior of the RFD could be established.

In analytical practice, sulfur and phosphorus luminescences in the FPD are monitored through interference filters. We therefore include calibration curves for two popular wavelengths in Figs. 5 and 6. No unexpected features appear to be present. The minimum detectable amounts are slightly worse than under filterless conditions, as one would expect [46].

We also include, via Fig. 7, the calibration curve for "linear sulfur" [47] (HSO [48]). Increasing the relative response of the red HSO vs. the blue S_2 bands through the use of different hydrogen–air ratios, while helpful in the flame, proved of only limited value in the glow. Instead, the RFD was operated at an overall larger supply rate of reactant gases; an approach that appeared to depress S_2 slightly more than HSO. Also, a red-sensitive PMT was used and two

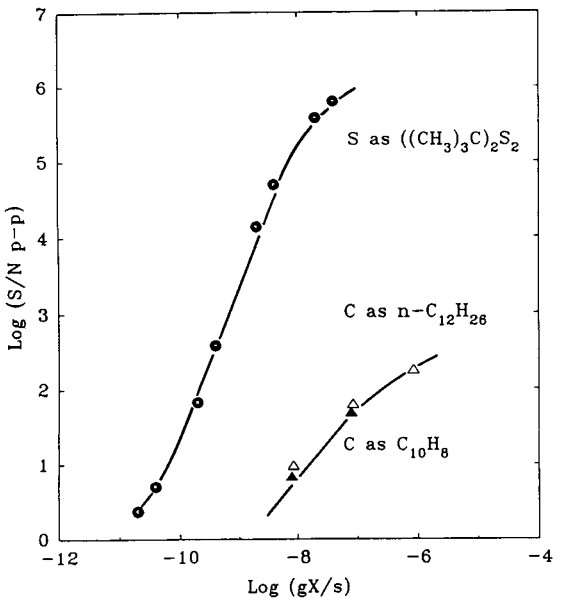

Fig. 5. Calibration curves of sulfur and hydrocarbon analytes through a 405-nm narrowband interference filter of 11 nm bandpass. Other conditions as in Fig. 3.

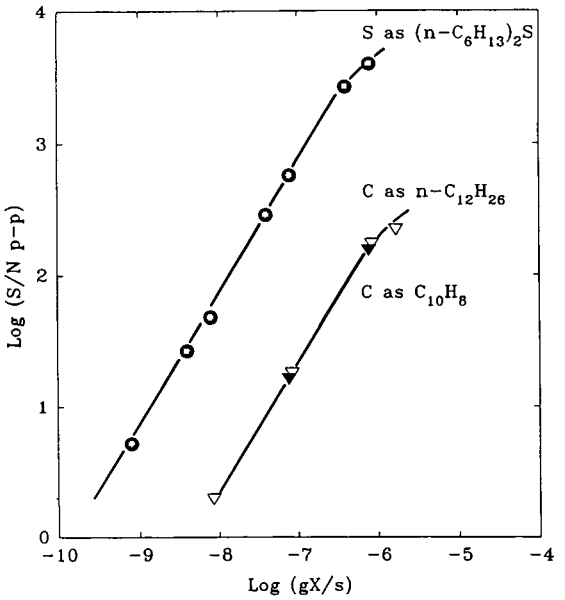

Fig. 7. Calibration curves of sulfur (X = S) and hydrocarbon (X = C) analytes through a 750-nm wideband interference filter of 40 nm bandpass, with a 600-nm longpass colored-glass filter added for increased blocking. Hydrogen 100, air 85 ml/min; Hamamatsu R-374 PMT. Both lines are drawn at exactly unity slope.

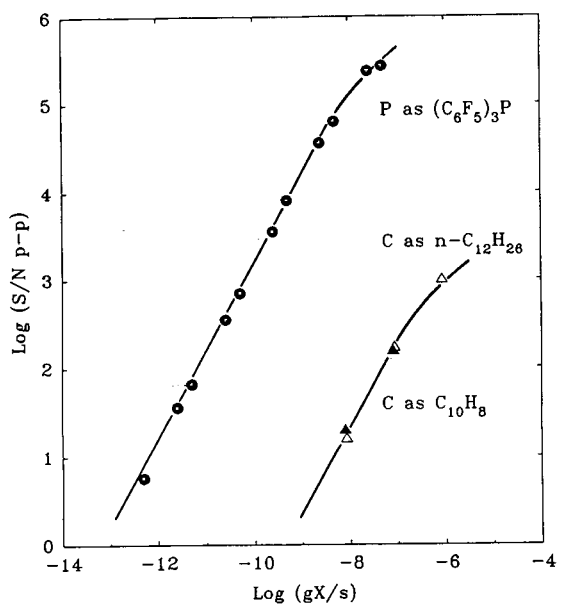

Fig. 6. Calibration curves of phosphorus and hydrocarbon analytes through a 524-nm broadband interference filter of 40 nm bandpass. Other conditions as in Fig. 3.

optical filters restricted the light input to the $0 \rightarrow 1$ 750-nm band of HSO ($^2A' \rightarrow {}^2A''$) [48]. The HSO luminescence was not as strong in the glow as it had been in the FPD flame [47]; also, its selectivity against carbon was lower. It is interesting to note in this context that, in the RFD, carbon compounds give rise to conventional peaks, while in the FPD they usually produce negative peaks (decreases in baseline luminescence) at wavelengths above, very roughly, 600 nm.

Taken together, the RFD behavior vis-à-vis sulfur, phosphorus and carbon suggests that the glow responds frequently, though not always, in a manner similar to that of the FPD. But why? It could be argued, of course, that the FPD flame should contain a region similar in composition to the reactive flow. Yet the existence of such a region is neither a necessary nor, obviously, a

sufficient criterion for observing luminescence. When, in an unrelated earlier study, sulfur compounds were introduced into an FPD from the top, strong sulfur response could still be obtained [49,50]. Since both the point of introduction and the luminescent region were situated clearly above the (visible) flame region in those early experiments, we are forced to conclude that high-energy species (e.g. hydrogen atoms) had to transcend the visible flame in large enough numbers to excise a significant fraction of sulfur atoms from the analyte molecules above {and perhaps excite (cf. [3,5,9]) them to the $S_2(B^3\Sigma^-)$ [51] state}. By general principle as well as optical analogy, such free radicals (H, OH, peroxy-type structures, etc.) must likewise be present in reactive flows.

The suggested excision scenario is also in general agreement with the measured survival rates of various hetero-organics (containing N, O or S) en route *through* the low-temperature, hydrogen-rich flame of the above-mentioned reactor: their survival rates are much lower than those of the pure hydrocarbons [1,2]. It is also possible to introduce test compounds *above the flame of the reactor* (in fact, that is what the reactor was in part designed for). However, no thorough study of analyte survival under such conditions has yet been carried out.

Nor, indeed, have the contents of typical *reactive flows* been collected and analyzed for residual molecules of, or products from, hydrocarbons and hetero-organics of interest. These analytes/reagents are easily added as vapors —via a continuous doping stream or as chromatographic peaks— to the premixed hydrogen–air supply gas. Such an "RFR" (a reactive-flow *reactor*) may indeed prove attractive to some of the earlier-mentioned areas of spectral or kinetic cognates; it may even appeal to synthetic interests.

That would certainly be helpful: the RFD is in dire need of basic understanding (a need not unlike that of the FPD; never mind the latter's much longer history [4–9]). Similar to many other chromatographic detectors that appear to represent simplicity itself —and certainly similar to the FPD— the RFD may yet turn out to be much appreciated before it is much understood.

4. Note added in revision

Our reviewer suggested that we "discuss the applicability of this detector to capillary GC". Aware of the dinosaurian aura of packed columns, we are pleased to oblige. We do not, however, want to test the RFD with capillary columns: for us, packed columns are easier to use. More importantly, still, they offer a bigger challenge to detector performance because of their greater bleed, their larger solvent volumes, their broader analyte peaks. Thus, the RFD should, if anything, perform better with capillary than with packed columns.

That leaves only one problem to be addressed in this context: the detector speed (cell time constant). Some detectors broaden sharp peaks. Will the RFD do likewise? Judged from Fig. 1, considerable deadspace exists near the detector base. To reduce it is easy: by a tighter construction; by combining the hydrogen–air premix with the column effluent within the capillary flow regime; or by simply inserting the capillary column right up to restriction. But it would not be as easy to reduce the volume of the glow itself. Could *it* contribute to peak broadening?

The glow used in this study is a cylinder of 1.8 mm diameter and 35 mm length —of which, say, 10 mm are within view of the 6-mm diameter image conduit. The typical supply flow-rates are hydrogen 40 and air 60 ml/min. That amounts to a detector cell constant of ca. 15 ms, or to an analyte residence time within the whole reactive flow region of ca. 50 ms —far shorter than the chromatographic dispersion of even the sharpest capillary peak.

5. Note added in proof

One of us described briefly the RFD in a recent lecture [52]. In the ensuing discussion it

was noted that a micro-flame ionization detector–radioactivity detector (μFID–RAD) [53], which used a premixed oxy–hydrogen flame, had also monitored photometric flame response. This multi-channel detector should therefore be included in our literature citations (see second page) of *premixed flames*.

Acknowledgements

The consummate artistry of J. Müller (glassblowing) provided the capillaries for the new detector; the cooperative assistance of M.R. Conrad and C.G. Eisener (machining) succeeded in putting it together; and the cost-conscious adaptations of B. Millier and C. Wright (electronics) helped to monitor its response. Only this full array of Departmental support made our study possible and allowed it to proceed with minimal drain on our much appreciated financial support, NSERC research grant A-9604.

References

[1] K.B. Thurbide, Dalhousie University, Halifax, unpublished thesis research, 1991–1994.
[2] K.B. Thurbide and W.A. Aue, presented at the *77th CIC (Chemical Institute of Canada) Conference, Winnipeg, June 1994.*
[3] W.A. Aue and X.-Y. Sun, *J. Chromatogr.*, 641 (1993) 291.
[4] M. Dressler, *Selective Gas Chromatographic Detectors (Journal of Chromatography Library*, Vol. 36), Elsevier, Amsterdam, 1986, pp. 152–156.
[5] S.O. Farwell and C.J. Barinaga, *J. Chromatogr. Sci.*, 24 (1986) 483.
[6] E.R. Adlard, *CRC Crit. Rev. Anal. Chem.*, 5 (1975) 13.
[7] S. Kapila, K.O. Duebelbeis, S.E. Manahan and T.E. Clevenger, in R.M. Harrison and S. Rapsomanikis (Editors), *Environmental Analysis Using Chromatography Interfaced with Atomic Spectroscopy*, Ellis Horwood, Chichester, 1989, Ch. 3.
[8] R.S. Hutte and J.D. Ray, in H.H. Hill and D.G. McMinn (Editors), *Detectors for Capillary Chromatography*, Wiley Interscience, New York, 1992, Ch. 9.
[9] P.T. Gilbert, in R. Mavrodineanu (Editor), *Analytical Flame Spectroscopy*, Philips Technical Library/Macmillan, London, 1970, pp. 181–377, particularly pp. 240, 241, 247, 282 and 287.
[10] A.G. Gaydon and H.G. Wolfhard, *Flames*, Chapman & Hall, London, 1970.
[11] C.T.J. Alkemade, T. Hollander, W. Snelleman and P.J.T. Zeegers, *Metal Vapours in Flames*, Pergamon, Oxford, 1982.
[12] C.T.J. Alkemade and R. Herrmann, *Fundamentals of Analytical Flame Spectroscopy*, Adam Hilger, Bristol, 1979.
[13] R.M. Fristrom and A.A. Westenberg, *Flame Structure*, McGraw-Hill, New York, 1965.
[14] E. Pungor, *Flame Photometry Theory*, Van Nostrand, London, 1965.
[15] G.J. Minkoff and C.F.H. Tipper, *Chemistry of Combustion Reactions*, Butterworths, London, 1962.
[16] A.G. Gaydon, *The Spectroscopy of Flames*, Chapman & Hall, London, 2nd ed., 1974.
[17] B. Lewis and G. von Elbe, *Combustion, Flames and Explosions of Gases*, Academic Press, Orlando, FL, 3rd ed., 1987.
[18] A. Smithells and H. Ingle, *J. Chem. Soc. Trans.*, 61 (1892) 204.
[19] P.L. Patterson, R.L. Howe and A. Abu-Shumays, *Anal. Chem.*, 50 (1978) 339.
[20] T.L. Chester, *Anal. Chem.*, 52 (1980) 1621.
[21] R.M. Dagnall, K.C. Thompson and T.S. West, *Analyst*, 93 (1968) 72.
[22] N.B. Lowery, Dalhousie University, Halifax, unpublished doctoral research, 1993–1994.
[23] H.A. Moye, *Anal. Chem.*, 41 (1969) 1717.
[24] J.W. Birks (Editor), *Chemiluminescence and Photochemical Reaction Detection in Chromatography*, VCH, New York, 1989.
[25] I.M. Campbell and D.L. Baulch, in P.G. Ashmore and R.G. Donovan (Senior Reporters), *Gas Kinetics and Energy Transfer*, Vol. 3, Chemical Society, London, 1978, Ch. 2.
[26] M.A.A. Clyne, in B.P. Levitt (Editor), *Gas Phase Reactions of Small Molecules*, Plenum, London, 1973, Ch. 4.
[27] M.F. Golde and B.A. Thrush, in D.R. Bates and B. Bederson (Editors), *Advances in Atomic and Molecular Physics*, Vol. 11, Academic Press, New York, 1975, pp. 361–409.
[28] S. Toby, *Chem. Rev.*, 84 (1984) 277.
[29] B. Millier, X.-Y. Sun and W.A. Aue, *J. Chromatogr. A*, 675 (1994) 155.
[30] C.G. Flinn and W.A. Aue, *Can. J. Spectr.*, 25 (1980) 141.
[31] L.B. Graiff, *Nature*, 203 (1964) 856.
[32] H.H. Hill and W.A. Aue, *J. Chromatogr. Sci.*, 12 (1974) 541.
[33] W.A. Aue, H. Singh and X.-Y. Sun, *J. Chromatogr. A*, in press.
[34] V.A. Joonson and E.P. Loog, *J. Chromatogr.*, 120 (1976) 285.
[35] X.-Y. Sun, B. Millier and W.A. Aue, *Can. J. Chem.*, 70 (1992) 1129.

[36] X.-Y. Sun, H. Singh, B. Millier, C.W. Warren and W.A. Aue, *J. Chromatogr. A*, submitted for publication.
[37] S. Cheskis, E. Atar and A. Amirav, *Anal. Chem.*, 65 (1993) 539.
[38] S.J. Hill, M.J. Bloxham and P.J. Worsfold, *J. Anal. Atomic Spectr.*, 8 (1993) 499.
[39] B.D. Quimby and J.D. Sullivan, *Anal. Chem.*, 62 (1990) 1027.
[40] J.T. Andersson and B. Schmid, *Fresenius' J. Anal. Chem.*, 346 (1993) 403.
[41] S. Pedersen-Bjergaard, T.N. Asp and T. Greibrokk, *Anal. Chim. Acta*, 265 (1992) 87.
[42] S.E. Eckert-Tilotta, S.B. Hawthorne and D.J. Miller, *J. Chromatogr.*, 591 (1992) 313.
[43] W. Wardencki and B. Zygmunt, *Anal. Chim. Acta*, 255 (1991) 1.
[44] W.A. Aue and C.G. Flinn, *J. Chromatogr.*, 158 (1978) 161.
[45] S.S. Brody and J.E. Chaney, *J. Gas Chromatogr.*, 4 (1966) 42.
[46] C.R. Hastings, D.R. Younker and W.A. Aue, *Trace Subst. Environ. Health*, 8 (1974) 265.
[47] W.A. Aue and X.-Y. Sun, *J. Chromatogr.*, 633 (1993) 151.
[48] U. Schurath, M. Weber and K.H. Becker, *J. Chem. Phys.*, 67 (1977) 110.
[49] Y.-Z. Tang, *Doctoral Thesis*, Dalhousie University, Halifax, 1987.
[50] Y.-Z. Tang and W.A. Aue, presented at the *71st CIC (Chemical Institute of Canada) Conference and 3rd Chemical Congress of North America, Toronto, June 1988.*
[51] R.W.P. Pearse and A.G. Gaydon, *The Identification of Molecular Spectra*, Chapman & Hall, London, 4th ed., 1976.
[52] W.A. Aue, presented at the *25th Ohio Valley Chromatography Symposium, Hueston Woods, OH, June 1994*, plenary lecture.
[53] P.A. Rodriguez and C.L. Eddy, presented at the *ACS 15th Central Regional Meeting joint with the Ohio Valley Chromatography Symposium, Miami University, Oxford, OH, May 1983*, abstract No. 65.

ELSEVIER

Journal of Chromatography A, 684 (1994) 269–275

JOURNAL OF CHROMATOGRAPHY A

Determination of low concentrations of trimellitic anhydride in air

Pirkko Pfäffli

Institute of Occupational Health, Topeliuksenkatu 41 a A, FIN-00250 Helsinki, Finland

First received 20 October 1993; revised manuscript received 1 July 1994

Abstract

Trimellitic anhydride is used in the polymer industry as a hardener in epoxy formulations and as a component in paint resins and surface coatings. It has been reported to be a severe respiratory irritant and to cause pulmonary oedema, immunological sensitisation and asthma-like symptoms. It has been previously analysed as the corresponding acid by high-performance liquid chromatography with ultraviolet detection, and with flame ionisation detection after esterification to trimethyl trimellitate. In this study, the trimellitate ester was assayed by gas chromatography using electron-capture detection. The detection limit, 0.6 $\mu g/m^3$ (12 l of air sample; sampling rate 0.2 l/min), was superior compared with methods using flame ionisation or ultraviolet detection and also in view of the occupational reference value, 0.04 mg/m^3. The method will also be suitable for short-term sampling of the anhydride.

1. Introduction

Trimellitic anhydride (TMA; CAS No. 552-30-7; M_r 192.13; vapour pressure at 25°C $1.6 \cdot 10^{-5}$ Pa) [1] is a common industrial chemical used in the production of coatings, enamels and plasticisers for plastics. It is used also at elevated temperatures (ca. 200°C) as a multifunctional hardener for epoxy resins [2].

TMA is considered to be an extremely toxic substance [3–5]. In exposed humans, it can cause non-cardiac pulmonary oedema, immunological sensitisation and severe respiratory irritation. In many countries, the occupational reference value for this compound has been set as low as 0.04 mg/m^3, this being in most cases the ceiling value [6,7].

Sampling of airborne TMA has been carried out with poly(vinyl chloride) (PVC) copolymer membrane filters [8] or glass fibre filters [9–11]. PVC filter cassettes mounted on 10-mm cyclonic separators [12] have been used for collecting respirable particles while vapours have been sampled with Tenax tubes [9]. Apart from Tenax tubes, even charcoal tubes, two types of silica gel tubes, octadecyl silica gel, XAD-2 resin and Chromosorb 104 adsorption tubes have been tested for sampling TMA [1]. Tenax and Chromosorb 104 were the most promising sampling media for TMA vapours.

After sampling, the sampling medium is eluted with a mixture acidic acetonitrile and water [9] or with a dilute sodium hydroxide solution [10,11]. TMA in the eluate is then determined as its corresponding acid using high-performance liquid chromatography (HPLC) with ultraviolet (UV) detection. Alternatively, the filters are extracted with methanol, the extract derivatised

0021-9673/94/$07.00
SSDI 0021-9673(94)00617-2

with boron trifluoride–methanol, and TMA assayed as its trimethyl ester by gas chromatography (GC) with flame ionisation detection (FID) [8,12,13]. Solutions consisting of diazomethane in diethyl ether have also been used for derivatisation of the anhydride and the corresponding acid, followed by GC–FID [14].

The detection limits of the above methods are roughly on the same level as the current occupational reference value. However, large sample volumes are required for determination of concentrations close to the reference value. On the other hand, nothing is known about the lowest concentrations causing sensitisation. Therefore, it would also be important to be able to measure TMA at any concentration suspected of causing allergy.

We modified the NIOSH method [8] where TMA is determined as the corresponding methyl ester, i.e. trimethyl trimellitate (TME), by GC–FID. It has been found that phthalate esters with a conjugated structure resembling that of trimellitic esters, sometimes cause considerable contamination in the electron-capture detection (ECD) in environmental analyses [15]. TME could thus be assumed to yield a good response by ECD. Using ECD, one could easily reach a detection limit corresponding to 0.6 μg TMA/m^3 air with samples of 12 l.

2. Experimental

2.1. Chemicals

The chemicals used were boron trifluoride–methanol (BF_3 14%; E. Merck, Darmstadt, Germany), methanol and acetonitrile (Lab-Scan, Dublin, Ireland), methyl *tert.*-butyl ether (MTBE; Rathburn Chemicals, Walkerburn, UK), pyridine (Pierce, Rockford, IL, USA), dimethyl phthalate (DMP) and phthalic anhydride (PA) (E. Merck). The solvents were of HPLC grade (dried with anhydrous sodium sulphate), and the other chemicals of analytical grade.

2.2. Sampling

For sampling of airborne TMA, glass fibre filters (binder-free, Type AE, diameter 1 cm, pore size 0.3 μm; SKC, Eighty Four, PA, USA) and Tenax tubes (No. 226-35, SKC) mounted in series and a flow-rate of 0.2 l/min produced by SKC Aircheck Samplers, Model 224-43 XR, were used.

2.3. Derivatisation

For the analysis, the filters and the Tenax polymer were separately desorbed overnight with 2 ml methanol, with 0.2 pmol phthalic anhydride as an internal standard. Filter fibres and Tenax corns were removed from the solution by centrifugation (2000 *g*) and then washed with an additional 1 ml methanol which was thereafter combined with the desorption solution. After addition of 5 mg fine sodium chloride (for drying purposes), the solution was evaporated to near dryness and esterified with 150 μl boron trifluoride–methanol solution at 100°C for 1 h. After cooling, the solution was again carefully evaporated to near dryness under a nitrogen stream and the residue dissolved in 1 ml of MTBE. A 40-μl volume of pyridine was added to the MTBE solution, and the precipitate formed was removed by centrifugation (2000 *g*). Acetonitrile (0.5 ml) was added to 0.5 ml of the clear supernatant, and the mixture was used for GC analysis. As TME is a polar compound, the addition of the more polar acetonitrile to the solvent avoided the memory effect which otherwise might occur in chromatography.

2.4. Gas chromatography

The apparatus consisted of a Hewlett-Packard series 5790A gas chromatograph (Palo Alto, PA, USA) with a Ni^{63} electron-capture detector and a HP 5 column (5% phenylmethyl silicone; 25 m × 0.32 mm I.D., 0.17 μm). The temperature program for the column oven was 60°C for 0.5 min, 15°C/min, and 250°C for 3 min. The injector temperature was 230°C and that of the

detector 250°C. Helium was used as the carrier gas at a flow-rate of 1 ml/min, and argon with 5% of methane as an additional detector gas at 56 ml/min. These conditions gave a retention time of 15.04 min for TME.

2.5. Identity confirmation

The identity of the ester was confirmed by mass spectrometry (Hewlett-Packard, HP-5989A MS Engine) using electron impact ionisation at 70 eV. The optimal esterification period was determined by infrared (IR) spectrometry (20 SXC Fourier transform IR spectrometer; Nicolet, Madison, WI, USA). The anhydride was esterified as described above, but the heating was stopped alternatively after 15, 30, 45 or 60 min. After solvent evaporation, the ester was mixed with dried potassium bromide powder, and the mixture was pressed onto disks for IR spectroscopy.

2.6. Calibration

Calibration was performed with external standards by the phase (solid–liquid) balance method, i.e. a glass fibre filter or the contents of a Tenax tube of the same batch and in the same amount as for the samples were added to 2 ml of a standard solution of TMA in methanol. The standard solutions were allowed to stabilise overnight before derivatisation of TMA in the same way as with the samples. PA was used as an internal standard.

3. Results and discussion

A plot of ln $KT^{3/2}$ versus T^{-1} [15] has been used to provide insight into the detection mechanism of a compound and to indicate its optimum temperature (T) for ECD. Since K, electron-capture affinity, is proportional to the peak area, A, recorded on the chromatogram, K can be replaced by A in the plot. The graph for TME (Fig. 1) with its positive slope, indicates that TME is detected non-dissociatively and that the

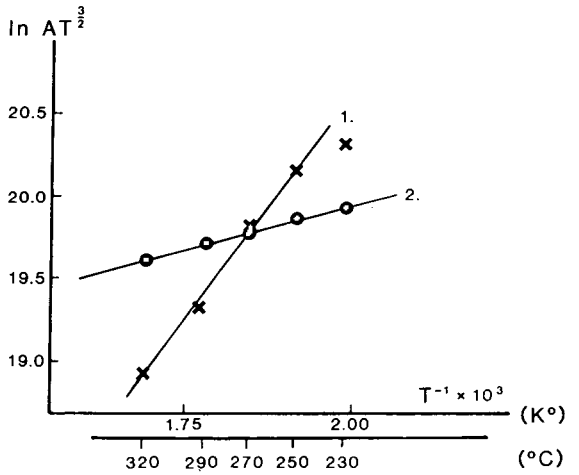

Fig. 1. Temperature dependence of the ECD response towards a fixed mass of trimethyl trimellitate (1; 0.71 pmol) and of dimethyl phthalate (2; 3.7 pmol). A = Area counts of the peaks; T = temperature (K).

detector response is stronger at lower temperatures. For a fixed amount of TME, the detector response was about six times stronger at 225°C than at 350°C (Fig. 2). Injection temperatures higher than 230°C caused the ester to decompose back to the anhydride [16], which was also

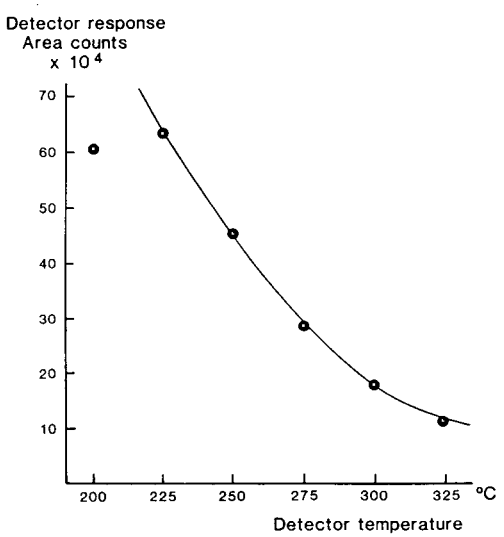

Fig. 2. Effect of the detector temperature on the detector response of a fixed mass (0.47 pmol) of trimethyl trimellitate.

evident in the chromatogram as a broad anhydride peak.

The identity of TME was confirmed by mass spectrometry. Fig. 3 shows a molecular ion at m/z 252 and a confirmatory ion at m/z 221 corresponding to the loss of an OCH_3 group [14]. The identity of the ester was also confirmed by IR spectrometry (Fig. 4). After a 30-min esterification period at 100°C, no sign of the anhydride was apparent in the wavenumber range 1860–1780 cm^{-1}, which is specific for anhydrides [17]. It was therefore also concluded that the esterification had been adequate.

A chromatogram of an external standard and of a sample collected on a glass fibre filter from the factory air are presented in Fig. 5. The chromatograms also show an internal standard (DMP) at 10.34 min. The ratio between the responses of the same molar amounts of TME and DMP at the detection temperature used (250°C) was 4 (response factor).

A calibration graph prepared with external standards is presented in Fig. 6. The regression is linear ($y = 35.96x + 0.065$; $r = 0.999$) up to a concentration of 0.5 μg/ml. The relative standard deviation of the method (including sampling and analysis) was 6.3% when measuring a concentration of 0.04 mg/m^3 ($n = 6$) of TMA in the air of an exposure chamber (6 m^3). The concentration in the chamber was developed by heating an epoxy hardener (4% TMA) in an open Petri dish (165 cm^2) at 185°C and using a fan to mix the emitted vapour with the chamber air.

TMA has a low vapour pressure, and, therefore, it can be expected to appear in the air as a

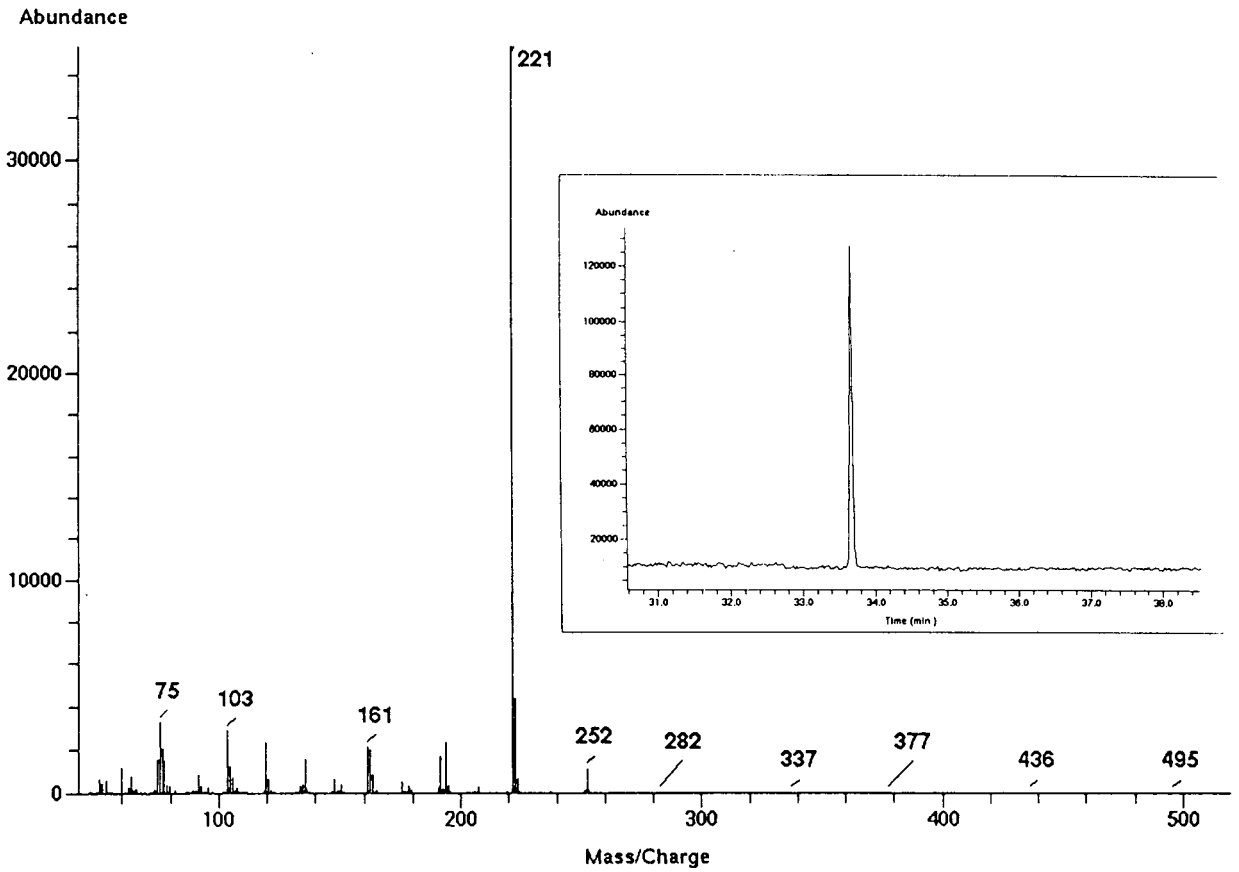

Fig. 3. Mass spectrum of trimethyl trimellitate (M^+ 252; $M - OCH_3$ 221).

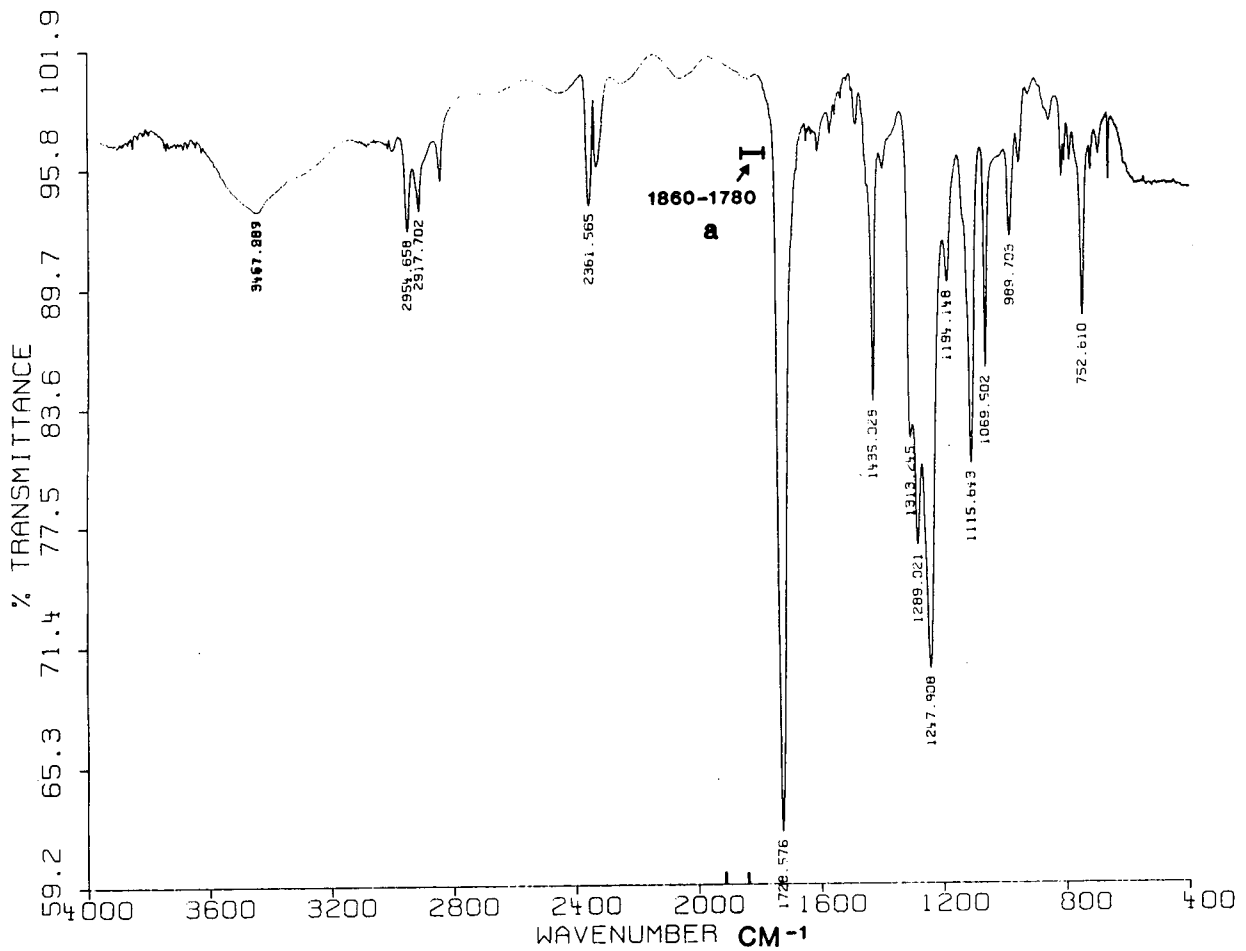

Fig. 4. Infrared spectrum of trimethyl trimellitate (a = wavenumber range for anhydrides).

mixture of gas and very fine particles [18]. Depending on TMA concentration in the air, 65 to 11% of the total amount of TMA retained was found on the filters and 35 to 89% in the Tenax tubes (Table 1). The anhydride was undetectable in the back-up sections of the tubes, indicating that no breakthrough had occurred in the tubes. The distribution of TMA between the filter and the Tenax tube did not seem to be significantly dependent on the sampling rate in the range of 0.2 to 0.5 l min^{-1}.

The anhydride, which reacts readily with water, may partly be converted to the corresponding acid in the moist ambient air. The same can happen on glass fibre filters, which are, unlike Tenax [19], polar material and may thus collect some water from the air. The esterification methods do not distinguish between the anhydride and the acid if present in the sample at the same time.

The analytical recovery of the anhydride (and the acid) from the spiked glass fibre filters was 100%, thus corroborating the previous results [9–11]. The recovery from Tenax polymer was 74.8 to 96.8% depending on the concentration (Table 2).

The collected samples can be stored at least four weeks at 6°C. Likewise, the esterified samples can be stored in dry solvent at 6°C for at least four weeks.

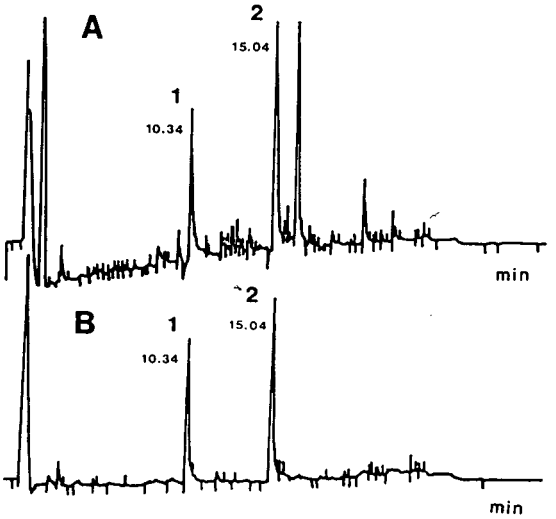

Fig. 5. Chromatograms of a sample (A) collected on a glass fibre filter and of a calibration standard (B) (0.22 μg/ml) of trimethyl trimellitate. TME (2) has a retention time of 15.04 min. Peak 1 is the internal standard, DMP (10.34 min; 0.72 μg/ml).

The detection limit of the ester in solution was 10 pg/μl (0.01 μg/ml), corresponding to 7.6 pg of the anhydride in each μl injected and 0.6 μg of the anhydride in each m^3 of air (12 l, sampling time 60 min). This detection limit is superior to methods using UV detection and FID, and good compared with the current occupational reference values (40 μg/m^3). The low detection limit also allows the use of short sampling periods, which might be valuable, e.g. when analysing profiles of fluctuating atmospheric concentrations. Such analyses are important when evaluating the role of peak concentrations in the development of allergy in workers [4].

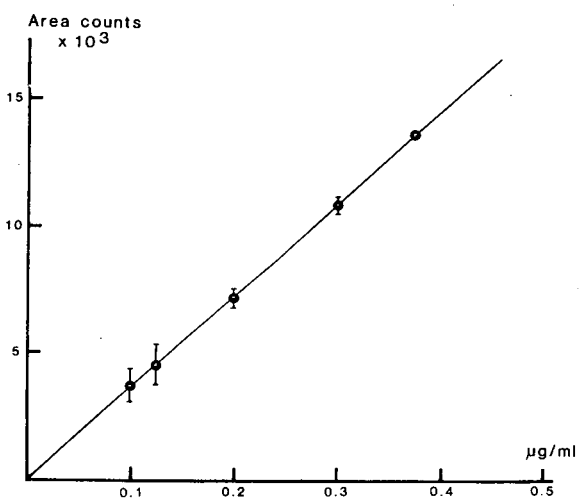

Fig. 6. Calibration graph for trimethyl trimellitate.

Table 1
Distribution of TMA fume between glass fibre filter and Tenax tube in the sampling apparatus (mean proportion, %, retained in each medium)

Concentration of TMA in air (mg/m^3) (± R.S.D., %)	Retained on filter (%)	Retained in Tenax tube (%)
0.042 (± 6.3)	65.2	34.8
0.026 (± 2.9)	11.3	88.7

R.S.D. = Relative standard deviation. Six samples were analysed at each of the two concentration levels. Of the six samples, two were collected at 0.2 l/min, two at 0.35 l/min and two at 0.5 l/min.

Personal samples collected from the workplace of a patient with suspected work-derived asthma showed TMA concentrations ranging from 2 to 24 μg/m^3 of TMA in the air. The factory in question used epoxy resin which was hardened with TMA to produce components for the electronics industry.

4. Conclusions

Determination of trimellitic anhydride by GC–ECD is superior in sensitivity to other detection

Table 2
Recovery of spiked trimellitic anhydride amounts from sampling media

Amount of TMA (μg)	Recovery (%)	
	Glass fibre filter	Tenax polymer (± R.S.D., %)
1.127	100	96.8 ± 2.2
0.375	100	78.5 ± 5.1
0.209	100	77.8 ± 6.3
0.125	100	74.8 ± 8.0

Number of samples was 6 in each concentration.

methods used for determining this toxic compound. The good sensitivity permits also short-term sampling.

Acknowledgements

Thanks are due to Ms. Leila Valtonen for skillful technical assistance and Ms. Mervi Hämeilä, M.Sc., for performing mass spectrometry.

References

[1] R.E. McCoy, J.A. Pauls and R.L. Stoffer, *Am. Ind. Hyg. Assoc. J.*, 46 (1985) 704.
[2] C.E. Freitag, in H. Buchholz-Meisenheimer, J. Frenzel and R. Pfefferkorn (Editors), *Ullmanns Ensyklopädie der technischen Chemie*, Vol. 9, Verlag Chemie, Weinheim, 4th ed., 1975, p. 150.
[3] National Institute of Occupational Safety and Health (NIOSH), *Current Intelligence Bulletin 21: Trimellitic anhydride; Publication No. 78-121*, Department of Health, Education and Welfare, Cincinnati, OH, 1978.
[4] K.M. Venables, *Br. J. Ind. Med.*, 46 (1989) 222.
[5] *Toxicity Review 8*, Health and Safety Executive, London, 1983.
[6] *Threshold Limit Values and Biological Exposure Indices, 1993–1994*, American Conference of Governmental Industrial Hygienists, Cincinnati, OH, 1993.
[7] Anon., *Appl. Occup. Environ. Hyg.*, 6 (1991) 625.
[8] National Institute of Occupational Safety and Health (NIOSH), *Manual of Analytical Methods, Vol. 6, Method No. P and CAM 322; Trimellitic Anhydride*, US Department of Health, Education and Welfare, Washington, DC, 2nd ed., 1985.
[9] *Aromatic Carboxylic Acid Anhydrides in Air —Laboratory Method using Glass Fibre Filter/Tenax Tube Sampling and High Performance Liquid Chromatography (MDHS Series* No. 62), Health and Safety Executive, London, 1988.
[10] J. Purnell and C.J. Warwick, *J. High Resolut. Chromatogr. Chromatogr. Commun.*, 3 (1980) 482.
[11] R. Geyer, R.C. Jones and N. Mezin, *J. High Resolut. Chromatogr. Chromatogr. Commun.*, 9 (1986) 308.
[12] J. Palassis, J.C. Posner, E. Slick and K. Schulte, *Am. Ind. Hyg. Assoc. J.*, 42 (1981) 785.
[13] P.A. Biondi and M. Gagnasso, *J. Chromatogr.*, 109 (1975) 389.
[14] L.G. Rushing, J.R. Althaus and H.C. Thompson, *J. Anal. Toxicol.*, 6 (1982) 290.
[15] C.F. Poole and A. Zlatkis, in A. Zlatkis and C.F. Poole (Editors), *Electron Capture —Theory and Practice in Chromatography*, Elsevier, Amsterdam, 1982, pp. 151–190.
[16] M. Windholz, S. Budavari, L.Y. Stroumtsos and M. Noether Fertig (Editors), *The Merck Index, An Encyclopedia of Chemicals and Drugs*, Merck & Co., Rahway, NJ, 1976, p. 1244.
[17] C.J. Pouchert, *The Aldrich Library of FT-IR Spectra*, Edition I, Vol. 2, Aldrich, Milwaukee, WI, 1985, pp. 308, 334.
[18] C. Perez and S.C. Soderholm, *Appl. Occup. Environ. Hyg.*, 6 (1991) 859.
[19] U. Giese, in A. Kettrup (Editor), *Analyses of Hazardous Substances in Air*, Working Group Analytical Chemistry, Deutsche Forschungsgemeinschaft, VCH, Weinheim, Vol. 2, 1993, pp. 7–8.

ELSEVIER

Journal of Chromatography A, 684 (1994) 277–287

JOURNAL OF CHROMATOGRAPHY A

Gas chromatographic–mass spectrometric determination of chlorinated *cis*-1,2-dihydroxycyclohexadienes and chlorocatechols as their boronates

N.H. Kirsch, H.-J. Stan*

Institute of Food Chemistry, Technical University of Berlin, D-13355 Berlin, Germany

First received 5 May 1994; revised manuscript received 1 July 1994

Abstract

The aerobic degradation of mono- and dichlorobenzenes proceeds via the chlorinated *cis*-1,2-dihydroxycyclohexa-3,5-dienes, which are subsequently reduced to their chlorocatechols. It is necessary to derivatize the vicinal hydroxyl groups in both polar metabolites to obtain volatile compounds amenable to capillary gas chromatography–mass spectrometry. Butyl- and phenylboronic acids were found to be the most suitable and easy to handle reagents because of their inherent selectivity in forming cyclic boronates. These derivatives were found to be stable and exhibit good chromatographic properties and clear mass spectra, which are presented for all mono- and dichlorocatechols, as well as for 3-chloro-, 3,5- and 3,6-dichloro-*cis*-1,2-dihydroxycyclohexa-3,5-diene.

1. Introduction

Aerobic microbial degradation of lower chlorinated benzenes starts with the initial oxygenation of the benzene nucleus by (chloro-)-benzenedioxygenases and leads to the chlorinated *cis*-1,2-dihydroxycyclohexa-3,5-dienes (*cis*-Ds) [1–3]. These metabolites are substrates for the following dihydroxydihydrobenzene-oxidoreductases, which rearomatize the *cis*-Ds by dehydrogenation to their chlorinated catechols [1–6]. Subsequently these substituted catechols are transformed by the ring cleaving catechol dioxygenases, with fission mainly occurring between the hydroxyl groups (modified *ortho* pathway) to the corresponding chlorinated muconic acids. The reaction with a catechol-2,3 dioxygenase (*meta* pathway) leads to chlorinated 2-hydroxymuconic semialdehydes, which were reported to be dead-end metabolites that bind irreversibly to enzymes [7].

The degradation of chlorobenzenes by suitable microbes in bioreactors has been recently reported [8]. The efficiency of such biological treatments is controlled by the determination of the chlorobenzene concentrations in inlet and effluent of the bioreactors, as well as by measuring the rate of chloride release and the growth of bacterial populations. Additionally, the screening for exuded metabolites in the effluent is a useful tool for the optimized operation of the reactors with regard to chlorobenzene loading, to temperature and to pH, as well as with regard to oxygen and supplementary substrate concentration. The optimized operation of bioreactors will be described elsewhere. In accordance with

* Corresponding author.

0021-9673/94/$07.00
SSDI 0021-9673(94)00619-9

the observations of other working groups [1,3,5,6], we sometimes observed blue–purple discoloured media during the enrichment of chlorobenzene degrading cultures grown in a chemostat. This phenomenon has been explained as the secretion of chlorinated catechols, which give coloured complexes with transient metal ions and tend to polymerize in their reactive quinone form to yield dark coloured polymerisates. The chlorocatechols are toxic compounds and their secretion might occur at overdoses of substrate [1] or with insufficient availability of catechol dioxygenase.

Knuutinen and Korhonen [9] presented the mass spectral data of all nine underivatized chlorinated catechols and the mass spectra of some derivatized chlorocatechols have also been briefly discussed [10,11]. Chlorinated catechols have been mainly analyzed as their ethyl [10,11], silyl [2,3,12] and acetyl [13] derivatives. These methods exhibit no selectivity for vicinal diols and may result in loaded chromatograms with poor separation of the isomers. Better results were expected by using reagents for the selective derivatization of bifunctional compounds.

As early as 1958, Sugihara and Bowman [14] studied the applications of "benzeneboronic acid" to react with polyhydroxyl compounds to yield stable five-, six- and seven-membered rings. They used the different structures and accordingly different melting and boiling points of *cis*- and *trans*-boronate isomers to achieve separation. Brown and Zweifel [15] applied butylboronate esters to separate *cis*- and *trans*-cycloalkanediols by distillation. In 1967 Brooks and Watson [16] introduced the use of cyclic boronates into analytical GC–MS and reported that the reaction is specific for certain cyclic *cis*-diols and can therefore be used to distinguish between *cis*- and *trans*-isomers. Brooks and Maclean [17] investigated in 1971 the GC and MS properties of cyclic *n*-butylboronates as derivatives of polar bifunctional compounds. Later, Brooks and co-workers [18–20] introduced ferroceneboronates as derivatives of diols and related compounds for similar analytical purposes. Poole and Zlatkis [21] reviewed the properties and wide applications of boronic acids to yield cyclic boronic esters. Recently, the use of phenylboronic acid for the exclusive derivatization of side-chain diols was reported for the chromatography of ecdysteroids [22,23]. To our knowledge, however, the method was not applied for the detection of the first two metabolites of aerobic degradation of chlorobenzenes. The suitability of boronates to analyze catechols selectively with GC–MS was demonstrated with a number of available test substances [24].

In this paper, the GC and MS data of several chlorocatechols and their precursor metabolites, the chlorinated benzene-*cis*-dihydrodiols as their boronic acid derivatives are reported, as well as their detection in biological samples.

2. Experimental

2.1. Materials

3-Chlorocatechol was kindly provided by F. Lingens, University of Stuttgart-Hohenheim, Germany. 4-Chlorocatechol was purchased from Aldrich, Milwaukee, WI, USA. All four isomeric dichlorocatechols were prepared and stored as previously described [25]. Each catecholic compound was dissolved in acetone to prepare stock solutions containing 1 mg/ml. From these stock solutions standard mixtures containing 1 mg per compound in 10 ml of acetone were prepared.

Butyl- and phenylboronic acids were purchased from Fluka, Buchs, Switzerland. Solutions were prepared by dissolving 20 mg of each boronic acid in 10 ml of dry acetone. All solutions were stored at 4°C in the dark until used.

Acetone, hexane and dichloromethane were Pestanal grade from Riedel-de Haen, Seelze, Germany. Methanol and water for HPLC were Chromosolv grade and purchased from Riedel-de Haen as well.

Analytical-reagent grade sodium sulfate was obtained from Merck, Darmstadt, Germany and dried at 400°C for at least 1 h before use. All other chemicals were of analytical-reagent grade.

2.2. Instrumentation and methods

GC–MS was performed by using a Hewlett-Packard (HP) 5890 Series II gas chromatograph

with hot splitless injector (210°C) and an OV-17 column, 50 m × 0.32 mm I.D. and 0.25 μm film thickness from Seekamp, Achim, Germany. The analytical column was connected to a deactivated, uncoated retention gap of 2 m × 0.32 mm I.D. by a press-fit connector. The injection volume was 2 μl; injection was performed by an automatic liquid sampler HP 7673.

Helium was used as carrier gas with a flow of 3 ml/min. The applied temperature programs differed for butyl- and phenylboronic derivatives, according to optimized separation of the chlorocatechol isomers. The temperature program for butylboronates was: 90°C (2 min), 5°C/min to 140°C (1 min), 10°C/min to 240°C (10 min).

The temperature program for phenylboronates was: 90°C (2 min), 20°C/min to 160°C (10 min), 10°C/min to 240°C (10 min).

The quadrupole mass spectrometer HP 5989 A was operated in the electron impact (EI) mode at 70 eV with an ion source temperature of 240°C and full scan in the range of 50–350 u (1.7 scans/s). When running in the chemical ionization (CI) mode, methane was used as reactant gas with a source pressure of 1.2 Torr (1 Torr = 133.322 Pa) and a source temperature of 170°C.

Preparative HPLC was performed using a Beckman System Gold system equipped with solvent module 126 and UV–Vis detector 166 and a column Beckman Ultrasphere Octyl 5 μm (25 cm × 10 mm). Solvents were methanol (A) and 0.005 *M* KH_2PO_4 in water of pH 2.5 (B); the elution was isocratic 30:70 (A–B) with a flow of 4 ml/min. Catechols and dienes were detected at 250 nm.

^1H NMR data were obtained from a Bruker AM 400 (Rheinstetten, Germany) instrument, processed with Aspect 3000 processor. NMR was operated with 400 MHz and tetramethylsilane (TMS) as internal standard and C^2HCl_3 as solvent.

2.3. Extraction of metabolites

A 200–500-ml volume of chemostat medium or bioreactor effluent was centrifuged at 9000 rpm (ca. $1.3 \cdot 10^4$ *g*) for 20 min. The almost clear supernatant was adjusted to a pH of 10–11 by the addition of 1 *M* sodium hydroxide solution. Subsequently, liquid–liquid extraction with 50 ml of *n*-hexane was performed twice, in order to eliminate all non-polar compounds from the aqueous phase, which then was acidified to pH 4–5 by 1 *M* hydrochloric acid and extracted twice with 50 ml of dichloromethane. The combined dichloromethane extracts were dried with sodium sulfate and after filtration evaporated to dryness.

2.4. Derivatization procedure

The residue was dissolved in 800 μl of dry acetone, transferred to an autosampler vial and mixed with 200 μl of the boronic acid solution. The vials were capped, shaken and kept at 50°C for 10 min. The extracts so treated were ready for GC–MS analysis. For the preparation of reference chromatograms and spectra, standard solutions or mixtures containing 20 μg per compound in 800 μl of dry acetone were derivatized.

3. Results and discussion

3.1. GC and MS data of monochloro- (MCC) and dichlorocatechol (DCC) isomers after derivatization to boronates

The well known derivatization with boronic acids represents a reversible reaction with an equilibrium constant sufficiently high for the formation of boronate esters in the particular case of coplanar and vicinal diols. A test for long time stability of derivatized extracts was carried out with different vials containing equal amounts of chlorocatechols that were derivatized successively for six days and stored at 4°C until measured on the last day in one sequence. No significant difference between peak areas could be observed with all the derivatives produced within this period of time.

The derivatization of all chlorocatechols used in this study was found to be reproducible and probably complete with both boronic acids, because the plots of the measured areas of the derivative peaks versus concentrations of chlorocatechols resulted in a linear relationship over a wide concentration range. An excess of boronic

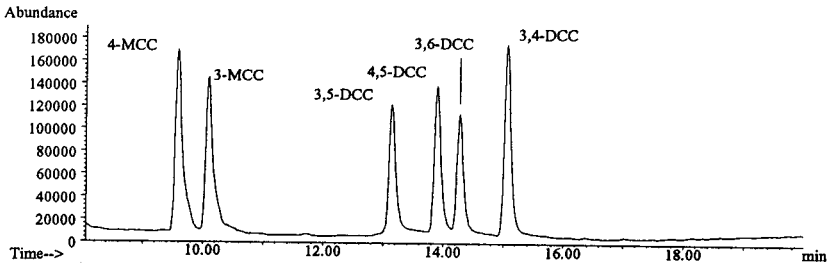

Fig. 1. TIC chromatogram of a standard mixture of all isomeric MCCs and DCCs as their butylboronates.

acid in the reaction mixture was found not to impair the chromatography, because no additional peaks appeared in the relevant part of the chromatogram and the peaks of the derivatives showed good peak shapes (Figs. 1 and 4). The excessive boronic acids were found to react to volatile trimers as described in the literature [21], which was proved by their mass spectra in this study (data not shown).

3.2. Mass spectra of butylboronates

In Fig. 1 a chromatogram of a standard mixture of all MCCs and DCCs after derivatization to their butylboronates is presented. With the GC conditions elaborated in preliminary experiments, a satisfactory separation of all the target compounds can be easily achieved, which is necessary because the isomers show very similar mass spectra. In Fig. 2, mass spectra of the butylboronates of 3-MCC and 3,6-DCC are presented as examples. The isotopic patterns of boron (^{10}B:$^{11}B = 1:4$) and chlorine (^{35}Cl:$^{37}Cl = 3:1$) make the identification of the diol derivatives an easy task.

The spectra of the butylboronates of all MCCs and DCCs exhibit the molecular ion at m/z 210 and 244, respectively, with relative intensities of 30–40%. The base peaks in all spectra are m/z 154 or 188, respectively, which arise from the loss of butene $[M - C_4H_8]^+$. Due to the stability of the cyclic boronate and the favourable loss of butene, all other fragments are of low intensity and negligible.

When negative CI with methane is performed, different but also simple spectra of the butylboronates of MCCs and DCCs are obtained, as can be seen from Fig. 3. Each spectrum provides the molecular ion M^- as base

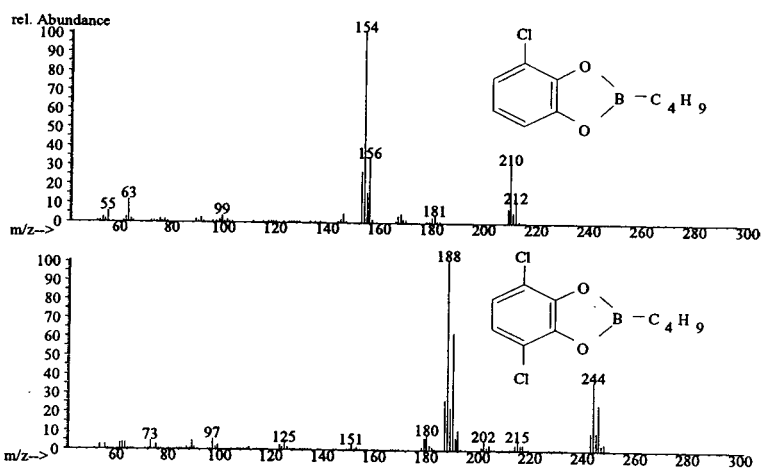

Fig. 2. EI mass spectra of 3-MCC and 3,6-DCC as their butylboronates.

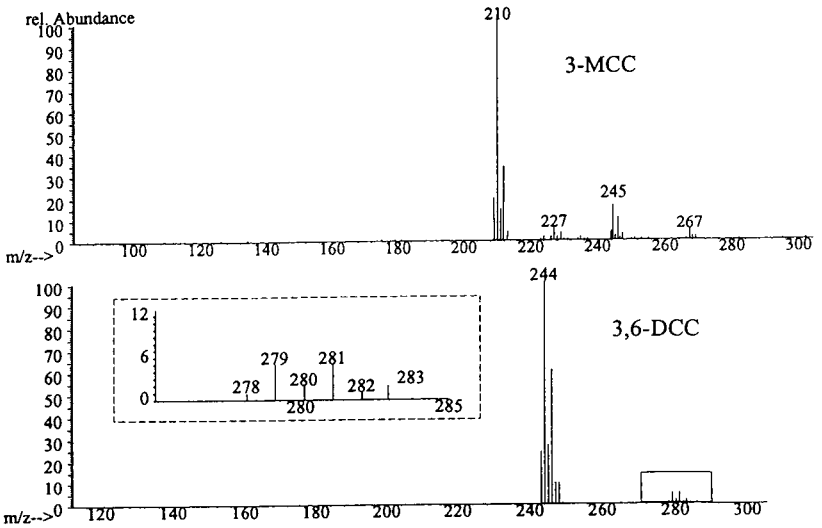

Fig. 3. Mass spectra of 3-MCC and 3,6-DCC as their butylboronates obtained with negative CI using methane as reactant gas.

peak without further fragmentation to be observed. Additionally the attachment of a chlorine results in the formation of $[M + 35]^-$, which can be easily recognized by checking for the typical chlorine clusters at m/z 245 and m/z 279, respectively.

3.3. Mass spectra of phenylboronates

The total ion current (TIC) chromatogram of a standard mixture of chlorocatechols derivatized with phenylboronic acid is shown in Fig. 4. The chromatogram shows prolonged retention times due to their higher molecular masses with also satisfactory separation of all isomers. Note the different order of elution between 3,6-DCC and 4,5-DCC when compared with butylboronates.

By means of the spectra, the isomers can hardly be distinguished. The great stability of the phenylboronates shows almost only molecular ions without remarkable fragmentation, as can be seen from the spectra of Fig. 5 for 3-MCC and 3,6-DCC.

Note the ion cluster at m/z 132 with 3,6-DCC, which is obviously the double charged molecular ion M^{2+}, often observed with compounds producing very stable ions. The fragment m/z 123 can be found in any chlorocatechol spectrum in various intensities.

The clusters of the ion m/z 123 indicate that this fragment contains the boron and one chlorine atom. Due to the absence of this fragment ion with the butylboronates, its formation is proposed to occur by loss of the stable boronphenyl group and the attachment of a cleaved chlorine from the chlorinated catechol to the electrophilic boron.

In Table 1 the intensities of m/z 123 related to M^+ observed with the different derivatives are compiled. They are in agreement with our interpretation of a rearrangement taking place, because the intensities of m/z 123 with the 3-substituted isomers are obviously larger than that observed with other isomers not containing chlorine adjacent to the boron.

The mass spectra obtained from negative CI show the molecular ions M^- without any fragmentation, but in analogy to the butylboronates,

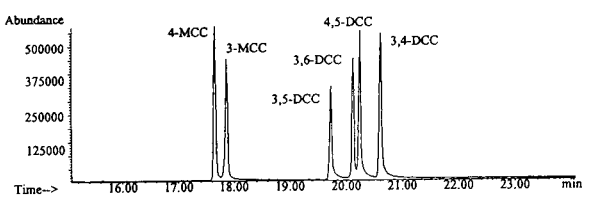

Fig. 4. TIC chromatogram of all isomeric MCCs and DCCs as phenylboronates.

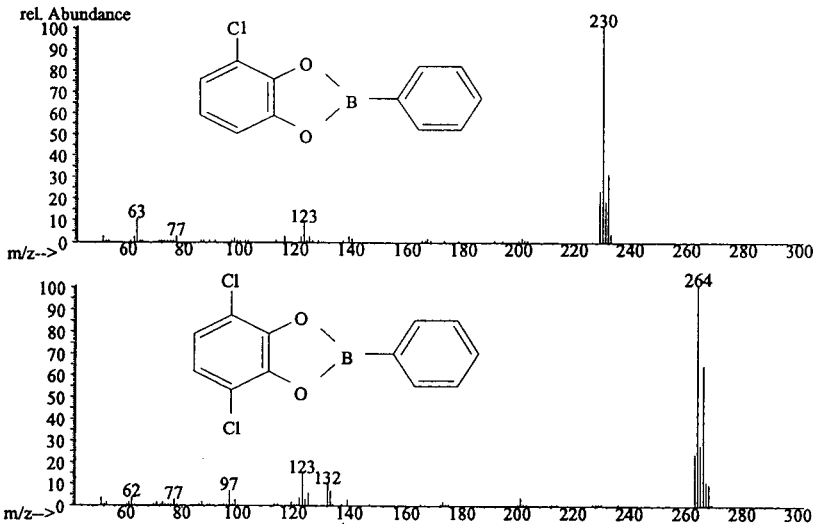

Fig. 5. EI mass spectra of 3-MCC and 3,6-DCC as their phenylboronates.

the attachment of chlorine to $[M+35]^-$ is observed. While the ion m/z 265 in the spectra from 3- and 4-MCC is present with 10–15%, the corresponding ion m/z 299 from DCC spectra is only observed in low abundancies of about 5% of the base peak (data not shown).

3.4. Derivatization of extracts

The derivatization of extracts could be easily carried out without interference by the matrix. Some case studies will be given here as examples. When extracts from bioreactor effluent or from medium of the chemostat were analyzed, a standard mixture of chlorocatechols was derivatized and measured within the same sequence, in order to calibrate the system.

In the first case chosen, the medium of a chemostat was extracted and derivatized with butylboronic acid. This chemostat contained a pure culture of *Pseudomonas aeruginosa* sp., which is able to utilize 1,4-dichlorobenzene (1,4-DCB) only. A typical TIC chromatogram and the relevant spectra of the boronate peaks obtained from such an extract is given in Fig. 6. As can be seen, only small amounts of the expected 3,6-DCC were detectable (10–15 μg/l), whereas another compound appeared at 15.3 min in a larger quantity. The mass spectrum of this compound was not that of a catechol derivative. The spectrum of this unknown compound exhibits ions with isotopic clusters indicative for boron esters (m/z 246, 211 and 146) and such that are indicative for a dichlorinated compound (m/z 246) as well as an one chlorine-containing fragment (m/z 211). Therefore, it is probable a dichloro compound as its butylboronate. The ion with the largest mass is most likely the molecular ion with a mass 2 u higher than that of a DCC butylboronate.

Since the compound shows more fragmentation than the aromatic catechol, a non-aromatic

Table 1
Relative intensity of the fragment at m/z 123 from different CCs as their phenylboronates

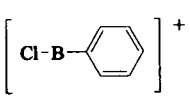

proposed m/z 123

Chlorinated catechol	Intensity related to M^+ (%)
3-MCC	9.5
4-MCC	1.7
3,4-DCC	14
3,5-DCC	11
3,6-DCC	15
4,5-DCC	2.7

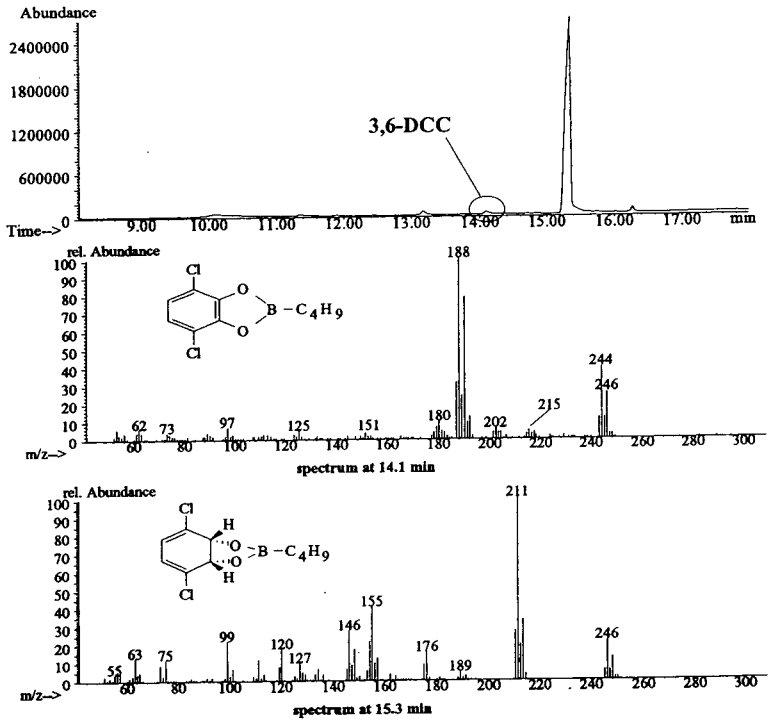

Fig. 6. TIC chromatogram and mass spectra from butylboronates of metabolites extracted from a chemostat experiment eluting at 14.1 and 15.3 min.

structure is probable. The pattern of the chlorine and the boron isotopes at the molecular ion proves the presence of two chlorines in this derivative. The base peak of the spectrum at m/z 211 obviously results from the loss of one chlorine $[M-35]^+$. The loss of the second chlorine is also observed resulting in m/z 176. Although not all fragments can be reasonably explained, we suggested the presence of the first metabolite of the aerobic degradation of chlorobenzenes, a chlorinated benzene-*cis*-dihydrodiol. Since the microbes were fed with 1,4-DCB only, this metabolite is strongly indicated to be 3,6-dichloro-*cis*-D. The structure of the derivatized metabolite is shown in the spectrum of Fig. 6. The content of the *cis*-diol in the medium of the chemostat was estimated to be 200 μg/l by semi-quantitative analysis. In order to isolate this compound for further characterization, 18 l of chemostat medium were extracted with dichloromethane and the residue was purified by preparative HPLC. The fraction containing the metabolite yielded an amount of 1.9 mg and was subjected to ^{1}H NMR. The spectrum provided two resonances, which were in accordance with the predictions for this symmetrical compound. Related to TMS as internal standard, one singlet was observed at $\delta = 4.45$ ppm, which was assigned to the olefinic protons. A second singlet appeared at $\delta = 6.08$ ppm, assigned to the *cis*-located protons beneath the hydroxy groups. These data are in agreement with the ^{1}H NMR data of 4-chloro-2,3-dihydroxy-1-methylcyclohexa-4,6-diene, the corresponding metabolite originating from 4-chlorotoluene, reported by Gibson et al. [26].

The isolated *cis*-dihydrodiol was also measured with negative CI under the conditions described above after derivatization with butylboronic acid. The spectrum is presented in Fig. 7 and shows the quasi molecular ion $[M-1]^-$ at m/z 245 with an intensity of only 23%. The consider-

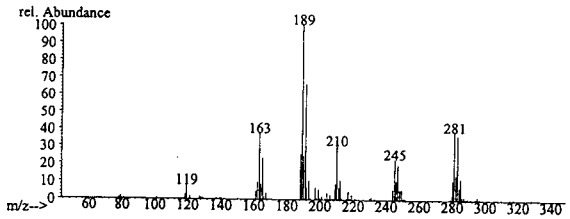

Fig. 7. Mass spectrum of 3,6-dichloro-*cis*-D obtained with negative CI with methane as reactant gas.

able fragmentation as well as the abstraction of one proton is again indicative to a non-aromatic structure. While m/z 210 originates from the loss of one chlorine, m/z 281 is indicative to an attachment of a chlorine; a reaction that could be observed under the same conditions with butylboronates of DCCs only with intensities below 5% (see Fig. 3). The base peak at m/z 189 is easily explained by the loss of butene.

In a second case study, a bioreactor loaded with mono- and all three isomers of dichlorobenzene was investigated. The clearly arranged TIC chromatogram of the butylboronates is presented in Fig. 8 and offers only a few peaks. Four of them are marked and the appropriate spectra of compounds I and II are also shown in Fig. 8.

The spectra of compounds I and III can easily be assigned to the structure of MCC and DCC isomers, their retention times were identical with those of 3-MCC and 3,6-DCC. By performing reconstructed ion chromatograms based on m/z 154 and 188, respectively, the presence of other isomers can be checked even in small amounts, but this type of screening was negative in this case.

The spectra of compounds II and IV offer molecular ions, whose masses are again 2 u higher than those of MCC and DCC isomers. The spectra also provide more fragmentation compared to the aromatic catechols. While com-

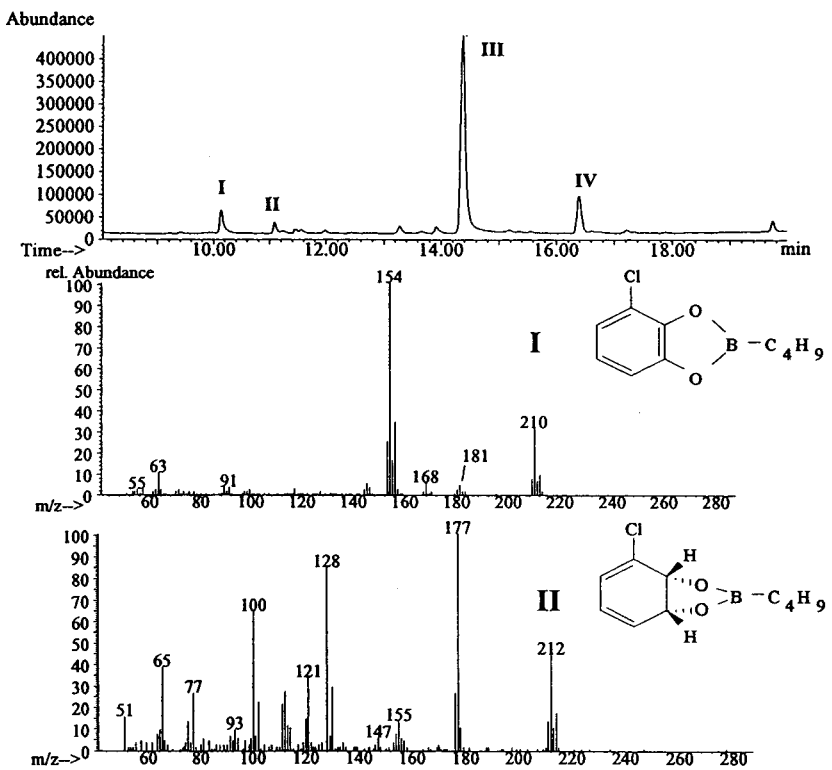

Fig. 8. TIC chromatogram of an extract from bioreactor effluent derivatized with butylboronic acid and mass spectra of two of the compounds indicated.

pound IV shows a spectrum identical to that of 3,6-dichloro-*cis*-D, compound II provides a spectrum unknown so far (see Fig. 8). The boron and chlorine isotope cluster of the probable molecular ion at *m/z* 212 indicates the presence of one chlorine, whose loss produces the base peak at *m/z* 177. The fragmentation of $M^{+\cdot}$ with loss of butene leads to *m/z* 155, while the cleavage of $O–B–C_4H_9$ leads to the intense peak at *m/z* 128. Ion *m/z* 121 can be explained by the loss of butene (C_4H_8) from the fragment ion *m/z* 177. The appearance of a chlorinated fragment at *m/z* 100 can be explained by the rearrangement of a chlorinated cyclopentadiene radical.

Summarizing the MS information it is strongly evident that compound II is a chloro-*cis*-D, which probably is the 3-chloro isomer, the natural precursor metabolite of the 3-MCC (compound I in Fig. 8) also detected. The position of the chlorine in 3-MCC is certain (known retention time). Hitherto, the formation of 4-MCC during the degradation of monochlorobenzene could not be observed in our analyses and has not yet been reported by others. Therefore, compound II is unlikely to be 4-chloro-*cis*-D, which would be the natural precursor of 4-MCC.

As a last example, the extract of the medium of a bioreactor was analyzed, loaded with an inlet concentration of about 30 mg/l of 1,3-dichlorobenzene as single substrate. The chromatogram of the butylboronates is presented in Fig. 9, as well as the mass spectra of the dominant peak V at 13.4 min.

The spectrum of compound V eluting at 13.4 min exhibits the ion masses of *m/z* 246, 211, 189, 146 and 99 already known from the 3,6-dichloro-*cis*-D, so that *m/z* 246 is probably the molecular ion of this compound (cf. Fig. 6). However, the ion intensities are different and additionally the ions of *m/z* 162 representing the base peak of the spectrum and *m/z* 134 next in intensity are found only in this compound. As can be seen, the fragment ion *m/z* 162 lacks the boron cluster, but contains the double chlorine cluster. Therefore its occurrence can be explained with the cleavage of the $O–B–C_4H_9$ group from the molecular ion with formation of a dichlorophenol ion. Phenols are known to lose CO forming a cyclopentadiene fragment, which is observed with a high abundance at *m/z* 134 as the corresponding dichloro compound. The cleavage of one chlorine from *m/z* 134 results in the formation of ion *m/z* 99, exhibiting the ion cluster of an one chlorine containing fragment. When compared with the 3,6-dichloro-*cis*-D derivative the loss of chlorine seems less favourable and can be

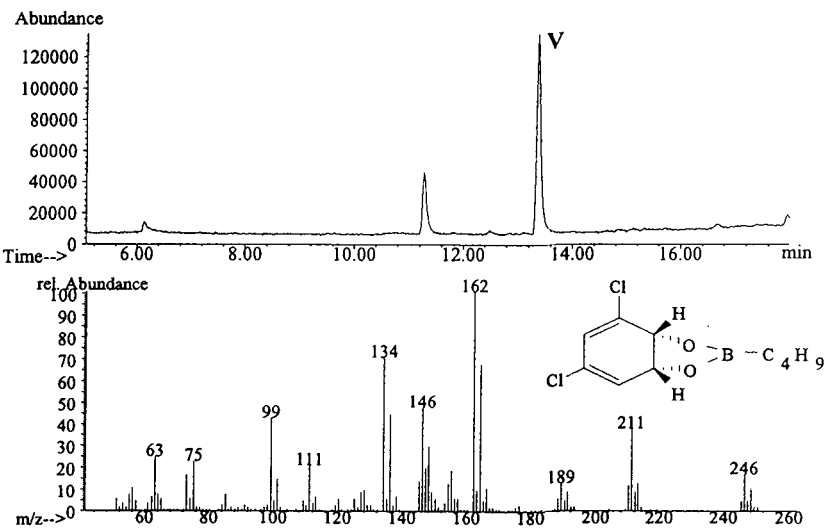

Fig. 9. TIC chromatogram of an extract of a bioreactor effluent dervatized with butylboronic acid and mass spectrum of compound V.

explained only with the different chlorine substitution. Since the microbes of the bioreactor have only degraded the 1,3-dichlorobenzene, it seems reasonable to propose the metabolite obtained to be 3,5-dichloro-*cis*-D. The structure of its butylboronate is given in Fig. 9. Due to the small amounts produced in the bioreactor it was not possible to isolate this compound in order to support the proposed structure by NMR.

4. Conclusions

For the GC determination of metabolites of the aerobic degradation of chlorobenzenes the derivatization of these compounds is a prerequisite. Butyl- and phenylboronic acids have proven to be suitable reagents for the selective derivatization of diol-containing metabolites. The advantages of using these reagents are: easy handling of the derivatization procedure, quantitative reaction under mild conditions, stability of the derivatives, good GC behavior and clear MS fragmentation pattern. The boron isotope cluster adds to the assignment of fragments. Additionally to note is that boronic acids are less toxic than other derivatization reagents.

The isomers of derivatized chlorocatechols show a good separation with an OV-17 column. The MS detection provides spectra with minor fragmentation and characteristic base peaks for the homologues, whereas the isomers produce very similar spectra.

In contrast, the chlorinated *cis*-Ds, the precursor metabolites of the chlorocatechols, exhibit significant MS fragmentation, which allows their distinction as could be proved with the 3,5- and 3,6-dichloro-*cis*-D isomers. The isotopic pattern of boron and chlorine again represent valuable tools for the interpretation of the spectra. The loss of chlorine from the non-aromatic *cis*-Ds is observed at a significant higher rate than from the more stable chlorocatechols. This also applies to electron capture with negative CI which produces with chlorocatechols almost only the molecular anion while the chlorocyclodienediol boronates show considerable fragmentation.

The screening on the exuded metabolites of chlorobenzene degradation delivered helpful information about the operation of the bioreactors as well as data about the chemical pathways and properties of microbial metabolism.

Acknowledgement

Financial support by the "Deutsche Forschungsgemeinschaft" as part of "Sonderforschungsbereich 193" (Biological Treatment of Industrial Wastewaters) is gratefully acknowledged.

References

[1] W. Reineke and H.-J. Knackmuss, *Appl. Environ. Microbiol.*, 47 (1984) 395–402.
[2] B.E. Haigler, S.F. Nishino and J.C. Spain, *Appl. Environ. Microbiol.*, 54 (1988) 294–301.
[3] J.C. Spain and S.F. Nishino, *Appl. Environ. Microbiol.*, 53 (1987) 1010–1019.
[4] J.A.M. de Bont, M.A.W. Vorage, S. Hartmans and W.J.J. van den Tweel, *Appl. Environ. Microbiol.*, 52 (1986) 677–680.
[5] G. Schraa, M.J. Boone, M.S.M. Jetten, A.R.W. Neerven, P.J. Colberg and A.J.B. Zehnder, *Appl. Environ. Microbiol.*, 52 (1986) 1374–1381.
[6] S.F. Nishino, J.C. Spain, L.A. Belcher and C.D. Litchfield, *Appl. Environ. Microbiol.*, 58 (1992) 1719–1726.
[7] W. Reineke, D.J. Jeenes, P.A. Williams and H.-J. Knackmuss, *J. Bacteriol.*, 150 (1982) 195–201.
[8] J. Nowak, M. Schäfer, W. Hegemann, N.-H. Kirsch, H.-J. Stan, P. Kämpfer, W. Dott, C. Sommer, E. Spiess and H. Görisch, *GWF Wasser-Abwasser*, 134 (1993) 379–385.
[9] J. Knuutinen and I.O.O. Korhonen, *Org. Mass Spectrom.*, 18 (1983) 438–441.
[10] J. Knuutinen, J. Tarhanen and M. Lahtiperä, *Chromatographia*, 15 (1982) 9–12.
[11] K. Lindström and J. Nordin, *J. Chromatogr.*, 128 (1976) 13–26.
[12] G.E. Garlberg, N. Gjös, M. Möller, K.O. Gustavsen and G. Tveten, *Sci. Total Environ.*, 15 (1980) 3–11.
[13] R.H. Voss, J.T. Wearing and A. Wong, *CPAR Project No. 828*, Pulp and Paper Research Institute of Canada, Pointe Claire, Canada, 1979.
[14] J.M. Sugihara and C.M. Bowman, *J. Am. Chem. Soc.*, 80 (1958) 2443–2446.
[15] H.G. Brown and G. Zweifel, *J. Org. Chem.*, 27 (1962) 4708–4709.

[16] C.J.W. Brooks and J. Watson, *Chem. Commun.*, (1967) 952–953.
[17] C.J.W. Brooks and I. Maclean, *J. Chromatogr. Sci.*, 9 (1971) 18–24.
[18] C.J.W. Brooks and W.J. Cole, *J. Chromatogr.*, 362 (1986) 113–116.
[19] C.J.W. Brooks and W.J. Cole, *J. Chromatogr.*, 399 (1987) 207–221.
[20] C.J.W. Brooks, W.J. Cole and D.J. Robins, *Heterocycles*, 28 (1989) 151–156.
[21] C.F. Poole and A. Zlatkis, *J. Chromatogr.*, 184 (1980) 99–183.
[22] J. Pís and J. Harmatha, *J. Chromatogr.*, 596 (1992) 271–275.
[23] J.-H. Shim, I.D. Wilson and E.D. Morgan, *J. Chromatogr.*, 639 (1993) 281–285.
[24] H.-J. Stan, T. Döring, M. Linkerhägner and N.H. Kirsch, *Schriftenreihe Biologische Abwasserreinigung 1*, Sonderforschungsbereich 193, TU Berlin, Berlin, 1992, pp. 43–57.
[25] N.H. Kirsch and H.-J. Stan, *Chemosphere*, 28 (1994) 131–137.
[26] D.T. Gibson, J.R. Koch, C.L. Schuld and R.E. Kallio, *Biochemistry*, 7 (1968) 3795–3802.

ELSEVIER

Journal of Chromatography A, 684 (1994) 289–296

JOURNAL OF CHROMATOGRAPHY A

Determination of polychlorinated biphenyls in sewage sludges from Catalonia (N.E. Spain) by high-resolution gas chromatography with electron-capture detection☆

F. Pauné*, J. Rivera, I. Espadaler, J. Caixach

Laboratori d'Espectrometria de Masses, CID–CSIC, J. Girona 18, 08034 Barcelona, Spain

First received 6 December 1993; revised manuscript received 17 June 1994

Abstract

A study was carried out on the presence of polychlorinated biphenyls (PCBs) in sewage sludges from Catalonia (N.E. Spain) using high-resolution gas chromatography with electron-capture detection. Aroclor 1254 and 1260 were characterized. The concentrations were between 2310 and 69 μg/kg (dry mass). High-resolution gas chromatography coupled with low-resolution mass spectrometry was used for screening the samples. No reports of the presence of PCBs in Spanish sewage sludges have been published previously. These analyses were performed in order to establish the availability of these sludges for disposal in agricultural soils.

1. Introduction

Polychlorinated biphenyls (PCBs) were once widely used as industrial chemicals, particularly as dielectric fluids in electrical transformers and capacitors, hydraulic fluids, lubricating and cutting oils, and as additives in sealants, plastics, paints, copying paper, adhesives and casting agents [1,2]. Their thermal stability and resistance to degradation contributed to their commercial usefulness, but also their long-term environmental effects. PCBs were extensively used commercially between the 1930s and 1970s, when their use was restricted because of their toxicity.

PCB residues have been detected in almost all compartments of the global ecosystem and the occurrence of these compounds in the environment has been extensively documented [3–9]. Over the years, PCBs have entered the environment following direct release from "open systems" and from industrial effluents, landfills, agricultural application of sewage sludges and the failure of electrical equipment. The PCBs enter the atmosphere by volatilization or in association with aerosols and can be transported over long distances before deposition on land or water surfaces. Consequently, PCBs and other organochlorine compounds (OCs) are now ubiquitous across the globe, even in remote polar regions. They come biomagnified through the food chain and may have adverse effects in aquatic and terrestrial organisms [10]. These often subtle ecotoxicological effects have sus-

* Corresponding author.

☆ Presented at the *22nd Annual Meeting of the Spanish Chromatography Group, Barcelona, October 20–22, 1993.*

0021-9673/94/$07.00
SSDI 0021-9673(94)00577-V

tained and stimulated research on the environmental importance of PCBs into 1990s.

Much attention has been drawn to the problem of polychlorinated dibenzo-*p*-dioxins (PCDDs) and dibenzofurans (PCDFs) and their environmental effects. More recently, however, research on other substances with similar toxic properties such as 2,3,7,8-TCDD (2,3,7,8-tetrachlorinated dibenzo-*p*-dioxin) has increased [1]. Recent studies indicate that the levels of individual PCBs expressed as 2,3,7,8-TCDD toxic equivalents equals or precedes that of PCDDs and TCDDs [11,12].

Every year thousands of tons of sludge are produced in sewage treatment plants. Application to agricultural land, disposal in landfills and incineration are the most popular sludge disposal practices in Europe. Chemicals contained in the sludge have the potential to directly enter the biogeochemical cycle after application to land. This work was carried out in order to consider the presence and amount of PCBs in different samples of sludges from sewage treatment plants in Catalonia (N.E. Spain). The production of sludges in Catalonia is expected to be 0.25 million tons per year by the year 2000, and part of this can be used in amendment of agricultural soils. Sampling was performed in six different sewage treatment plants selected to give overall information about the quality of sludges.

Usually the analyses of these samples performed in Spain have given information about conventional agronomic parameters such as organic matter, nutrients, humic acids and other pollution parameters such as heavy metals, but very little information is known about specific organic contaminants. This paper reports a wide-ranging analysis of these selected pollutants, especially PCBs. Prior to analysis a procedure was established for the determination of PCBs in these particular samples.

2. Experimental

2.1. Chemicals

Aroclor 1242, 1248, 1254, 1260 and 1262 PCB standard mixtures and individual 28, 52, 101, 118, 138, 153 and 180 congener standards were purchased from Cromlab (Barcelona, Spain). The internal standard, 2,2′,5-tribromobiphenyl, was purchased from Ultra Scientific (Hope, USA). Florisil for residue analysis (60–100 mesh, 0.15–0.25 mm) from Merck (Darmstadt, Germany) was used as a chromatographic adsorbent. It was activated at 500°C for 10 h and used immediately. Granular anhydrous sodium sulphate for residue analysis from Carlo Erba (Milan, Italy) was dried under the same conditions as Florisil. Copper for removal of sulphur was purchased from Merck. Glass-wool was cleaned by extraction in a Soxhlet apparatus with dichloromethane for 24 h.

The solvents, dichloromethane and acetone, were doubly distilled in glass to obtain residue analysis-grade materials. The purity of the solvents was tested by concentration of 100 ml to 100 μl and injection of 1 μl of the extract into a gas chromatographic–electron capture detector (HRGC–ECD) system. Isooctane and *n*-hexane were purchased from Merck. All glass materials were cleaned with Extran AP 13 alkaline soap (Merck) by sonification for 5 min and dried at 60°C overnight.

Standard solutions of PCB mixtures containing 1 ng/μl of individual Aroclors 1242, 1248, 1254, 1260 and 3.5 ng/μl of 1262 and 91 pg/μl of individual congeners 28, 52, 101, 118, 153, 138, 180 were prepared in isooctane for residue analysis (Merck).

2.2. Apparatus

Gas chromatography was carried out on a Model KNK-3000 gas chromatograph (Konik, Barcelona, Spain) equipped with a Tracor (Austin, TX, USA) electron-capture detector using nitrogen as make-up gas. A BP-5 (SGE, Ringwood, Australia) fused-silica capillary column (25 m × 0.22 mm I.D.) with a 0.25-μm film thickness was used with hydrogen as the carrier gas at a linear velocity of 35 cm/s. The temperature programme was from 70°C (held for 0.7 min) at 20°C/min.to 125°C (held isothermally for 1 min) and then to 280°C (maintained for 10 min) at 4°C/min; the injector and detector temperatures were 250 and 310°C respectively. The

injection mode was splitless for 45 s. The chromatographic data were processed using a Merck–Hitachi Model D-2000 integrator.

For HRGC–low-resolution MS (HRGC–LRMS) a VG TS-250 mass spectrometer (VG Instruments, Manchester, UK) interfaced to a VG 11-250 data system with a KNK-3000 (Konik) was used. The column and conditions were the same as for HRGC–ECD.

2.3. Sampling and analysis

Six sewage plant sludges from Catalonia were selected to give overall information about the presence, type and levels of PCBs in this kind of setting. The samples were collected bimonthly for 1 year in each place. The analyses were carried out on a total of 29 samples. The towns selected were Sant Feliu de Guíxols, Vilafranca del Penedès, Cadaqués, Manresa, Girona and Reus (abbreviated to SF, VI, CA, MA, GI and RE in the tables and figures).

Samples were dried at 110°C for 18 h, ground with a centrifuge mill and sieved to 750 μm. Two methods of extraction (sonification and Soxhlet) were compared. Soxhlet extraction was performed on 5 g of dried sludge in a solution of acetone–*n*-hexane (1:1) [13,14]. The sonification method, used extensively [15,16], was finally chosen because of the minimal amount of co-extracted impurities. It is less time consuming and good recoveries are obtained.

Five grams of homogenized dried sample were extracted with three 50-ml aliquots of dichloromethane–hexane (1:1) for 5 min. The organic extract was concentrated by rotary evaporation and solvent exchange with *n*-hexane (5 ml), then dried through anhydrous sodium sulphate. Subsequently, freshly activated copper was added to remove elemental sulphur (S_8) [17]. The sample clean-up was tested with different adsorbents, such as deactivated alumina and Florisil. Better results were obtained when 8 g of Florisil and 4 g of anhydrous sodium sulphate were used. A 5-ml volume of extract was cleaned up and eluted with 50 ml of *n*-hexane [18]. An internal stan-

Table 1
Congeners identified in samples (Ballschmiter and Zell's nomenclature [20])

No.	Structure	No.	Structure	No.	Structure	No.	Structure	No.	Structure
DiCBs		49	2,2′,4,5′	97	2,2′,3′,4,5	156	2,3,3′,4,4′,5[a]	190	2,3,3′,4,4′,5,6
5	2,3[a]	51	2,2′,4,6′	99	2,2′,4,4′,5	158	2,3,3′,4,4′,6	191	2,3,3′,4,4′,5′,6
7	2,4[a]	52	2,2′,5,5′	100	2,2′,4,4′,6	159	2,3,3′,4,5,5′[a]	192	2,3,3′,4,5,5′,6
15	4,4′[b]	53	2,2′,5,6′	101	2,2′,4,5,5′	163	2,3,3′,4′,5,6	193	2,3,3′,4′,5,5′,6
TriCBs		60	2,3,4,4′[a]	110	2,3,3′,4′,6	164	2,3,3′,4′,5′,6	*OctaCBs*	
16	2,2′,3	64	2,3,4′,6	118	2,3′,4,4′,5[a]	167	2,3′,4,4′,5,5′[a]	194	2,2′,3,3′,4,4′,5,5′
17	2,2′,4	66	2,3′,4,4′[a]	*HexaCBs*		*HeptaCBs*		195	2,2′,3,3′,4,4′,5,6
18	2,2′,5	70	2,3′,4′,5[a]	128	2,2′,3,3′,4,4′	170	2,2′,3,3′,4,4′,5	196	2,2′,3,3′,4,4′,5,6′
22	2,3,4′[a]	71	2,3′,4′,6	130	2,2′,3,3′,4,5′	171	2,2′,3,3′,4,4′,6	197	2,2′,3,3′,4,4′,6,6′
28	2,4,4′[a]	72	2,3′,5,5′[a]	131	2,2′,3,3′,4,6	172	2,2′,3,3′,4,5,5′	198	2,2′,3,3′,4,5,5′,6
31	2,4′,5[a]	74	2,4,4′,5[a]	132	2,2′,3,3′,4,6′	173	2,2′,3,3′,4,5,6	199	2,2′,3,3′,4,5,6,6′
32	2,4,′,6	76	2′,3,4,5[a]	134	2,2′,3,3′,5,6	174	2,2′,3,3′,4,5,6′	201	2,2′,3,3′,4,5,5′,6
33	2′,3,4[a]	*PentaCBs*		135	2,2′,3,3′,5,6′	177	2,2′,3,3′,4′,5,6	203	2,2′,3,4,4′,5,5′,6
37	3,4,4′[b]	82	2,2′,3,3′,4	138	2,2′,3,4,4′,5′	178	2,2′,3,3′,5,5′,6	205	2,2′,3′,4,4′,5,5′,6
TetraCBs		84	2,2′,3,3′,6	141	2,2′,3,4,5,5′	179	2,2′,3,3′,5,6,6′	*NonaCBs*	
41	2,2′,3,4	87	2,2′,3,4,5′	144	2,2′,3,4,5′,6	180	2,2′,3,4,4′,5,5′	206	2,2′,3,3′,4,4′,5,5′,6
42	2,2′,3,4′	89	2,2′,3,4,6′	146	2,2′,3,4′,5,5′	182	2,2′,3,4,4′,5,6′	207	2,2′,3,3′,4,4′,5,6,6′
44	2,2′,3,5′	91	2,2′,3,4′,6	148	2,2′,3,4′,5,6′	183	2,2′,3,4,4′,5′,6	208	2,2′,3,3′,4,5,5′,6,6′
45	2,2′,3,6	92	2,2′,3,5,5′	149	2,2′,3,4′,5′,6	185	2,2′,3,4,5,5′,6		
47	2,2′,4,4′	94	2,2′,3,5,6′	151	2,2′,3,5,5′,6	187	2,2′,3,4′,5,5′,6		
48	2,2′,4,5	95	2,2′,3,5′,6	153	2,2′,4,4′,5,5′	189	2,3,3′,4,4′,5,5′[a]		

[a] Mono-*ortho*-PCBs.
[b] Non-*ortho*-PCBs.

dard, 2,2',5-tribromobiphenyl, was added and the final volume of extract was adjusted to 0.5 ml under a gentle flow of nitrogen. Samples were then analysed by HRGC–ECD.

In order to validate the method used, the recoveries of seven individual congeners added to a simple sewage sludge, PCB free, were determined; this sample was extracted in a Soxhlet apparatus with three aliquots of acetone–*n*-hexane (1:1) until PCBs were totally removed. In all instances the recoveries were >95%. The feasibility of the method was also tested in two intercalibration exercises with the BCR (Bureau Communitaire de Réference) [19].

2.4. Chromatographic analysis

Qualitative determination

Purified PCB extracts were analysed by HRGC–ECD. Compounds were assigned by their GC retention times compared with standard Aroclor mixtures and individual selected congeners. The determination of specific congeners was carried out using Aroclor 1242, 1248, 1254, 1260 and 1262. Identification of congeners was done following Ballschmiter and Zell's nomenclature [20] (see Table 1).

Quantitative determination

Quantification was done by comparing Aroclor standards and individual congeners. The results were compared using different methods. The detection level was 1–5 pg injected. The sensitivity of method was 10–50 pg/g. One system of quantitative analyses involved the congener-specific methodology using the Aroclor 1260. Sample chromatographic peaks were determined using an internal standard, 2,2',5-tribromobiphenyl. Seven recommended BCR congeners were analysed to obtain calibration graphs and response factors. The feasibility of this method was checked in a BCR intercalibration exercise.

3. Results

Aroclor 1260 was clearly identified in all samples, as a main constituent (Fig. 1 shows a sample containing Aroclor 1260 without other

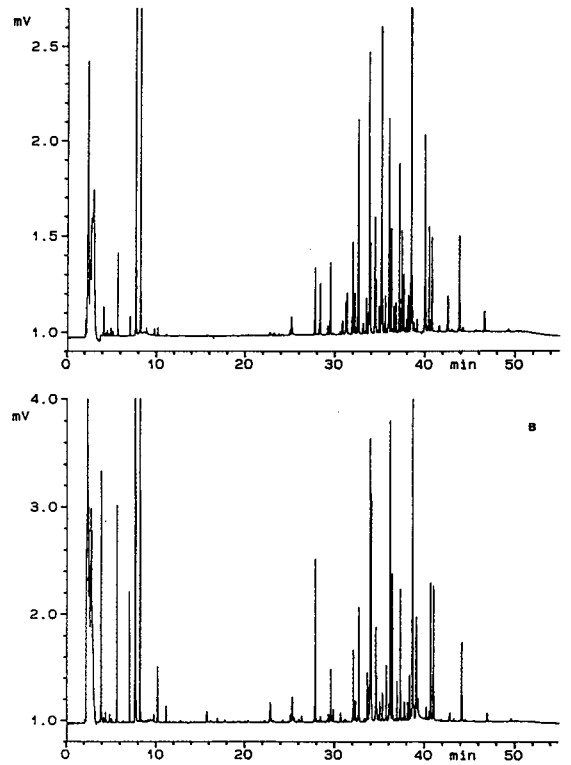

Fig. 1. HRGC–ECD (25-m BP-5 column) of (A) Aroclor 1260 and (B) sample VI (Vilafranca del Penedès).

Aroclor interferences). Other samples, however, showed complex mixtures with smaller retention times corresponding to Aroclors having a lower degree of chlorination (Fig. 2). Construction of a bar diagram (percentage of individual congener from total PCBs) proved the presence of Aroclor

Table 2
Results (μg/kg) obtained by BCR recommended method (seven individual congeners)

Congener	Sample					
	SF	VI	RE	CA	MA	GI
28	14	4	21	11	12	9
52	92	4	28	22	109	10
101	22	6	29	12	18	11
118	76	9	50	16	41	13
153	167	17	218	39	109	20
138	119	4	147	24	79	17
180	88	23	161	21	80	19
Total	578	69	653	143	447	100

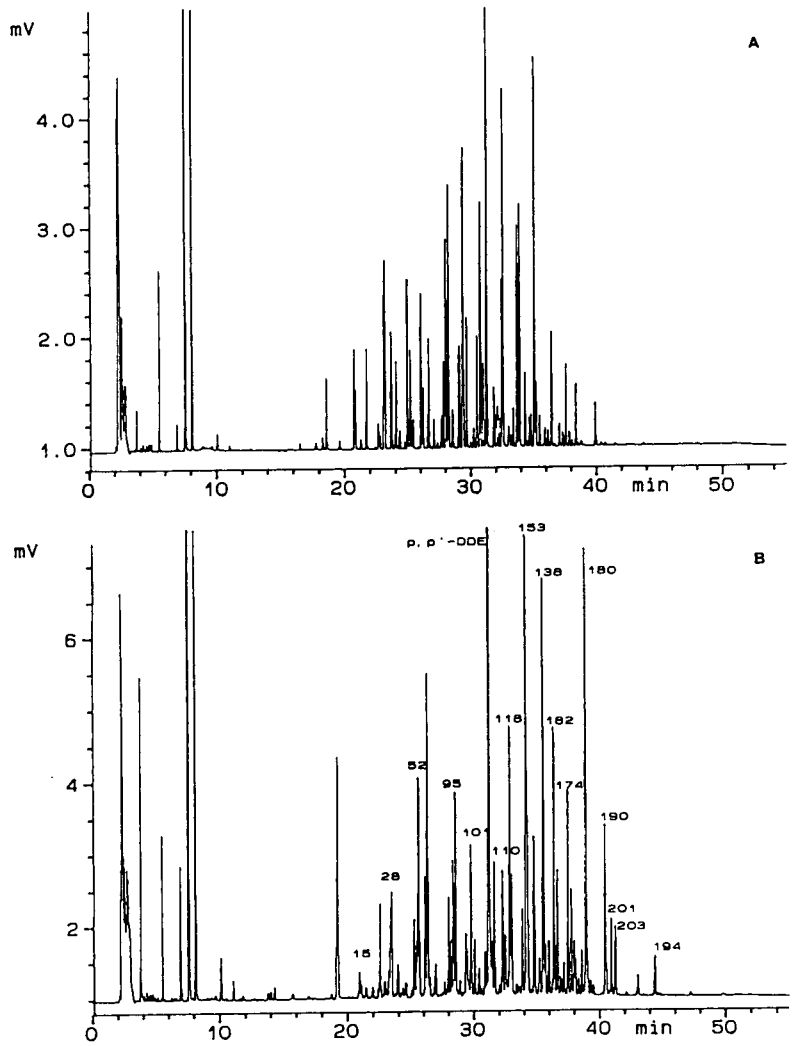

Fig. 2. HRGC–ECD (25-m BP-5 column) of (A) Aroclor 1254 and (B) sample SF (Sant Feliu de Guíxols). PCB congener numbers and p,p'-DDE are indicated.

1254 (Fig. 3). Fig. 4 shows the overall trends of the samples.

Aroclor 1260 is the most frequently identified compound because of its extensive commercial use and high degree of chlorination. As described [21–23], the degradation most frequently occurs in less chlorinated congeners (1–3 chlorine atoms) by photodegradation, microbiological action and volatilization. The degree of chlorination of the identified congeners was 4–8.

Other compounds identified were 1,2,3-trichlorobenzene, 1,2,4-trichlorobenzene and 1,3,5-trichlorobenzene. These pollutants are ubiquitous and are also associated with PCBs because they are used commerciallly together in Askarel mixtures which are used as electrical insulating media in transformers and electric capacitors. The most common transformer Askarels showed 30% of trichlorobenzene–70% of Aroclor 1254 and 40% of trichlorobenzene–60% of Aroclor 1260 [1,2].

The results obtained with both methods are given in Tables 2 and 3. The application of the method to the seven BCR individual congeners

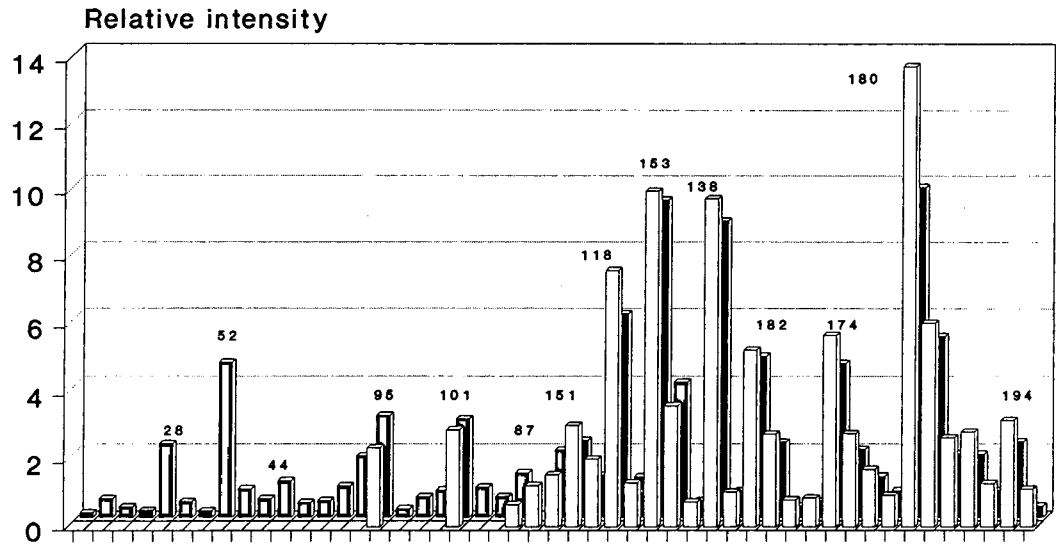

Fig. 3. Bar diagram showing relative intensities in percentages of SF sample (■; Sant Feliu de Guíxols) compared with an Aroclor 1260 standard mixture (□).

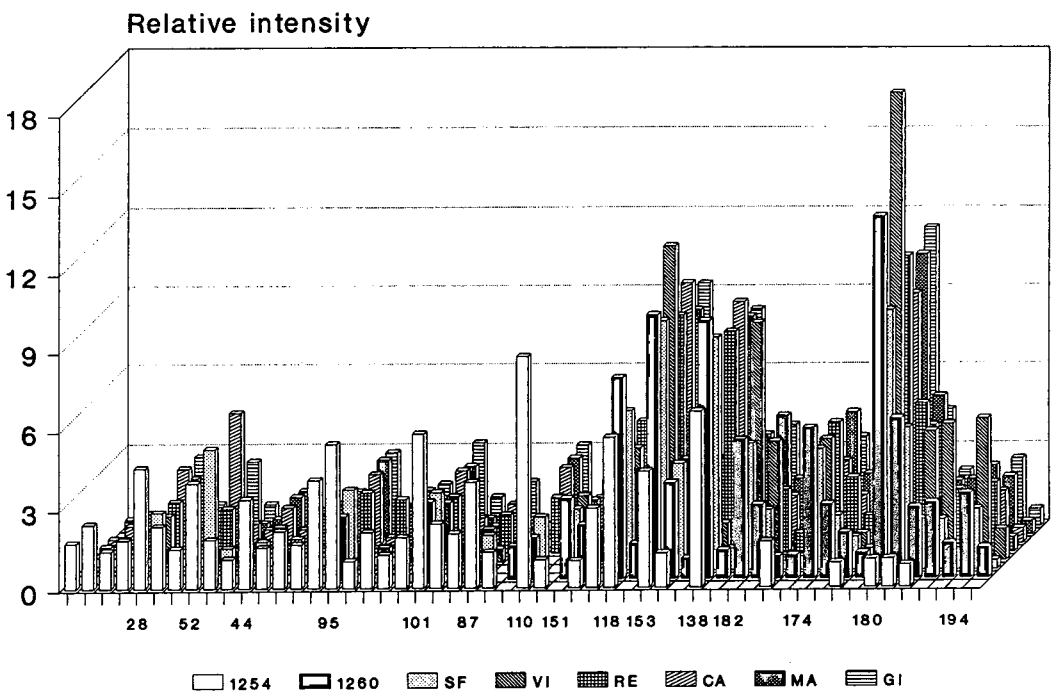

Fig. 4. Bar diagram showing relative intensities in percentages of all samples compared with the Aroclor 1254 and 1260 standard mixtures.

Table 3
Comparison of results obtained by two different methods

Sample	PCB level (μg/kg)	
	BCR congeners[a]	Aroclor 1260[b]
SF	578	1421
VI	69	382
RE	653	2310
CA	143	623
MA	447	1239
GI	100	501

[a] Quantification based on seven individual congeners recommended by BCR.
[b] Quantification based on Aroclor 1260 mixture.

is presented in Table 2. Table 3 gives the quantitative results using Aroclor 1260, and a comparison with those obtained by the BCR method. The levels found are similar to published data [24–26].

The peak eluting between the 110 and 87 PCB congeners was identified as *p,p'*-DDE [1,1-dichloro-2,2-bis(4-chlorophenyl)ethylene] by HRGC–LRMS; this compound was only found in some of the samples analysed. *p,p'*-DDE is one of the major metabolites of DDT [1,1,1-trichloro-2,2-bis(*p*-chlorophenyl)ethane]. In the environment, DDT is metabolized to DDD [1,1-dichloro-2,2-bis(*p*-chlorophenyl)ethane] and DDE. In some samples DDD is the major metabolite whereas in others DDE predominates. Aliphatic hydrocarbons were detected together with PCBs in the same fraction. A background of aliphatic hydrocarbons, typically due to an unresolved complex mixture, did not allow the determination of PCBs using LRMS with selected ion monitoring. Other compounds identified in the screening, prior to the special clean-up for PCBs, were polycyclic aromatic hydrocarbons (PAHs), fatty acids and sterols.

4. Conclusions

PCBs from several municipal sewage sludge treatment plant were characterized and quantified. The analysis revealed PCBs in all these samples. Prior to analysis a procedure was established for the determination of PCBs in these particular samples. The recovery of the extraction procedure was >95% and the feasibility of this method was tested in a BCR intercalibration programme.

The PCBs levels found were similar to those already published. Aroclor 1260 was detected most frequently in the commercial mixture. The specific sources of these pollutants in the samples analysed are still unknown, but extensive commercial use of these compounds, their ubiquitous presence, high resistance to degradation, sediment uplift and suspended particulate permitted detection.

The PCB content of municipal sewage sludges is a critical point concerning their treatment, management and agricultural use. Further developments in the analysis of these compounds and a quantitative normalization procedure in sludges are necessary to allow an integrated assessment of the behaviour and impact of these contaminants according to the type of processing techniques and use of the sludges.

Acknowledgements

Samples were collected by the Agricultural Superior School of Barcelona. We thank J.J. Llerena, J. Saña and M. Morén for their collaboration.

References

[1] R.D. Kimbrough and A.A. Jensen (Editors), *Halogenated Biphenyls, Terphenyls, Naphthalenes, Dibenzodioxins and Related Products*, Elsevier, Amsterdam, 1989.
[2] D. Erickson, *Analytical Chemistry of PCBs*, Butterworth, Guildford, 1986.
[3] S. Jensen, A.G. Johnels, M. Olsson and G. Olterlind, *Nature*, 224 (1969) 247.
[4] M. El-Dib, *Bull. Environ. Contam. Toxicol.*, 34 (1985) 216.
[5] S. Georgii, G. Bachour, K. Failing, U. Eskens, I. Elmadfa and H. Brunn, *Arch. Environ. Contam. Toxicol.*, 26 (1994) 1.

[6] M.C. Kennicutt, T.L. Wade, B.J. Presley, A.G. Raquejo, J.M. Brooks and G.J. Denoux, *Environ. Sci. Technol.*, 28 (1994) 1.
[7] J.R. Kucklick, T.F. Bidleman, L.L. Mcconnell, M.D. Walla and G.P. Ivanov, *Environ. Sci. Technol.*, 28 (1994) 31.
[8] Y. Ohsaki and T. Matsueda, *Chemosphere*, 28 (1994) 47.
[9] F.F. Daelemans, F. Mehlum and J.C. Schepens, *Bull. Environ. Contam. Toxicol.*, 48 (1992) 828.
[10] G. Sanders, K.C. Jones, J. Hamilton and H. Dörr, *Environ. Sci. Technol.*, 26 (1992) 1815.
[11] J. Tarhanen, J. Koistinen, J. Paasivirta, P.J. Vuorinen, J. Koivusaari, I. Nuuja, N. Kannan and R. Tatsukawa, *Chemosphere*, 18 (1989) 1067.
[12] U. Järnberg, L. Asplund, C. de Wit, A.K. Grafström, P. Haglund, B. Jansson, K. Lexén, M. Strandell, M. Olsson and B. Jonsson, *Environ. Sci. Technol.*, 27 (1993) 1364.
[13] J. Japenga, W. Wagensar, F. Smedes and W. Salomons, *Environ. Technol. Lett.*, 8 (1987) 9.
[14] B.G. Oliver and A.J. Niimi, *Environ. Sci. Technol.* 22 (1988) 388.
[15] A.L. Alford-Stevens, W.L. Buddle and T.A. Bellar, *Anal. Chem.*, 57 (1985) 2452.
[16] V. López-Ávila, J. Benedicto, E. Baldin and W.F. Beckert, *J. High Resolut. Chromatogr.*, 15 (1992) 319.
[17] N.I. Rubinstein, R.J. Pruell, B.K. Taplin, J.A. Livolsi and C.B. Norwood, *Chemosphere*, 20 (1990) 1097.
[18] A.C. Alder, M.M. Häggblom, S.R. Oppenhelmer and L.Y. Young, *Environ. Sci. Technol.*, 27 (1993) 530.
[19] X. Santos and M. Galceran, *Certification of Chlorobiphenyls in Waste Fuel Oil, Intercalibration Exercise*, BCR, Brussels, 1990.
[20] K. Ballschmiter and M. Zell, *Fresenius' Z. Anal. Chem.*, 302 (1980) 20.
[21] K. Furukawa and F.J. Matsumara, *Agric. Chem.*, 24 (1976) 251.
[22] R. Moolenaar, in R. Davenport and B. Bernard (Editors), *Advances in Exposure, Health and Environmental Effects Studies of PCBs, Symposium Proceedings*, US Environmental Protection Agency, Washington, DC, 1983, pp. 67–96.
[23] P. Moza, J. Scheunert, W. Klein and F.J. Korte, *Agric. Food. Chem.*, 27 (1979) 1120.
[24] P. Brunner, U. Weberrub and H. Hagemayer, presented at the *18th International Symposium on Environmental Analytical Chemistry, 4th International Congress on Analytical Techniques in Environmental Chemistry, Barcelona, 1988.*
[25] S. Wild and K. Jones, *Chemosphere*, 19 (1989) 1765.
[26] R.E. Alcock and K.C. Jones, *Chemosphere*, 26 (1993) 2199.

ELSEVIER

Journal of Chromatography A, 684 (1994) 297–309

JOURNAL OF CHROMATOGRAPHY A

Evaluation of β-cyclodextrin-based chiral stationary phases for capillary column supercritical fluid chromatography

P. Petersson[a], S.L. Reese[b], G. Yi[b], H. Yun[b], A. Malik[b], J.S. Bradshaw[b], B.E. Rossiter[b], M.L. Lee[b], K.E. Markides[a,*]

[a] *Department of Analytical Chemistry, Uppsala University, P.O. Box 531, S-751 21 Uppsala, Sweden*
[b] *Department of Chemistry, Brigham Young University, Provo, UT 84602, USA*

First received 6 May 1994; revised manuscript received 6 July 1994

Abstract

The chromatographic performance of two series of chiral stationary phases (CSPs) based on β-cyclodextrin, one copolymeric and one side-arm substituted, was investigated to improve the applicability of cyclodextrin-based CSPs in open-tubular column supercritical fluid chromatography. For the side-arm approach, the influence on performance of different amount of cyclodextrin in the CSP, attachment of the cyclodextrin at the wide or narrow opening, different substituents on the cyclodextrin, the structure of the spacer and the film thickness was studied. The immobilization of these CSPs was also investigated. In addition, the chromatographic performance in gas and supercritical fluid chromatography of one of these CSPs was compared at optimal conditions using test solutes having relatively large differences in size and functionality.

1. Introduction

Chiral stationary phases based on β-cyclodextrin are, today, the most widely applicable stationary phases available for chiral separations performed by open-tubular column gas chromatography (GC) [1–3] and supercritical fluid chromatography (SFC) [4]. The latter technique has proved to be able to separate the underivatized enantiomers of a wide range of compounds, e.g. alcohols, lactones, ketones, amines, carboxylic acids and steroids, including relatively large and polar compounds such as ibuprofen, flurbiprofen, warfarin, dihydrodiazepam, norgestrel and 10,2-camphorsultam, which are not readily analyzed by GC due to low volatility or thermal instability [5–13].

In previous work on CSPs with cyclodextrin functionalities for open-tubular column SFC, three approaches can be identified for the design of the CSPs: (i) a polysiloxane having permethylated β-cyclodextrin attached to aliphatic side-arms [5–8,10], (ii) a copolymer consisting of alternating β-cyclodextrin and polysiloxane units [9,11,12] and (iii) methylated β-cyclodextrin having short polysiloxane units as substituents [13,14].

In the present study the chromatographic performance of a number of β-cyclodextrin-based CSPs, synthesized according to the copolymeric (CSP **1–3**, Table 1) and side-arm approach (CSP **4–21**), was compared. For the side-arm approach, the influence on performance

* Corresponding author.

0021-9673/94/$07.00
SSDI 0021-9673(94)00640-7

Table 1
Structures of the CSPs used in this study

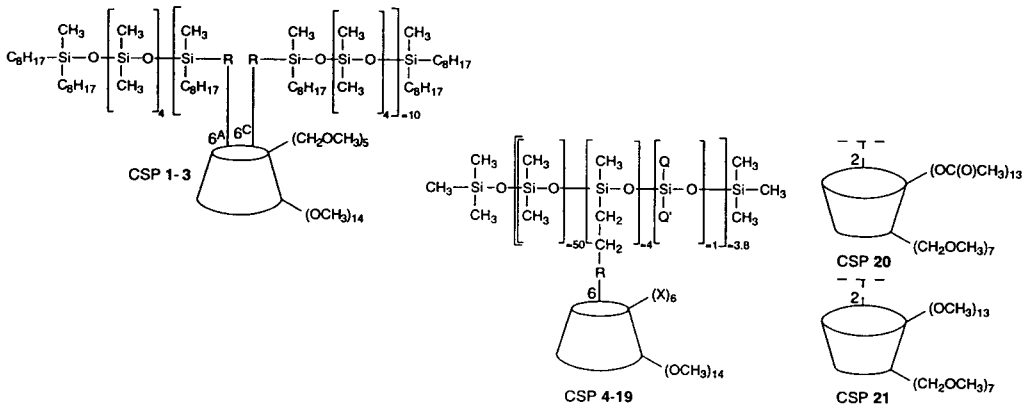

CSP	R[a]	Q, Q'	X	% n/n[b]	% w/w[c]
1	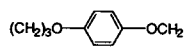				56
2	$(CH_2)_3OCH_2$				59
3	$(CH_2)_{10}OCH_2$				57
4-11[d]	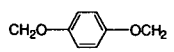	C_8H_{17}, CH_3	CH_2OCH_3	0.4-9.5	12-72
12	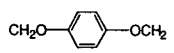	C_8H_{17}, CH_3	$CH_2OC(O)CH_3$	3.6	59
13	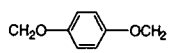	C_8H_{17}, CH_3	CH_3	3.6	50
14	None	C_8H_{17}, CH_3	CH_2OCH_3	3.6	56
15	CH_2CH_2	C_8H_{17}, CH_3	CH_2OCH_3	3.6	56
16	CH_2OCH_2	C_8H_{17}, CH_3	CH_2OCH_3	3.6	55
17	$CH_2(CH_2)_8OCH_2$	C_8H_{17}, CH_3	CH_2OCH_3	3.6	53
18	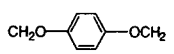	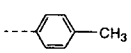	CH_2OCH_3	4.3	56
19[e]	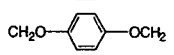	C_8H_{17}, CH_3	CH_2OCH_3	4.0	53
20	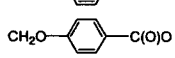	C_8H_{17}, CH_3		3.6	59
21	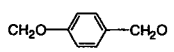	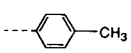		4.3	56

[a] The left side of the spacer is attached to the siloxne.
[b] Amount of cyclodextrin expressed in % by substituent.
[c] Amount of cyclodextrin expressed in % by weight. The spacer is assigned to the achiral part of the CSP.
[d] Synthesized in eight versions with different amounts of cyclodextrin (0.4, 0.8, 1.5, 2.1, 2.7, 3.6, 5.4 and 9.5% by substituent, or 12, 21, 34, 42, 46, 53, 63 and 72 % w/w).
[e] Contains 4.0% cyclodextrin, 1.0% octyl and 5% cyanopropyl by substituent.

of different amounts of cyclodextrin in the CSP, attachment of the cyclodextrin at the wide or narrow opening, different substituents on the cyclodextrin, the structure of the spacer and the film thickness was studied. The possibility to immobilize these CSPs was also investigated. In addition, the chromatographic performance in GC and SFC of one of these CSPs was compared at optimal conditions for a number of test solutes having different size and functionality.

2. Experimental

2.1. Preparation of CSPs

The synthesis of the CSPs used in this study (Table 1) have previously been described (CSP **9, 12–17** [15]) or are in the process of being published (CSP **1–3, 4–8, 10–11** and **18–21** [16]).

2.2. Column preparation

The fused-silica capillaries, 5 m × 50 μm I.D. for SFC and 10 m × 100 μm I.D. for the comparison of SFC and GC (Polymicro Technologies, Phoenix, AZ, USA) were deactivated as previously described [17].

The deactivated capillaries were statically coated at 25°C using dichloromethane as solvent for the CSPs. The concentration of the coating solution, C_{CSP}, was calculated according to the following equation assuming a stationary phase density, ρ_{CSP}, of 1 g ml^{-1}:

$$C_{CSP} = \rho_{CSP}(r^2 - (r - d_f)^2)/r^2 \quad (1)$$

where r represents the internal radius of the capillary and d_f the approximate film thickness. In order to immobilize the CSPs by crosslinking, 5% (w/w, relative to the amount of CSP in the coating solution) dicumylperoxide (Aldrich, Steinheim am Albuch, Germany) was added as a free radical initiator.

The CSPs were immobilized by heating the coated capillaries from room temperature to 170°C at 4°C min^{-1} under a slow nitrogen purge (ca. 0.05 ml min^{-1}) and subsequently keeping the capillaries at 170°C for 40 min plus an additional 60 min at an increased nitrogen flow (ca. 0.20 ml min^{-1}). Prior to evaluation, the columns were rinsed with supercritical CO_2 for 60 min in a dynamic extraction (SFE) at temperatures and densities slightly above the testing conditions. The columns used in the evaluation of the immobilization procedure and stability test were subjected to repeated SFE at 415 atm and 120 and/or 60°C.

2.3. Samples

(±)-3,3-Dimethyl-1,2-butanediol, (±)-γ-phenyl-γ-butyrolactone, (±)-2-phenylcyclohexanone, (±)-pantolactone, (±)-diethyl tartrate, (±)-1-phenyl-1-ethanol, (±)-*trans*-1,2-cyclohexanediol and (±)-*trans*-2-phenylcyclohexanol were obtained from Aldrich (Steinheim am Albuch, Germany). (±)-Ibuprofen was obtained from Sigma Chemical Company (St. Louis, MO, USA). The following compounds were gifts from persons and companies listed below and are gratefully acknowledged: (±)-carboranylalanine derivative [(*N*-trifluoroacetyl)-propylester], S. Sjöberg (Uppsala University, Uppsala, Sweden); (±)-chlor-mezanone, Sanofi Winthorp Ltd. (Wythenshawe, Manchester, UK); (±)-dihydrodiazepam and (±)-γ-heptalactone, W. Walther (Hoffman-La Roche, Basel, Switzerland); (±)-2,8-di(hydroxyethyl)-6*H*,*H*-5,11-methanodibenzo-[*b*,*f*]-[1,5]-diazocine and (±)-1-(4-phenyl)phenylethanol, B.E. Rossiter (Brigham Young University, Provo, UT, USA) and (±)-glutethimide, K. Grolimund (Ciba-Geigy, Basel, Switzerland).

All racemates were dissolved in ethanol with the exception of the carboranylalanine derivative which was dissolved in dichloromethane.

2.4. Instrumentation

SFC–FID was performed with a Series 600-D SFC system (Dionex, Salt Lake City, UT, USA) equipped with a flame ionization detector (FID, 350°C). The injector consisted of a Model CI4W.5 high-pressure four port valve injector

with a 0.5 μl sample loop (Valco Instruments, Houston, TX, USA) combined with a splitter (300 μm I.D., SGE, Austin, TX, USA). The density of the mobile phase was kept approximately constant along the column using an in-house made deactivated integral [18] or frit restrictor (Dionex, Salt Lake City, UT, USA). SFC–MS was performed by coupling the system above to an API-III (SCIEX Perkin Elmer, Thornhill, Ontario, Canada) [19]. GC–FID was performed with a GC 6000 Vega Series 2 (Carlo Erba, Milan, Italy) equipped with a split injector (250°C) and an FID (350°C). Hydrogen was used as mobile phase at an average linear velocity of 75 cm s^{-1} at 100°C.

The chromatograms were registered with an SP4290 or ChromJet integrator (SpectraPhysics, San Jose, CA, USA), transferred to a Macintosh IIfx computer (Apple Computer, Cupertino, CA, USA) and subsequently decoded with an routine written in-house in Microsoft QuickBasic (Microsoft, Redmond, WA, USA). A program for general graphing and data analysis, Igor (Wave Metrics, Lake Oswego, OR, USA) was used for determination of peak widths, retention times etc.

3. Results and discussion

3.1. Evaluation of CSP performance

The chromatographic performance of the CSPs in SFC was investigated by the injection of ten racemic test compounds **I–X** (Table 2) under isopycnic and isothermal conditions. The repeatability of the column preparation procedure was estimated by the preparation of five columns coated with CSP **18**. Based on injections of (±)-*trans*-2-phenylcyclohexanol **IX**, confidence intervals at the 95% level were calculated for the capacity factor, $k' \pm 0.17$, selectivity, $\alpha \pm 0.006$, and efficiency, $N \pm 380$ plates m^{-1}. The relatively large but quite normal variance in efficiency made it difficult to compare efficiency and resolution for different CSPs and emphasis has therefore been put on chiral selectivity instead.

As the densities of the different CSPs are unknown, the film thicknesses of columns coated with different CSPs may vary somewhat (Eq. 1) and consequently the comparison of retention may be somewhat biased. This bias should be most pronounced in the comparison of CSP **4–11**

Table 2
Compounds used to compare chromatographic performance on CSPs **1–21** in SFC

I	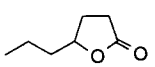	**II**	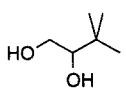		
III	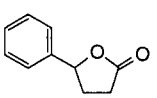	**IV**	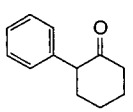	**V**	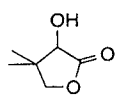
VI	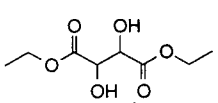	**VII**	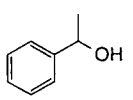		
VIII	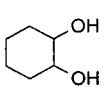	**IX**	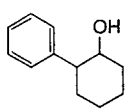	**X**	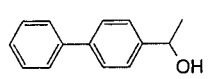

Conditions: **I** 60°C, 0.20 g ml^{-1}, **II** 50°C, 0.30 g ml^{-1}, **III–VII** 60°C, 0.30 g ml^{-1}, **VIII–IX** 60°C, 0.35 g m^{-1}, **X** 60°C, 0.40 g ml^{-1}.

as there is a large variation in cyclodextrin content between these CSPs. The selectivity should however not, according to theory, be influenced by differences in film thickness.

Initially it was decided to compare the chromatographic performance of the CSPs at equal chromatographic conditions, as well as equal retention. The relatively small changes in density required to achieve equal retention did, however, not cause any differences in chiral selectivity for (±)-2-phenylcyclohexanone **IV**, when chromatographed on the different CSPs. It was therefore decided that a comparison of selectivity and retention at identical conditions should suffice as this approach reduces the number of experiments.

3.2. Comparison of the copolymeric and the side-arm approach

Previously reported copolymeric CSPs based on cyclohexylenebisbenzamides showed, in contrast to the cyclodextrin-based copolymeric CSPs **1–3**, large differences in both retention and selectivity in response to small changes in the structure of the spacers between the chiral unit and the achiral siloxane block [17]. In the case of cyclodextrin-based CSPs it could, on the other hand, only be concluded that short and rigid spacers favour the selectivity somewhat (Fig. 1). These results indicate that the copolymeric approach require relatively small chiral units and not macrocycles like cyclodextrins for which the structure of the spacers does not seem to be critical (cf. section 3.6, Structure of the spacer).

As shown in Fig. 1, CSP **1**, representing the copolymeric approach, and CSP **9**, representing the side-arm approach [56 and 53% (w/w) cyclodextrin respectively], did not show any large differences in retention and chiral selectivity. The side-arm CSP gave, for all compounds in the test set, similar or somewhat better chiral selectivity, indicating that the secondary structure of the copolymers does not contribute to the chiral selectivity.

Considering these results and the fact that the copolymeric cyclodextrin-based CSPs are more complex to synthesize it was logical to focus further studies on the side-arm approach, CSP **4–21**.

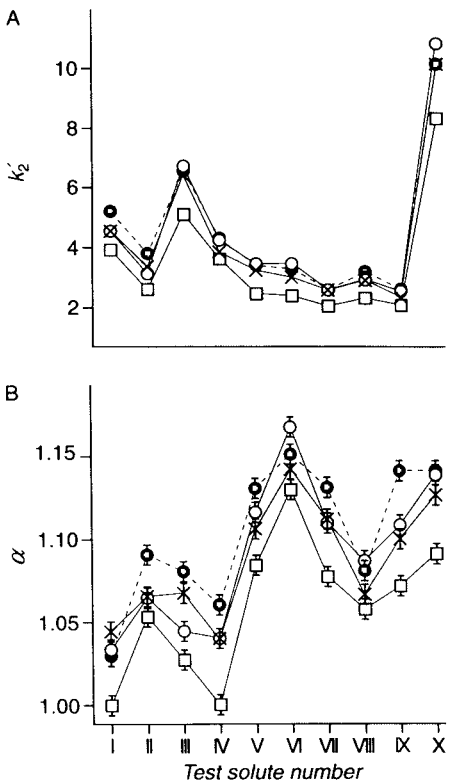

Fig. 1. Comparison of copolymeric (CSP **1** ○, **2** × and **3** □, solid line) and side-arm CSPs (CSP **9** ●, dashed line). (A) retention of the last eluting enantiomer and (B) chiral selectivity versus test solute number (SFC–FID cf. Table 2). Error bars correspond to confidence intervals at the 95% level ($k' \pm 0.17$ and $\alpha \pm 0.006$ estimated from 5 columns coated with CSP **18**).

3.3. Amount of cyclodextrin in the CSP

For CSPs similar to CSP **17** it has previously been found by Jung and Schurig [20] that the chiral selectivity in GC increases with increasing amount of cyclodextrin in the CSP (16–36%) up to a certain limit above which little or no chiral selectivity is gained, i.e. 20–30%. This phenomenon was explained on the basis of theoretical models for the relationship between the chiral selectivity and the amount of cyclodextrin in the CSP [21]. Comparisons of the chiral selectivity of CSP **4–11** (12–72% cyclodextrin) using SFC

showed similar trends for all compounds in the test set **I–X**. This suggest that the models can be applied also in SFC and for higher amounts of cyclodextrin than previously reported.

An increase of the amount of cyclodextrin in the CSP from 12 to 72% resulted in a significant increase of the capacity factor, often in the order of 300%. It is likely that this difference in retention is related to some extent to differences in the CSP density as mentioned above.

The influence of the amount of cyclodextrin on sample capacity was investigated by the injection of different amounts of (±)-γ-phenyl-γ-butyrolactone **III** on columns coated with CSP **8** and **11**, i.e. CSPs containing 46 and 72% cyclodextrin. By plotting the asymmetry factor for the first eluting enantiomer versus peak area it was found that the CSP having a higher content of cyclodextrin also had an enhanced sample capacity (Fig. 2). Large sample capacity is an important property of chiral columns as closely eluting enantiomers often have to be quantified at an enantiomeric impurity level of less than 1%. The sample capacity is usually low in comparison with achiral columns due to the relatively low number of chiral substituents. It may therefore be favourable to use a relatively large amount of cyclodextrin in the CSP, especially since this does not seem to influence the efficiency dramatically (CSP **4** 1400, **5** 1200, **6** 1900, **7** 600, **8** 2200, **9** 2200, **10** 1800 and **11** 1800 plates m^{-1}, (±)-*trans*-2-phenylcyclohexanol **IX**, SFC–FID cf. Table 2).

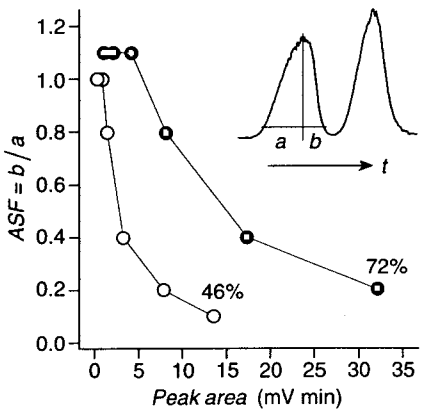

Fig. 2. A comparison of sample capacity for two columns (5 m × 50 μm I.D., $d_f \approx 0.25$ μm) coated with CSP **8** and **11** having different amounts of cyclodextrin (46 and 72% w/w). Asymmetry factor versus peak area was monitored in SFC–FID for (±)-γ-phenyl-γ-butyrolactone **III** at 60°C and 0.30 g ml^{-1}. The smallest and largest peak areas correspond to concentrations of 1.25 and 40.00 mg ml^{-1}, respectively, i.e. approximately 62 and 2000 ng on the columns.

3.4. Attachment to the siloxane backbone

The stationary phases **18** and **21** are structurally similar and differ only in that CSP **18** has the cyclodextrin attached at the narrow opening and CSP **21** at the wide opening. A comparison of the chromatographic performance (Fig. 3) shows that the attachment of the wide opening of the cyclodextrin to the siloxane backbone resulted in

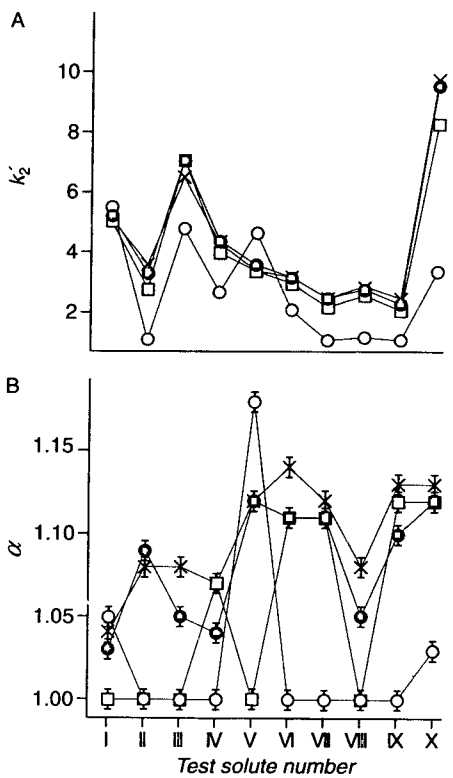

Fig. 3. Effect of attachment of the cyclodextrin on (A) retention of the last eluting enantiomer and (B) chiral selectivity versus test solute (SFC–FID cf. Table 2). Attachment at the narrow opening (CSP **12** □ and **18** ×) and the wide opening (CSP **20** ○and **21** ●).

a reduced chiral selectivity for 60% of the compounds in the test set. By comparing the performance of CSP **12** and **20** (Fig. 3) it is seen that such an attachment in combination with the acetylation of the hydroxyl groups at the opening on the side of attachment, i.e. narrow opening for CSP **12** and wide opening for CSP **20**, resulted in shorter retention and lower chiral selectivity for most compounds in the test set with exception of compound **V**. In other words, there was a loss of general selectivity but a gain in specific selectivity. Both CSP **12** and **20** showed a poorer general chiral selectivity than any other CSP in this study.

These results indicate that the acetylation of and/or the attachment of the wide opening of the cyclodextrin to the siloxane backbone will reduce the access to the cyclodextrin cavity and thereby hamper the chiral selectivity.

3.5. Substitution at the narrow opening of the cyclodextrin

The replacement of the hydroxyl groups at the narrow opening of the cyclodextrin with hydrogen, CSP **13**, resulted in a somewhat shorter retention and a chiral selectivity that was different from that of the permethylated versions (Fig. 4). It is, with the present number of test compounds, not possible to state which CSP, **9** or **13**, that would be most widely applicable.

The acetylation of the hydroxyl groups at the narrow opening, i.e. CSP **12**, resulted in a significant decrease in chiral selectivity in comparison to the permethylated versions, e.g. CSP **9** (Fig. 4). One explanation for this loss in selectivity could be a disturbance of the interactions at the narrow opening, while another explanation is a change of the shape of the cyclodextrin torus. Molecular modelling studies [22] indicate that a derivatization of the narrow opening of the cyclodextrin may influence, i.e. distort, the shape of the wide opening.

3.6. Structure of the spacer

The different spacers connecting the cyclodextrin to the siloxane backbone, evaluated in this study, CSP **9, 14–17**, showed similar retention and selectivity. It is therefore not possible to distinguish between the influence of a long and short spacer or between an aromatic and aliphatic spacer. Thus it is reasonable to believe that the structure of the spacer is not critical for this type of CSPs.

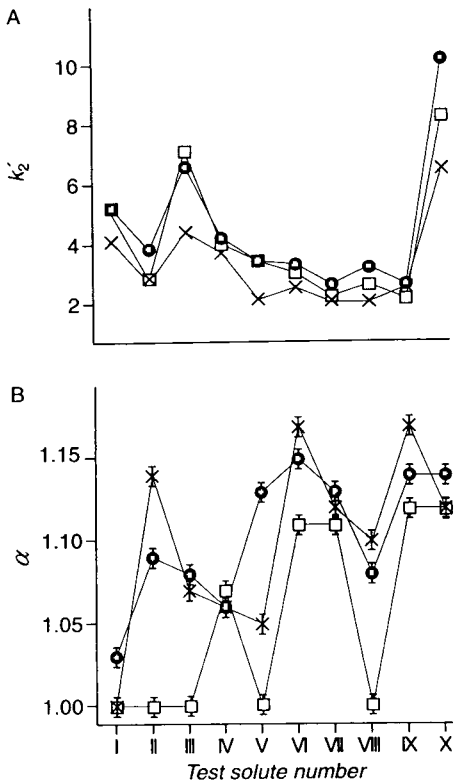

Fig. 4. Substitution at the narrow opening of the cyclodextrin, (A) retention of the last eluting enantiomer and (B) chiral selectivity versus test solute (SFC–FID cf. Table 2). CSP **9** ●, **12** □ and **13** ×.

3.7. Film thickness

Five capillaries (5 m × 50 μm I.D.) were coated with CSP **9** to give columns having film thicknesses of approximately 0.125, 0.25, 0.375, 0.50 and 0.625 μm, respectively. The peak asymmetry was then monitored for (±)-γ-phenyl-γ-butyrolactone **III** in analogy with the study of the influence of substitution ratio above.

An increasing film thickness is expected to

give both increased sample capacity and retention whereas the selectivity should remain constant. While retention and selectivity behaved as expected, the sample capacity, measured in terms of peak asymmetry, did not differ significantly between columns with different film thicknesses. This unexpected result, for which we have no reasonable explanation, indicates that it is not advisable to increase the film thickness of these CSPs above ca. 0.25 μm to increase the sample capacity as this would mainly increase the retention and decrease the efficiency.

3.8. Substitution of the siloxane backbone

CSPs having octyl, CSP **9**, and tolyl, CSP **18**, groups attached to the siloxane backbone to enhance immobilization did not differ significantly with respect to chromatographic performance (Fig. 5). The addition of a cyanopropyl group, CSP **19**, did, however, result in increased retention as well as chiral selectivity for most compounds in the test set. It must consequently be concluded that the polar cyano groups participate in and improve the chiral recognition of certain solutes. It is therefore not unlikely that the presence of other small polar groups on the siloxane backbone, or the rim(s) of the cyclodextrin, could enhance the chiral selectivity.

3.9. Immobilization and column stability

Due to the solvating power of the supercritical mobile phase, it is necessary to immobilize the stationary phase in order to obtain a stable column and allow the analysis of non-volatile compounds. In open-tubular column SFC, the CSP is generally immobilized by thermal or radical initiated crosslinking, as has successfully been done for achiral columns [23]. In the presence of the bulky chiral selector, however, radical initiated crosslinking is often disturbed and it becomes necessary to incorporate groups in the non-chiral part of the CSP that facilitate crosslinking. A small amount of octyl, CSP **1–17, 19** and **20**, or tolyl, CSP **18** and **21**, groups (ca. 1% by substituent) was therefore incorporated in

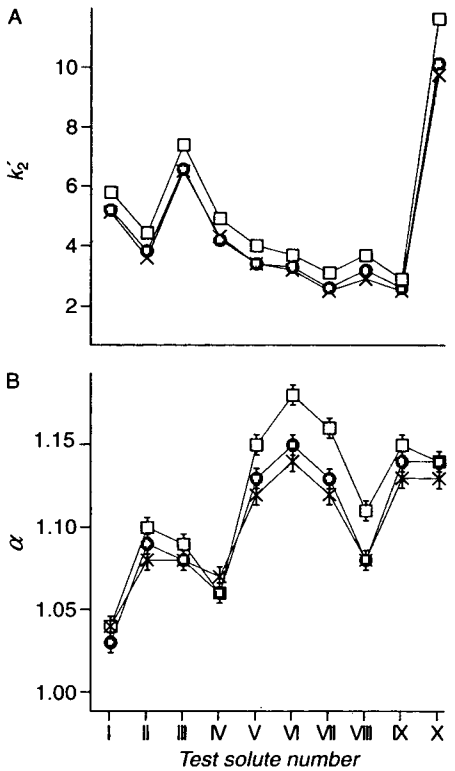

Fig. 5. Substitution of the siloxane backbone, (A) retention of the last eluting enantiomer and (B) chiral selectivity versus test solute (SFC–FID cf. Table 2). CSP **9** O, **18** × and **19** □.

the siloxane for this purpose. The use of dicumylperoxide as a free radical initiator was found to reduce the α values for CSP **9** and **18** with about 3% in comparison with the non-immobilized CSPs. A rinsing with supercritical CO_2 at 60°C and 0.89 g ml^{-1} (415 atm, the upper pressure limit of the instrument) for five hours followed by a rinsing at 120°C and 0.71 g ml^{-1} (415 atm) for another five hours resulted, for the dicumylperoxide treated CSP **9**, in a 30% decrease in k', a 37% decrease in N but no decrease in α. For the dicumylperoxide treated CSP **18** the same rinsing procedure resulted in a 22% decrease in k', a 14% decrease in N and no decrease in α, a result promoting the use of tolyl substitution of the CSP. Tolyl substituted polysiloxanes should have a solubility that is more compatible with cyclodextrin than the corresponding octyl substituted polysiloxanes, an im-

portant consideration for reproducible and uniform synthesis.

The relatively large decrease in k' indicates that the CSPs might contain a low-molecular mass fraction that can not be immobilized. In an attempt to decrease the loss of stationary phase during rinsing, 10 mg of CSP **18** was coated on the walls of a piece of glass tubing and subsequently subjected to dynamic SFE to remove low-molecular-mass material from the CSP prior to the coating of columns. Even though the CSP was extracted at 60°C and a density of 0.80 g ml^{-1} for two hours no decrease in mass could be observed which indicates that the CSP should have a uniform molecular mass. However, a column coated with the extracted CSP did not show any improved degree of immobilization. One explanation for this could be that the relatively thick polymer film on the glass prevented an efficient extraction. During the SFE treatment it was realized that the CSP becomes milky and non-transparent after a rapid density decrease in contrast to its otherwise colorless and transparent appearance. This observation stresses the need to avoid drastic density changes in order to maintain good column performance.

Column stability was investigated by subjecting a column coated with CSP **18** to extremely rapid density programs to the maximal density allowed by the instrument. The chromatographic performance was monitored after 0, 25, 50, 75 and 100 density programs respectively and, as is illustrated in Fig. 6, no degradation could be observed.

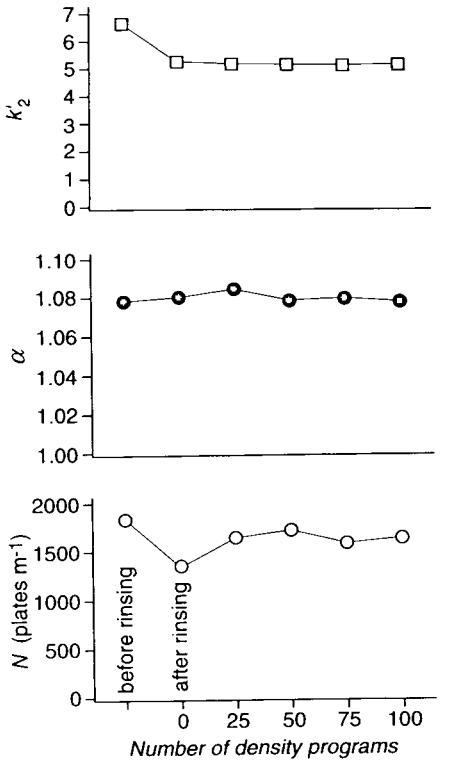

Fig. 6. Immobilization and column stability, chromatographic performance of a column (5 m × 50 μm, $d_f \approx 0.25$ μm) coated with CSP **18** monitored by the injection of (±)-γ-phenyl-γ-butyrolactone **III** (SFC–FID 60°C and 0.30 g ml^{-1}) before and after rinsing as well as after 25, 50, 75 and 100 extremely rapid density programs to the maximal density allowed by the instrument (from 0.20 to 0.89 and 0.20 g ml^{-1} at ± 0.20 g ml^{-1} min^{-1} and 60°C).

3.10. Chromatographic performance with different mobile phases

According to our observations and previous studies by Schurig and co-workers [7], CSPs based on cyclodextrins give lower α values in SFC than in GC *at the same temperature* due to solvation effects. A comparison of efficiencies also revealed that GC provides higher efficiencies (250 μm I.D. columns, ca. 3000 plates m^{-1}) than SFC (50 μm I.D. columns, ca. 2000 plates m^{-1}).

However, the fact that the chiral selectivity increases with decreasing temperature can in some cases be used to compensate for the lower chiral selectivities and efficiencies in SFC. As the retention is usually controlled by the density of the mobile phase the temperature thus becomes a free variable. In addition, the use of low temperatures reduces the risk of thermal decomposition and racemization.

In most comparisons of the behaviour of a CSP in SFC and GC, retention, selectivity, resolution (R_s) and efficiency have been monitored at the same temperatures. In the present study, the separations of ten compounds with different polarity and molecular mass were com-

pared at "iso-conditions" yielding an R_s value of 1.5 within the shortest possible time or, if this was not obtainable, at a retention time of 60 min with as large resolution as possible (Table 3). Deviations of ±0.1 R_s units and ±5 min between predicted and experimental values were accepted, as the predictions were made by *extrapolation* from a small number of experiments [24–28]. A maximum working temperature of 200°C was used in order to prevent degradation of the column. From these comparisons it can be concluded that when using the same column, 10 m × 100 μm I.D., in both techniques, GC provides significantly shorter retention times than SFC for volatile compounds such as 1-phenylethanol and diethyl tartrate. However, the enantiomers of more polar compounds or compounds of higher molecular mass, e.g. 2,8-di(2-hydroxyethyl) - 6*H*,12*H* - 5,11 - methanodibenzo-[*b*,*f*]-[1,5]-diazocine, ibuprofen and dihydrodiazepam, are often difficult or even impossible to separate with GC.

It should be pointed out that this comparison was performed with a 10 m × 100 μm I.D. column which is theoretically favourable for GC and unfavourable for SFC. If instead a 50 μm I.D. column is used in SFC it is possible to decrease the retention times significantly. For example, with the 10 m × 100 μm I.D. column it was, for (±)-*trans*-2-phenylcyclohexanol **IX**, only possible to obtain baseline resolution at a retention time of 56 min whereas the use of a 5 m × 50 μm I.D. column allowed baseline resolution within 14 minutes, one minute shorter than in the GC separation (Table 3). Other examples of separations of the compounds listed in Table 3 using 5 m × 50 μm I.D. columns are shown in Figs. 7 and 8.

3.11. Examples of separations

The broad applicability of CSP **9** and **18** is exemplified in Figs. 7 and 8 in which the enantiomers of non-volatile compounds of pharmaceutical interest have been efficiently separated by SFC.

Fig. 7A shows the separation of the racemic (*N*-trifluoroacetyl)propylester of carboranylalanine, a compound which is not readily analyzed by either GC or LC as it requires a relatively

Table 3
Comparison between SFC and GC at optimal conditions using the same 100 μm I.D. column coated with CSP **18**

Compound	SFC 5 m × 50 μm I.D. [a,b]				SFC 10 m × 100 μm I.D. [a,c]				GC 10 m × 100 μm I.D. [a,d]		
	T (°C)	ρ (g ml^{-1})	t_{R2} (min)	R_s	T (°C)	ρ (g ml^{-1})	t_{R2} (min)	R_s	T (°C)	t_{R2} (min)	R_s
(±)-*trans*-2-Phenylcyclohexanol **IX**	60	0.35	14.1	1.6	40	0.20	56.1	1.6	120	15.3	1.5
(±)-1-Phenyl-1-ethanol **VII**					48	0.17	31.8	1.6	114	2.7	1.5
(±)-Pantolactone **V**					50	0.16	56.8	1.3	130	2.5	1.6
(±)-Diethyl tartrate **VI**					50	0.18	55.6	1.4	140	4.6	1.6
(±)-Glutethimide Fig. 7D					58	0.27	63.0	1.1	144	61.6	0.9
(±)-1-(4-Phenyl)phenylethanol **X**					51	0.29	59.9	1.6	139	60.2	1.0
(±)-Ibuprofen Fig. 7B					60	0.30	62.3	1.0	200	>60	–
(±)-Dihydrodiazepam Fig. 8					58	0.52	14.2	1.6	200	>60	–
(±)-2,8-Di(2-hydroxyethyl)-6H,-12H-5,11-methanodibenzo-[*b*,*f*]-[1,5]-diazocine (Fig. 7E)					53	0.61	64.9	1.5	200	>60	–
(±)-Carboranylalanine as its (N-trifluoroacetyl)propylester (Fig. 7A)					56	0.32	55.2	1.2	143	61.1	0.0

[a] For both the 50 and 100 μm I.D. columns the film thickness was ca. 0.25 μm.
[b] CO_2 at an average linear velocity of 1.9 cm s^{-1} at 60°C and 0.30 g ml^{-1}.
[c] CO_2 at an average linear velocity of 2.5 cm s^{-1} at 60°C and 0.30 g ml^{-1}.
[d] H_2 at an average linear velocity of 75 cm s^{-1} at 100°C.

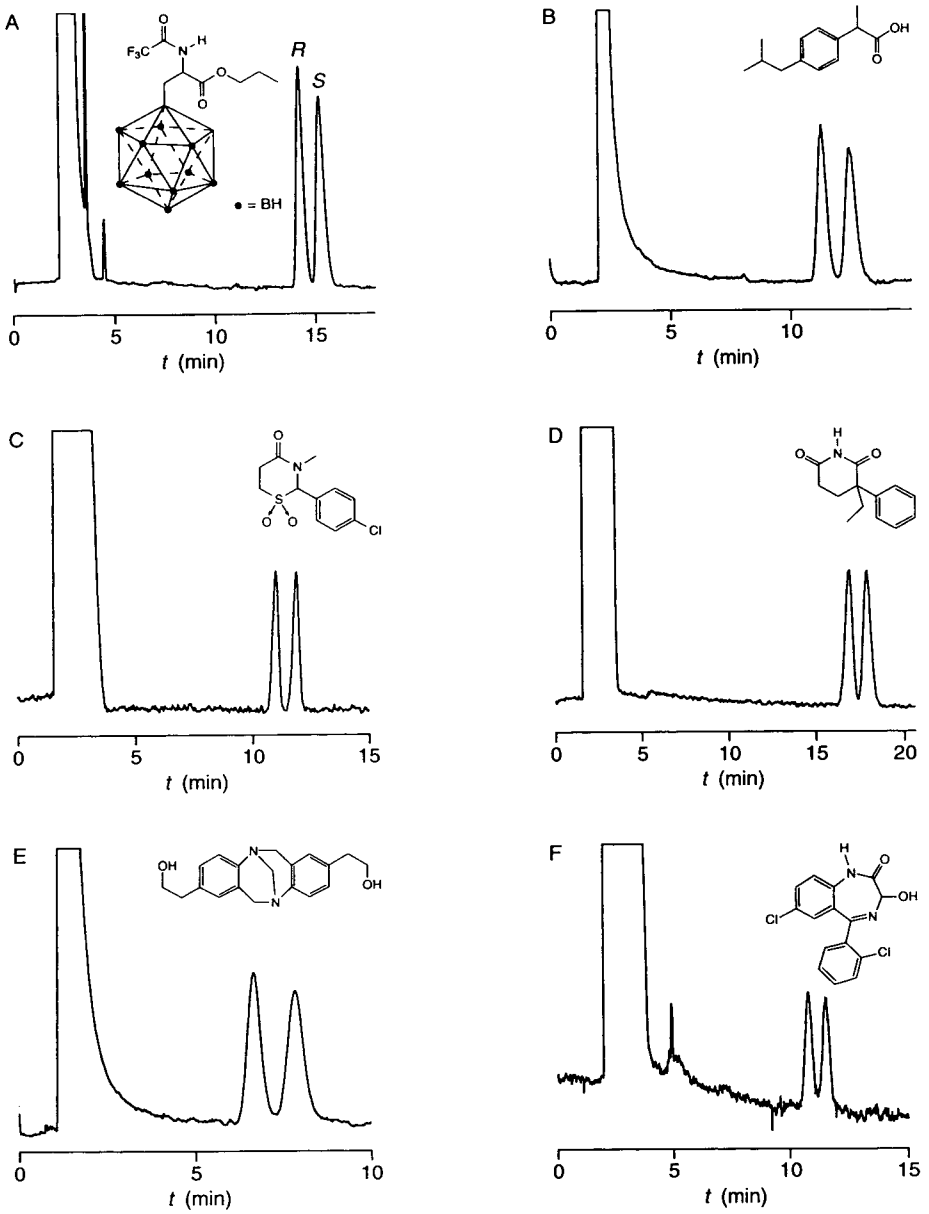

Fig. 7. Examples of separations performed by SFC–FID and columns coated with CSP **9** (A,B) and **18** (C–F), respectively. Column: 5 m × 50 μm I.D., $d_f \approx 0.25$ μm. Conditions: CO_2, 60°C, (A) (±)-carboranylalanine as its (N-trifluoroacetyl) propylester density programmed from 0.20 to 0.485 g ml^{-1} at 0.20 g ml^{-1} min^{-1} after a 2 min isopycnic period, (B) (±)-ibuprofen density programmed from 0.18 to 0.375 g ml^{-1} at 0.20 g ml^{-1} min^{-1} after a 2 min isopycnic period, (C) (±)-chlormezanone density programmed from 0.18 to 0.51 g ml^{-1} at 0.20 g ml^{-1} min^{-1} after a 2 min isopycnic period, (D) (±)-glutethimide density programmed from 0.18 to 0.375 g ml^{-1} at 0.20 g ml^{-1} min^{-1} after a 2 min isopycnic period, (E) (±)-2,8-di(2-hydroxyethyl)-6H,12H-5,11-methanodibenzo-[*b*,*f*]-[1,5]-diazocine isopycnic at 0.74 g ml^{-1} and (F) (±)-lorazepam density programmed from 0.20 to 0.79 g ml^{-1} at 0.20 g ml^{-1} min^{-1} after a 2 min isopycnic period.

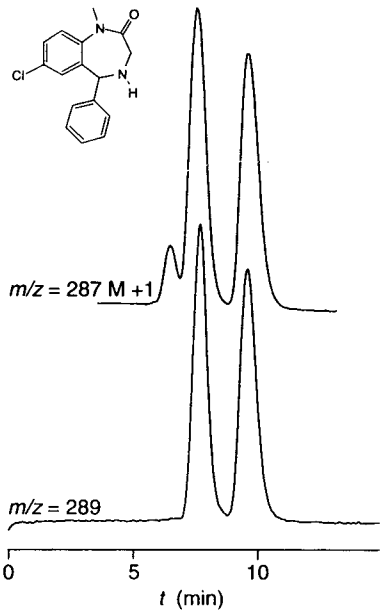

Fig. 8. SFC–MS, selected ion monitoring allowing the elimination of the signal from a compound coeluting with the analyte (±)-dihydrodiazepam. Column: CSP **18**, 5 m × 50 μm I.D., $d_f \approx 0.25$ μm. Conditions: CO_2 isopycnic at 0.48 g ml^{-1} and 85°C.

high temperature to elute in the former technique and only absorbs light at short wavelengths making LC detection difficult [27].

Also benzodiazepines, such as dihydrodiazepam, lorazepam and oxazepam [28] can be separated with this type of CSPs. Unfortunately, the FID response is quite small for lorazepam and oxazepam in comparison with other compounds (Fig. 7F), but this problem can probably be circumvented by the use of a UV detector, electron capture detector or mass spectrometer. The latter solution has several advantages as it is, for example, possible to eliminate the signals from coeluting compounds by employing selected-ion monitoring, as is illustrated in Fig. 8 for the enantiomers of dihydrodiazepam and an unknown impurity.

4. Conclusions

The copolymeric approach for the construction of CSPs seems to have no benefits over the side-arm approach when the chiral selector consists of macrocycles like β-cyclodextrin. Consequently, further development of cyclodextrin-based CSPs should be focused on the latter approach as this approach requires a less complicated synthesis.

Among the side-arm substituted CSPs evaluated in this study, the permethylated β-cyclodextrin and the permethylated β-cyclodextrin having the hydroxyl groups at the narrow opening replaced with hydrogen proved to be the most widely applicable CSPs. This result is well in line with previous observations in GC for alkyl and acetyl substituted cyclodextrins dissolved in polysiloxanes [2]. The structure of the spacer between the cyclodextrin and the siloxane part of the CSP does not seem to be critical. A small amount of cyanopropyl groups attached to the siloxane backbone improved the chiral selectivity. This indicates that a small number of polar groups on the siloxane backbone or the rim(s) of the cyclodextrin could be beneficial.

Since the sample capacity increased and the efficiency did not decrease dramatically with increasing substitution ratio it should be favourable to utilize relatively large amounts of cyclodextrin in the CSP, e.g. 70%.

Even though the present approach does not allow a complete immobilization of the CSPs (ca. 20% was lost in terms of decrease in k'), the stability study clearly shows that the obtained columns are stable enough to allow a more widespread use.

As illustrated in the comparison between open-tubular column GC and SFC, SFC should be a valuable complement to GC for the analysis of non-ionic compounds of low to medium volatility.

References

[1] D. Schmalzing, M. Jung, S. Mayer, J. Rickert and V. Schurig, *J. High Resolut. Chromatogr.*, 15 (1992) 723.
[2] W. Keim, A. Köhnes, W. Meltzow and H. Römer, *J. High Resolut. Chromatogr.*, 14 (1991) 507.
[3] W.A. König, *Gas chromatographic separation with modified cyclodextrins*, Hüthig, Heidelberg, 1992.
[4] P. Petersson and K.E. Markides, *J.Chromatogr. A*, 666 (1994) 381.

[5] V. Schurig, Z. Juvancz, G.J. Nicholson and D. Schmalzing, *J. High Resolut. Chromatogr.*, 1 (1991) 58.
[6] V. Schurig, D. Schmalzing and M. Schleimer, *Angew. Chem. Int. Ed. Engl.*, 30 (1991) 987.
[7] D. Schmalzing, G.J. Nicholson, M. Jung and V. Schurig, *J. Microcol. Sep.*, 4 (1992) 23.
[8] V. Schurig, M. Schleimer and M. Jung, in V. Schurig (Editor), *Book of Abstracts of the 3rd International Symposium on Chiral Discrimination, Tübingen, Germany, Oct. 1992*, p. 76.
[9] G. Yi, J.S. Bradshaw, B.E. Rossiter, S.L. Reese, P. Petersson, K.E. Markides and M.L. Lee, *J. Org. Chem.*, 58 (1993) 2561.
[10] M. Jung and V. Schurig, *J. High Resolut. Chromatogr.*, 16 (1993) 215.
[11] P. Petersson, K.E. Markides, G. Yi, S.L. Reese, B.E. Rossiter, J.S. Bradshaw and M.L. Lee, in P. Sandra, M.L. Lee, F. David, G. Devos (Editors), *Proceedings of the 14th International Symposium on Capillary Column Chromatography, Baltimore, MD, May 1992*, Foundation for the International Symposium on Capillary Chromatography, Miami, FL, 1992, p. 750.
[12] J.S. Bradshaw, G. Yi, B.E. Rossiter, S.L. Reese, P. Petersson, K.E. Markides and M.L. Lee, *Tetrahedron Lett.*, 34 (1993) 79.
[13] D.W. Armstrong, Y. Tang, T. Ward and M. Nicholas, *Anal. Chem.*, 65 (1993) 1114.
[14] Y. Tang, Y. Zhou and D.W. Armstrong, *J. Chromatogr.*, 666 (1994) 147.
[15] G. Yi, J.S. Bradshaw, B.E. Rossiter, A. Malik, W. Li and M.L. Lee, *J. Org. Chem.*, 58 (1993) 4844.
[16] G. Yi, J.S. Bradshaw, B.E. Rossiter, H. Yun, A. Malik and M.L. Lee, *in preparation.*
[17] P. Petersson, K.E. Markides, D.F. Johnsson, B.E. Rossiter, J.S. Bradshaw and M.L. Lee, *J. Microcol. Sep.*, 4 (1992) 155.
[18] K.E. Markides and M.L. Lee (Editors), *Analytical Supercritical Fluid Chromatography and Extraction*, Chromatography Conferences Inc., Provo, UT, 1990, p. 172.
[19] L.N. Tyrefors, R.X. Moulder and K.E. Markides, *J. Am. Chem. Soc.*, 65 (1993) 2835.
[20] M. Jung and V. Schurig, *J. Microcol. Sep.*, 5 (1993) 11.
[21] M. Jung, D. Schmalzing and V. Schurig, *J. Chromatogr.*, 552 (1991) 43.
[22] B.E. Rossiter, S.S. Zimmerman, D.F. Johnsson, J.S. Bradshaw, K.E. Markides and M.L. Lee, *in preparation.*
[23] L.G. Blomberg, *J. Microcol. Sep.*, 2 (1990) 62.
[24] P. Petersson, N. Lundell and K.E. Markides, in P. Sandra and G. Devos (Editors), *Proceedings of the 15th International Symposium on Capillary Chromatography, Riva del Garda, Italy, May 1993*, Hüthig Verlag, Heidelberg, 1993, p. 1566.
[25] E.V. Dose, *Anal. Chem.*, 59 (1987) 2414.
[26] D.E. Bautz, J.W. Dolan, W.D. Raddatz and L.R. Snyder, *Anal. Chem.*, 62 (1990) 1560.
[27] P. Petersson, J. Malmquist, K.E. Markides and S. Sjöberg, *J. Chromatogr A.*, 670 (1994) 239.
[28] S.R. Almquist, P. Petersson, W. Walther and K.E. Markides, *J. Chromatogr A.*, 679 (1994) 139.

ELSEVIER

Journal of Chromatography A, 684 (1994) 311–322

JOURNAL OF CHROMATOGRAPHY A

Dependence of the electroosmotic mobility on the applied electric field and its reproducibility in capillary electrophoresis

Michael S. Bello[1], Laura Capelli, Pier Giorgio Righetti*

Faculty of Pharmacy and Department of Biomedical Sciences and Technologies, University of Milan, Via G. Celoria 2, 20133 Milan, Italy

First received 5 April 1994; revised manuscript received 8 June 1994

Abstract

Experimental results on the electroosmotic mobility in fused-silica capillaries are presented for different applied voltages and solutions of different pH. The electroosmotic mobility is shown to be dependent on the applied voltage and this dependence cannot be attributed to the temperature effects. Results of the electroosmotic mobility measurements are found to be dependent also on the electrophoresis unit they have been performed in. The explanation given and the relevant theory presented are based on the hypothesis that these effects are produced by a radial electric field inevitably existing in any electrophoresis unit. The concept of the limiting electrophoretic mobility, i.e. extrapolated to the zero applied voltage, is introduced in order to characterize the properties of the solution–wall interface. The slope of the electroosmotic mobility dependence on the applied voltage depends on the solution pH and the surroundings of the capillary. Theoretical estimations agree well with both experimentally found limiting mobilities and slopes. Long-term variations of the electroosmotic mobility are supposed to be related with the cation penetration into the capillary wall.

1. Introduction

The electroosmotic flow in a capillary column is produced by an electric field and transmitted by the drag of ions acting in a thin sheath of charged fluid adjacent to the silica wall column. The origin of charge in this sheath is an unbalance between positive and negative ions in the bulk solution which have to balance the fixed negative charge on the silica wall. Electroosmosis (EO) in capillary electrophoresis has attracted much attention because of its importance for understanding results of separation and run reproducibility. EO flow is superimposed on the electrophoretic motion of the analyte and, thus, effects its migration time. If the direction of the EO flow is the same as that of the electrophoretic motion, it reduces the migration time and decreases resolution. For micellar electrokinetic chromatography with neutral micelles, electroosmosis is the only source of motion and, therefore, determines the reproducibility of the analysis.

A traditional explanation of electroosmosis [1–3], based on the concept of the electric double layer at the boundary of the solid-phase–electrolyte solution, assumes that the mobile part of

* Corresponding author.

[1] Permanent address: Institute of Macromolecular Compounds, Russian Academy of Sciences, Bolshoi 31, St. Petersburg 199004, Russian Federation.

0021-9673/94/$07.00
SSDI 0021-9673(94)00545-K

the double layer moves parallel to the boundary with a certain velocity U under the influence of the applied tangential electric field E. The mobile part of the double layer has an opposite charge to the immobilized surface charge originating from the dissociation of surface molecules or ion adsorption to the surface.

Electroosmotic mobility (EM) μ is defined as the ratio of the electroosmotic velocity to the intensity of the electric field which generates the electroosmotic flow. The well-known formula of Von Smoluchowski relates μ with the properties of the liquid (dielectric constant and viscosity) and ζ potential.

$$\mu = \frac{\varepsilon \varepsilon_0 \zeta}{\eta} \quad (1)$$

where ε is the dielectric constant of the electrolyte solution, ε_0 is the dielectric permittivity of vacuum, η is the solution viscosity and ζ is the zeta potential, which is, as a first approximation, equal to the electric potential drop between the wall and the bulk of the electrolyte solution.

The surface charge determining ζ potential is formed by the dissociated charged groups and is known to be controlled by the solution pH (as shown by Lukacs and Jorgenson [4], Schutzner and Kenndler [5], Schwer and Kenndler [6], Kohr and Engelhardt [7]), by organic modifiers [6], and its ionic strength and composition, see Van Ormann [8]. The important feature of the EO mobility generated by the immobilized surface charge is that it does not directly depend on the applied axial electric field. Indirectly, EO mobility depends on the electric field through the dependence of the solution viscosity on temperature which, in case of inadequate cooling, depends on the square of the electric field strength.

A way to control EO directly by applying a radial electrical field was proposed recently by Lee and co-workers [9,10] and by Ghowsi and Gale [11]. This radial electric field is produced by applying a potential difference between the electrolyte solution within the capillary and the outer surface of the capillary [12–17]. The effect of the radial electric field on the EO is explained in the literature as it induces an additional surface charge density on the inner fused-silica surface which effects the total ζ potential and, thus, according to Eq. 1, the EO mobility.

The dependence of the EO mobility on the electric field measured in conventional CE units was experimentally observed and reported by Rasmussen and McNair [18] and by Issaq et al. [19] and was attributed to the viscosity dependence on the temperature mentioned above. Another explanation for the dependence of the EO mobility on the applied electric field, based on new findings [9–17], was recently proposed by Van De Goor et al. [20] and by the present authors [21]. The idea was that the electric potential difference between the part of the capillary maintained at high voltage and the grounded parts of the equipment creates a radial electric field in the capillary wall. Therefore, application of the electric field to the capillary leads to effects similar to those reported for capillaries with a voltage offset at the outer surface.

In this paper we present a theoretical model for explaining the existence of the radial electric field in conventional CE units and experimental data showing direct dependence of the EO mobility on the applied voltage in two types of commercially available CE units. In the theoretical treatment the capillary surroundings in conventional CE units are modelled by an outer grounded cylinder containing the capillary. The theory derives a formula for the EO mobility in this system from the basic equations of the electric field. Reproducibility of the EO flow is studied and discussed for various experimental conditions.

2. Theory

A capillary in conventional CE units is contained in a grounded box or a cartridge and has nearby other parts of the unit, such as a carousel or a detector having the electric potential of the ground. The high positive voltage applied to the anode creates not only a uniform electric field within the capillary bore, but also an electric field of a very complex configuration outside the capillary, and, in particular, a radial electric field

in the capillary wall. Obviously, if two points in space have different electric potential, an electric field exists between them. In the case of a capillary these points are the high voltage part of the capillary and grounded parts of the unit. Additionally, for a coiled capillary, parts of the capillary with different electric potential are close to each other and, thus, produce a radial electric field [22].

The radial electric field directed outward from the capillary can only be created by a positive electric charge. As the buffer solution is electrically conductive, the only possible location of the positive charge is in the vicinity of the capillary wall. This positively charged layer, having the thickness of the Debye–Hückel radius, generates the EO flow under the influence of the axial electric field. Note that in the case of an induced positive charge, the existence of the neutralizing negative immobilized charge is not necessary.

In order to calculate the electric field outside and inside the capillary one has to solve the three-dimensional Poisson equation taking into account the geometry of the capillary surroundings and their electrical properties. Although this problem can be solved in principle, it is extremely laborious. As an approximation, we propose to model the surroundings of the capillary by an outer grounded metal cylinder of the large radius r_c.

Consider a cross-section of the capillary at a distance z from the high voltage end of the capillary and having the inner wall radius r_w and the outer capillary radius r_o (Fig. 1). The capillary is contained within an outer metal cylinder of the radius r_c large enough to be assumed as a model of a container, a box or a cartridge surrounding the capillary and having the electrical potential of the ground. The potential difference between the metal cylinder and the bulk of the solution is $V(z)$.

Assume the capillary to be long in comparison with the radius of the outer cylinder. Then, when calculating the radial electric field for the high voltage part of the capillary the axial electric field may be neglected in comparison to the radial one. This approximation should be valid for the part of the capillary distant enough from both ends of the capillary. Therefore, we consider a simplified one-dimensional model for the electric field distribution within the capillary instead of a complex three-dimensional one. The errors caused by this simplification do not allow us to suppose a quantitative agreement with experiments, although a qualitative agreement is expected.

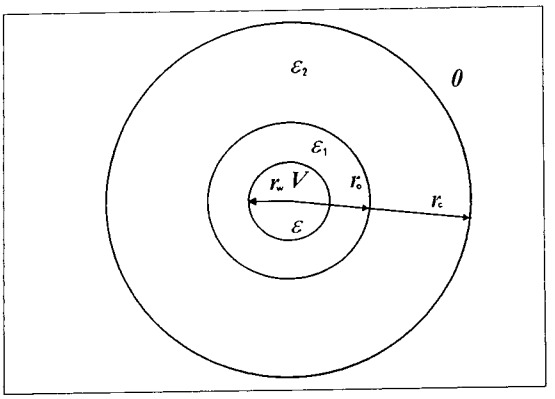

Fig. 1. Scheme of the capillary cross section and its surroundings. r_w is the inner capillary radius, r_o is the capillary outer radius, r_c is the radius of the imaginary grounded outer cylinder, modeling the capillary surroundings, ε is the dielectric constant of the solution, ε_1 and ε_2 are the dielectric constants of the capillary wall and the substance filling the space between the capillary and the grounded parts of the CE unit.

2.1. ζ Potential

At this point it is possible to derive the electric potential drop between the bulk of the electrolyte solution in the capillary and its surface, i.e. the ζ potential, and, hence, according to Eq. 1, the expression for the EO mobility. The equation governing electric field in the electrolyte solution is the well-known Poisson–Boltzmann equation

$$\nabla^2\varphi = -\frac{1}{\varepsilon\varepsilon_0}F\sum_i z_i C_{i0}\exp\left(-\frac{z_i F(\varphi - V)}{RT}\right) \quad (2)$$

where ∇^2 is the Laplace differential operator, φ is the electric potential in the capillary bore, ε is the solution dielectric constant, ε_0 is the dielectric permittivity of vacuum, F is the Faraday

constant, $_i$ is the counting index of ions in the solution, z_i the valence of the ion $_i$, C_{i0} is its concentration in the bulk, R is the gas constant and T is the absolute temperature in Kelvin.

The first boundary condition at the interface electrolyte–capillary wall follows from the Gauss electrostatic theorem and is given by

$$\varepsilon \frac{\partial \varphi(r_w^-)}{\partial r} = \varepsilon_1 \frac{\partial \varphi_1(r_w^+)}{\partial r} + \frac{\sigma_w}{\varepsilon_0} \tag{3a}$$

where r is the radial coordinate, ε_1 is the dielectric constant of the capillary wall, σ_w is the surface density of the immobilized electric charge, the arguments r_w^- and r_w^+ mean that the derivatives are calculated at the inner and outer side of the boundary $r = r_w$, respectively.

The surface charge density σ_w includes all charges bound to the wall: ionized groups (silanols in case of fused silica) and adsorbed cations. We do not distinguish here the Stern layer but assume it to be included in the immobilized surface charge and to belong to the solid phase.

The second boundary condition at $r = r_w$ expresses the continuity of the electric potential

$$\varphi(r_w^-) = \varphi_1(r_w^+) \tag{3b}$$

In the bulk of the solution the radial electric field should be equal to zero as the radial electric current does not exist and, thus, the electric potential should be equal to V. The term "bulk" means here a domain of the capillary bore distant several Debye–Hückel radii inward from the capillary wall. We denote a length equal to several Debye–Hückel radii by δ_∞ and set the third boundary condition for Eq. 2 as

$$\varphi(r_w - \delta_\infty) = V \tag{3c}$$

The ion concentrations in the bulk are subject to the electroneutrality condition

$$\sum_i z_i C_{i0} = 0. \tag{4}$$

The electric potentials φ_1 in the capillary wall and φ_2 in the space between the capillary and the outer cylinder are governed by the Poisson equation.

$$\nabla^2 \varphi_1 = 0, \qquad \nabla^2 \varphi_2 = 0. \tag{5}$$

The boundary conditions at the surfaces $r = r_o$ and $r = r_c$ are the continuity of the electric displacement, continuity of the electric potential, and the equality of the potential φ_2 to zero at the grounded surface of the outer cylinder.

$$\varepsilon_1 \frac{\partial \varphi_1(r_o^-)}{\partial r} = \varepsilon_2 \frac{\partial \varphi_2(r_o^+)}{\partial r}, \tag{6}$$

$$\varphi_1(r_o^-) = \varphi_2(r_o^+), \qquad \varphi_2(r_c) = 0.$$

Linearizing the Poisson–Boltzmann Eq. 2[2] for relatively small $F(\varphi - V)/RT$ and ignoring the curvature of the capillary inner surface on the space scale of δ_∞ one obtains for the electric potential in the solution

$$\varphi = V - \varphi_s \exp\left(-\frac{r - r_w}{\delta}\right), \tag{7}$$

$$\delta = \frac{1}{F}\sqrt{\frac{\varepsilon_0 \varepsilon RT}{\Sigma_i C_{i0} z_i^2}}$$

where φ_s is an integration constant and δ is the Debye–Hückel radius.

Solutions to Eqs. 5 have the form

$$\varphi_1 = A_1 + A_2 \ln(r), \qquad \varphi_2 = B_1 + B_2 \ln(r) \tag{8}$$

where A_1, A_2, B_1 and B_2 are constants.

All five unknown constants in Eqs. 7 and 8 can easily be found from the five boundary conditions in Eqs. 3a, 3b, and 6. Eq. 3b can be substituted by a simpler one: $\varphi_1(r_w^+) = V$ because the electric potential difference between the bulk of the electrolyte and the capillary inner surface is not expected to be greater than a hundred millivolts which is negligible in comparison with V (kilovolts).

The solution for the intensity of the electric field in the capillary wall at the interface with the capillary bore is

$$E_1(r_w^+) = \frac{V}{r_w}\left(\ln\frac{r_o}{r_w} + \frac{\varepsilon_1}{\varepsilon_2}\ln\frac{r_c}{r_o}\right)^{-1} \tag{9}$$

[2] Linearization of the Poisson–Boltzmann equation does not lead to any significant errors for the results presented below.

where E_1 is the radial intensity of the electric field within the capillary wall.

For the ζ potential defined as the potential drop between the bulk of the solution and a capillary inner surface it follows from Eqs. 3a, 7 and 9

$$\zeta = \varphi_s = GV\delta - \frac{\sigma_w \delta}{\varepsilon\varepsilon_0}, \qquad (10)$$

$$G = \frac{\varepsilon_1}{\varepsilon r_w}\left(\ln\frac{r_o}{r_2} + \frac{\varepsilon_1}{\varepsilon_2}\ln\frac{r_c}{r_o}\right)^{-1}$$

where G is the geometrical factor. It can be seen from Eq. 10 that the ζ potential comprises two terms. The first term in the right-hand side of Eq. 10 represents an induced ζ potential, vanishing if the applied voltage reduces to zero. The second term is associated with the immobilized surface charge. In the general case, Eq. 10 is not linear but an implicit non-linear equation for ζ, since, as will be discussed below, the surface charge density depends on ζ.

2.2. Induced electroosmotic mobility

According to Eq. 1, EO mobility is directly proportional to the ζ potential. Since the first term in the right hand side of Eq. 10 is not zero if a voltage is applied, the EO mobility is not zero even at very low pH values when silanols are not ionized, and it is proportional to the electric field. We shall call the EO mobility at zero wall charge the "induced EO mobility"

In the case of zero surface charge, one obtains for the EO mobility from Eqs. 1 and 10

$$\mu_i = \beta V, \qquad \beta = \frac{\varepsilon\varepsilon_0 G\delta}{\eta} \qquad (11)$$

where μ_i is the induced electroosmotic mobility and β is the slope of the induced EO mobility dependence on the applied voltage. This slope has a dimension of $m^2\ V^{-2}\ s^{-1}$ and is proportional to the capacity of two cylindric capacitors in series. The expression for the induced electroosmotic mobility can formally be obtained from a capacitor model in a similar way to that presented in [14]. However, the interpretation is different. In a number of papers the induced EO mobility is explained by an additional polarization charge induced at the capillary surface by the radial electric field. Here, in contrast, we have shown that EO can exist even in the absence of both immobilized surface charge (set $\sigma_w = 0$ in Eq. 10) and the induced polarization charge (set $\varepsilon_1 = 1$ and $\varepsilon_2 = 1$, no polarization). Even if there is no polarization or immobilized surface charges, the mobile charged layer, which is responsible for electroosmosis, exists due to the existence of the radial potential gradient.

It follows from Eq. 11 that the factor β and, thus, the induced EO mobility depends both on the dielectric constant of the material (possibly coolant) filling the space between the capillary and the distance between the capillary and the grounded cylinder or grounded part of the unit. In general, if the surface charge is not zero the slope β depends on the surface charge due to the non-linearity of Eq. 10. An expression for the slope can be derived from Eqs. 1 and 10.

$$\beta = \frac{\varepsilon\varepsilon_0 G\delta}{\eta}\left(1 + \frac{d\sigma_w}{d\zeta}\frac{\delta}{\varepsilon\varepsilon_0}\right)^{-1} \qquad (12)$$

Evidently, Eq. 12 generalizes Eq. 11. It is seen from Eq. 12 that the slope of the EO mobility dependence on the applied voltage decreases when the surface charge density depends on the ζ potential.

The magnitude of the induced electroosmotic mobility can be estimated as follows. Assume the capillary I.D. to be equal to 75 μm, $r_o = 176$ μm, $r_c = 3$ cm, $\varepsilon_1 = 3$ (fused silica), $\varepsilon_2 = 1$ (air), $V = 10$ kV, $\delta = 5$ nm. Eq. 12 gives a mobility of $\mu_i \approx 0.21 \cdot 10^{-8}$ (m^2/Vs) which is not negligible. This value of the electroosmotic mobility corresponds to the induced ζ potential $\zeta_i \approx 3$ mV. This value lies within the limit (≈ 25 mV) of the applicability of the linearized Poisson–Boltzmann equation. If the space between the capillary and the outer cylinder is filled with a fluorocarbonic refrigerant having a dielectric constant $\varepsilon_2 \approx 2$ then $\mu_i \approx 0.38 \cdot 10^{-8}$ (m^2/Vs), which is twice as high as in air. One can imagine a situation in which the space is filled with water. For this case $\varepsilon_2 = 80$ and Eq. 12 gives $\mu_i \approx 2.1 \cdot 10^{-8}$ (m^2/Vs), which approaches the maximum

value of the induced EO mobility of $2.3 \cdot 10^{-8}$ (m^2/Vs). The latter value is derived from Eq. 12 by setting $r_c = r_o$ and neglecting the second term in the parentheses in the right hand side of Eq. 12. This situation corresponds to a conductive sheath installed at the surface of the capillary [15].

2.3. Limiting electroosmotic mobility and properties of the surface

It can be seen from Eqs. 10 and 11 that at the limit of zero applied voltage the ζ potential and, therefore, the EO mobility, approaches a certain value determined by the immobilized surface charge. We shall denote this limiting value of the ζ potential as ζ_0 and the corresponding EO mobility as μ_0. In order to calculate the surface charge density and the ζ potential one has to adopt a model of the surface reactions. Several models have been proposed in literature and all of them include the dissociation of the surface silanols. Additionally, Ghowsi and Gale [11] assumed formation of complexes $SiOH_2^+$, $SiOH_2Cl$ and SiOK at the surface; Salomon et al. [23] considered complexation of the ionized silanols with the metal ions SiOM; Huang et al. [13] included in their model only interaction between metal ions and non-ionized silanols. Almost all models supposed the existence of the Stern layer the width of which was used as an additional fitting parameter.

The model used in this paper assumes the following reactions taking place on the surface of the capillary wall, involving dissociation of the surface groups (silanols in the case of fused silica)

$$A^- + H^+ \overset{K_a}{\longleftrightarrow} AH \tag{12a}$$

$$A^- + M^+ \overset{K_1}{\longleftrightarrow} AM \tag{12b}$$

$$AH + M^+ \overset{K_2}{\longleftrightarrow} AHM^+ \tag{12c}$$

where A is the ionized surface group, H^+ is the proton and M^+ is the counter ion. Constants K_a, K_1 and K_2 are the equilibrium constants used for the algebraic relations between the concentrations.

The total surface density of the surface sites is assumed to be fixed and the following equation relates it with the surface concentrations of the ionized and non-ionized groups and positive and neutral complexes.

$$[A^-] + [AH] + [AHM^+] + [AM] = N \tag{13}$$

where quantities in brackets denote surface concentrations of the ionized groups, non-ionized groups, positive complexes and neutral complexes. N is the total surface concentration of sites.

The surface charge density can be found as

$$\sigma_w = -\frac{eNK_1(K_aK_2 - [M_s^+][H_s^+])}{K_1K_2K_a + [M_s^+]K_2K_a + [H_s^+][M_s^+]K_1 + [H_s^+]K_1K_2} \tag{14}$$

where e is the electron charge.

Concentrations $[M_s^+]$ and $[H_s^+]$ of the counter ions and protons are related to their bulk values by the Boltzmann factor [11,13]:

$$[M_s^+] = [M^+]\exp\left(\frac{F\zeta}{RT}\right),$$

$$[H_s^+] = [H^+]\exp\left(\frac{F\zeta}{RT}\right) \tag{15}$$

It's worth noting that the last relations, Eq. 15, are the source of non-linearity of Eq. 10 as they contain the ζ potential.

Constants of the surface group dissociation K_a and of the counter ion binding K_1 and K_2 were found from the fitting of the experimental data on the dependence of the limiting EO mobility on the solution pH. The geometrical factor G was found from the dependence of the induced EO mobility on the applied voltage and used the same in all calculations.

3. Experimental

Measurements of the EO mobility were performed for solutions in the pH range from 2.3 to 8 using a Beckman P/ACE System 2100 and at pH 4 using a Waters Quanta 4000. In order to exclude all effects of the initial treatment of the capillaries with strong base (a sharp increase in the EO mobility [6,14]), in most experiments the

capillaries were initially rinsed with water for 30 min and with the solution for another 30 min. Between runs the capillaries were stored in the solution. The EO mobility was assessed by measuring the migration time of a neutral marker (phenol or acrylamide). The electric current dependence on the applied voltage was always linear for runs made by using the Beckman system. This indicated no increase in the temperature of the solution. When working with the Waters system, the electric current dependence of the applied voltage was used to find mobilities recalculated to 25°C. The software package described in [24] was utilized for the recalculation. Fused-silica capillaries were from Polymicro (Phoenix, AZ, USA), 375 μm O.D., 75 μm I.D. In series of experiments with a given buffer, the capillary was rinsed with water and then with that particular buffer, as opposed to treatment with KOH (see Fig. 2). The ionic strength in the majority of experiments was kept constant and equal to 5 mM. The solutions used were acetic acid and Tris-acetate solutions. Acetic acid, Tris (hydroxymethylaminomethane) and phenol used as a neutral marker were obtained from Merck (Darmstadt, Germany). Acrylamide used as a neutral marker for measurements at high pH values was from Bio-Rad (Hercules, CA, USA).

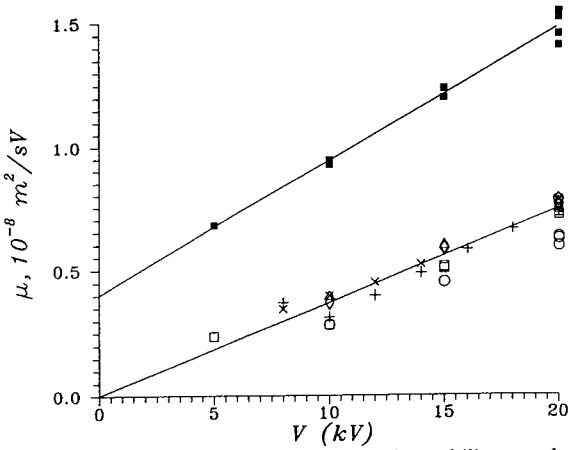

Fig. 2. Dependence of the electroosmotic mobility on the applied voltage in a 1.41 M solution of acetic acid, pH = 2.3, ionic strength 5 mM. Black boxes represent measurements made in a capillary treated before with KOH. Other symbols show results obtained in a capillary rinsed only with water and the solution. Different symbols represent series of measurements performed on different days. Beckman P/ACE System 2100.

4. Results and discussion

4.1. Experimental results

EO mobilities measured in two fused-silica capillaries in the solution of the acetic acid pH = 2.3 are shown in Fig. 2. The ionic strength of the solution is 5 mM and corresponds to the Debye–Hückel radius $\delta = 4.34$ nm; the concentration of the acetic acid is 1.41 M. The neutral marker is 1 mM phenol solution. The upper black boxes represent the mobilities obtained in the capillary treated with KOH before the EO measurements. The group of the experimental points clustering near the lowest line shows the mobilities obtained in different days in the capillary rinsed only with the solution and water. Different symbols correspond to the different days when the measurements were performed. Both groups of experimental points show the dependence of the electroosmotic mobility on the electric field. The significant difference in the mobilities obtained in the capillary treated with KOH and that treated only with the solution and water is in accord with previous findings [6,14]. However, in contrast to [14] the EO mobility shows a voltage dependence in the capillary pretreated with KOH. The limiting mobility in the capillary rinsed with KOH has a non-zero value even at this very low pH indicating a negative charge on the fused-silica surface, whereas in the capillary rinsed only with water and the solution the limiting mobility and the surface charge are negligible.

The best-fit solid line in Fig. 2 is given by the equation

$$\mu = 0.37 \cdot 10^{-12} V$$

where V is the applied voltage in volts. The slope $\beta = 0.37 \cdot 10^{-12}$ was used to calculate the geometrical factor G according to Eq. 11.

EO mobility as a function of the applied

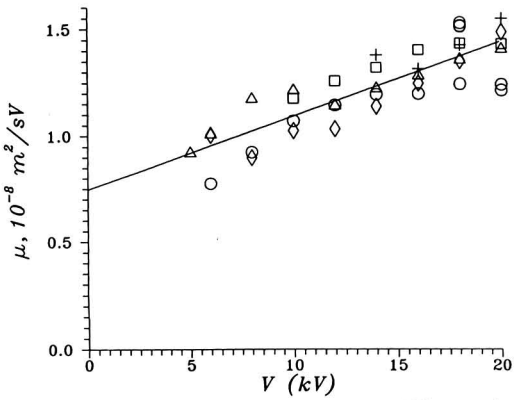

Fig. 3. Dependence of the electroosmotic mobility on the applied voltage in a 6 m*M* solution of acetic acid, pH = 3.5, ionic strength 0.32 m*M*. Different symbols represent series of measurements performed on different days. Beckman P/ACE System 2100.

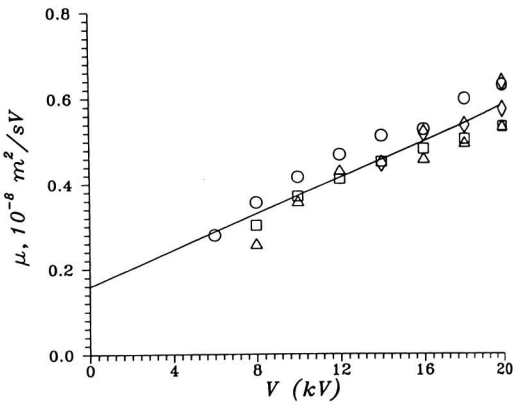

Fig. 4. Dependence of the electroosmotic mobility on the applied voltage in a solution of 93.9 m*M* acetic acid and 5 m*M* Tris, pH = 3.5, ionic strength 5 m*M*. Different symbols represent series of measurements performed on different days. Beckman P/ACE System 2100.

voltage for the 6 m*M* acetic acid solution pH = 3.5 is shown in Fig. 3. The ionic strength of the solution is 0.32 m*M* which corresponds to δ = 17.2 nm, i.e. about four times as the Debye–Hückel radius corresponding to the previous case. Different symbols again represent different days when measurements were performed. The linear best fit of the experimental points gives $\mu_0 = 0.75 \cdot 10^{-8}$ m^2 V^{-1} s^{-1} and $\beta = 0.35 \cdot 10^{-12}$ m^2 V^{-2} s^{-1}, indicating approximately the same slope as the best-fit line in Fig. 2. However, the limiting mobility μ_0 is rather high. It suggests that at this pH there exists not only induced ζ-potential but also the ζ-potential created by ionized silanol groups at the inner capillary wall.

Fig. 4 shows EO mobility as a function of the applied electric field for the 93.9 m*M* acetic acid solution and 5 m*M* Tris which corresponds to pH = 3.5 and ionic strength equal to 5 m*M* (the same as in Fig. 2). The best-fit line is described by $\mu = 0.16 \cdot 10^{-8}$ m^2 V^{-1} s^{-1} and $\beta = 0.21 \cdot 10^{-12}$ m^2 V^{-2} s^{-1} showing a gentler slope than the previous best-fit lines. The limiting mobility has a value lower than that for the solution of a low ionic strength. It is of interest to note that the slope β here is less than the slope in Fig. 2 corresponding to the solution of the same ionic strength but lower pH.

Fig. 5 shows the EO mobility as a function of the applied electric field in the Tris-acetate buffer, pH = 4.75; concentration of acetic acid is 10 m*M*, concentration of Tris is 5 m*M*, making the ionic strength equal to 5 m*M*. Black boxes in the figure show the first series of experiments with this buffer. The dashed line fitting open squares corresponds to the series of measurements obtained after a 40-hour pause (after a

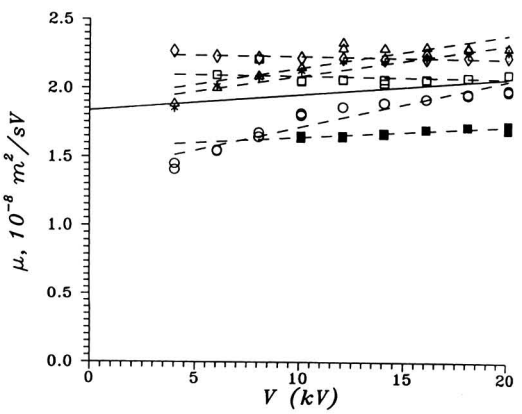

Fig. 5. Dependence of the electroosmotic mobility on the applied voltage in a solution of 10 m*M* acetic acid and 5 m*M* Tris, pH = 4.75, ionic strength 5 m*M*. Different symbols represent series of measurements performed on different days. Beckman P/ACE System 2100.

weekend) and is almost horizontal. The next line with a slope fits experimental points obtained in successive days. The upper horizontal dashed line fits points measured after the second 40-hour pause and the upper line with a slope fits data measured in successive days. It can be seen that the reproducibility of the EO flow improves with time suggesting a saturation of a slow transport process. The line fitting all experimental points gives $\mu_0 = 1.83 \cdot 10^{-8}$ m^2 V^{-1} s^{-1} and $\beta = 0.12 \cdot 10^{-12}$ m^2 V^{-2} s^{-1}.

The first series of measurements for a solution of 5 m*M* acetic acid and 5.25 m*M* Tris making pH = 7 and ionic strength 5 m*M* are shown by open circles in Fig. 6. Then, unexpectedly, the next day (open squares) the EO mobility dropped. The measurements performed on following days showed less dispersion and gave values grouped between the highest and lowest series. The values for μ_0 and β are $2.18 \cdot 10^{-8}$ m^2 V^{-1} s^{-1} and $0.6 \cdot 10^{-12}$ m^2 V^{-2} s^{-1}, respectively.

Experimental data for a solution of 5 m*M* acetic acid and 7.5 m*M* Tris making pH = 8 and ionic strength 5 m*M* are shown by open circles in Fig. 7. In contrast to the previous case but similar to the case of pH = 4.75, the lowest EO mobilities were found on the first day of measurements (open circles). The second day gave slightly higher values and then, after a 40-hour pause, the EO mobility increased significantly (triangles) and then remained approximately the same (diamonds). μ_0 and β are $2.25 \cdot 10^{-8}$ m^2 V^{-1} s^{-1} and $0.9 \cdot 10^{-12}$ m^2 V^{-2} s^{-1}, respectively.

Fig. 8 shows the EO mobility measured in a solution of 33.1 m*M* acetic acid and 5 m*M* KOH having pH = 4 and ionic strength 5 m*M*. The measurements were performed on the Waters Quanta 4000 having a geometry of the capillary environment different from that of the Beckman P/ACE 2100 system. Three groups of experimen-

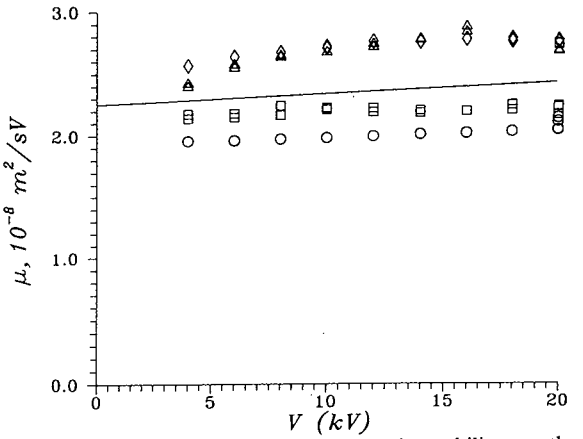

Fig. 7. Dependence of the electroosmotic mobility on the applied voltage in a solution of 5 m*M* acetic acid and 7.5 m*M* Tris, pH = 7, ionic strength 5 m*M*. Beckman P/ACE System 2100.

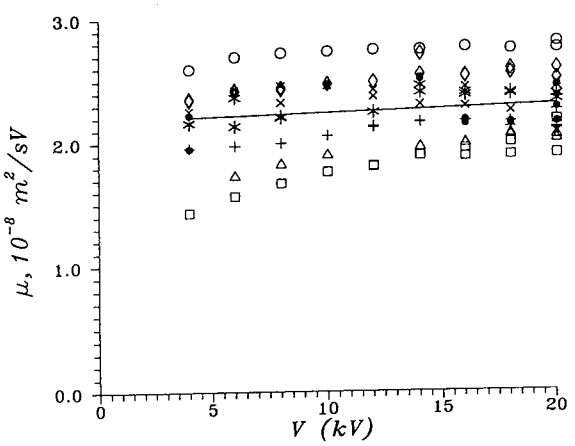

Fig. 6. Dependence of the electroosmotic mobility on the applied voltage in a solution of 5 m*M* acetic acid and 5.25 m*M* Tris, pH = 7, ionic strength 5 m*M*. Beckman P/ACE System 2100.

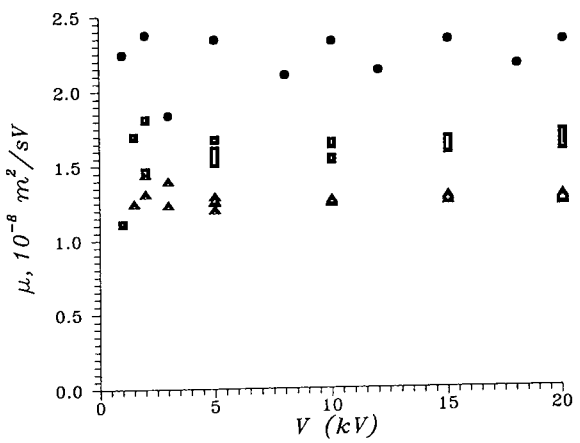

Fig. 8. Dependence of the electroosmotic mobility on the applied voltage in a solution of 33.1 m*M* acetic acid and 5 m*M* KOH, pH = 4, ionic strength 5 m*M*. Waters Quanta 4000.

tal points correspond to the measurements performed with the time interval of three weeks. During this time the capillary contained the buffer solution inside. The highest mobility corresponds to the latest series of measurements. The main characteristic for all the series of measurements shown in this figure is the absence of a measurable slope, i.e. $\beta = 0$.

4.2. Comparison of the experimental results with the theory

Limiting mobilities obtained as the results described in the previous section together with their confidence intervals are shown by the circles in Fig. 9. The solid line in this figure is found by numerically solving Eq. 10 with $V = 0$ and with the surface charge density given by Eqs. 14 and 15. The total surface density of silanol sites N was taken from literature as $N = 8.31 \cdot 10^{-6}$ mol/m^2 (5 nm^{-2}). The pK_a of silanols was found by fitting the experimental points and happened to be equal to 6.3 which is exactly the same value as found by Huang [13]. However, this could represent a mean pK value and does not per se exclude the existence of a spectrum of pK values. A pK_a less then 6.3 would contradict that the limiting mobility at pH = 2.3 is as close to zero as shown in Fig. 9. The binding constants

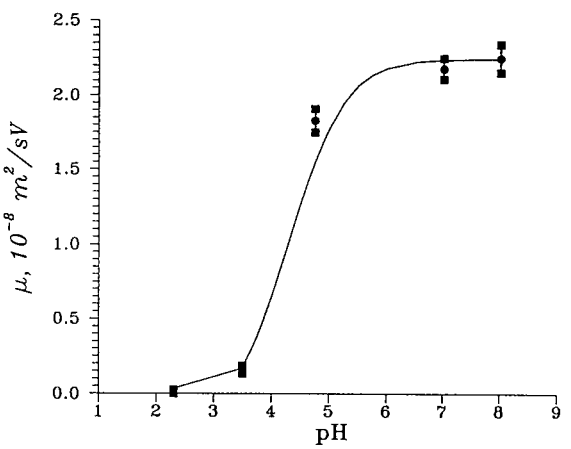

Fig. 9. Limiting EO mobilities corresponding to the measurements shown in Figs. 2, 4, 5, 6 and 7. Solid line represents simulation.

K_1 and K_2 were also determined from the fitting. Their pK's were found to be equal to $pK_1 = 4.92$ and $pK_2 = 0.25$, respectively. Neither scaling nor introduction of additional fitting parameters like Stern's layer capacity or immobile layer capacity was necessary to fit the experimental data.

It is of interest to note that the steep transition in Fig. 9 has the inflection point between pH 4 and 5 whereas pK_a of silanols was found to be 6.3. Therefore the transition should be attributed to the combined action of the ion complexation and silanol ionization at the capillary surface. The EO mobility at high pH is determined to a great extent by the value of the constant K_1, controlling complexation of the cations with the ionized silanols. If this mechanism were not taken into account in our model for the surface charge, Eq. 12b, we would obtain EO mobility values 6–7 times higher than those experimentally found. It was necessary to include in the model additional complexation of the neutral silanols with the buffer cations described by the constant k_2, Eq. 12c, to fit intermediate values of the limiting EO mobility at pH = 3.5 and 4.75.

A relatively high value for the experimentally obtained limiting mobility at pH = 4.75 suggests the possibility of an additional mechanism affecting the surface charge. It might be additional binding of protons by neutral silanols, a change of binding constants and silanol pK with the increase of the surface charge, or, finally, existence of a spectrum of the silanol pK's in stead of a single value.

Experimentally measured (circles) and theoretically found (asterisks) slopes β as a function of pH are plotted in Fig. 10. It can be seen from this figure that the theory explaining the EO voltage dependence based on the concept of the radial electric field is in agreement with experiments. Fig. 10 shows a decrease of the slope β, i.e. a decrease of the voltage control of the EO flow with the pH increase. This fact agrees with experiments performed in the capillaries with the radially applied electric field [13].

The results presented in Fig. 3 for the low ionic strength solution of acetic acid are in relative agreement for the limiting mobility [$0.75 \cdot 10^{-8}$ m^2 V^{-1} s^{-1} (experimental) and $1.15 \cdot$

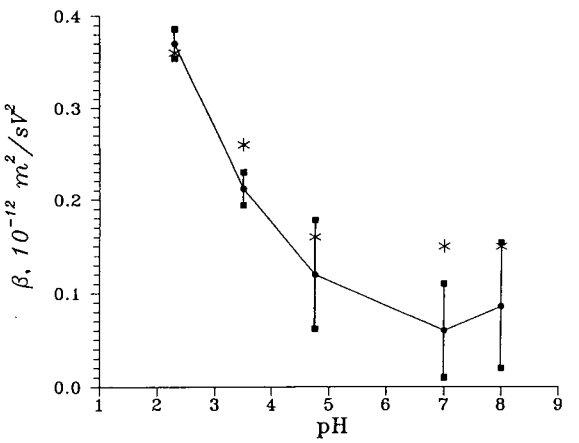

Fig. 10. Slopes of the dependencies of the EO mobilities against applied voltage corresponding to the measurements shown in Figs. 2, 4, 5, 6 and 7. Asterisks represent simulation.

10^{-8} m^2 V^{-1} s^{-1}, (theoretically calculated)] and show a discrepancy for the slope [$0.35 \cdot 10^{-12}$ m^2 V^{-2} s^{-1} (experimental) and $0.94 \cdot 10^{-12}$ m^2 V^{-2} s^{-1} (theoretical)]. Therefore, the model for the surface interaction with the electrolyte solution still needs improvement.

The short-term (within hours) and long-term (days and weeks) variations of the EO mobility found in this study were attributed to the ion-exchange properties of the silica wall [25] and, also, the influence of the radial electric field. This radial electric field keeps embedding cations into the silica wall (physically driving them to penetrate the wall) to such an extent as to continuously alter the EOF (which keeps increasing as the voltage is augmented). Only after several hours (or even days) of continuous operation does the EOF approach a plateau, probably as a compromise between electrical forces driving cations into the wall and diffusive forces pushing them out. It should also be noted that different geometries of the metal box surrounding the capillary can have a profound effect on the EOF. Thus in the Beckman unit, where the metal frame is very close to the capillary, there is a stronger dependence of EOF on voltage since the radial voltage is quite high. Conversely in the Waters Quanta, where the metal box is quite a distance from the capillary, such voltage dependence of the EOF is much reduced.

Therefore, we suppose that cations are not only attracted by the negatively charged surface, but that they can also enter the capillary wall. This continuous penetration of ions (strongly enhanced by the radial electric field) might result in an additional ionization of silanols (which would normally be protonated). An experimental evidence for the ion penetration into the capillary wall at high pH was given recently by Wu et al. [26].

As a final remark, our data could shed some light on the work of Lambert and Middleton [27], who reported a pH hysteresis effect with silica capillaries. They observed that the EOF would depend on the preconditioning of the fused-silica column. EOF values obtained from a column previously exposed to acidic conditions for varying periods of time were consistently lower than the values from columns previously exposed to alkaline conditions, particularly in the pH 4–6 region. The equilibration of surface charges on the capillary thus preconditioned could take as long as two weeks. These data can now be interpreted on the basis of our hypothesis of penetration of cations inside the wall: clearly, when preconditioning at pH 2 such penetration would be negligible, whereas a preconditioning step at pH 12 would considerably enhance this phenomenon.

5. Conclusions

1. The EO flow is observed in fused-silica capillaries even in solutions of very low pH as 2.3. However, the EO flow shows linear dependence on the applied voltage and the EO mobility extrapolated to zero voltage approaches zero.

2. The experimentally found dependence of the EO mobility on the intensity of the applied electric field is explained by the radial electric field caused by the surroundings of the capillary. The latter indicates that EO mobility measurements depend on the instrument used for measurements and that the characteristic of the

capillary wall should be evaluated from the EO mobility extrapolated to zero voltage.

3. The reproducibility of the EO flow decreases with the increase of the solution pH. A probable explanation is the interaction of cations (adsorption and diffusion enhanced by the electric field) with the fused-silica wall.

Acknowledgements

Supported in part by a grant from the European Community (Human Genome Analysis, N. GEN-CT93-0018) and by Progetto Strategico Comitato Chimica. (CNR, Roma).

Note added

After this manuscript was accepted, we heard of a paper from the group of E. Gruska [28] also describing the unreproducibility of EOF flow and ways to control it. According to them, additives such as amines added to the background electrolyte completely stabilize the EOF flow. Although they do not mention the radial electric field as a possible source for EOF unreproducibility, they mention a mechanism for such phenomenon which is indeed complementary to our observations. According to them (verbatim): the amines (added to the standard buffer) "should shield the wall from impurities in the buffer that otherwise might be adsorbed onto it. The adsorption of impurities will change the nature of the double layer on the wall and therefore change EOF". What we are saying is (verbatim): "this radial electric field keeps embedding cations into the silica wall (physically driving them to penetrate the wall) to such an extent as to continuously alter the EOF (which keeps increasing as the voltage is augmented)." Clearly, while hypothesizing different causes, we are talking about the same mechanism for EOF unreproducibility!

References

[1] D.J. Shaw, *Electrophoresis 1969*, Academic Press, London.
[2] P.D. Grossman, in P.D. Grossman and J.C. Colburn (Editors), *Capillary Electrophoresis 1992*, Academic Press, San Diego, 3–43.
[3] R.J. Hunter, in J.O'M. Bockris, B.E. Conway and E. Yeager (Editors), *Comprehensive Treatise of Electrochemistry, Vol. 1: The Double Layer*, Plenum Press, New York, 1980, pp. 397–437.
[4] K.D. Lukacs and J.W. Jorgenson, *J. High Resolut. Chromatogr. Chromatogr. Commun.*, 8 (1985) 407–411.
[5] W. Schutzner and E. Kenndler, *Anal. Chem.*, 64 (1992) 1991–1995.
[6] C.Schwer and E. Kenndler, *Anal. Chem.*, 63 (1991) 1801–1807.
[7] J. Kohr and H. Engelhardt, *J. Microcol. Sep.*, 3 (1991) 491–495.
[8] B.B. Van Ormann, G.G. Liversidge and G.L. McIntire, *J. Microcol. Sep.*, 2 (1991) 176–180.
[9] C.S. Lee, W.C. Blanchard and C.-T. Wu, *Anal. Chem.*, 62 (1990) 1550–1552.
[10] C.S. Lee, D. McManigill, C.-T. Wu and B. Patel, *Anal. Chem.*, 63 (1991) 1519–1523.
[11] K. Ghowsi and R.J. Gale, *J. Chromatogr.*, 559 (1991) 95–101.
[12] C.S. Lee, C.-T. Wu, T. Lopes and B. Patel, *J. Chromatogr.*, 559 (1991) 133–140.
[13] T.-L. Huang, P. Tsai, C.-T. Wu and C.S. Lee, *Anal. Chem.*, 65 (1993) 2887–2893.
[14] M.A. Hayes and A.G. Ewing, *Anal. Chem.*, 64 (1992) 512–516.
[15] M.A. Hayes, I. Kheterpal and A.G. Ewing, *Anal. Chem.*, 65 (1993) 27–31.
[16] M.A. Hayes, I. Kheterpal and A.G. Ewing, *Anal. Chem.*, 65 (1993) 2010–2013.
[17] C. A. Keeley, R.H. Holloway, T.A.A.M. van de Goor and D. McManigill, *J. Chromatogr. A*, 652 (1993) 283–289.
[18] H.T. Rasmussen and H.M. McNair, *J. Chromatogr.*, 516 (1990) 223–231.
[19] H.J. Issaq, I.Z. Atamna, G.M. Muschik and G.M. Janini, *Chromatographia*, 32, (1991) 155–161.
[20] T.A. van de Goor, C.A. Keely, R.R. Holloway and D. McManigill, presented at the *Sixth International Symposium on HPCE, Jan 31–Feb 3, 1994, San Diego, CA*.
[21] M.S. Bello, L. Capelli and P.G. Righetti, *Sixth International Symposium on HPCE, Jan 31–Feb 3, 1994, San Diego, CA*, poster p-335.
[22] W.D. Cole and D. McManigill, *Sixth International Symposium on HPCE, Jan 31–Feb 3, 1994, San Diego, CA*, poster p-326.
[23] K. Salomon, D.S. Burgi and J.C. Helmer, *J. Chromatogr.*, 559 (1991) 69–80.
[24] M.S. Bello, E.I. Levin and P.G. Righetti, *J. Chromatogr. A*, 652 (1993) 329–336.
[25] R. Virtanen, *Acta Polytechnica Scand.*, 123 (1974) 1–67.
[26] C.T. Wu, T.L. Huang and C.S. Lee, *J. Chromatogr. A*, 652 (1993) 277–281.
[27] W.J. Lambert and D.L. Middleton, *Anal. Chem.*, 62 (1991) 1585–1587.
[28] N. Cohen and E. Grushka, *J. Chromatogr. A*, 678 (1994) 167.

ELSEVIER

Journal of Chromatography A, 684 (1994) 323–328

JOURNAL OF CHROMATOGRAPHY A

Influence of the capillary edge on the separation efficiency in capillary electrophoresis

Nava Cohen, Eli Grushka*

Department of Inorganic and Analytical Chemistry, The Hebrew University, Jerusalem, Israel

First received 21 March 1994; revised manuscript received 14 June 1994

Abstract

The results of the present work show that the physical shape of the injection end of the capillary in CE has a major effect on the observed efficiencies. Straight-edge capillaries yield much more efficient electropherograms than do slanted edge capillaries. Also, injections into straight-edge capillaries give more symmetrical peaks. Indications are that the effect of the inlet shape is independent of molecular size. Moments analysis shows that the increase in size of the injected plug, due to the slanted shape of the capillary inlet, is not sufficient to explain the large decrease in efficiency.

1. Introduction

Separation efficiencies in capillary electrophoresis (CE) which are attainable in practice are often smaller than the theoretically predicted values. This loss in efficiency can be the result of extra broadening processes such as wall adsorption of solutes, parabolic flow profile due to temperature gradients etc. (e.g., [1,2]). Among these processes, excessive zone broadening due to sample introduction can be the dominating factor in the total zone dispersion.

While there are several methods of introducing solutes into the capillary in CE, the two most common injection techniques use either electrokinetic migration or pressure displacement. In both methods the injection protocol involves several manipulations of the running buffer and sample vials. Thus, the injection process is cumbersome and, intuitively, prone to problems.

There are several reports on difficulties related to sample introduction. Huang et al. [2], Burton et al. [3] and Terabe et al. [1] found that the injection length affects the efficiency. Rose and Jorgenson [4] compared the above two injection methods. While they could not find any significant difference in the efficiency between the two, they did notice a difference in peak size that they attributed to preferential sample introduction in the electrokinetic approach. Grushka and McCormick (5) described a ubiquitous sample introduction that resulted from the actual immersion of the capillary in the sample vial. This ubiquitous injection occurs over and above the conventional injection. The size of sample plug thus entering the capillary is quite large, resulting in lower than expected efficiencies. Schwartz et al. [6] confirmed the presence of the ubiquitous injection. Recently, Fishman et al. [7]

* Corresponding author.

0021-9673/94/$07.00
SSDI 0021-9673(94)00597-3

showed that the ubiquitous injection is caused by an interfacial pressure difference formed at the inlet of the capillary. They also discussed means of eliminating or greatly diminishing this undesirable mode of injection. Lux et al. [8] found that the injection process produces asymmetric peaks, which can be eliminated by rinsing the outer part of the capillary with clean buffer after the sample introduction part of the injection process. Dose and Guiochon [9] discussed the effects of diffusion and hydrodynamic flow on the amounts of solutes entering the capillary during the injection process.

In the present communication we show that the quality of the injection depends strongly on the physical condition of the inlet side of the capillary.

2. Experimental

2.1. Apparatus

The instrument used was a laboratory-made CE unit. A high-voltage power supply (Glassman, NJ, USA) was used to establish the electrical field across the capillary. The output voltage of the power supply was computer controlled. Capillaries were polyimide coated fused silica (Polymicro Technologies, CA, USA) 50 μm I.D. and 375 μm O.D., having separation lengths varying from 38 to 42 cm and total lengths from 72 to 74 cm. Detection was done with a Model 200 UVIS absorbance detector (Linear Instruments, CA, USA) at 280 or 200 nm for proteins. A section of about 1 cm of the capillary coating was removed by heat, to serve as a UV-detection window. The signals from the detector were fed to a Model 600 recorder (W + W Electronic, Switzerland) and a Model D-2000 Hitachi integrator (Merck, Germany).

2.2. Reagents

Buffers

The following buffers were used: (a) 0.02 *M* NaH_2PO_4 adjusted to pH 6 with NaOH (Frutarom, Israel), (b) 0.02 *M* sodium acetate (Merck) adjusted to pH 5 with acetic acid (Frutarom) and (c) 0.02 *M* Na_2HPO_4 (Mallinckrodt, USA) adjusted to pH 11 with NaOH.

Additives

The running buffer contained either 0.01 *M* triethylamine (TEA) or 0.001 *M* isoleucine as additives. The additives are used to maintain constant electroosmotic flow to ensure constant migration times [10].

Solutes

The solutes used were phenol (Mallinckrodt) and myoglobin (Sigma, MO, USA). The solutes were dissolved in the running buffer.

2.3. CE procedures

Injection of the sample into the capillary was made by electromigration at 5 kV for 1 s. Electrophoresis was run at 25 kV applied voltage. The current through the capillary did not exceed 50 μA.

2.4. Capillary treatment

Each new capillary was cleaned by flushing, sequentially, with 1 *M* KOH (Frutarom) for 15 min, triply distilled water for 30 min and the running buffer which contained an additive for a few seconds. The capillary was conditioned for 3 h, at 25 kV, to allow equilibration and consistency of migration times. This treatment eliminates the need for capillary washing between runs.

2.5. Preparation of the injection end of the capillary

The capillary edge was cut, usually with scissors, either on a slant or straight. Often, the capillary was cut having one shape, and after a few electrophoretic runs it was recut to give the other shape. The capillary edges were photographed through an Olympus Model SZH microscope at × 64 magnification.

3. Results and discussion

In our studies in CE we found that when we changed capillaries we could not reproduce peak shapes and, consequently efficiencies, for identical systems; i.e., same running buffers, solutes, injection conditions and applied voltages. Washing the injection end of the capillary after the injection process, as suggested by Lux et al. [8], did not seem to alleviate the problem since the phenomenon was dependent mainly on the capillary and not the actual injection process. While trying to establish whether the polyimide coating had an effect on the efficiency, we examined the capillary edge with a microscope. It became apparent that the capillary glass shape is the important factor.

A capillary with a straight injection end is shown in Fig. 1a and with a slanted end in Fig. 1b. An electropherogram of phenol obtained with the straight-cut capillary is given in Fig. 2a and one from the capillary with the slanted injection edge in Fig. 2b. The capillary in Fig. 1b is the same as in Fig. 1a but it was cut to give a slanted edge. The solute velocity was identical in both capillaries. The peak obtained with the straight-edge capillary is narrower than that obtained with the slanted-edge capillary; the plate numbers are 161 000 and 122 000, respectively.

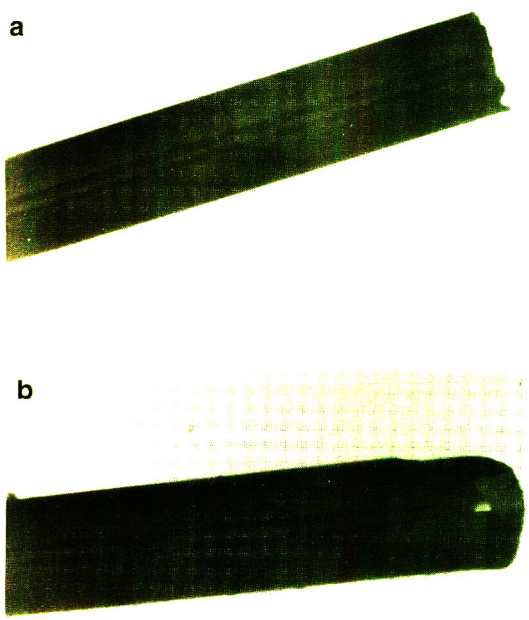

Fig. 1. Photographs of the injected end of a 50 μm I.D. 375 μm O.D. capillary used with phenol as solute. (a) Straight-edge capillary; (b) slanted-edge capillary.

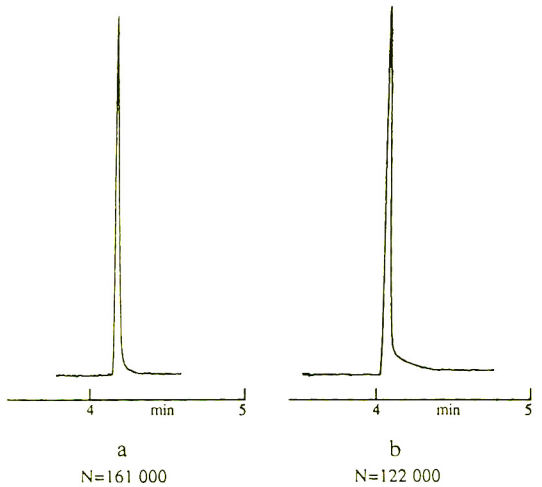

Fig. 2. Electropherograms of phenol, (a) obtained with the capillary in Fig. 1a and (b) obtained with the capillary in Fig. 1b. The electrophoresis conditions were: applied voltage 25 kV; 0.02 *M* NaH_2PO_4 buffer at pH 6; 0.01 *M* triethylamine added to the buffer to maintain constant electroosmotic flow.

Similar results were obtained with all buffers and additives mentioned in the Experimental section. For example, Fig. 3 gives a series of electropherograms of phenol, obtained under various conditions (different pH values and different additives) using several capillaries. The peaks on the right side of the figure resulted from injection into slanted-edge capillaries whereas the peaks on the left side are from the straight-edge capillaries. Injection into a straight-edge capillary resulted not only in increased efficiency but also in better peak symmetries.

The above results were obtained with small solutes. Similar results are observed with large solutes as well. As an example, Fig. 4a gives the electropherogram of the protein myoglobin (phosphate buffer at pH 11) obtained with the straight-edge capillary shown on the left side of Fig. 5. The result with the slanted-edge capillary (right side of Fig. 5), is shown in Fig. 4b. The

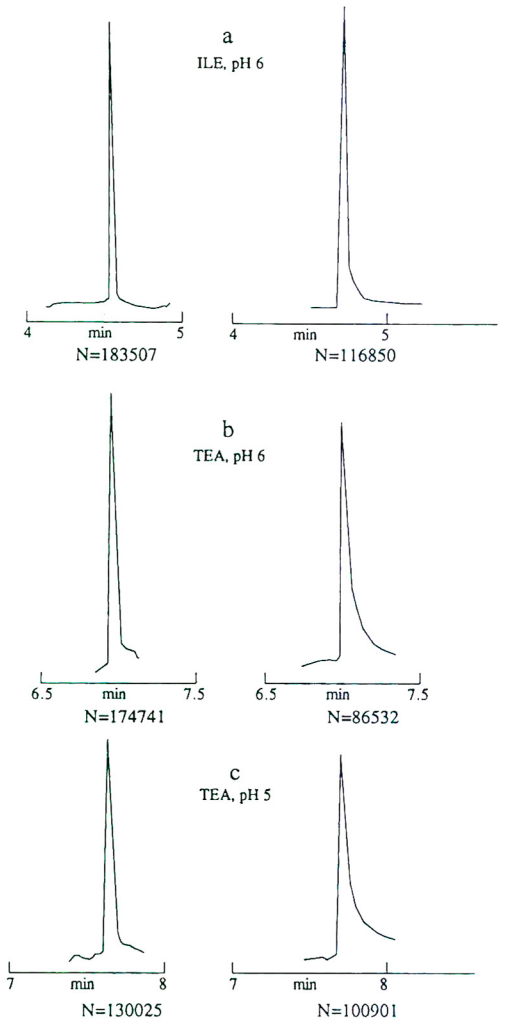

Fig. 3. Electropherograms of phenol under different conditions: (a) 0.02 *M* NaH_2PO_4 buffer pH 6 plus 0.001 *M* isoleucine additive, (b) 0.02 *M* NaH_2PO_4 buffer pH 6 plus 0.01 *M* TEA additive and (c) 0.02 *M* CH_3COONa buffer pH 5 plus 0.01 *M* triethylamine additive. In each case the right electropherogram was obtained with a slanted-edge capillary.

plate number for the peak in Fig. 4b is 87 000 as compared to 230 000 for the peak in Fig. 4a. The plate number for Fig. 4a is much lower than that predicted, most likely due to interaction of the protein with the capillary wall, even at pH 11. The peak in Fig. 4b is much smaller than that in Fig. 4a although both samples were injected under identical conditions. The small impurity

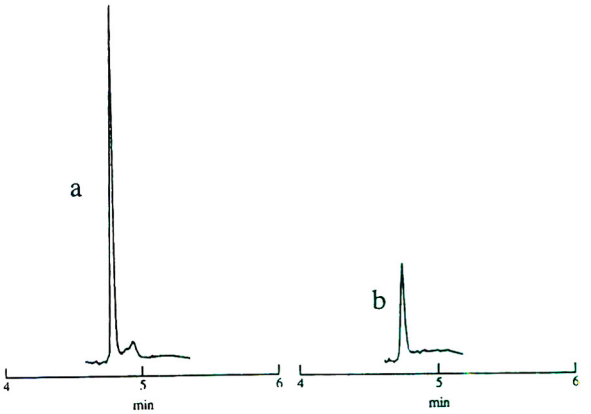

Fig. 4. Electropherograms of myoglobin; 0.02 *M* Na_2HPO_4 buffer, pH 11, 0.01 *M* TEA, 25 kV. (a) Straight-edge capillary; (b) slanted-end capillary.

peak evident in Fig. 4a is not observed in Fig. 4b due to the additional broadening effect of the slanted edge.

The peak-shape dependency on capillary edge geometry was examined by us with several different running buffers, with several different additives (used for electroosmotic flow control) and with several solutes (both small and large). Results similar to those observed above were obtained with all systems which we studied.

Our results indicate that the physical shape of the capillary end does influence the efficiency of the separation. Undoubtedly, the capillary edge affects the size of the injected sample plug. Fig. 6a shows, in a schematic manner, the shape of a sample plug obtained from a straight-edge capillary. The contribution of that sample zone to the overall peak variance is [11]:

$$\sigma_{inj}^2 = \frac{l^2}{12} \quad (1)$$

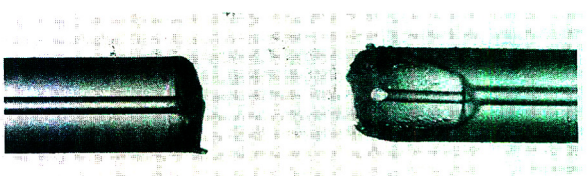

Fig. 5. The capillary with which the electrophoresis of myoglobin was done. Shown are the straight edge on the left and the slanted edge on the right.

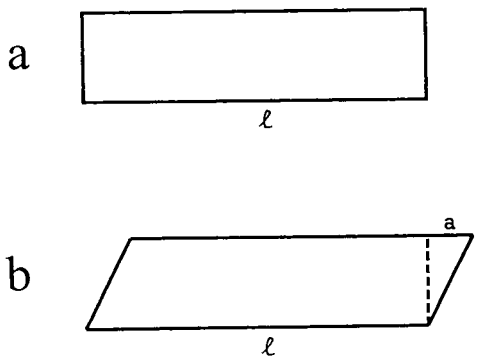

Fig. 6. Schematic representation of the injected plug. (a) Plug resulting from a straight-edge capillary; (b) plug resulting from a slanted-edge capillary.

σ^2_{inj} is the plug variance and l is the plug length. Fig. 6b represents the injected zone shape resulting from a slanted edge. The contribution here to the peak variance is:

$$\sigma^2_{inj(slant)} = \frac{1}{12} \cdot (l^2 + a^2) \quad (2)$$

where a is the extra length in the injection zone (Fig. 6b). Therefore, the increase in the size of the injected plug due to the slanted edge of the capillary is $a^2/12$.

The length of the parameter a depends on the angle of the slant. Simple trigonometric calculation shows that, for a 50 μm I.D. capillary, parameter a is 87, 50 and 29 μm for a slant angle of 30, 45 and 60°, respectively. In a straight-edge capillary, a typical size of the injected zone is about 350 μm. Thus, according to Eq. 2, the variance of the injected plug will increase only by about 10% for the most unfavorable slant angle of 30°. That modest increase in the variance of the injected sample does not explain the large decrease in efficiency that is observed in practice. If we assume that, due to diffusion, the injected zone will revert quickly to a plug shape having the length of $l + a$, the increase in the injected zone variance is still not sufficient to explain the large decrease in the observed efficiency.

Even with the straight-edge capillary, the plate height values are smaller than theoretically expected, based on estimated diffusion coefficient values of the solutes. For example, based on its size, the diffusion coefficient of myoglobin is estimated to be about $1 \cdot 10^{-6}$ cm^2/s [12]. Hence, the plate height for conditions similar to those in Fig. 4 should be around 0.12 μm. In practice we obtained 1.9 μm with a straight-edge capillary. With phenol as solute, the theoretical H value, for the conditions of Fig. 3, are around 1.2 μm as opposed to an observed value of 2.4 μm with a straight-edge capillary. Thus, in addition to molecular diffusion, there are other processes that add to the width of the solute zone. Still, even though the observed efficiency is lower than the prediction, the effect of the shape of the injection end of the capillary is most pronounced.

As discussed before, the increase in the size of the injected zone is not sufficient to explain the profound effect of the capillary edge shape. Other causes must be responsible for the large decrease in efficiency. The exact nature of these causes is not clear to us at the present stage. We do not feel that the decrease in efficiency can be explained by interfacial pressure difference, which seems to control sample penetration in CE [7]. Undoubtedly, the slanted edge causes a current density difference between the capillary inlet and outlet. This gradient in current density can effect electroosmotic and electrophoretic mobilities. A gradient in electroosmosis can in turn cause excessive zone broadening. In addition, because part of the capillary in the slanted inlet is not bound by a wall (as is the case in the actual capillary after the injection edge) the electroosmosis flow profile may be greatly distorted, as bulk liquid from the reservoir is trying to enter the capillary. This distortion in the electroosmosis will also have deleterious effects on the efficiency and on peak shape.

The exact mechanism by which the zone broadens due to slanted capillary inlet is yet to be found. However, the effect is real as judged from its observed reproducibility: relative standard deviation of $<1\%$ in migration times and $<2\%$ in H values. It is clear that more careful attention must be given to the exact shape of the capillary inlet. A straight-edge capillary inlet is

essential for high efficiencies in CE separations as well as for more symmetrical peaks.

Acknowledgements

We wish to thank Dr. Gil Shoham and Ms. Hadar Feinberg for their help photographing the capillaries. This research was supported by grant No. 88-00021 from the United States–Israel Binational Science Foundation (BSF), Jerusalem, Israel.

References

[1] S. Terabe, K. Otsuka and T. Ando, *Anal. Chem.*, 61 (1989) 251.
[2] X. Huang, W.F. Coleman and R.N. Zare, *J. Chromatogr.*, 480 (1989) 95.
[3] D.E. Burton, M.J. Sepaniak and M.P. Maskarinec, *Chromatographia*, 21 (1986) 583.
[4] D.J. Rose and J.W. Jorgenson, *Anal. Chem.*, 60 (1988) 642.
[5] E. Grushka and R.M. McCormick, *J. Chromatogr.*, 471 (1989) 421.
[6] H.E. Schwartz, M. Mellera and R.G. Brownlee, *J. Chromatogr.*, 480 (1989) 129.
[7] H.A. Fishman, N.M. Amudi, T.T Lee, R.H. Scheller and R.N. Zare, *Anal. Chem.*, 66 (1994) 2318.
[8] J.A. Lux, H.F. Yin and G. Schomburg, *Chromatographia*, 30 (1990) 7.
[9] E.V. Dose and G. Guiochon, *Anal. Chem.*, 64 (1992) 123.
[10] N. Cohen and E. Grushka, *J. Chromatogr. A*, 678 (1994) 167.
[11] J.C. Sternberg, *Adv. Chromatogr.*, 2 (1966) 205.
[12] D. Freifelder, *Physical Biochemistry*, W.H. Freeman, San Francisco, CA, 2nd ed., 1982.

ELSEVIER

Journal of Chromatography A, 684 (1994) 329–341

JOURNAL OF CHROMATOGRAPHY A

Influence of additives on resolution and focusing efficiency in free-flow isoelectric focusing

Gerhard Küllertz*, Gunter Fischer

Max-Planck-Gesellschaft zur Förderung der Wissenschaften eV, Arbeitsgruppe "Enzymologie der Peptidbindung", Weinbergweg 16a, 06120 Halle/Saale, Germany

First received 6 April 1994; revised manuscript received 28 June 1994

Abstract

In theory, the resolution of isoelectric focusing (IEF) depends directly on the electric field strength. However, at higher electric field strengths with free-flow IEF, focusing of proteins is impaired by electrodispersive effects. These effects cause a widening of protein peaks sharply focused at lower voltage. This was dependent on the electric field strength and thus reduced the focusing efficiency and resolution. Using 4-nitroaniline as a visible marker substance, the influence of concentration and molecular mass of various additives on the electrodispersive effects as a function of electric field strength was investigated. The efficiency to reduce electrodispersive effects was determined by various properties of the additives. However, the molecular mass of the additives only marginally influenced electrodispersive effects. In the most favourable case, the resolution R for the separation of bovine serum albumin and haemoglobin applied as a standard mixture increased from $R = 0.4$ without additive to $R = 3.4$ with 2% saccharose and 0.3% Servalyte 3–10 as ampholyte. Improvements in the resolution for the separation for the standard mixture were independent of the ampholyte used (Bio-Lyte, Ampholine, Servalyte).

1. Introduction

Isoelectric focusing (IEF) is a kind of electrophoresis performed in a pH gradient where amphoteric molecules are separated according to their individual isoelectric points (pI). This isoelectric pH value is a characteristic physicochemical property of each protein and is affected by the overall composition of the protein and the properties of the medium. The history of IEF is relatively short and dates back to the early 1960s [1,2].

Four techniques are useful for laboratory-scale preparative electrofocusing: (1) IEF in order on granular beds [3], (2) IEF in order on a separation chamber that is divided into compartments [4,5], (3) a recycling isoelectric focusing method [6,7] and (4) a continuous free-flow isoelectric focusing method [8].

IEF is a technique allowing enrichment of zwitterionic molecules with respect to their spatial pH distribution depending on a uniform d.c. voltage. The production of this stationary, steady-state sample distribution is time consuming because the electrophoretic velocity tends towards zero when the migration of the proteins in the pH gradient carries them towards their pI. The steady state is established where the electrokinetic transport of protein into the focusing zone is exactly balanced by the diffusion out of

* Corresponding author.

0021-9673/94/$07.00
SSDI 0021-9673(94)00599-0

this zone. For IEF in a column, experimental times of at least 18–24 h [9] and, in membrane-defined subcompartments [4,5], focusing times of 1.5–5 h are usually satisfactory. Free-flow IEF apparatus requires a transition time of about 3 h using a recycling system [10] and less than 20 min [8] as a continuous device.

The differential equation describing the equilibrium between the electrophoretic and diffusional mass transport was derived by Svensson [2]:

$$\frac{dC_i}{dx} = \frac{C_i \mu_i E}{D} \quad (1)$$

where C_i is the concentration of component i, μ_i is its mobility, E is the electric field strength, D is the diffusion coefficient of the solution and dC_i/dx is the concentration gradient. This equation shows that both increasing the mobility and electric field strength and reducing the diffusion will lead to an increase in the narrowing of the focusing zone. Because the viscosity of the solution has an opposite influence on the diffusion and the mobility of proteins, it is difficult to predict the effect of the viscosity on the focusing process.

In addition, the focusing of proteins will be affected by electrodispersive effects (EDE) depending on the electric field strength. Such effects can be seen as a broadening of otherwise sharply focused protein peaks depending on the electric field strength [8,10]. To manipulate the EDE with additives, extensive experiments have been carried out on capillary electrophoresis [11]. Based on these data, we determined the influence of different transport phenomena on the sample dispersion in continuous free-flow IEF to improve the resolution of this method.

2. Experimental

2.1. Standards for calibration of native IEF

Haemoglobin (human; pI = 7.0) was obtained from Boehringer (Mannheim, Germany). Bovine serum albumin (pI = 5.2), ovalbumin (chicken egg albumin; pI = 4.6) and 4-nitroaniline (pK_a = 1.3) were obtained from Sigma (Deisenhofen, Germany).

2.2. Solutions for IEF

Solutions of Servalyte (Serva, Heidelberg, Germany), pH range 3–10, 4–7, 4–5 or 5–8, solutions of Ampholine (Pharmacia, Uppsala, Sweden), pH range 5–8, and solutions of Bio-Lyte (Bio-Rad, Hercules, CA, USA), pH range 5–8 with concentrations of 0.1–0.4% (w/v), were prepared with deionized (Milli-Q Plus; Millipore, Eschborn, Germany) and CO_2-free water. The catholyte was 0.05 M sodium hydroxide and the anolyte was 0.5 M orthophosphoric acid. Both solutions were used as membrane rinse solutions at their appropriate position.

2.3. Additives to manipulate the focusing efficiency

Different concentrations of the following additives were used to manipulate the focusing efficiency and resolution: glycerol from Roth (Karlsruhe, Germany), polyethylene glycol (PEG) with a molecular mass of 10^6 (PEG 1-kDa) from Merck–Schuchardt (Hohenbrunn, Germany), PEG of molecular mass $6 \cdot 10^3$ (PEG 600-kDa) from Serva, saccharose, sorbose and polyvinylpyrrolidone (PVP) with a molecular mass of $3.6 \cdot 10^5$ (PVP 360-kDa) from Serva, PVP with a molecular mass of $2.5 \cdot 10^4$ (PVP 25-kDa) from Merck (Darmstadt, Germany), hydroxypropylmethylcellulose (HPMC) from Aldrich (Milwaukee, WI, USA) and dextrans with average molecular masses of 1000, $4 \cdot 10^4$, $7 \cdot 10^4$, $11 \cdot 10^4$ and $5 \cdot 10^5$ from Pfeifer & Langen Pharma (Dormagen, Germany).

2.4. Instruments

The principle of the preparative continuous isoelectrofocusing apparatus (Dr. Weber, Ismaning, Germany) and the equipment belonging to it and used here were described in detail previously [8].

The specific conductivity of solutions was determined in a conductivity cell with a cell con-

stant of 0.998 cm^{-1} connected to a Type LF530 precision conductivity meter (Wissenschaftliche-Technische Werkstätten, Weilheim, Germany).

Spectrophotometric measurements were carried out with a Type MR7000 microtitre plate reader (Dynatech, Chantilly, VA, USA).

The ionization data were calculated from titration curves according to Cohn et al. [12]. Titration curves were taken with a Type VIT90-video titrator (Radiometer, Copenhagen, Denmark).

2.5. Determination of protein, dextran and 4-nitroaniline concentrations

Protein concentrations were determined by the Bradford procedure [13] using bovine serum albumin as a standard at 625 nm. Dextran concentrations were confirmed with an anthrone method at 625 nm and dextran as standard [14]. 4-Nitroaniline concentration was measured utilizing the Lambert–Beer law at 390 nm (ε = 11 400 l mol^{-1} cm^{-1}).

2.6. Resolution and focusing efficiency

A method for specifying resolution (R) in IEF is in terms of the peak distance (Δx) in cm (Fig. 1), fraction numbers or pH values of the peak maximum of adjacent peaks. If the two detected peaks (a and b) have a symmetrical shape and Gaussian profiles with a baseline peak width of 4σ, the following equation will be used for the calculation of resolution in IEF experiments:

$$R = |\Delta x|/2(\sigma_a + \sigma_b) \quad (2)$$

The peak width (Fig. 1) at the peak half-height ($w_{1/2}$) is about 2.35σ for symmetrical peaks. Therefore, for practical purposes the focusing resolution of two symmetrical peaks can be defined as

$$R = |\Delta x|/0.85(w_{1/2a} + w_{1/2b}) \quad (3)$$

Peaks recorded in IEF are not always Gaussian. In a number of cases, especially with non-linear pH gradients, the bands are asymmetric. The resolution of such peaks was calculated using the equation

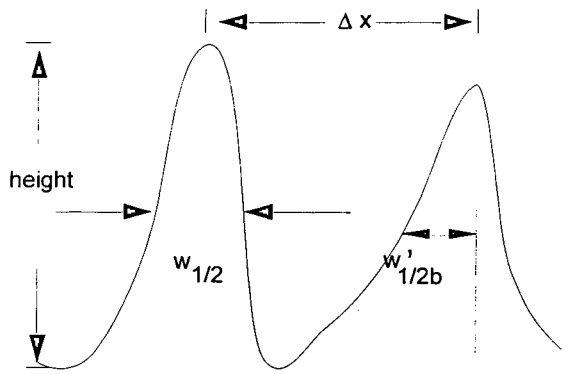

Fig. 1. Schematic representation of two peaks in IEF to characterize separation parameters: $w_{1/2}$ = peak width at half-height; $w'_{1/2}$ = segment of the baseline $w_{1/2}$ as intersection with the vertical from the peak maximum and $w_{1/2}$; Δx = distance in cm, fraction numbers or pH values of the peak maximum between adjacent peaks.

$$R = |\Delta x|/1.71(w'_{1/2a} + w'_{1/2b}) \quad (4)$$

The segment of the baseline $w'_{1/2}$ (Fig. 1) is defined by its intersection with the vertical from the peak maximum and $w_{1/2}$. For the calculation of R, two adjacent segments ($w'_{1/2a} + w'_{1/2b}$) of non-Gaussian peaks were used. For a quantitative description of the focusing efficiency (F_{eff}) of a single protein peak, we used the equation

$$F_{eff} = 1/\sigma^2 \quad (5)$$

or for practical purposes

$$F_{eff} = 5.54(1/\Delta pH_{1/2})^2 \quad (6)$$

where $\Delta pH_{1/2}$ is the pH difference of $w_{1/2}$ [8]. Because non-linear pH gradients intrinsically distort the Gaussian form of protein peaks, non-linear pH gradients were corrected by computational interconversion to a linear form before F_{eff} was calculated [8].

2.7. Determination of the apparent diffusion coefficient

The diffusion coefficient (D) of proteins was determined using the Gaussian spreading by

diffusion processes of the respective protein in the IEF separation chamber in the absence of an electric field. Based on Einstein's equation ($\sigma^2 = 2Dt$) we calculated D using the equation

$$D = \frac{(\Delta w_{1/2})^2}{3.07\Delta t} \quad (7)$$

where $\Delta w_{1/2}$ is the difference in the peak half-width at different transit times (Δt) of the sample.

3. Results and discussion

3.1. Influence of electrodispersive effects on focusing efficiency (F_{eff})

The negative influence of electrodispersive effects (EDE) on the resolution in IEF has been described by several workers [10,11,15,16] based on investigations with different electrophoretic devices. Fawcett [15] and others have explored the use of free-flow electrophoretic instruments for isoelectric focusing, but the results were described as "rather disappointing". Increasing the voltage resulted in "feathering", a breakdown of the flow lanes into feather-like structures.

Using colored marker substances such as haemoglobin, the line shape of these focused substances can be observed visually in the separation chamber. In contrast to the optimum electric field strength, at higher voltages broadening of substance distribution occurs [8]. The influence of a stepwise increase in electric field strength (from 50 to 200 V/cm^{-1}) on the F_{eff} of human haemoglobin is shown in Fig. 2. Between 100 and 110 V/cm^{-1} an optimum F_{eff} was detected whereas at higher electric field strengths F_{eff} decreased drastically. This optimum is caused by the concerted action of processes that mainly consist of electrophoresis, electroosmosis, streaming potential and sedimentation potential [17]. The total variance σ_T^2 ($\sigma_T^2 = 1/F_{eff}$) of these effects results from the sum of the contributing variances:

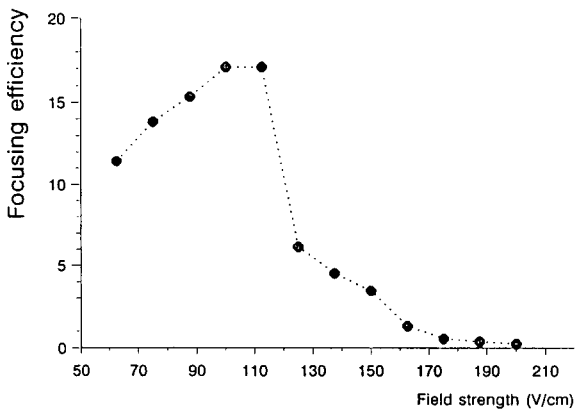

Fig. 2. F_{eff} of human haemoglobin as a function of the electric field strength in IEF. Experimental conditions of IEF: temperature of chamber, 4°C; medium, 0.3% (v/v) Servalyte 3–10/4% (w/v) glycerol; transit time, 8 min.

$$\sigma_T^2 = \sigma_{dif}^2 + \sigma_{conv}^2 + \sigma_{ads}^2 + \sigma_{eld}^2 + \sigma_{oth}^2 \quad (8)$$

where the subscripts refer to diffusion, convection by temperature gradients, adsorption on the walls of the electrophoresis chamber, electrodispersion and other effects, respectively. Electrodispersive effects can be caused by the potential gradient of the electric field in IEF (σ_{ief}^2), by conductivity gradients (σ_{cond}^2) and by the electroosmotic potential (σ_{eos}^2).

In relation to the electric field we can classify the variances into three groups. There are variances that are mainly independent of field strength (σ_{dif}^2 and σ_{ads}^2) and also variances that increase with increasing electric field strength (σ_{conv}^2, σ_{cond}^2 and σ_{eos}^2) and that will decrease with the electric field strength (σ_{ief}^2). The dependence of F_{eff} on the electric field strength in Fig. 2 is the overall result of these effects.

In order to measure exclusively electrokinetic phenomena, uncharged marker molecules may be helpful. Their migrations depend only on the passive transport by the focusing medium. Therefore, we investigated the effect of EDE using 4-nitroaniline as indicator substance. With a pK_a value of approximately 1.3 [18] this substance occurs uncharged in a solution with a

pH gradient of 3–10 and also at the starting pH of the separation medium (ca. 6.5). The 4-nitroaniline solution was introduced as a narrow stream in the middle of the bottom of the electrophoresis chamber. The widening of the 4-nitroaniline lane after applying an electric voltage was evaluated as a measure of EDE.

At a field strength above 120 V cm^{-1} there was a sharp decline for the F_{eff} of haemoglobin (Fig. 2). Concomitantly, an increase in the peak width at half-height of 4-nitroaniline (Fig. 3) occurred. In addition, a non-linear change of the electrical resistance as a result of increasing electric field strength enhances the value of EDE (Fig. 3). According to Ohm's law, the plot of the applied field strength versus the resulting current should be linear. Deviations from linearity described for capillary zone electrophoresis probably arise from enhanced heat generation at higher potential differences [19]. However, temperature measurements (standard error ca. 0.1°C) in the 96-channel outlet port during IEF showed no significant temperature drift depending on the electric field strength.

The peak broadening of the 4-nitroaniline concentration is directed to both electrodes. The drift to the anodic side is half as much as the drift to the cathode (Fig. 3). A similar effect can

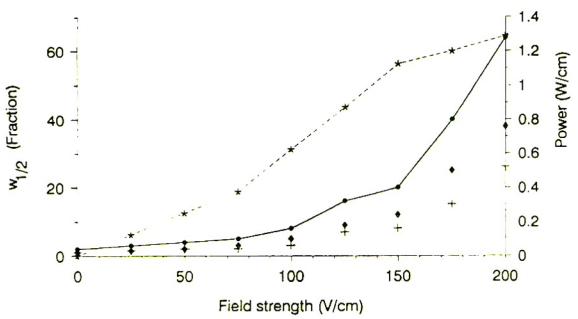

Fig. 3. Influence of the electric field strength on electric power and $w_{1/2}$ of a saturated 4-nitroaniline solution. Experimental conditions of IEF: temperature of chamber, 5°C; medium, 0.2% (v/v) Servalyte 3–10/3% (w/v) glycerol; transit time, 8 min. ● = Peak width at half-height; * = power (W cm^{-1}); + = $w'_{1/2}$ towards the anode; ◆ = $w'_{1/2}$ towards the cathode.

be obtained by investigating the EOF in recycling free-flow IEF [10].

3.2. *Influence of additives on electroosmotic flow (EOF)*

To control electroosmotic flow, surface modification has been used to manipulate the EOF in capillary zone electrophoresis [11,20]. It was shown that simple manipulation of the ionic composition of the buffer can reduce the EOF by decreasing the double-layer thickness [21]. The flow-rate in capillary zone electrophoresis was found to be inversely proportional to ionic strength [11]. The addition of organic solvents can dramatically influence the electroosmotic flow [11]. However, salts and organic solvents as additives may not be suitable for the separation of native proteins with IEF, because organic solvents lead to the formation of protein aggregates. On the other hand, ionic substances increase the conductivity of the focusing solution and may reduce the resolution by enhanced thermal convection.

It was recently established that the addition of amphiphilic copolymers or oligomers that contain both hydrophobic and hydrophilic groups can efficiently control the IEF in capillary electrophoresis [11,20]. These investigations also suggest [20] that the degree of reduction in EOF is proportional to the size of the hydrophilic portion of the surfactant. In a capillary the EOF could be adjusted to any desired value by adsorbing surfactants and polymers of various size on the capillary wall.

By adding to the flow solution one of the surfactants or polymers glycerol, sorbose, saccharose, polyvinylpyrrolidone (PVP), hydroxypropylmethylcellulose (HPMC), polyethylene glycol (PEG) and dextran, the influence on the resolution and focusing efficiency was tested with preparative continuous IEF. Coatings of the chamber walls were applied by passing about 50 chamber volumes of surfactant solution through the focusing chamber. Subsequent separations were carried out using ampholyte solutions containing the same concentration of surfactant.

Additives can have different effects on IEF. First, they modulate the EOF and reduce the adsorption of samples in the separation chamber. Second, an increase in the viscosity and/or density of the focusing solution is obtained. Hence impaired mobility of charged substances in an electric field may result. Because free-flow IEF has a limited focusing time, such reduced mobility may result in a poor pH gradient. The quality of the pH gradient in the IEF equipment used can be evaluated after measurement of the pH in each of the 96 fractions, which are continuously produced by the sample outlet connector [8]. With Servalyte 3–10 as ampholyte and sufficient time to create a linear pH gradient at an optimum electric field strength, a pH difference between fraction 20 (ca. pH 4) and fraction 76 (ca. pH 9) of about 5 pH units can be expected.

Fig. 4 shows that the quality of the pH gradient, expressed as $\Delta pH_{20/76}$ (pH difference between fractions 20 and 76), becomes worse if the concentration of glycerol is increased from 1 to 30% (w/v). In parallel, the value of $w_{1/2}$ of 4-nitroaniline as EDE marker substance is decreased. Increasing the electric field strength from 125 to 200 V cm^{-1} exerts an opposite effect on both EDE and the quality of the pH gradient (Fig. 4).

Additives that provide both an excellent pH gradient and a small EDE are 1% (w/v) PVP (10-kDa), 0.002% (w/v) HPMC, 2% (w/v) saccharose, 0.1% (w/v) dextran (1-kDa) and PEG. Other substances such as glycerol, sorbose, 2% (w/v) PVP (10-kDa), PVP (360-kDa) and dextran with a molecular mass of $4 \cdot 10^4$ and higher are apparently less suitable. Adsorption of polymers on surfaces is described as a loop-and-train mechanism [20]. As the molecular mass of the additives increases, the adsorbed coating becomes thicker and more viscous. In agreement with this finding, EOF was inversely related to the molecular mass of the coating polymer in capillary isoelectric focusing [20]. In our experiments however, we found that $w_{1/2}$ does not depend exclusively on molecular mass of the coating polymer. Whereas PVP and PEG decreased the EDE with increasing molecular mass, six different dextrans with molecular masses from 1000 to $5 \cdot 10^5$ did not show this size effect.

As can be seen in Fig. 4, large differences of EDE in IEF are achieved almost exclusively by a different chemical structure and are only margi-

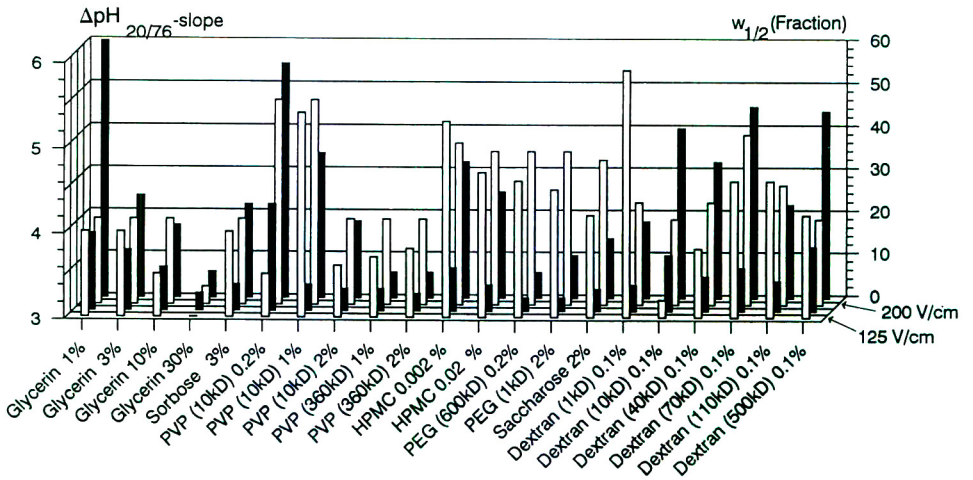

Fig. 4. Influence of additives on the peak width at half-height of a saturated 4-nitroaniline solution and the pH slope between fractions 20 and 76 ($\Delta pH_{20/76}$) as a function of electric field strength. Experimental conditions of IEF: temperature of chamber, 5°C; medium, 0.4% (v/v) Servalyte 3–10; transit time, 10 min. □ = Peak width at half-height; ■ = $\Delta pH_{20/76}$ slope.

Table 1
Isoelectric points and charges

Protein, amino acid or polypeptide	p*I*	Net charge (proton units)		Charge/radius coefficients at different pH[b] (proton units/cm)
		±0.3	±1.0	−0.4 0 0.4 0.8 1.2 1.6
Bovine serum albumin	5.7	9	39	
Bovine serum albumin[a]	4.8	6	41	
Human serum albumin	5.9	9	33	
Human haemoglobin[a]	7.0	4.5	23	
Ovalbumin	5.3	7.5	30	
Asparagine (D)	3.6	0.55	1.5	
NH_2-D_2-COOH	3.4	0.76	2.0	
NH_2-D_3-COOH	3.3	0.88	2.7	
NH_2-D_4-COOH	3.2	0.97	3.2	
NH_2-D_5-COOH	3.1	1.0	3.5	
NH_2-D_{10}-COOH	2.9	1.2	4.9	
Arginine (R)	10.1	0.04	0.2	
NH_2-R_2-COOH	12.0	0.70	1.6	
NH_2-R_3-COOH	12.3	0.90	2.2	
NH_2-R_4-COOH	12.5	1.02	2.9	
NH_2-R_5-COOH	12.6	1.11	3.4	
NH_2-R_{10}-COOH	13.0	1.7	4.8	

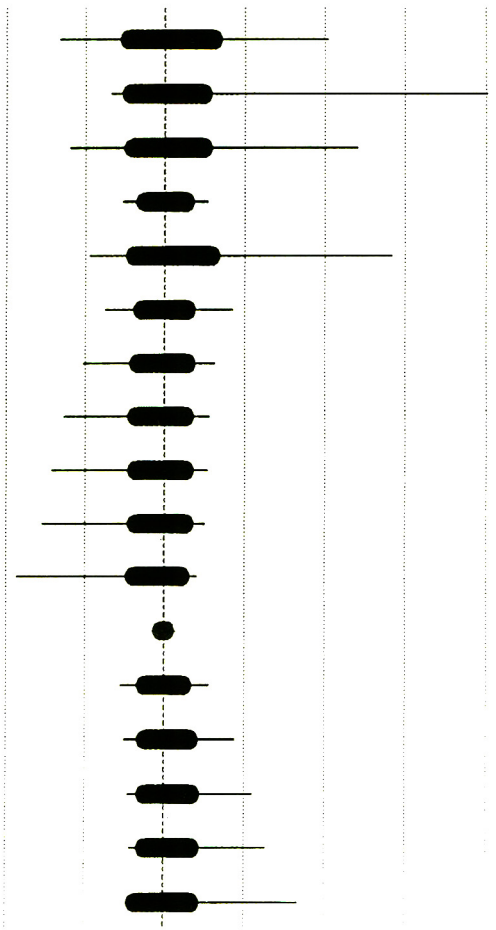

Sequences were taken from Protein Identification-Resource (PIR), the international association of protein sequence banks. The isoelectric points and net charge differences were calculated according to Ref. [25]. Partial specific radii of proteins or peptides were calculated from the amino acid composition according to the volumes of the constituent amino acids [26]. Ionization data were calculated from titration curves and are in accordance with values for haemoglobin [12][a] and ionization data for bovine serum albumin [24][a] or values were calculated from the amino acid sequence of proteins in a range of 0.3 and 1 pH units around the p*I* (calculated or determined by IEF [b]) of selected proteins, peptides and amino acids and their charge/radius coefficients at this pH.

nally influenced by the molecular mass of polymers with a homologous structure. Earlier data [8] showed that EDE can be reduced by adding zwitterionic substances which exhibit very flat titration curves around their p*I* values (Table 1), e.g., N,N-bis(2-hydroxyethyl)glycine (bicine). The influence of increasing concentrations of bicine on the EDE is shown in Fig. 5. Higher concentrations of bicine clearly reduced the EDE. In comparison with monoionic additives, zwitterionic substances strongly affect the shape of the pH gradient [8]. Therefore, the application of these compounds will be limited to special separation problems in IEF.

3.3. Mobility of proteins in free-flow IEF

It is assumed that proteins require a longer time for focusing than ampholytes. Therefore, it was predicted that continuous-flow systems cannot be applied to IEF since the method lacks the long residence times required for protein focusing [10]. To test this prediction, we investigated the relationship between the transition time, R and F_{eff}. We investigated the separation of a sample containing bovine serum albumin and haemoglobin in IEF by stepwise changing the transition time. The results are summarized in Fig. 6. A transition time of 5–7 min at 150 V cm^{-1} gave a favourable resolution, whereas a significant deterioration below 5 min and a minor deterioration above 7 min were observed.

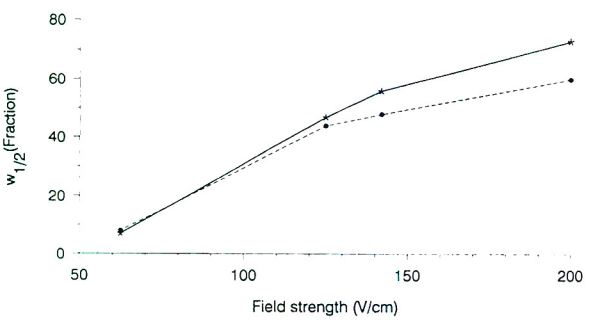

Fig. 5. Influence of bicine on the peak width at half-height of a saturated 4-nitroaniline solution as a function of electric voltage. Experimental conditions of IEF: temperature of chamber, 5°C; medium, 0.2% (v/v) Servalyte 3–10/4% (w/v) glycerol. ● = Peak width at half-height with 1% (w/v) bicine; ∗ = peak width at half-height without bicine.

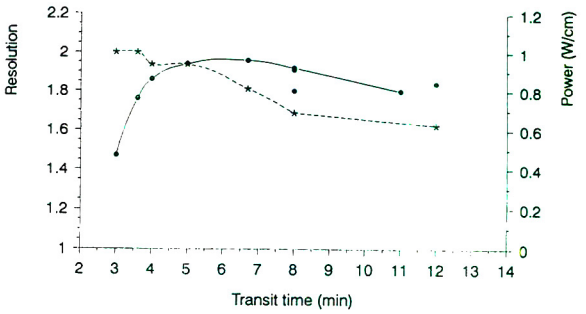

Fig. 6. Influence of transit time at a constant electric field strength on power and the peak resolution of bovine haemoglobin and bovine serum albumin. Experimental conditions: temperature of chamber, 5°C; medium, 0.2% (v/v) Servalyte 3–10/0.1% dextran 110-kDa; conductivity, 8.4 μS; electric field strength, 175 V cm^{-1}; sample solution, 1 mg ml^{-1} haemoglobin and 1 mg ml^{-1} bovine serum albumin in medium. ● = Resolution; ∗ = power (W cm^{-1}).

The short focusing times of these proteins can be explained in terms of the electric mobility of molecules that bear a relatively high net charge around their p*I* values. In detail, the electrophoretic mobility of proteins depends on the mobility slope ($d\mu/dpH$). A high value of this term results from the presence of many amino acids with dissociable groups having pK_a values close to the p*I* of the protein. Reasonable approximations can be obtained by calculation of net charge depending on the pH from the amino acid composition [22,23]. To estimate the mobility slope ($d\mu/dpH$) of different polypeptides, we calculated the net charge within 0.3 and 1.0 pH units around the p*I* value (Table 1) based on the amino acid sequence according to Ref. [25], and/or calculated the net charges from titration curves according to Ref. [12]. As expected, the net charge of the investigated proteins is higher than that of the investigated small zwitterionic substances. To calculate the electrophoretic mobilities (μ) we utilized the equation [27]

$$\mu = \frac{Q}{6\pi\eta a} \tag{9}$$

where Q is the effective charge of the ion, η the viscosity of the solution and $2\pi a$ the hydrodynamic circumference of the ion. Using the

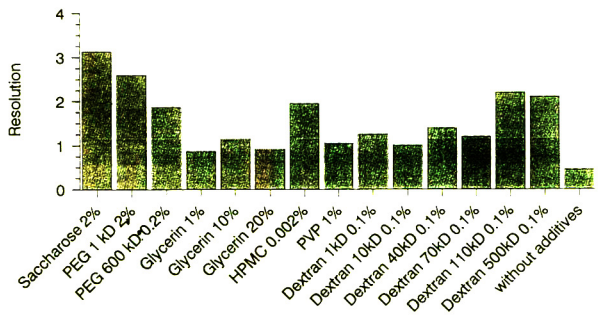

Fig. 7. Influence of additives on the resolution of a sample containing haemoglobin and bovine serum albumin. Experimental conditions: temperature of chamber, 4°C; medium, 0.2% Servalyte 3–10; sample solution, 1 mg ml^{-1} haemoglobin and 1 mg ml^{-1} bovine serum albumin in medium; electric field strength, 175 V cm^{-1}; transit time, 8 min. Concentrations of additives in % (w/v).

partial specific volumes of the constituent amino acids [26], the circumferences of proteins can be calculated. Commercial carrier ampholytes are mixed polymers of aliphatic amino and carboxylic acids of molecular mass ca. 300–1000 [16,28,29]. To calculate the magnitude of the differences between the electrophoretic mobilities of proteins and of carrier ampholytes we calculated the ratio of charge to radius (a) for proteins and polypeptides as a function of the pI of such molecules (Table 1). In contrast to electrophoretic methods in gels, where proteins are subject to sieving effects, in free solution the investigated proteins can migrate in an electrical field with velocities comparable to or even faster than those of small molecules.

3.4. *Influence of additives on resolution (R) of proteins*

To investigate the influence of various additives on the separation of proteins in free-flow IEF, we used a mixture of two proteins with different isoelectric points. Both proteins, human haemoglobin with a pI of ca. 7 and bovine serum albumin with a pI of ca. 5.2, were separated with a resolution of 0.8–3 depending on the nature and concentration of the additive. In contrast to the investigations with 4-nitroaniline as marker substance, a direct correlation between the molecular mass of the additives and

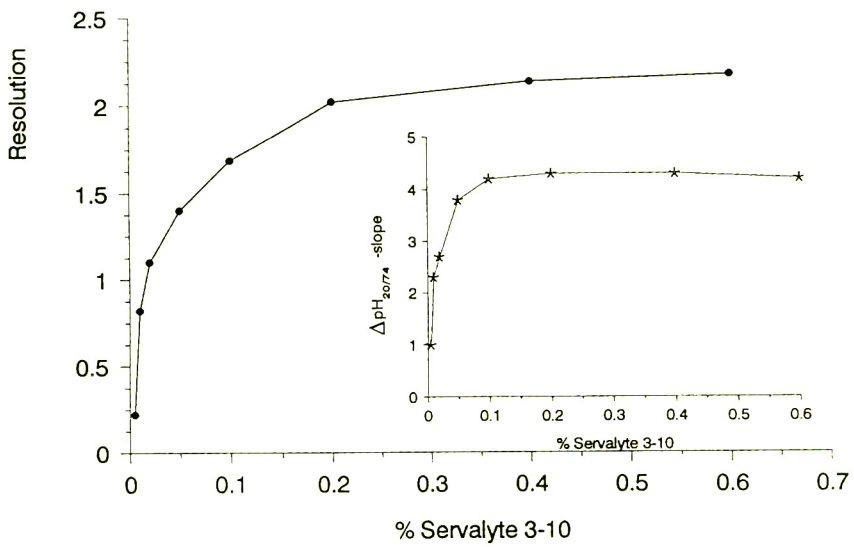

Fig. 8. Influence of ampholyte concentration on the resolution of a sample containing haemoglobin and bovine serum albumin and influence on the pH slope between fractions 20 and 76 ($\Delta pH_{20/76}$). Experimental conditions: temperature of chamber, 5°C; medium, 0.1% (w/v) dextran 110-kDa; sample solution, 1 mg ml^{-1} haemoglobin and 1 mg ml^{-1} albumin in medium; electric field strength, 200 V cm^{-1}; transit time, 9 min. ● = Resolution; ∗ = pH slope ($\Delta pH_{20,76}$).

R was observed (Fig. 7). An improved separation of proteins by raising the molecular mass of the additives was also found in investigations with capillary isoelectric focusing [20]. It was suggested from the experiments that the EOF is influenced by additives [20]. In our investigations on 4-nitroaniline there is an obvious lack of evidence for a correlation of EOF with the molecular mass of additives. We conclude that there is a concerted action between electroosmotic effects and effects on the diffusion of the proteins by changes in the viscosity and density of the solution. However, less than a twofold change in EOF was achieved by varying the molecular mass of the polymer ranging from 1000 up to $5 \cdot 10^5$.

3.5. Effect of ampholyte concentration on resolution

An increase in the ampholyte concentration from 0 to 0.6% Servalyte 3–10 improved the resolution from 0 to about 2 for the separation of a sample containing human haemoglobin and bovine serum albumin (Fig. 8). There was no further substantial improvement in resolution when the ampholyte concentration became higher than 0.3%. The data in the inset in Fig. 8 show that a maximum pH slope is achieved even at a Servalyte concentration of 0.3%. Therefore, we suggest that a maximum pH slope should be applied for high resolution.

3.6. Effect of small ions on resolution

In contrast to zwitterionic substances, which focus at their intrinsic pI and have only a limited contribution to the current flux, unipolar ions will be transported in the direction of the counter-charged electrodes. Heat development, generated by passage of electric current, renders problems as it can cause non-uniform temperature gradients, local changes in viscosity and subsequent zone broadening [30]. Independent of this thermal convection, small ions affect the diffusion of large molecules. The small counter ions of proteins diffuse more rapidly than the oppositely charged macromolecules and increase the diffusion rate of the macroion [17]. Both an increase in thermal convection during IEF and an increase in diffusion at higher conductivity deteriorate R and F_{eff}. Our investigations (Fig. 9) shows that the resolution of the standard mixture containing haemoglobin and bovine serum albumin decreases with increasing conductivity. This is in agreement with experiments on IEF in gels. In the gel IEF method high salt concentrations cause band broadening [16].

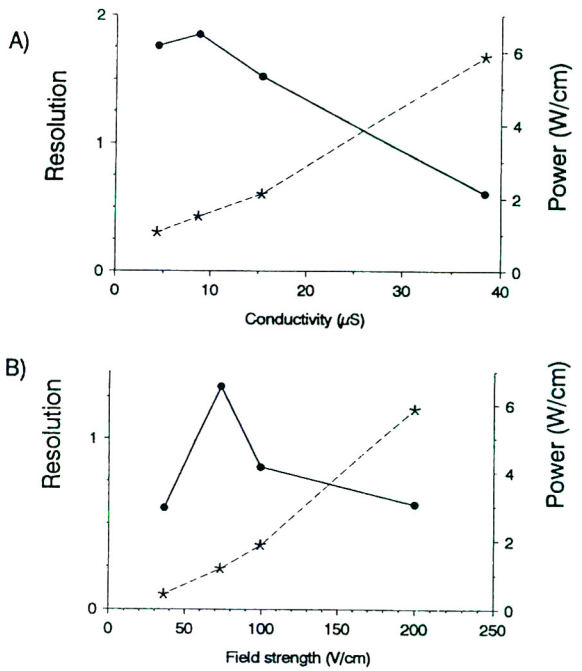

Fig. 9. (A) Effect of conductivity of the medium on the resolution of a sample containing haemoglobin and bovine serum albumin at an electric field strength of 200 V cm^{-1}. (B) Dependence of the resolution on the electric field strength (conductivity = 38.6 μS). Experimental conditions: temperature of chamber, 5°C; medium, 0.1% (w/v) dextran 110-kDa–0.2% (v/v) Servalyte 3–10 enriched with various amounts of sodium chloride; sample solution, 1 mg ml^{-1} haemoglobin and 1 mg ml^{-1} bovine serum albumin in medium; transit time, 9 min. ● = Resolution; ∗ = power (W cm^{-1}).

3.7. Effect of different pH gradients on resolution

The resolution in IEF with respect to pI differences of focused proteins in IEF is given by [31,32]

$$\Delta pI = K\left[\frac{D(\mathrm{dpH/d}x)}{E(-\mathrm{d}\mu/\mathrm{dpH})}\right]^{0.5} \quad (10)$$

where K is the mean zone width (usually 4σ), D is the diffusion constant, E is the electric field strength, $\mathrm{d}\mu/\mathrm{dpH}$ is the mobility slope at the pI that depends on the charge of the protein around its pI value (Table 1) and $\mathrm{dpH/d}x$ is the pH gradient at this zone. As described by Eq. 10, high resolution should be obtained with a shallow profile of pH change. To check this relationship between R and the pH gradient in the continuous free-flow IEF, investigations on R and F_{eff} as a function of four different pH gradients produced with Servalyte 3–10, 5–8, 4–5 and 4–7 using a mixture of three different

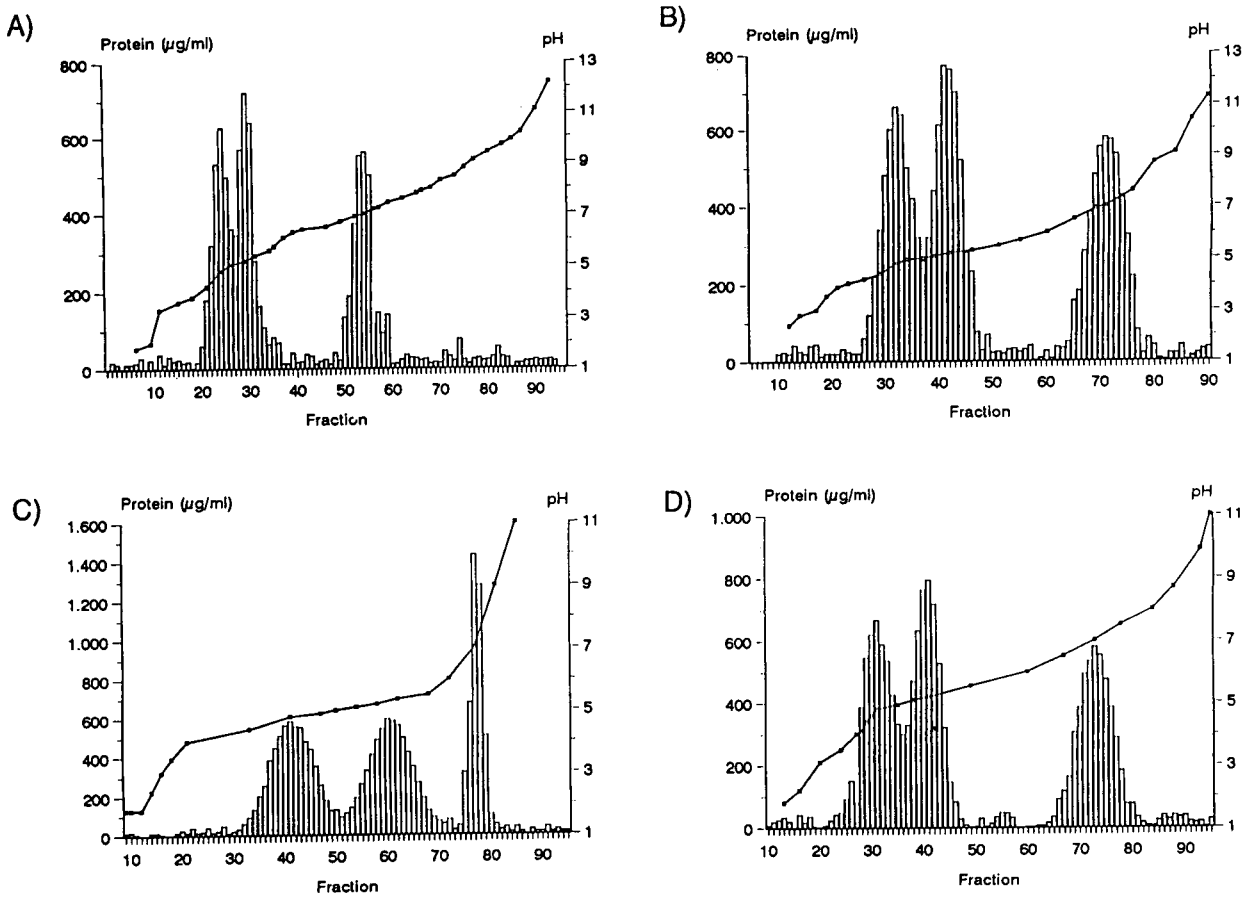

Fig. 10. Effect of different pH gradients on the separation of a sample containing ovalbumin, bovine serum albumin and haemoglobin. Experimental conditions: temperature of chamber, 5°C; medium, 3% (w/v) saccharose–0.35% (v/v) Servalyte; sample solution, 1 mg ml^{-1} ovalbumin, 1 mg ml^{-1} haemoglobin and 1 mg ml^{-1} bovine serum albumin in medium; electric field strength, 200 V cm^{-1}; transit time, 7 min. O = pH gradient. (A) Servalyte 3–10; (B) Servalyte 4–5; (C) Servalyte 4–7; (D) Servalyte 5–8.

Table 2
Influence of different pH gradients on R and F_{eff}

Parameter	Protein	pH gradient			
		3–10	4–7	4–5	5–8
F_{eff}	Ovalbumin	12.3	12.7	19.0	6.1
	Bovine serum albumin (BSA)	19.0	21.3	21.3	17.7
	Haemoglobin	11.0	3.0	1.13	4.24
R	Ovalbumin–BSA	0.66	0.83	1.13	0.82
	Ovalbumin–haemoglobin	3.2	3.46	3.11	2.97
	BSA–haemoglobin	2.89	2.48	1.38	2.24

The values were calculated from IEF of a mixture containing ovalbumin, bovine serum albumin (BSA) and haemoglobin as described in Fig. 10.

proteins (Fig. 10) were undertaken. To estimate F_{eff} values, each protein was individually focused in a separate experiment. The calculated constants F_{eff} and R inferred from Fig. 10 are summarized in Table 2. Compared with bovine serum albumin and ovalbumin, F_{eff} for haemoglobin is smaller in each of the Servalyte types used. This may be caused by the significantly smaller value of the mobility slope ($d\mu/dpH$) for haemoglobin (Table 1). According to Eq. 6, the influence of different pH gradients on F_{eff} is negligible if the pH gradients show a linear behaviour, as the pH gradients for albumin did (Fig. 10C).

On the other hand, non-linear pH gradients deteriorate F_{eff}, as is found for haemoglobin within a pH gradient between 4–7 and 4–5 or ovalbumin within a pH gradient between 5 and 8 pH units. As expected from Eq. 10, for the separation of bovine serum albumin and ovalbumin an improvement in resolution with decreasing pH gradient is fulfilled in practice.

3.8. *Influence of different ampholytes on resolution*

It is possible that the effects produced by additives may differ based on the chemistry of the ampholytes used. Therefore, we investigated the influence of different ampholytes [Servalyte 5–8, Bio-Lyte 5–8 and Ampholine 5–8, 0.35% (v/v) solutions] on R in the free-flow IEF of the protein standard mixture with and without addition of 3% (w/v) of saccharose. The ampholytes used produced minor differences in the declared pH gradients. The resolution increased in each instance on addition of 3% of saccharose (Table 3).

Table 3
Influence of different ampholytes on resolution

Conditions	Resolution		
	Bio-Lyte	Pharmalyte	Servalyte
Without additives	1.35	1.42	1.67
With 3% saccharose	2.3	1.93	2.11

The values were calculated from IEF of a mixture containing bovine serum albumin (BSA) and human haemoglobin. Experimental conditions: temperature of chamber, 5°C; medium, 0.35% (v/v) ampholyte with and without 3% (w/v) saccharose; sample solution, 1 mg ml^{-1} BSA and haemoglobin in medium; electric field strength, 175 V cm^{-1}; transit time, 7 min.

4. Conclusions

The separation of a protein mixture consisting of bovine serum albumin, ovalbumin and haemoglobin by preparative continuous free-flow IEF was mainly characterized by two parameters: resolution and focusing efficiency. Hydrophilic additives to the IEF medium can effectively control the resolution and focusing efficiency of proteins in free-flow IEF and caused up to an

eightfold improvement in resolution. This effect is mainly caused by the influence of these additives on electrodispersive effects. Shallow pH gradients have a minor influence on the focusing efficiency, but improve the resolution. For the proteins investigated, transit times as short as ca. 7 min gave optimum resolution. These limited transit times may be very helpful for separating biomolecules having a short lifetime.

References

[1] A. Kolin, in D. Glick (Editor), *Methods of Biochemical Analysis*, Vol. VI, Interscience, New York, 1958, pp. 259–288.
[2] H. Svensson, *Acta. Chem. Scand.*, 15 (1961) 325–341.
[3] T. Laas, in J.-C. Janson and L. Ryden (Editors), *Protein Purification —Principles, High Resolution Methods, and Applications*, VCH, Weinheim 1989, pp. 376–403.
[4] M. Bier, J. Ostrem and R.B. Marquez, *Electrophoresis*, 14 (1993) 1011–1018.
[5] D.E. Garfin, *Methods Enzymol.*, 182 (1990) 475–477.
[6] M. Bier and N.B. Egen, *Dev. Biochem.*, 7 (1979) 35–48.
[7] M. Bier, G.E. Twitty and J.E. Sloan, *J. Chromatogr.*, 470 (1989) 369–376.
[8] G. Küllertz, S. Meyer and G. Fischer, *Electrophoresis*, 7 (1994) 960–967.
[9] A.T. Andrews, *Electrophoresis —Theory, Techniques, and Biochemical and Clinical Applications*, Oxford University Press, Oxford, 1985, pp. 257–258.
[10] C. Burgaud, M.J. Clifton and V. Sanchez, *Electrophoresis*, 13 (1992) 128–135.
[11] W.G. Kuhr, *Anal. Chem.*, 63 (1990) 403R–414R; and references cited therein.
[12] E.J. Cohn, A.A. Green and M.H. Blanchard, *J. Am. Chem. Soc.*, 59 (1937) 509–513.
[13] M.M. Bradford, *Anal. Biochem.*, 72 (1976) 248–254.
[14] E. van Handel, *Anal. Biochem.*, 19 (1967) 193–194.
[15] J.S. Fawcett, *Ann. N.Y. Acad. Sci.*, 200 (1972) 112–116.
[16] *Isoelectric Focusing Principles and Methods*, Vol. 1, Pharmacia Fine Chemicals, Uppsala, 1982, pp. 9–10.
[17] M.A. Lauffer, *Motion in Biological Systems*, Alan R. Liss, New York, 1989, pp. 80–81.
[18] D.D. Perrin, *Dissociation Constants in Aqueous solutions*, Butterworths, London, 1965.
[19] R. Kuhn, and S. Hofstetter-Kuhn, *Capillary Electrophoresis: Principles and Practice*, Springer, Berlin, 1993, pp. 43–50.
[20] X.-W. Yao and F.E.J. Regnier, *J. Chromatogr.*, 632 (1993) 185–193.
[21] S. Fujiwara and S. Honda, *Anal. Chem.*, 58 (1986) 1811–1814.
[22] A.-S. Yang, M.R. Gunner, R. Sampogna, K. Sharp and B. Honig, *Proteins*, 15 (1993) 252–265.
[23] A. Sillero and J.M. Ribeiro, *Anal. Biochem.*, 179 (1989) 319–325.
[24] K. Linderstrom-Lang and S.O. Nielsen, in M. Bier (Editor), *Elecrophoresis*, Vol. 1, Academic Press, New York, 1959, p. 85.
[25] J.M. Ribero and A. Sillero, *Comput. Biol.*, 21 (1991) 131–141.
[26] A.J. Reynolds and D.R. McCaslin, *Methods Enzymol.*, 117 (1985) 41–53.
[27] E. Hückel, *Phys. Z.*, 25 (1924) 204–210.
[28] W.J. Gelsema, C.L. de Ligny and N.G.J. van der Veen, *J. Chromatogr.*, 173 (1979) 33–41.
[29] A.B. Bosisio, R.S. Snyder and P.G. Righetti, *J. Chromatogr.*, 209 (1981) 265–272.
[30] D.A. Saville, in B.J. Radola (Editor), *The Dynamics of Electrophoresis*, VCH, Weinheim, 1992, pp. 11–70.
[31] H. Svensson, *J. Chromatogr.*, 25 (1966) 266–273.
[32] J.C. Giddings, *Unified Separation Science*, Wiley, New York, 1991, pp. 180–184.

ELSEVIER

Journal of Chromatography A, 684 (1994) 343–349

JOURNAL OF CHROMATOGRAPHY A

Behaviour of periodate ion in isotachophoresis using cyclodextrins

Keiichi Fukushi[a,*], Kazuo Hiiro[b]

[a]*Research Institute for Marine Cargo Transportation, Kobe University of Mercantile Marine, 5-1-1 Fukaeminami-machi, Higashinada-ku, Kobe 658, Japan*

[b]*Kobe Women's Junior College, Minatojima, Chuo, Kobe 658, Japan*

First received 19 April 1994; revised manuscript received 24 June 1994

Abstract

The effects of α-, β- and γ-cyclodextrins on the migration behaviour of periodate ion in capillary isotachophoresis were investigated. The qualitative index R_E for periodate ion increased linearly with increasing cyclodextrin concentration in the leading electrolyte. The magnitude of the increase was in the order β- > α- > γ-cyclodextrin. During migration, periodate ion was decomposed to iodate ion in the presence of cyclodextrins. The decomposition rate was in the order γ- > β- > α-cyclodextrin. For the simultaneous determination of iodate and periodate ions, β-alanine was better than histidine as the buffer added to the leading electrolyte. Triton X-100 was also better than poly(vinyl alcohol) as the additive to the leading electrolyte.

1. Introduction

In a previous paper [1] it was shown that each ion of groups of inorganic anions such as nitrite and nitrate ions, cyanate, thiocyanate and selenocyanate ions, chlorate and perchlorate ions and chloride and iodide ions was separable by capillary isotachophoresis using leading electrolytes containing α-cyclodextrin (CD); it is difficult to separate these ions by the use of ordinary leading electrolytes.

In general, periodate ion oxidizes carbohydrates to give iodate ion [2,3]. In this work, first the following conditions were examined for the simultaneous determination of iodate and periodate ions: two kinds of buffers for the leading electrolyte, histidine and β-alanine; and two kinds of additives to the leading electrolyte, poly(vinyl alcohol) and Triton X-100. Then the isotachophoretic migration behaviour of periodate ion when α-, β- or γ-CD was added to the leading electrolyte was studied in detail. The effects of α-, β- and γ-CDs on the qualitative index R_E for other anions (e.g., chromate, tetrathionate, fluoride, perchlorate and iodide ions) were also studied.

2. Experimental

2.1. Apparatus

A Shimadzu Model IP-2A isotachophoretic analyser was used with a potential gradient detector. The main column was a fluorinated ethylene–propylene (FEP) copolymer tube (15

* Corresponding author.

0021-9673/94/$07.00
SSDI 0021-9673(94)00594-Y

cm × 0.5 mm I.D.), and the precolumn was a polytetrafluoroethylene (PTFE) tube (4 or 10 cm × 1.0 mm I.D.). A Hamilton Model 1701-N microsyringe was used for the injection of samples into the isotachophoretic analyser. Distilled, demineralized water was obtained from a Yamato-Kagaku Model WG-25 automatic still and a Nihon Millipore Milli-QII system.

2.2. Reagents

All reagents were of analytical-reagent grade and used as received. Distilled, demineralized water was used throughout. The α-, β- and γ-CDs were obtained from the Nacalai Tesque. Standard solutions of various anions were prepared by dissolving their sodium or potassium salts in water; those of periodate ion were prepared from sodium metaperiodate once a week because periodate is liable to cause hydrolysis.

3. Results and discussion

3.1. Determination of iodate and periodate ions

Volumes of 5 μl of solutions containing 1.0 m*M* periodate ion, 1.0 m*M* iodate ion or their mixtures were injected into the isotachophoretic analyser. The migration current was maintained at 150 μA for the first 10 or 11 min and then reduced to 50 μA. The following leading electrolytes were examined for the simultaneous determination of iodate and periodate ions; (I) 5 m*M* histidine hydrochloride–0.01% (w/w) Triton X-100 (pH 4.3); (II) 5 m*M* hydrochloric acid–0.01% (w/w) Triton X-100–β-alanine (pH 3.6). The terminating electrolyte was 10 m*M* sodium acetate solution. The R_E value [4] was used as a parameter of identification of the analyte ions, and is defined by the equation

$$R_E = \frac{\bar{m}_L}{\bar{m}_A} = \frac{E_A}{E_L} \quad (1)$$

where $\bar{m}_L$ and $\bar{m}_A$ are the effective mobilities of the leading and the analyte ion A and E_L and E_A are the potential gradients. When 1.0 m*M* periodate ion was measured, two zones were observed with the use of leading electrolyte I, as shown in Fig. 1A. The R_E value of zone c in Fig. 1A is almost equal to those in Fig. 1B and C. The length of zone c in Fig. 1C is almost equal to the sum of those in Fig. 1A and B. Therefore, zones b and c in Fig. 1A correspond to periodate and iodate ions, respectively. This phenomenon seemed to be caused by the insufficient buffering capacity of histidine at the pH of leading electrolyte I. On the other hand, only one zone of periodate ion was obtained with the use of leading electrolyte II, as shown in Fig. 2A. Clearly separated and stable zones with sharp boundaries for iodate and periodate ions were obtained as shown in Fig. 2C. It was not possible to separate these ions when poly(vinyl alcohol) (degree of polymerization 500 and 2000) was used instead of Triton X-100.

Linear calibration graphs were obtained for iodate and periodate ions with the use of leading electrolyte II. The regression equations for iodate and periodate ions were $y = 15.1x + 0.1$ ($0 \leq x \leq 2.5$, $0 \leq y \leq 38.1$) and $y = 13.2x - 0.1$ ($0 \leq x \leq 2.5$, $0 \leq y \leq 33.2$), respectively, where x is the concentration of the ion in m*M* and y the

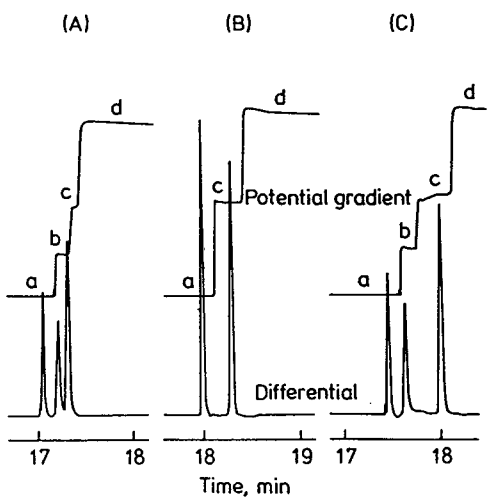

Fig. 1. Isotachopherograms for iodate and periodate ions by use of the leading electrolyte I. (A) 1 m*M* IO_4^-; (B) 1 m*M* IO_3^-; (C) 1 m*M* IO_3^- + 1 m*M* IO_4^-. (a) Cl^-; (b) IO_4^-; (c) IO_3^-; (d) CH_3COO^-.

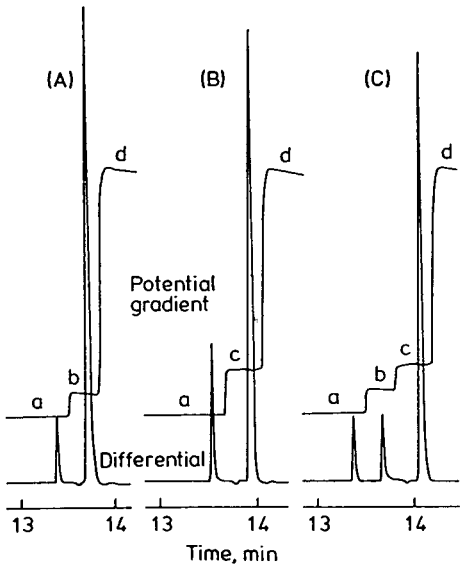

Fig. 2. Isotachopherograms for iodate and periodate ions by use of the leading electrolyte II. (A) 1 mM IO_4^-; (B) 1 mM IO_3^-; (C) 1 mM IO_3^- + 1 mM IO_4^-. (a) Cl^-; (b) IO_4^-; (c) IO_3^-; (d) CH_3COO^-.

zone length in mm when the recording speed is adjusted to 40 mm/min. Both correlation coefficients were 0.9999. The relative standard deviations were obtained by calculating the zone length per 1.0 mM at each point on the calibration graphs. They were 2.2% and 0.87% (n = 5), respectively. The limits of determination for iodate and periodate ions were 6.6×10^{-3} and 7.6×10^{-3} mM, respectively, corresponding to a 0.1-mm zone length. When 5-μl volumes of solutions containing various concentrations of iodate and periodate ions were injected and analysed by use of the calibration graphs, the error in the simultaneous determination of these anions was less than ±12%, as shown in Table 1. Therefore, leading electrolyte II was adopted for subsequent experiments.

3.2. Effects of concentration of CDs on R_E values for periodate and iodate ions

A solution containing 1.0 mM periodate or iodate ion was analysed and the R_E values were calculated as above. The concentration of α- or γ-CD in the leading electrolyte was increased to 50 mM and that of β-CD to 15 mM owing to the poor solubility in water. It was possible to prepare a leading electrolyte containing 50 mM β-CD by the addition of 3 M urea [5]. Urea was not used in this study because this leading electrolyte contained a lot of impurities. The R_E value of periodate ion increased linearly with increasing concentration of α-, β- and γ-CDs up to 30, 15 and 30 mM, respectively, as shown in Fig. 3. The magnitude of the slope of the regression line of R_E vs. α-, β- or γ-CD concentration for periodate ion was in the order β- > α- > γ-CD, which corresponds to that of the magnitude of the interaction between periodate ion and α-, β- or γ-CD. The effective mobilities of analyte ion A ($\bar{m}_A$) in the presence of an electrically neutral ligand N_1 or N_2 are expressed as follows by modifications of the equations derived by Tazaki et al. [6]:

Table 1
Analytical results for iodate and periodate ions

Mixture	Added (mM)		Found (mM)		Error (%)	
	IO_3^-	IO_4^-	IO_3^-	IO_4^-	IO_3^-	IO_4^-
1	0.50	2.5	0.56	2.4	+12	−4.0
2	1.0	1.0	1.1	0.96	+10	−4.0
3	1.0	2.0	1.1	1.9	+10	−5.0
4	1.5	1.5	1.5	1.5	0.0	0.0
5	2.0	1.0	2.1	0.94	+5.0	−6.0
6	2.5	0.50	2.6	0.45	+4.0	−10

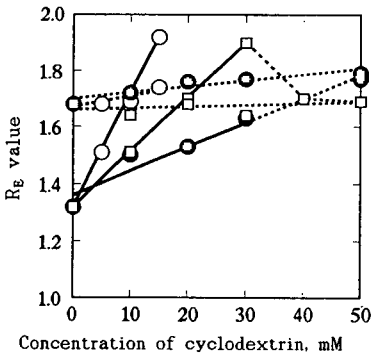

Fig. 3. Effect of cyclodextrin concentration on the R_E values of iodate and periodate ions. Solid lines, IO_4^-; dotted lines, IO_3^-. □ = α-CD; ○ = β-CD; ● = γ-CD.

$$\bar{m}_A = \frac{m_A + m_{AN_1} K_{AN_1}[N_1]_A}{1 + K_{AN_1}[N_1]_A} \quad (2)$$

$$\bar{m}_A = \frac{m_A + m_{AN_2} K_{AN_2}[N_2]_A}{1 + K_{AN_2}[N_2]_A} \quad (3)$$

where m_A, m_{AN_1} and m_{AN_2} are the ionic mobilities of the free analyte ion A and the complexed analyte ions AN_1 and AN_2, respectively, K_{AN_1} and K_{AN_2} are the complex formation constants of A with the ligand N_1 and N_2, respectively, and $[N_1]_A$ and $[N_2]_A$ are the ligand concentrations in each zone. By use of both calculated and experimental data, Tazaki et al. [6] showed that $\bar{m}_A$ decreases with increasing $[N_1]_A$ or $[N_2]_A$ (that is, the R_E value increases); if $K_{AN_1} > K_{AN_2}$, $\bar{m}_A$ in Eq. 2 is less than $\bar{m}_A$ in the Eq. 3 (the R_E value for the former $\bar{m}_A$ is greater than that for the latter $\bar{m}_A$) and if $K_{AN_1} < K_{AN_2}$, $\bar{m}_A$ in Eq. 2 is greater than $\bar{m}_A$ in the Eq. 3 (the R_E value for the former $\bar{m}_A$ is less than that for the latter $\bar{m}_A$). Therefore, if $K_{AN_1} > K_{AN_2}$, the slope of the regression line of R_E vs. the ligand N_1 concentration is larger than that vs. the ligand N_2 concentration and if $K_{AN_1} < K_{AN_2}$, the former slope is smaller than the latter. The R_E value of iodate ion remained almost constant, increased or slightly increased when the concentration of α-, β- or γ-CD increased, respectively.

3.3. Behaviour of periodate ion in the presence of CDs

When solutions containing 1.0 m*M* periodate ion were analysed, the zone length of periodate ion decreased with increasing concentration of α-, β- and γ-CDs and the zone disappeared at 40 m*M* α-CD and 50 m*M* γ-CD, as shown in Fig. 4. The zone length of periodate ion at 10 m*M* CD concentration was in the order of α- > β- > γ-CD. Another zone began to appear and increased with decreasing zone length of periodate ion. The new zone was presumed to correspond to iodate ion for the same reason as in the explanation of Fig. 1.

In order to confirm above phenomena, the following experiments were carried out by the modified procedure proposed by Honda and coworkers [2,3]. Two kinds of solutions were prepared: leading electrolyte II containing 2 m*M* periodate ion (solution A) and leading electrolyte II containing 2 m*M* α-CD or 10 m*M* α-, β- or γ-CD (solution B). A 1-ml volume of solution A was mixed with 1 ml of solution B in a test-tube. The test-tube was allowed to stand at room temperature (21.9–23.4°C). A 5-μl volume of the mixture was taken and injected into the

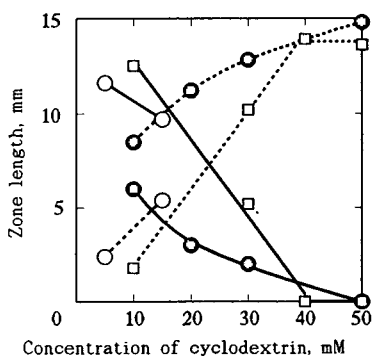

Fig. 4. Decomposition of periodate ion in the presence of α-, β- or γ-cyclodextrin during migration. Solid lines, IO_4^-; dotted lines, IO_3^-. □ = α-CD; ○ = β-CD; ● = γ-CD.

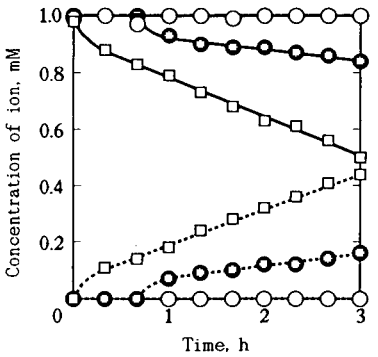

Fig. 5. Decomposition rates of periodate ion. Solid lines, IO_4^-; dotted lines, IO_3^-. ● = Addition of 1 m*M* α-CD; □ = addition of 5 m*M* α-CD; ○ = without α-CD.

isotachophoretic analyser every 20 min. Figs. 5 and 6 show the results. With 1 m*M* α-CD, the concentration of periodate ion began to decrease after 40 min and then decreased linearly up to 0.84 m*M* after 3 h. On the other hand, the concentration of iodate ion began to increase after 40 min and then increased linearly up to 0.16 m*M* after 3 h. The total concentration of periodate and iodate ions at each sampling time was 0.99–1.0 m*M* over 3 h. With 5 m*M* α-CD, the concentration of periodate ion began to decrease after mixing and then decreased linearly up to 0.50 m*M* after 3 h. The concentration of iodate ion began to increase after mixing and then increased linearly up to 0.44 m*M* after 3 h. The total concentration was 0.94–0.99 m*M*. Without α-CD, the concentration of periodate ion was almost constant (0.97–1.0 m*M*) over 3 h. With 5 m*M* β-CD, the concentration of periodate ion began to decrease after mixing and then decreased up to 0.30 m*M* after 3 h. The concentration of iodate ion began to increase after mixing and then increased up to 0.68 m*M* after 3 h. The total concentration was 0.98–1.0 m*M*. With 5 m*M* γ-CD, the concentration of periodate ion began to decrease just after mixing and then decreased up to 0 m*M* after 1 h 40 min. The concentration of iodate ion began to increase just after mixing, increased up to 0.91 m*M* after 1 h 40 min and then gradually increased up to 0.98 m*M* after 3 h. The total concentration was 0.91–1.0 m*M*.

Consequently, it was concluded that periodate ion was decomposed by its reduction to iodate ion in the presence of CDs; the magnitude of the decomposition rate was in the order of γ- > β- > α-CD and depended on the concentration of CDs. This order was not contradictory to that of the zone length of periodate ion at a 10 m*M* CD concentration in Fig. 4. It may be possible to estimate the ease of oxidation of CDs from the order of the magnitude of the decomposition rate for periodate ion. Hence the phenomena observed during the migration of periodate ion with CDs were confirmed.

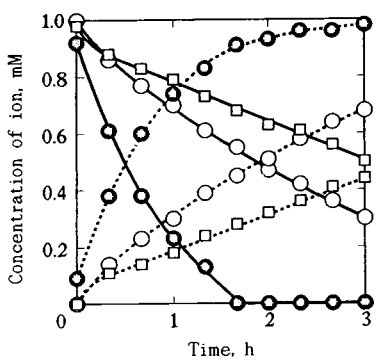

Fig. 6. Decomposition rates of periodate ion. Solid lines, IO_4^-; dotted lines, IO_3^-. □ = Addition of 5 m*M* α-CD; ○ = addition of 5 m*M* β-CD; ● = addition of 5 m*M* γ-CD.

3.4. Effects of concentration of CDs on R_E values for other anions

The R_E values of other anions such as chromate, tetrathionate, fluoride, perchlorate and iodide ions were obtained when the concentration of α-, β- or γ-CD in the leading electrolyte was changed. A 2-μl volume was adopted as the injection volume for a solution of 1.0 m*M* of tetrathionate ion when the leading electrolyte containing α-CD or that without CDs was used, because a mixed zone with leading anion was formed on injection of 5 μl of the solution. The injection volume was 5 μl for the other anions.

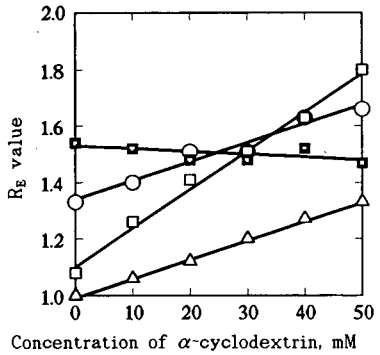

Fig. 7. Effect of α-CD concentration on the R_E values of anions. ○ = CrO_4^{2-}; ■ = F^-; □ = ClO_4^-; △ = I^-.

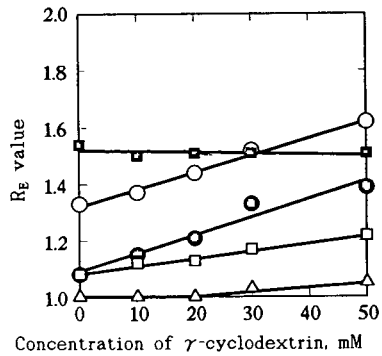

Fig. 9. Effect of γ-CD concentration on the R_E values of anions. ○ = CrO_4^{2-}; ● = $S_4O_6^{2-}$; ■ = F^-; □ = ClO_4^-; △ = I^-.

Figs. 7–9 show the results. The R_E values of chromate, perchlorate and iodide ions increased linearly with increasing concentration of α-CD. The magnitude of the slope of the regression line for these anions was in the order perchlorate > chromate ≈ iodide, which corresponds to that of the magnitude of the interaction between these anions and α-CD. This is explicable in a similar manner as described in Section 3.2. The R_E value of fluoride ion slightly decreased. The R_E value of tetrathionate ion was constant over the range 0–20 m*M* α-CD, although this is not shown in Fig. 7. Therefore, the solution of tetrathionate ion was not injected for leading electrolytes containing α-CD at concentrations above 20 m*M*. The R_E values of chromate, tetrathionate and perchlorate ions increased linearly with increasing concentration of β-CD. The magnitude of the slope for these anions was in the order tetrathionate > perchlorate > chromate. Iodide ion was faintly detected and the R_E value was 1.01 when the concentration of β-CD was 15 m*M*. The R_E value of fluoride ion decreased slightly similarly to the result for the addition of α-CD. The R_E values of chromate, tetrathionate and perchlorate ions increased linearly with increasing concentration of γ-CD. The magnitude of the slope for these anions was in the order chromate ≈ tetrathionate > perchlorate. The R_E value of fluoride ion was almost constant. A weak indication of the detection of iodide ion was recognized when the concentration of γ-CD was 20 m*M*. The zone for iodide ion began to appear at 30 m*M* γ-CD concentration and its R_E value increased slightly.

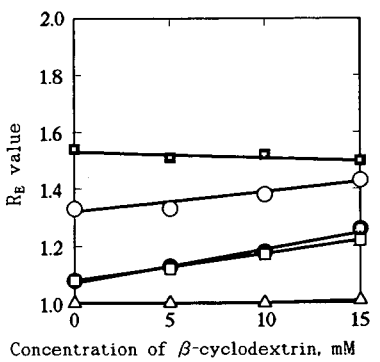

Fig. 8. Effect of β-CD concentration on the R_E values of anions. ○ = CrO_4^{2-}; ● = $S_4O_6^{2-}$; ■ = F^-; □ = ClO_4^-; △ = I^-.

The magnitude of the slope of the regression line of R_E vs. α-CD concentration was compared with that of R_E vs. β- or γ-CD concentration for each anion. The following indications were obtained: the magnitude of the interaction between chromate ion and α-CD was almost equal to that for β- or γ-CD; the magnitude of the interaction for tetrathionate ion was in the order β- > γ- > α-CD; the magnitude of the interaction for

perchlorate ion was in the order α- > β- > γ-CD; and the magnitude of the interaction for iodide ion was in the order α- > β- ≈ γ-CD.

References

[1] K. Fukushi and K. Hiiro, *J. Chromatogr.*, 518 (1990) 189.
[2] S. Honda, H. Wakasa, M. Terao and K. Kakehi, J. Chromatogr., 177 (1979) 109.
[3] S. Honda, K. Suzuki and K. Kakehi, *Anal. Biochem.*, 177 (1989) 62,
[4] T. Hirokawa, N. Aoki and Y. Kiso, *J. Chromatogr.*, 312 (1984) 11.
[5] H. Nishi, Y. Kokusenya, T. Miyamoto and T. Sato, in *Proceedings of the 12th Symposium on Capillary Electrophoresis, Himeji, December 2–4, 1992*, Japan Discussion Group of Electrophoretic Analysis, Japan Society for Analytical Chemistry, Tokyo, 1992, p. 49.
[6] M. Tazaki, T. Hayashita, Y. Fujino and M. Takagi, *Bull. Chem. Soc. Jpn.*, 59 (1986) 3459.

ELSEVIER

Journal of Chromatography A, 684 (1994) 350–353

JOURNAL OF CHROMATOGRAPHY A

Short communication

Separation and determination of allantoin, uric acid, hydantoin and urea

L. Terzuoli, M. Pizzichini, L. Arezzini, M.L. Pandolfi, E. Marinello*, R. Pagani

Istituto Biochimica e Enzimologia, Università di Siena, Siena, Italy

First received 24 January 1994; revised manuscript received 5 July 1994

Abstract

Hydantoin and urea, obtained by reducing the allantoin ring with hydroiodic acid or uric acid after treatment with uricase, were separated from each other and from their starting compounds by high-performance liquid chromatography and anion-exchange chromatography.

1. Introduction

Purine metabolism, followed by the incorporation of [^{14}C]formate into uric acid and allantoin in the rat liver, has long been used as an index of purine nucleotide catabolism [1–3]. The specific radioactivity of allantoin was found to be higher than that of uric acid a short time after administration of the precursor (17 and 30 min after administration of [^{14}C]formate). After 60 min, the values started to return to the same levels as for uric acid [4]. This quite unexpected result opens a new field in the study of purine catabolism.

One way to study this point and to explain these results is to measure the radioactivity of C-2 and C-8 in allantoin and uric acid. The procedure is based on the facts that: (1) during nucleotide catabolism, both compounds are selectively labeled in positions C-2 and C-8 when [^{14}C]formate is used as precursor; (2) purified uric acid is transformed in vitro into allantoin by treatment with uricase; (3) allantoin, however obtained, is transformed into hydantoin and urea by reductive hydrolysis with phosphonium iodide. The labeled carbons, originally in positions 8 and 2 of uric acid and allantoin, end up in hydantoin and urea, respectively (Fig. 1) The reduction of allantoin is reported in the literature [5] and involves the precipitation of hydantoin, but the working conditions used were not suitable for our study. Since we used about 0.1 mg of allantoin or uric acid, we could not obtain the hydantoin precipitate.

This made it necessary to use another specific procedure for the separation and determination of hydantoin, urea and allantoin; small amounts of allantoin were still present under our conditions and had to be separated from urea and hydantoin. The separation of these reaction products has never been reported in the literature. The three substances had a very similar chromatographic pattern and we could not use an ammonium buffer, because the urea determination was extremely sensitive to ammonium salts. We succeeded in separating hydantoin,

* Corresponding author.

0021-9673/94/$07.00
SSDI 0021-9673(94)00650-4

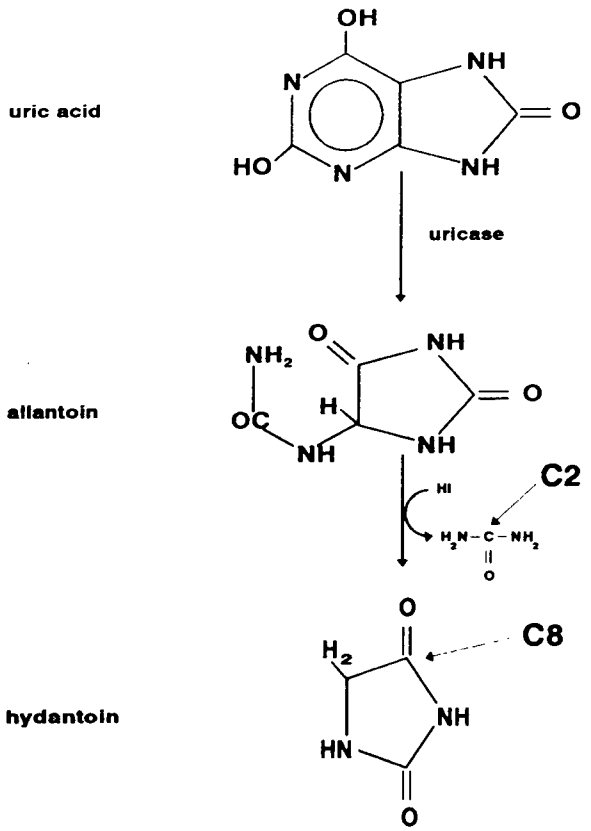

Fig. 1. Formation of hydantoin and urea.

urea and allantoin by HPLC and anion-exchange chromatography.

2. Experimental

2.1. Chemicals

Allantoin, uric acid, hydantoin and urea were purchased from Sigma (St. Louis, MO, USA). Uricase and urea stain were obtained from Boehringer Mannheim (Mannheim, Germany). Red phosphorus and hydroiodic acid were purchased from Fluka (Buchs, Switzerland). Anhydrous acetic acid was obtained from Farmitalia Carlo Erba (Milan, Italy). Methanol (HPLC grade) was obtained from Baker (Phillipsburg, NJ, USA).

2.2. Preparation of hydantoin and urea

We placed 0.1 mg of allantoin, 10 mg of red phosphorus, 0.1 ml of anhydrous acetic acid and 0.1 ml of hydroiodic acid, in a 1-ml vial. The mixture was refluxed for 4 h and filtered with cotton after cooling. The unreacted phosphorus was washed on the filter with two 0.05-ml portions of glacial acetic acid and discarded. The filtrate was applied to Dowex 1-X8 to remove all compounds used to reduce the allantoin. The column was equilibrated and then eluted with distilled water (flow-rate 0.2 ml/min). A 15-ml volume of eluate was collected. The mixture contained residual allantoin, urea and hydantoin, free of impurities. After neutralization, the solution was reduced in volume to 2 ml, using a rotary evaporation under vacuum, and separated by HPLC. Elution was carried out with distilled water pH 6.0 for 10 min at a flow-rate of 4 ml/min. In this way, hydantoin was separated from urea and allantoin. The urea–allantoin mixture was brought to pH 12 with NaOH, applied to an anion-exchange column (Dowex 1-X8) and eluted with distilled water (flow-rate 0.2 ml/min, fractions collected every 1.5 min). Fractions 13–27 contained only urea. Residual allantoin was eluted with 0.1 *M* NaOH.

Urea was determined by an enzymatic colorimetric method [6]. When treated with urease it produced ammonium carbonate which reacts with sodium hydroxide and hypochlorite to give a coloured complex (wavelength: 600 nm) (Fig. 2).

The same procedure was used for uric acid but 0.1 mg of compound was brought to pH 9.5 with NaOH and treated with uricase (12 μg) for 1 h to obtain allantoin [7]. The recovery of hydantoin and urea after the final step was about 70%.

Allantoin was assayed by the Rimini–Schryver reaction (see Ref. [8]).

2.3. Apparatus and chromatographic conditions

A Vista 5500 high-performance liquid chromatograph (Varian, Sunnyvale, CA, USA) equipped with a variable-wavelength UV detector (Model 2550, Varian) and an electronic inte-

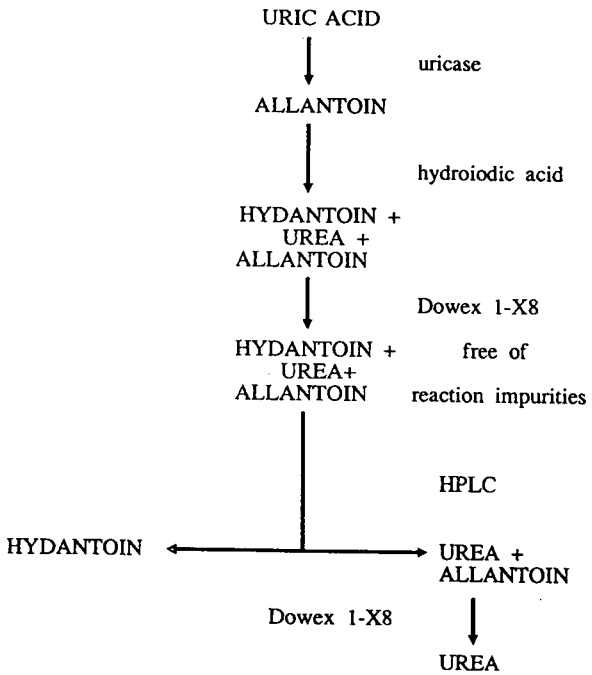

Fig. 2. Preparation and separation of hydantoin and urea.

grator (Model 4290, Varian) was used. A ready-for-use, prepacked Supelcosil LC-18 semipreparative column (250 × 10 mm I.D.), 5 μm (Supelco, Bellefonte, PA, USA) completed the analytical system. The mobile phase consisted of distilled water (pH 6.0), at a flow-rate of 4 ml/min. Detection was performed at 220 nm. Partisil 10 Sax (250 × 4.6 mm I.D.), 5 μm, was from Whatman, Supelcosil LC-SCX (250 × 4.6 mm I.D.), 5 μm, was from Supelco. A pH of 3 was obtained by acidifying distilled water with CF_3COOH; the pH of 6 was that of boiled distilled water; pH 3 and 6 were found to be constant during 10 min of HPLC analysis. Separation and retention times were the same using acidified water or 5 m*M* $NH_4H_2PO_4$ buffer.

A Dowex 1-X8 (200–400 mesh, anion-exchange resin) column (20 × 0.4 cm) was connected to an LKB Microperpex peristaltic pump and an LKB 2112 Redirac fraction collector (Pharmacia LKB Biotechnology, Uppsala, Sweden). The column was equilibrated and eluted with distilled water at a flow-rate of 0.2 ml/min.

3. Results and discussion

Allantoin, urea and hydantoin were tested with three different types of chromatographic column (Table 1), but showed similar patterns when elution was carried out at pH 3 or 6, with water or buffer. Only with a LC-18 column we succeed in separating hydantoin from urea and allantoin. In our procedure, we prefer to use distilled water, since we had no trouble in detecting radioactivity. The compounds were detected at 220 nm. At this wavelength, urea did

Table 1
Retention times of hydantoin, urea and allantoin under different HPLC conditions

Compound	Retention time (min)		Column
	pH 3.0	pH 6.0	
Allantoin	3.50	3.60	Supelcosil LC-18
Urea	3.30	3.31	
Hydantoin	4.70	4.75	
Allantoin	3.37	3.38	Partisil SAX
Urea	3.47	3.49	
Hydantoin	3.38	3.41	
Allantoin	3.53	3.53	Supelcosil LC-SCX
Urea	3.48	3.48	
Hydantoin	3.85	3.85	

not show any significant absorption (molar absorption 0.03 $mmol^{-1}$ cm^{-1}). It can be detected at 200 nm (molar absorption 0.23 $mmol^{-1}$ cm^{-1}) and has a retention time of 3.3 min which is very similar to that of allantoin. The hydantoin peak eluted at 4.6 min and allantoin at 3.6 min (Fig. 3). Good linearity was obtained for all amounts of hydantoin and allantoin used (16–0.2 nmol). The correlation coefficients for hydantoin and allantoin were both 0.998 and the regression equations of the calibrations were $A = 68733C + 977$ and $A = 56777C + 8411$, respectively, where A = peak area and C (nmol) = amount of hydantoin or allantoin. The separation was reproducible column to column.

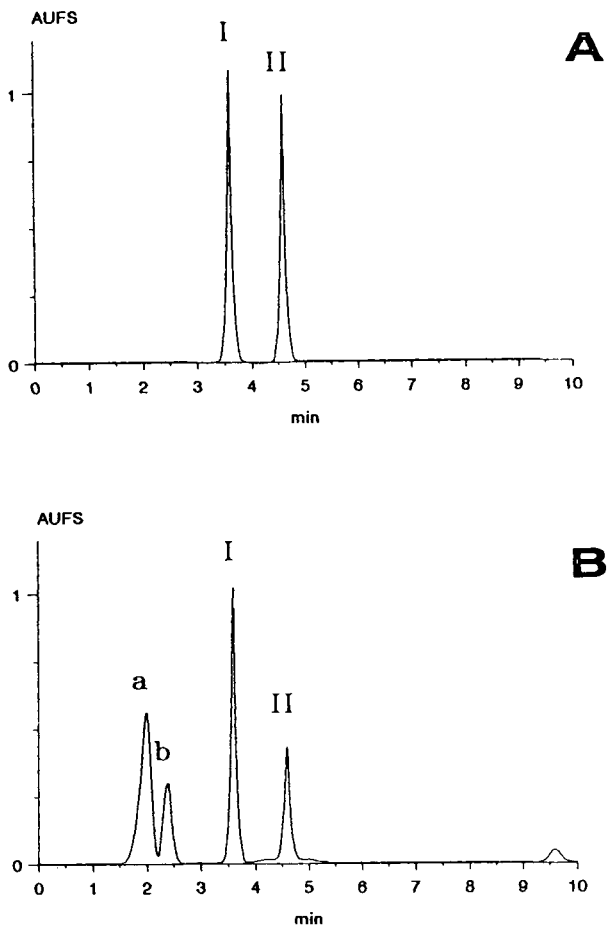

Fig. 3. (A) Separation of (I) allantoin and (II) hydantoin was carried out on a Supelcosil LC-18, with distilled water as mobile phase, at a flow-rate of 4 ml/min. Detection was performed at 220 nm. Injection volume: 20 μl of 1 mM solution of each standard. (B) Mixture containing reaction impurities (a, b), allantoin residues (I) and hydantoin (II). Urea is not visible because it is eluted at the same retention time as allantoin. Injection volume: 20 μl of solution diluted 1:20 with distilled water.

We obtained pure urea by applying the allantoin–urea mixture (pH 12) to the anion-exchange column (Dowex 1-X8) and collecting fractions 13–27. Separation of hydantoin and urea allowed the radioactivity of the labeled carbons to be measured. These were originally in positions 8 and 2 of uric acid and allantoin. Specific radioactivity was calculated.

3.1. Conclusions

The present method for the separation and determination of hydantoin, urea, allantoin and uric acid makes it possible to estimate, separately, the radioactivity of C-2 urea and C-8 hydantoin, obtained by reductive hydrolysis of allantoin with phosphonium iodide. The specific radioactivity of C-2 and C-8 obtained will be useful in the investigation of purine nucleotide catabolism and will help to explain why the incorporation of [^{14}C]formate into allantoin is much higher than into uric acid, a short time after administration of the labelled precursor in rat liver.

References

[1] M.N. Welch and F.B. Rudolph, *J. Biol. Chem.*, 257 (1982) 13 253.
[2] E. Zoref-Shani, G. Kessler-Icekson, L. Wasserman and O. Sperling, *Biochim. Biophys. Acta*, 804 (1984) 161.
[3] A. Di Stefano, M. Pizzichini and E. Marinello, *Biochim. Biophys. Acta*, 926 (1987) 1.
[4] A. Di Stefano, M. Pizzichini, R. Leoncini, D. Vannoni, R. Pagani and E. Marinello, *Biochim. Biophys. Acta*, 1117 (1992) 1.
[5] H.B. Gillespie and H.R. Snyder, *Org. Synth. Coll. Vol.II*, (1969) 489.
[6] J.K. Fawcett and J.E. Scott, *J. Clin. Pathol.*, 13 (1960) 156.
[7] E. Praetorius and H. Poulsen, *Scand. J. Clin. Lab. Invest.*, 5 (1953) 273.
[8] E.G. Young and C.F. Conway, *J. Biol. Chem.*, 142 (1942) 839.

ELSEVIER

Journal of Chromatography A, 684 (1994) 354–359

JOURNAL OF CHROMATOGRAPHY A

Short communication

Determination of platinum by ion-pair reversed-phase high-performance liquid chromatography with 4,4′-bis(dimethylamino)thiobenzophenone

Xiaosong Zhang*, Changshan Lin, Luzhou Liu, Guijuan Qiao

Department of Applied Chemistry, University of Science and Technology of China, Hefei, Anhui 230026, China

First received 7 March 1994; revised manuscript received 28 June 1994

Abstract

Platinum (II) was separated and determined by ion-pair reversed-phase high-performance liquid chromatography with spectrophotometric detection at 520 nm. 4,4′-Bis(dimethylamino)thiobenzophenone (TMK) was used as a precolumn complexing agent. The optimum conditions for the separation and determination of the Pt(II)–TMK complex were investigated. The complex was separated on a Nucleosil C_{18} column (250 mm × 4.0 mm I.D.) with tetrahydrofuran–water (48:52, v/v) containing 0.035 *M* acetic acid–sodium acetate buffer (pH 3.5), 0.20 *M* sodium perchlorate and $8.5 \cdot 10^{-5}$ *M* TMK. The proposed method was applied to the determination of platinum in cisplatin and carboplatinum samples.

1. Introduction

The separation and determination of mixtures of platinum metals as their complexes with organic reagents by high-performance liquid chromatography (HPLC) has received increasing attention and has been used in platinum metals analysis in recent years. Sometimes this technique has advantages over other instrumental methods of analysis, e.g., atomic absorption spectrometry or voltammetry, with regard both to detection limits and time requirements, which are of special importance in routine analyses of large numbers of sample.

The complexing agents that have been used for HPLC determination of platinum metals can be divided into two groups. The first group contains a nitrogen donor atom, such as 4-(2-pyridylazo)resorcinol [1], 1-(2-pyridylazo)-2-naphthol [2,3], 2-(5-bromo-2-pyridylazo)-2-diethylaminophenol [4], 2-(5-bromo-2-pyridylazo)-5-(N-propyl-N-sulphopropylamino)phenol [5], 1-(2-thiazolylazo)-2-naphthol [6], 2-(2-thiazolylazo)-5-diethylaminophenol [7], 2-(6-methylbenzolthiazolylazo)-5-diethylaminophenol [8] and 8-hydroxyquinoline [9,10]. The second group contains a sulphur donor atom, such as maleonitriledithiol [11], disubstituted dithiocarbamate [12–14], 1-hydroxy-2-pyridinethione [15] and diphenylthiourea [16]. Amongst the chromophoric agents, only diethyldithiocarbamate (DDTC) has been used for the determination of platinum in cisplatin [*cis*-dichlorodiammineplatinum (II)], an anti-cancer agent, as a complex of platinum based on precolumn derivatization [17–21]. To date, there have been no

* Corresponding author.

0021-9673/94/$07.00
SSDI 0021-9673(94)00641-5

reports on the separation and determination of platinum in carboplatinum [*cis*-diammine-1,1-cyclobutyldicarboxylate platinum(II)], another anti-cancer drug, as a complex of platinum with any chromophoric agent using HPLC.

The sensitive co-colour reaction of Pt(IV) and Pd(II) with 4,4′-bis(dimethylamino)thiobenzophenone (TMK) in the presence of ascorbic acid and Triton X-100 has been used previously for the spectrophotometric determination of platinum and palladium [22]. Using this reagent, the conditions for the precolumn derivatization and for the separation and determination of platinum in cisplatin and carboplatinum as complexes with TMK by ion-pair (IP) reversed-phase (RP) HPLC were investigated in this work.

2. Experimental

2.1. Apparatus

Liquid chromatography was performed using a Shimadzu Mode LC-4A HPLC instrument equipped with an SPD-1 spectrophotometric detector and a Chromatopac C-R2A data processor. A Nucleosil C_{18} column (250 mm × 4.0 mm I.D.) with a particle size of 5 μm was used in all experiments. A Shimadzu UV-240 recording spectrophotometer was used for spectral measurements. A Shanghai Model pH S-2 pH meter was also used.

2.2. Reagents and solutions

A stock standard solution of Pt(IV) was prepared by dissolving platinum wire (99.95%) in aqua regia on a hot-plate, evaporating nearly to dryness. The residue was treated with concentrated hydrochloric acid and evaporated to a small volume. After repeating this process three times to destroy oxides of nitrogen, the reaction mass was dissolved in and diluted with 1 *M* hydrochloric acid to give a concentration of 1.00 mg ml^{-1} of platinum. Working standard solutions of the required strength were prepared by appropriate dilution with water. A stock standard solution of Pd(II) was prepared by dissolving $PdCl_2$ in 1 *M* hydrochloric acid to give a concentration of 1.00 mg ml^{-1} of palladium. Working standard solutions of the required strength were prepared by appropriate dilution with water.

4, 4′ - Bis(dimethylamino)thiobenzophenone (Third Chemicals Factory of Shanghai) was dissolved in ethanol to give a concentration of 0.04% (w/v), stored in a brown-coloured bottle and kept in a refrigerator (a solution was prepared freshly every week). An ascorbic acid solution (8%, w/v) was prepared by dissolving the compound in water, adjusting the pH to 7 with dilute sodium hydroxide solution, and then kept in a refrigerator (a solution was prepared freshly every 3 days).

The mobile phase was tetrahydrofuran–water (48:52, v/v) containing 0.035 *M* acetic acid–sodium acetate buffer (pH 3.5), 0.20 *M* sodium perchlorate and $8.5 \cdot 10^{-5}$ *M* TMK, prepared freshly each day. All other chemicals were of analytical-reagent grade.

2.3. Procedure

To a slightly acidic solution containing 0.2–25 μg of Pt(IV) in a 10-ml calibrated flask, add 10 μg of Pd(II) solution and 1 ml of 8% ascorbic acid solution and mix thoroughly. After 1 min, add 2 ml of 2 *M* acetic acid–sodium acetate buffer solution (pH 3.5) and mix again thoroughly. After a further 3 min, add 1.5 ml of 0.04% TMK solution and 4 ml of 10% Triton X-100 solution and heat the mixture in a boiling water-bath for 20 min. After cooling immediately in tap water, dilute to volume with water. Filter the solution through a 0.3-μm membrane (mixed cellulose) and inject a 20-μl aliquot of the filtered solution on to the column. Elute the Pt(II)–TMK complex with the tetrahydrofuran–water mobile phase at a flow-rate of 0.6 ml min^{-1} and detect the complex in the eluate at 520 nm. Determine the amount of platinum by measuring the peak height.

Sample analysis

A cisplatin sample, or a carboplatinum sample, was dissolved in concentrated nitric acid–perchloric acid (1:10) on a hot-plate and evaporated nearly to dryness. This process was repeated twice to destroy organic chain bonds in the sample. The resulted residue was dissolved in 2 ml of 1 *M* hydrochloric acid by warming on the hot-plate. The solution was transferred into a 50-ml calibrated flask and diluted to volume with 1 *M* hydrochloric acid. An aliquot of this solution was diluted to volume with water in another 50-ml calibrated flask. A 1-ml aliquot of the last sample solution was taken and the Pt(II)–TMK complex was formed by reaction with TMK and determination by IP-RP-HPLC as described above.

3. Results and discussion

3.1. Selection of conditions for pre-column derivatization and detection wavelength of the Pd(II)–TMK complex

In a solution containing Pd(II), ascorbic acid and Triton X-100 in the pH range 2.5–4.2, buffered with acetic acid–sodium acetate, Pt(II) forms a violet complex with TMK at 100°C, exhibits an absorption maximum at 520 nm and has a molar absorptivity of $2.90 \cdot 10^5$ l mol^{-1} cm^{-1}. Ascorbic acid has the function of reducing Pt(IV) to Pt(II), which reacts with TMK to form the Pt(II)–TMK complex; Pd(II) plays a catalytic role in accelerating the colour development and making the reaction more completely. Although Pd(II) alone reacts with TMK to form an orange-red complex, the complex is labile and is decomposed rapidly at 100°C, and the amount of Pd(II) present in the sample solution does not affect the peak height of the Pt(II)–TMK complex.

In order to accelerate both the decomposition of the Pd(II)–TMK complex and the colour development of the Pt(II)–TMK complex, the sample solution had to be heated in a boiling water-bath for 15–20 min. As the reagent and the complex are insoluble in water, the concentration of Triton X-100 as a solubilizing agent in the sample solution should not be less than 4%. Reagents should be added to the solution containing Pt(IV) and Pd(II) as in the sequence described, as any change in the sequence affects the colour development of the Pt(II)–TMK complex.

The Pt(II)–TMK complex formed under the above-mentioned conditions had a stable peak height for at least 3 h.

3.2. Effect of concentration of tetrahydrofuran in the mobile phase

Some organic solvents, such as methanol, ethanol, isopropyl alcohol, acetone, acetonitrile and tetrahydrofuran, combined with water, were investigated as binary and ternary mobile phases. The tetrahydrofuran–water binary system was found to be suitable for the separation of the Pt(II)–TMK complex. A simple tetrahydrofuran–water mobile phase, however, gave a poor peak shape and low sensitivity; moreover, with a delay of injection of the sample solution, the peak height of the Pt(II)–TMK complex decreased distinctly because part of the complex was decomposed on the column. When acetic acid–sodium acetate buffer, sodium perchlorate and TMK were added to the mobile phase in order to suppress the decomposition of the complex, an excellent peak shape and high sensitivity were obtained. The effect of the concentration of tetrahydrofuran in the mobile phase on the retention time and peak height of the complex is shown in Fig. 1. The optimum results were obtained with tetrahydrofuran–water (48:52, v/v).

3.3. Effect of pH of buffer added to the mobile phase

The effect of the pH of the buffer to be added to the mobile phase containing 0.20 *M* sodium perchlorate and $8.5 \cdot 10^{-5}$ *M* TMK was examined in the pH range 2.5–5.0 by using acetic acid–sodium acetate. A good peak shape and a higher peak of the Pt(II)–TMK complex were obtained in the pH range 3.0–4.0, but below or above this

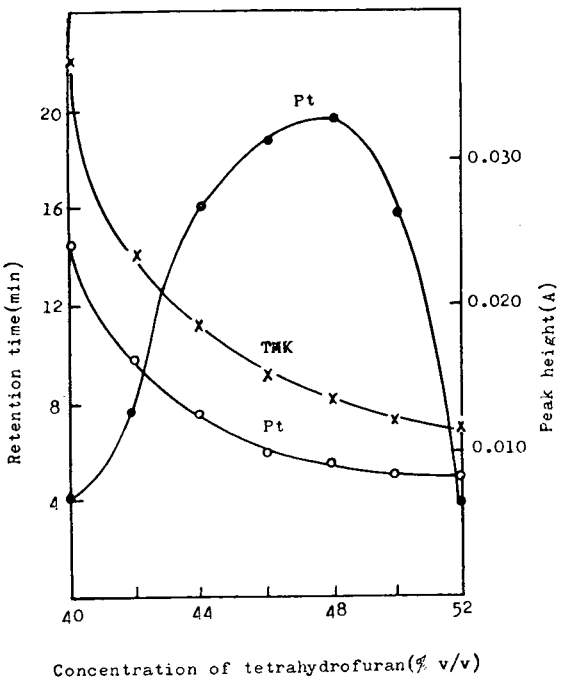

Fig. 1. Effect of concentration of tetrahydrofuran in the mobile phase on the retention time and the peak height of the complex of Pt(II)–TMK. Mobile phase, 0.035 *M* acetic acid–sodium acetate (pH 3.5), 0.20 *M* sodium perchlorate and $8.5 \cdot 10^{-5}$ *M* TMK, flow-rate, 0.6 ml min^{-1}; column, Nucleosil C_{18} (250 mm × 4.0 mm I.D.). × = Retention time of TMK; ○ = retention time of Pt; ● = peak height of Pt.

range the peak shape and peak height became worse because protonation and decomposition of the ligand occurred at high and low pH, respectively. Therefore, acetic acid–sodium acetate buffer solution of pH 3.5 was added to the mobile phase to give a concentration of 0.035 *M*.

3.4. Effect of TMK concentration in the mobile phase

If there was no TMK in the mobile phase, the peak height of the Pt(II)–TMK complex was very low. Because it is poorly stable, the complex injected may be gradually dissociated owing to dilution by a large volume of mobile phase without adding TMK. To suppress the decomposition of the complex, TMK was added to the mobile phase. An almost constant peak height was obtained at TMK concentrations greater $5 \cdot 10^{-5}$ *M*. The optimum concentration was obtained with $8.5 \cdot 10^{-5}$ *M* TMK in the mobile phase.

3.5. Effect of concentration of sodium perchlorate in the mobile phase

The effect of the concentration of sodium perchlorate in the mobile phase was investigated. As expected, the greater the concentration of sodium perchlorate, the longer was the retention time and the higher was the peak of the Pt(II)–TMK complex, and the better the resolution of peaks for the complex and unreacted reagent became. It is thought that the retention time of the complex increases on increasing the distribution of the complex to the stationary phase, based on the formation of an ion pair between the complex cation [22], $[Pt(TMK)_4]^{6+}$, and perchlorate anion. A concentration of 0.2 *M* sodium perchlorate in the mobile phase was selected.

3.6. Chromatogram and calibration graph

A typical chromatogram for the separation of the Pt(II)–TMK complex and unreacted reagent is shown in Fig. 2. The peak-height calibration graph was linear over the Pt(IV) concentration range 0.02–2.5 μg ml^{-1}, which is represented by the equation y (absorbance) = $0.0274x(\mu g\ ml^{-1}) + 0.0084$. The absolute detection limit, calculated as the amount injected that gave a signal that was three times the background noise (i.e., a signal-to-noise ratio of 3:1), was 0.11 ng.

3.7. Effect of foreign ions

The effect of possible interferences was studied by adding each foreign ion in turn to the sample before precolumn derivatization of the Pt(II)–TMK complex. The maximum levels (in μg) of foreign ions which gave a change of less than ±5% in the peak height of the Pt(II)–TMK complex that could be tolerated in the determination of 10 μg of platinum were as follows:

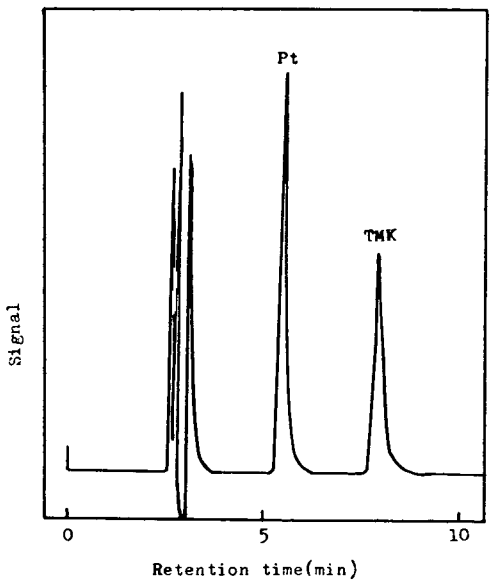

Fig. 2. Chromatogram of Pt(II)–TMK complex on a Nucleosil C_{18} column (250 × 4.0 mm I.D.) with a 20-μl injection of a solution containing 10 ppm of Pt(IV) and 20 ppm of Pd(II) using tetrahydrofuran–water (48:52, v/v) containing 0.035 *M* acetic acid–sodium acetate buffer (pH 3.5), 0.2 *M* sodium perchlorate and $8.5 \cdot 10^{-5}$ *M* TMK as the mobile phase at a flow-rate of 0.6 ml min^{-1}. Detection wavelength, 520 nm.

Cd(II), Co(II), Fe(II, III) and Ni(II), 40; Ru(IV), Rh(III), Pd(II), Os(VIII) and Ir(IV), 20; and Ag(I), Au(III), Cu(II) and Hg(II), 10. Of the metal ions tested, only Pb(II) caused a serious interference in the determination of platinum.

Table 1
Determination of platinum in cisplatin and carboplatinum

Added (μg)		Found[a] (μg)	
Cisplatin	Carboplatinum	Cisplatin	Carboplatinum
0.50	0.50	0.48	0.49
1.00	1.00	1.02	0.98
5.00	5.00	5.03	4.92
10.0	10.0	10.2	9.84
20.0	20.0	20.3	19.5

[a] Average of two parallel determinations.

3.8. Application to the determination of platinum in cisplatin and carboplatinum

The results for the determination of platinum in cisplatin and carboplatinum are given in Table 1 and show good agreement with the standard values, with satisfactory accuracy.

Acknowledgement

The financial support provided by National Natural Science Foundation of China is gratefully acknowledged.

References

[1] E. Watanabe, H. Nakajima, T. Ebina, H. Hoshino and T. Yotsuyanagi, *Bunseki Kagaku*, 32 (1983) 469.
[2] E.M. Basova, T.A. Bol'shova, V.M. Ivanov and N.B. Morozova, *Zh. Anal. Khim.*, 44 (1989) 680.
[3] T.A. Bol'shova, P.N. Nesterenko, E.M. Ivanov and N.B. Morozova, *Zh. Anal. Khim.*, 42 (1987) 1648.
[4] R.S. Chen, M.C. Liu and Z.D. Hu, *Sepu*, 6 (1988) 34; *Anal. Abstr.*, 50 (1988) 9B124.
[5] N. Uehara, Y. Annoh, T. Shimizi and Y. Shijo, *Anal. Sci.*, 5 (1989) 111.
[6] N.A. Beketova, E.M. Basova, V.M. Ivanov and T.A. Bol'shova, *Zh. Anal. Khim.*, 45 (1990) 2178.
[7] E.M. Shapovalova, I.V. Mishenina, E.M. Basova, T.A. Bol'shova and O.A. Shpigun, *Zh. Anal. Khim.*, 46 (1991) 1503.
[8] Q.F. Liu, Y.C. Wang, J.C. Liu and J.K. Cheng, *Fenxi Huaxue*, 20 (1992) 1088.
[9] I.R. Alimarin, E.M. Basova, A.Yu. Malykhin and T.A. Bol'shova, *Talanta*, 37 (1990) 485.
[10] B. Wenclawiak and F. Bickmann, *Bunseki Kagaku*, 33 (1984) E67.
[11] T. Ebina, H. Suzuki and T. Yotsuyanagi, *Buseki Kagagu*, 32 (1983) 575.
[12] B.J. Mueller and R.S. Lovett, *Anal. Chem.*, 57 (1985) 2693.
[13] B.J. Mueller and R.S. Lovett, *Anal. Chem.*, 59 (1987) 1405.
[14] M. Gill, Y.T. Shih and P.W. Carr, *Talanta*, 36 (1989) 293.
[15] K.-H. Konig, I. Kessler, M. Schuster and B. Sleinbrech, *Fresenius' Z. Anal. Chem.*, 322 (1985) 33.
[16] L.Y. Li, D.R. Li and S.R. Zhang, *Chem. Reagents*, 13 (1991) 236.
[17] S.J. Bannister, L.A. Sternson and A.J. Repta, *J. Chromatogr.*, 173 (1979) 333.

[18] R.F. Borch, J.H. Markorvitz and M.E. Pleasants, *Anal. Lett.*, 12 (1979) 917.
[19] P.A. Andrews, W.E. Wung and S.B. Howell, *Anal. Biochem.*, 143 (1984) 46.
[20] N.P. Feng, S.L. Lu, M.L. Lu and R.X. Xue, *Acta Acad. Med. Shanghai*, 17 (1990) 555.
[21] N.P. Feng, M.L. Lu, Y.F. Zhu and X.Y. Shi, *Acta Acad. Med. Shanghai*, 17 (1990) 459.
[22] W.B. Chang, X.P. Li, R.Y. Kang and Y.X. Ci, *Rare Met.*, 5 (1986) 122.

ELSEVIER

Journal of Chromatography A, 684 (1994) 360–365

JOURNAL OF CHROMATOGRAPHY A

Short communication

Enantiomeric and isotopic analysis of flavour compounds of some raspberry cultivars

Hervé Casabianca*, J. Bernard Graff

Service Central d'Analyse du CNRS, B.P. 22, F-69390 Vernaison, France

First received 7 March 1994; revised manuscript received 1 July 1994

Abstract

Analytical results from enantiomeric and isotopic analyses of four typical raspberry aroma compounds, α- and β-ionones, δ-decalactone and raspberry ketone, are reported. Different raspberry cultivars and commercial raspberry flavoured products were analysed, and a principal component analysis was carried out on the results. Using these methods, a cultivar discrimination was possible and significant information was obtained on the flavour of different cultivars. It was also possible to discriminate between natural and adulterated samples.

1. Introduction

Raspberry is a fruit mainly used in the food industry (baking, jam, syrup and juice). Therefore many authors have worked on its chemical characterization. Chromatographic methods of authentification were carried out [1] in 1965 and increasing numbers of components have been identified with the modernisation of analytical techniques since the study of Winter and Enggist [2]. Latrasse [3] proposed an aroma index in order to evaluate the flavour intensity and the "hedonic" part of several raspberries cultivars. In the 1980s particular attention was paid to a flavour impact molecule, 4-(*p*-hydroxyphenyl)-2-butanone, called raspberry ketone, whose olfactory impact was closely related to the fresh raspberry fruit. Several correlations between different cultivars were carried out [4,5].

New methods of detecting adulteration made it possible for the analyst to discard sensory evaluation of raspberry ketone and to replace it by the examination of the chirality of certain raspberry aroma compounds such as α-ionone or theaspirane diastereoisomers [6].

In our study, we aimed to use modern methods to check the chiral and isotopic "quality" and to quantify flavour impact molecules. The present report shows that these two aspects of the analysis of the fruit can be described by principal component analysis (PCA) and can also determine the authenticity and sensory quality of the product.

2. Experimental

2.1. Samples

Natural samples of Mecker, Heritage and Williamette raspberry cultivars were provided by Sicoly and Flores. The origin of other cultivars

* Corresponding author.

0021-9673/94/$07.00
SSDI 0021-9673(94)00618-0

was Ardeche (South of France). Raspberry-flavoured products (tea, syrup, juice) were bought on the local market.

2.2. Apparatus

Concentrated raspberry oils were analysed by GC–MS (Hewlett-Packard 5890 mass-selective detector) using the specific ion monitoring (SIM) method, which is specific and sensitive for particular molecules. Column: HP1, 25 m × 0.25 mm I.D., film thickness: 0.25 μm (Hewlett-Packard); carrier gas: He, 138 kPa; temperature program: 50°C for 5 min, 5°C min^{-1} to 200°C, 25°C min^{-1} to 295°C, 10 min at 295°C; temperature of injection: 280°C. Selected ions: m/z 192, 1 to 24.8 min (α- and β-ionones); m/z 99, 24.8 to 26 min (δ-decalactone); m/z 164, 26 min to end of run (raspberry ketone). Splitless injection; injection volume: 0.4 μl.

Chirality measurements were carried out on a Sichromat II (Siemens, Karlsruhe, Germany) with double ovens and pneumatic heart cut switching, allowing multidimensional gas chromatography (MDGC). Precolumn : 25 m × 0.32 mm I.D. coated with BP 20 from SGE; film thickness: 0.5 μm; carrier gas: He, 138 kPa; injection temperature: 250°C (flame ionization detection, FID); detector temperature: 250°C; program: 120°C for 5 min, 10°C min^{-1} to 220°C. Main column: 25 m × 0.22 I.D. coated with 10% octakis-2,6-dimethyl-3-trifluoroacetyl-γ-cyclodextrin in OV-1701 (MEGA, Milan, Italy); carrier gas: He, 96 kPa; detector temperature: 250°C (FID); program: 110°C for 10 min, 1°C min^{-1} to 180°C; injection volume: 1 μl.

Isotope ratios $^{13}C/^{12}C$ were measured on a MAT 252 (Finnigan, Bremen, Germany) with combined GC–combustion unit on CuO at 800°C–isotopic ratio mass spectrometry (IRMS) set on m/z 44, 45, 46. Column: HP1, 25 m × 0.25 mm I.D., film thickness: 0.25 μm (Hewlett-Packard); injection temperature: 285°C, splitless; carrier gas: He, 90 kPa; injection volume: 0.4 μl; temperature program: 50°C for 15 min, 5°C min^{-1} to 140°C, 2°C min^{-1} to 250°C, 15 min at 250°C.

Results are expressed as $\delta = [(R_{exp} - R_{ref})/R_{ref}] \cdot 1000$, where R is the isotope ratio $^{13}C/^{12}C$ and where the reference is a calcium carbonate (the P.D. Belemnita of South Carolina). δ is expressed in ‰ [7].

PCA was carried out on Statgraphics US (STSC, Rockville, MD, USA) integral software.

2.3. Sample preparation

A 500-g amount of fresh raspberries was ground with 300 ml distilled water and 200 ml distilled acetone to improve the extraction from the pulp of certain aroma compounds such as raspberry ketone. Pulp and juice were separated by filtration through sand.

After acetone removal under vacuum at ambient temperature, the aqueous raspberry juice was extracted in a separatory funnel with 250 ml of a mixture of pentane–diethyl ether (50:50). The organic layer, containing most of the aroma compounds, was dried over anhydrous Na_2SO_4 and concentrated at 40°C to a volume of 25 ml. An injection volume of 1 μl is taken for the GC–MS analysis. The 25 ml were reduced further to 2 ml and 1 μl of the residual oil injected for MDGC and GC–IRMS analysis.

If the chromatogram is complex, the sample can be cleaned up by a 2-step process, viz. first washing the ether extract with sodium hydrogencarbonate (10%) and then with water, and then pouring the ether extract through a column of activated Florisil and eluting the flavour compounds with dichloromethane–acetone (90:10). After such a treatment, the quality of resolution and background are optimised.

3. Results and discussion

In the natural fruit one enantiomer predominates whereas synthetic molecules have a racemic distribution. In the same way, the ^{13}C content of natural molecules can differ from the synthetic ones. The authentification methods are based on these two possibilities of discrimination [8].

Table 1
Chiral and isotope $^{13}C/^{12}C$ measurements with quantitative ratios of natural raspberry samples

Cultivar and characterization		δ-Decalactone enantiomeric excess (%)	δ-Decalactone isotope ratio $^{13}C/^{12}C$ (‰)	α-Ionone enantiomeric excess (%)	α-Ionone isotope ratio $^{13}C/^{12}C$ (‰)	Raspberry ketone isotope ratio $^{13}C/^{12}C$ (‰)	*cis*-3-Hexen-1-ol isotope ratio $^{13}C/^{12}C$ (‰)[a]	Quantitative ratio R1 = δC_{10}/α-ionone	Quantitative ratio R2 = α-ionone/β-ionone	β-Ionone isotope ratio $^{13}C/^{12}C$ (‰)
Natural Mecker (1993)	July	98 to 100 (*S*)	−34 to −39	98 to 100 (*R*)	−33 to −35	−28.9 to 31.9	−39.1	20 to 130	0.4 to 2.4	−32.2 to −33.9
	August	98 to 99 (*S*)	−36 to −39.1	98 (*R*)	−33 to −36	−30.6 to −32	−39.1	20 to 31	0.9 to 1.0	−32.3 to −31
Natural Heritage X (August 1993)		100 (*S*)	−33.3 to −35.9	98 (*R*)	−36.5 to −37.5	−28.8 to −30.2	−35.2	7 to 20	0.6 to 1.5	−32.2 to −34.1
		99 (*S*)	−40.2	98 (*R*)	−36	−30.1	n.d.	55	1.0	−33.7
Natural wild (1993)		100 (*S*)	−37.2	99 (*R*)	−33.6	−35.1	−34.6	8	0.9	−33.0
Natural Williamette (1992)		99 (*S*)	−35.0	99 (*R*)	−34.3	−30.0	−35.4	50	0.6	−34.4
Natural Malling Promise (1992)		99 (*S*)	−34.0	100 (*R*)	−32.5	−30.0	−33	16	0.7	n.d.

n.d. = Not detected. X is a Mecker's sample supplied under the name Heritage.
[a] Measurements made on a mixture of different samples.

Table 2
Chiral and isotope $^{13}C/^{12}C$ measurements with quantitative ratios of raspberry-flavoured products

Commercial Samples		δ-Decalactone enantiomeric excess (%)	δ-Decalactone isotope ratio $^{13}C/^{12}C$ (‰)	α-Ionone enantiomeric excess (%)	α-Ionone isotope ratio $^{13}C/^{12}C$ (‰)	Raspberry ketone isotope ratio $^{13}C/^{12}C$ (‰)	*cis*-3-Hexen-1-ol isotope ratio $^{13}C/^{12}C$ (‰)	Quantitative ratio R1 = δC_{10}/α-ionone	Quantitative ratio R2 = α-ionone/β-ionone	β-Ionone isotope ratio $^{13}C/^{12}C$ (‰)
Syrups	SA	100 (*S*)	−34	100 (*R*)	−35.8	−31.9	n.d.	11	50	−29.5
	SB	2 (*S*)	−26.3	4 (*R*)	−27.8	−24.0	n.d.	0.5	9	−26.3
Heavy Juice	BA	100 (*S*)	−28.3	100 (*R*)	−34.3	−29.1	n.d.	23	3	−33.1
	BB	100 (*S*)	−29.5	4 (*R*)	−26.0	−29.3	n.d.	4	2.1	−26.0
Tea		0	−27.6	8 (*R*)	n.m.	−25.2	n.d.	0.2	100[a]	n.d.

n.m. = Detected but not measurable; n.d. = not detected.
[a] R2 theorically equal to $+\infty$.

Four flavour impact molecules of raspberry were selected: α- (CAS No. 127-41-3) and β-ionones (CAS No. 14901-07-6), giving for the first a woody violet-like odor, whereas the second makes a more floral impact; δ-decalactone (CAS No. 705-86-2) which provides a peachy/apricot-like olfactory impression and the raspberry ketone or 4-(*p*-hydroxyphenyl)-2-butanone (CAS No. 5471-51-2), whose impact is clearly reminiscent of fresh raspberry.

From previous chiral studies, the enantiomeric distribution was expected to be strongly in favour of the *R* form for the *trans*-α-ionone [9] whereas the δ-decalactone occurs only in its *S* form [10] in the fruit.

The observed strong enantiomeric excesses of α-ionone and δ-decalactone in the natural products (Table 1) agreed with the literature [6], whereas in some cases commercial raspberry-flavoured products (Table 2) gave nearly racemic distributions.

The $^{13}C/^{12}C$ isotope ratio of the raspberry ketone (Table 1) and δ-decalactone revealed significant differences between the nature of identical molecules of synthetic origin and the natural molecules, particularly for δ-decalactone which showed a strong negative isotopic deviation ($-34‰$ to $-40‰$). *cis*-3-Hexen-1-ol showed a relatively low ^{13}C content. Table 1 gives the isotope ratios found in the different cultivars. Wild fruits showed lower δ values for raspberry ketone than cultivated species and this can help to distinguish the two groups.

Concentrations of the four chosen molecules are useful parameters. There was an increase in the level of aroma compounds within the Mecker cultivars from July to August; these measurements explain the fact that July raspberries did not have as pronounced a taste as those from August. The results we obtained are quite different from those given in the literature [5]. However, in the determination of such concentrations, the initial quantity of raspberries extracted needs to be known accurately. Such accurate information is rarely available in the case of commercial products. In order to avoid having to depend on the initial quantity, we chose to compare internal ratios such as those shown in Table 1. This made it possible to compare the results from our natural samples and from samples where the quantity extracted and the method of extraction were not known.

When PCA was applied to the data a two-dimensional representation explained 77% of the variations. The six parameters chosen were δ-decalactone enantiomeric excess, α-ionone enantiomeric excess, raspberry ketone $^{13}C/^{12}C$ isotope ratio, δ-decalactone $^{13}C/^{12}C$ isotope ratio, quantitative ratio of raspberry ketone to δ-decalactone and quantitative ratio of δ-decalactone to α-ionone.

The first steps of PCA analysis extracted α-ionone enantiomeric excess and δ-decalactone $^{13}C/^{12}C$ isotope ratio as the physicochemical properties which distinguish between the synthetic group on the left of Fig. 1 and the natural group on the right. A third discriminant axis is obtained with the isotope ratio of raspberry ketone but that parameter is not sufficient to authenticate a sample because the values for natural and synthetic products are too close.

Further conclusions can be drawn in a second step of PCA (Fig. 1) when ratios of flavour compounds are examined. It is interesting to note that the quantity ratio of δ-decalactone/α-ionone appears as a discriminant axis between different natural samples. From July to August, the Mecker cultivar zone has dropped due to the increase in α-ionone which is responsible for the development of a woody odour like in the wild species. The Heritage cultivar is close to the August Meckers, but forms a distinct group, the quantity ratios α/β-ionones being somewhat higher than those of the Meckers. The cultivars, Malling Promise and Williamette, can be grouped by PCA with the Meckers from August and July respectively. The wild raspberries form a group with low δ-decalactone/α-ionone quantity ratios, which correlates with the fact that these fruits have a strong woody wild odour. A second factor which separates the wild variety from the cultivated ones is its very low $^{13}C/^{12}C$ isotope ratio for raspberry ketone.

To test the power of PCA, sample X was provided under the name "Heritage". An analysis of the parameters and comparison with the

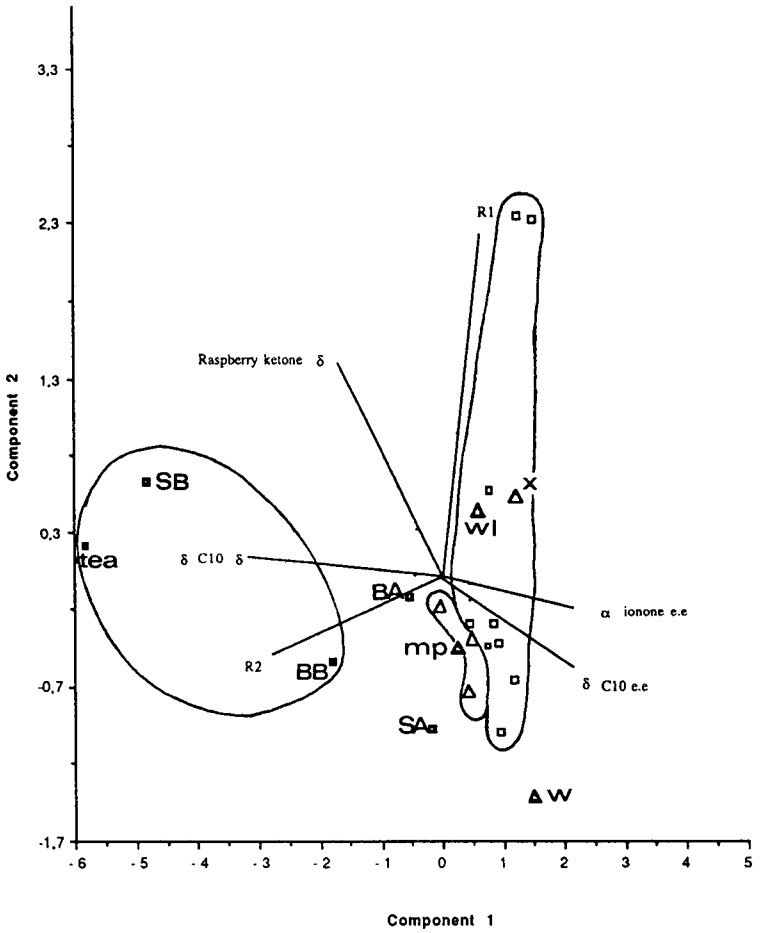

Fig. 1. Principal component analysis of raspberries samples. ■ = Raspberry-flavoured products (tea, syrup, heavy juice); □ = Mecker cultivar; △ = Heritage cultivar; ▲ = other raspberry cultivars: W = wild, mp = Malling Promise, WL = Williamette; e.e. = enantiomeric excess; δ = isotope ratio $^{13}C/^{12}C$; X = sample supplied to test discriminant power of the method; R1 = quantitative ratio raspberry ketone/δ-decalactone; R2 = quantitative ratio δ-decalactone/α-ionone.

PCA showed that sample X belonged to the Mecker group, a fact which was confirmed by the supplier.

Commercial samples like syrup SB, heavy juice BB and the tea were found to belong to the synthetic area on the left.

PCA provides a great deal of information about the nature of the fruit both with respect to authenticity and flavour. However, there is no correlation between naturalness and olfactory impressions.

4. Conclusions

The simultaneous chiral and isotopic measurement of aroma compounds together with their quantification produces results that can be used to perform PCA. The introduction of quantification parameters to an analysis brings out important points:

(1) A cultivar discrimination is possible and significant information about the taste of the different cultivars can be obtained.

(2) Although climatic variations influence the level of aroma compounds in natural samples it is still possible to discriminate between natural and adulterated samples.

Chiral chromatography and IRMS are powerful complementary methods for screening raspberry flavour in authentification problems.

Acknowledgements

We are very grateful to Mr. Massardier (Sicoly, St. Laurent d'Agny, France) and Mr. Meurisse (Flores, Grenoble, France) for providing samples and for profitable collaboration.

References

[1] R. Mestres and J. Soulie, *Trav. Soc. Pharm. Montpellier*, 25 (1965) 239.
[2] M. Winter and P. Enggist, *Helv. Chim. Acta*, 54 (1971) 1891.
[3] A. Latrasse, *Lebensm. Wiss. Technol.*, 15 (1982) 49.
[4] W. Borejsza-Wysocki, S.K. Goers, R.N. McArdle and G. Hrazdina, *J. Agric. Food Chem.*, 40 (1992) 1176.
[5] R. Renner and U. Hartmann, *Lebensmittelchem. Gerichtl. Chem.*, 39 (1985) 29.
[6] P. Werkhoff and W. Bretschneider, *Chem. Mikrobiol. Technol. Lebensm.*, 13 (1991) 129.
[7] H. Craig, *Geochim. Cosmochim. Acta*, 12 (1957) 133.
[8] A. Mosandl, *J. Chromatogr.*, 624 (1992) 267.
[9] P. Werkhoff, W. Bretschneider, M. Guentert, R. Hopp and H. Surburg, *Z. Lebensm.-Unters.-Forsch.*, 192 (1991) 111.
[10] D. Lehmann, C. Askari, D. Henn, F. Dettmar, U. Hener and A. Mosandl, *Dtsch. Lebensm. Rundschau*, 87 (1991) 75.

ELSEVIER

Journal of Chromatography A, 684 (1994) 366–369

JOURNAL OF CHROMATOGRAPHY A

Short communication

Determination of tris(2-chloroethyl) phosphate in leachates from landfills by capillary gas chromatography using flame photometric detection

Akio Yasuhara

Environmental Chemistry Division, National Institute for Environmental Studies, 16-2 Onogawa, Tsukuba, Ibaraki 305, Japan

Received 16 May 1994

Abstract

Tris(2-chloroethyl) phosphate (TCEP) in leachates from landfills for hazardous wastes was determined by wide-bore capillary gas chromatography using flame photometric detection. Its concentration levels ranged from 0.137 to 5.43 mg/l. The origin of TCEP seems to be waste plastics. No TCEP was detected in underground water and tap water.

1. Introduction

Tris(2-chloroethyl) phosphate (TCEP) is widely used as a plasticizer and a fire retardant in various kinds of synthetic resins. As the LD_{50} value of TCEP aqueous solution in acute toxicity using carp has been estimated to be 5 mg/l [1], environmental contamination with TCEP has attracted strong interest. Careless disposal of waste plastics might cause important problems. Several studies on environmental contamination with TCEP have been reported. The concentration of TCEP in water samples in Japan [2–4] has been found to be higher than that in the USA [5] or Spain [6]. It is of serious concern to people who live near waste disposal sites and use underground water or river water as drinking water how high the concentration of TCEP in leachates from landfill sites is. This paper describes the determination of the concentration of TCEP in leachates in Japan.

2. Experimental

2.1. Materials and samples

TCEP (analytical-reagent grade) was purchased from Wako (Osaka, Japan). Dichloromethane, anhydrous sodium sulfate, hexane, benzene and acetonitrile were of pesticide grade (Wako). Hydrochloric acid and sodium hydroxide were of extra-pure grade (Wako). Silica gel (particle size 75–150 μm) (Wako) was used without any activation procedure. Pure water was prepared by passing distilled water through a Milli-Q system (Millipore).

Leachates from landfill sites located in the central area and in the north-eastern part of Japan, underground water from the north-eastern part of Japan, and tap water from the National Institute for Environmental Studies were used as samples.

0021-9673/94/$07.00
SSDI 0021-9673(94)00643-1

2.2. Sample preparation

The pH of a water sample was adjusted at 7.5–4.0 with 1 *M* hydrochloric acid or 1 *M* sodium hydroxide solution. TCEP in each water sample (1 l) was extracted three times with dichloromethane (100, 50 and 50 ml) using a separating funnel for 5 min and the extracts were combined. The combined extract was passed through a short column packed with anhydrous sodium sulfate and concentrated by distillation of the solvent under atmospheric pressure. The concentrated extract solution (1 ml) was subjected to silica gel column chromatography on a glass column (150 × 12 mm I.D.) containing 5 g of silica gel packed with hexane. The following solvents were used for chromatography; fraction A, dichloromethane–hexane (1:9), 40 ml; fraction C, dichloromethane, 40 ml; and fraction D, acetonitrile–dichloromethane (1:9), 50 ml. TCEP eluted in fraction D. Fraction D was concentrated by distillation under atmospheric pressure and an aliquot of the concentrated solution was injected into a gas chromatograph (see below).

2.3. Chromatographic analysis

The gas chromatographic conditions were as follows: gas chromatograph, Hewlett-Packard Model 5890A equipped with a Hewlett-Packard Model 3396A integrator; column, J&W DB-1 (1.5 μm) (30 m × 0.53 mm I.D.); column temperature, 180°C for 5 min, increased to 240°C at 8°C/min; carrier gas (helium) flow velocity, 43.1 cm/s at 25°C; injector temperature, 250°C; injection mode, whole injection; detector, flame photometric; detector temperature, 230°C; and make-up gas (nitrogen) flow-rate, 33.5 ml/min.

3. Results and discussion

The distribution coefficients of TCEP between organic solvents and water were measured in order to select the best solvent for the extraction of TCEP. The distribution coefficients were 0.320 for hexane, 16.3 for benzene and 115 for dichloromethane. Therefore, dichloromethane was chosen as the extraction solvent.

The relationship between pH and recovery was studied. The recoveries were 94, 89 and 78% at pH 4, 7 and 10, respectively. Hence alkaline conditions are not to be preferred, and also strongly basic or acidic conditions should be avoided because of hydrolysis of TCEP. Therefore, neutral or weakly acidic conditions are suitable for the extraction of TCEP.

Recovery experiments were performed using aqueous solutions of TCEP at the concentrations of 300, 900 and 3000 ng/l. The recoveries were 98.1, 102.0 and 97.4%, respectively. As mean recovery was 99.2%, it is concluded that all the TCEP was recovered.

Instrumental stability in the measurement of TCEP was studied by replicated measurements of standard TCEP solution at a concentration of 139 ng/ml. The relative standard deviation was around 9%. This fairly high relative standard deviation might be due to the flame photometric detector.

Linearity of the detector response with respect to TCEP concentration was investigated. The calibration graph is shown in Fig. 1. The linearity range was fairly narrow. The reason seems to be the strong absorbability of TCEP on the inner surface of the capillary column. The ratio of the inner surface area to the inner volume of the

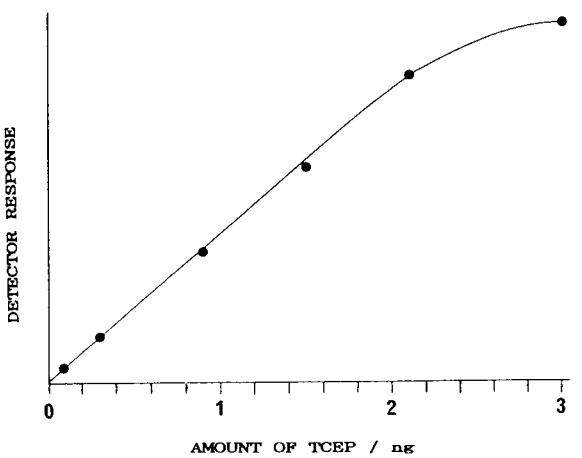

Fig. 1. Calibration graph for TCEP using flame photometric detection.

capillary column affects the range of linearity. The larger the inner diameter of a capillary column is, the wider the linearity range becomes. This phenomenon has been observed in the determination of TCEP by other workers [7]. Therefore, a wide-bore capillary column was used in this study.

The blank in the analytical procedure was examined using pure water. No contamination with TCEP was observed.

The detection limit (DL) and quantification limit (QL) were calculated according to the following equation [8] defined by the Japan Environmental Agency on instrumental analysis for chemical components in replicated recovery experiments using water samples:

$$DL = 3D$$

$$QL = 10D$$

$$D = t(n-1, 0.05) \cdot (\text{S.D.}/n) \cdot (C/R)$$

where $t(n-1, 0.05)$, S.D., n, C and R are a value in a Student's t examination for 95% reliability, standard deviation in the response of the detector, total run number, concentration in water sample and the mean of the detector responses, respectively. D is called the detection power. In this recovery experiment, it is most important that the concentration in the water sample should be near the estimated value, which is calculated to be around ten times the instrumental detection limit. Generally D is the mean obtained in experiments using several different concentrations. In this study, aqueous solutions of TCEP of concentrations 200 and 400 ng/l were prepared and recovery experiments were performed. The mean D value was 22.5 ng/l. Therefore, DL and QL were 67.5 and 225 ng/l, respectively. When the concentration of TCEP in actual samples is below 67.5 ng/l, the concentration is considered as "not detected". When the concentration of TCEP in actual samples ranges between 67.5 and 225 ng/l, the concentration is considered as "detected, but not determined".

The effect of clean-up by silica gel column chromatography is shown in Fig. 2. Large amounts of organic components give false signals

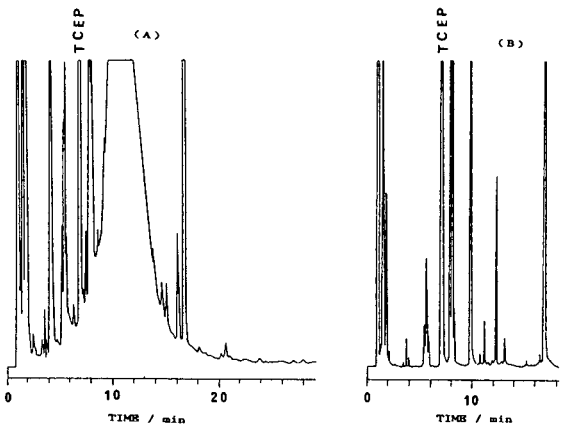

Fig. 2. Gas chromatograms of extracts of the leachate from landfill site D. (A) Before clean-up; (B) after clean-up with silica gel column chromatography.

with flame photometric detection. As especially leachates from landfill sites contain large amounts of chemical components, this clean-up procedure is essential. On the other hand, this clean-up procedure may be omitted for underground water and tap water, which contain only trace amounts of organic components.

Analytical results for actual samples are given in Table 1. No TCEP was detected in underground water and tap water. High concentrations of TCEP were detected in all leachate samples. These high concentrations were much higher than those in river waters in Japan [2–4]. These high concentrations of TCEP can reasonably be expected because large amounts of municipal, industrial and sewage wastes are disposed of every day. Kawagoshi et al. [9] reported that concentrations of TCEP in leachates from landfills in Japan reach extremely high levels. Also,

Table 1
Concentrations of TCEP in water samples

Samples	TCEP concentration (mg/l)
Tap water	Not detected
Underground water	Not detected
Leachate from landfill site A	0.137
Leachate from landfill site B	0.336
Leachate from landfill site C	0.534
Leachate from landfill site D	5.43

high concentrations of TCEP in leachates were confirmed by gas chromatography–mass spectrometry. It is serious that the concentration of TCEP in the leachate from the landfill site D exceeded the LD_{50} value. Experiments on leaching TCEP from plastics are in progress. Most waste plastics are buried rather than burned in the Japanese administration system. Detailed investigations on TCEP in leachates from landfills will be performed in near future.

References

[1] L.P. Burkhard, E.J. Durhan and M.T. Lukasewycz, *Anal. Chem.*, 63 (1991) 277–283.
[2] S. Ishikawa, M. Taketomi and R. Shinohara, *Water Res.*, 19 (1985) 119–125.
[3] K. Kenmotsu, Y. Okamoto, Y. Ogino, K. Matsunaga and T. Ishida, *Okayamaken Kankyo Hoken Senta Nenpo*, 9 (1985) 160–169.
[4] S. Ishikawa, K. Shigezumi, K. Yasuda and N. Shigemori, *Suishitsu Odaku Kenkyu*, 8 (1985) 529–535.
[5] G.L. LeBel, D.T. Williams and F.M. Benoit, *Adv. Chem. Ser.*, 214 (1987) 309–325.
[6] D. Barceló, C. Porte, J. Cid and J. Albaigés, *Int. J. Environ. Anal. Chem.*, 38 (1990) 199–209.
[7] Papers presented at the *2nd Meeting on Leachates from Landfill Buried with Hazardous Wastes, March 8, 1994, Tsukuba, Japan.*
[8] *Manual on Development of Analytical Methods for Hazardous Chemical Compounds*, Japan Environmental Agency, Tokyo, 1987, pp. 186–191.
[9] Y. Kawagoshi, I. Fukunaga and M. Fukushima, *Haikibutsu-Gakkai Kenkyu Hapyokai Koen Ronbunshu*, 4 (1993) 527–530.

ELSEVIER

Journal of Chromatography A, 684 (1994) 370–373

JOURNAL OF CHROMATOGRAPHY A

Short communication

Simple, inexpensive system for using thin-layer chromatography for micro-preparative purposes

Konrad Läufer, Jochen Lehmann*, Stefan Petry, Markus Scheuring, Markus Schmidt-Schuchardt

Institut für Organische Chemie und Biochemie der Universität Freiburg, Albertstrasse 21, D-79104 Freiburg im Breisgau, Germany

First received 4 March 1994; revised manuscript received 9 June 1994

Abstract

Glass high-resolution TLC plates were used to separate very small amounts of material (ng–mg). Either spots or linear zones can be quantitatively eluted after separating them from the surroundings with a fast-moving drill, which removes thin lines of layer material. Elution is carried out by siphoning eluent through a specially formed sintered glass on to one end of the zone or spot and picking up the eluate at the other with a piece of filter-paper carton. The latter can be extracted by soaking and centrifugation. Application in the carbohydrate field is demonstrated by a preparative isolation for structural analysis of three components and the determination of different amounts of one compound for analytical purposes.

1. Introduction

Separation, purification and isolation of chemical products from complex mixtures in minute amounts has been the aim of generations of chemists, especially those working with natural products and biochemists searching for metabolites. Of all micro-scale methods, TLC is by far the most popular owing to its simplicity, flexibility in trying out conditions and speed. This is especially so since industry has developed coatings, mostly silica gel, which are equal to GLC in their resolving capacity. Working with small amounts (ng–mg) of complex mixtures of radioactively labelled compounds and compounds carrying chromophor or fluorescent groups, we apply TLC or high-performance (HP) TLC plates, depending on the amount and separability of the mixture to be resolved. A procedure generally used is to scrape off the coating with the adsorbed compound and extract this compound [1].

2. Experimental and results

2.1. Chromatography

Commercial glass TLC plates (Merck, Darmstadt, Germany) are used for the separation of a mixture of compounds. The substances should normally be visible, or made visible under UV radiation or by autoradiography. There is also the possibility of detecting the compounds with a

* Corresponding author.

0021-9673/94/$07.00
SSDI 0021-9673(94)00571-P

reagent on part of the plate and to mark the corresponding zones for elution. Here the best approach is to cut a narrow strip off the plate for detection. In this paper we describe a preparative application with an artificial mixture of three monosaccharides, D-glucose (Glc), D-galactose (Gal) and D-N-acetylglucosamine (GlcNAc) and an analytical application by establishing a calibration graph for a maltose derivative to follow the rate of enzymic maltose liberation.

For the purpose of demonstrating the stages of the procedure in Figs. 1 and 2 a mixture of three dyes was applied to a TLC plate, clearly visible in daylight.

2.2. Zone extraction

The zone to be extracted has to be separated from its neighbours by cutting lines into the coating with a microdrill and then totally remove the adsorbent from the glass support (Fig. 1). A vacuum pipe should be used to suck up loose silica gel dust, especially when the compounds separated are toxic or radioactive.

In a case, which can be tightly closed with a glass plate (Fig. 2) to ensure saturation with the solvent, the TLC plate is placed on a rectangular plateau flanked on the sides with two basins containing the solvent. With a specially cut

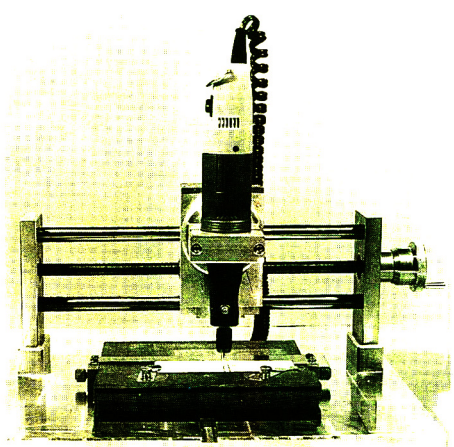

Fig. 1. Microdrill for the separation of zones.

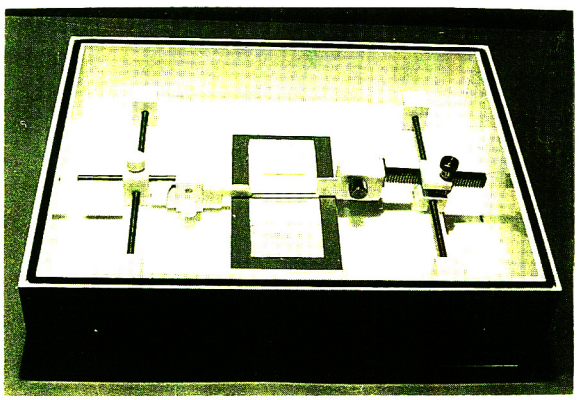

Fig. 2. Elutor for the elution of chemical substances from commercially available TLC and HPTLC plates.

sintered glass the solvent is applied to one end of the zone, where elution of the compound begins. At the other end a rectangular piece of filter-paper carton (Whatman 17 Chr, 3 × 1 cm) is positioned with one tip touching the coating. The extract is collected in the paper in a circular zone. Extraction is usually quantitative when the radius of the wet segment is ca. 0.5 cm.

2.3. Filter-paper extraction

The paper segment containing the compound is cut into strips (ca. 1 mm) and placed upright in a PTFE cartouche, which has a small perforation in the lower tip and fits into an Eppendorf reaction vessel (Eppendorf–Netheler–Hinz, Hamburg, Germany). The paper strips are soaked with an appropriate solvent mixture (a mixture of water and methanol or ethanol dissolves a great number of different products, especially carbohydrate derivatives). Usually 0.1 ml is optimal. After 10 min the solution is centrifuged for 3 min in an Eppendorf Model 5415 C desk centrifuge into the reaction vessel. This procedure is repeated twice, to ensure quantitative extraction of the compound. Centrifugal freeze-drying (SpeedVac concentrator; Savant Instruments, Farmingdale, NY, USA) yields a uniform compound, without any measurable loss, as could be demonstrated with radioactively labelled substances.

Including concentration to dryness, which con-

sumes the most time, the procedure, starting with the chromatographic separation, lasts not longer than 3 h.

2.4. Application

Preparative

Three monosaccharides (Glc, Gal, GlcNAc), each ca. 2 mg (together not more than 8 mg), representing a typical mixture of a poly- or oligosaccharide hydrolysate, are derivatized with 4-nitroaniline (4-NA) in dimethyl sulphoxide (DMSO) and aqueous formic acid as catalyst by mixing three solutions, a, b and c [a = 1 mg of reducing sugar–40 μl of DMSO; b = formic acid–water (9:1); c = 69 mg of 4-NA–100 μl of DMSO] in the ratio 4:1:2 and heating at 95°C for 75 min as described previously [2]. The product mixture, still containing relatively large amounts 4-NA, is applied to TLC plates (10 × 10 cm, 0.25- or 0.5-mm layer). The solution should be not more than 5% (w/v) and should be applied in only one stroke.

Separation is carried out using ethyl acetate–methanol–water (7:2:1). Three zones (I, II and III) are visible under UV–radiation (254 and 320 nm). The zones [I = 4-NA, R_F 0.75; II = N-4-nitrophenyl-β-D-glucopyranosylamine, R_F 0.57; III = N-4-nitrophenyl-β-D-galactopyranosyl- and N-acetyl-β-D-glucopyranosylamine, R_F 0.53 (these two cannot be separated under these conditions)] are separately eluted [methanol–water (3:1)] and isolated as described in Sections 2.2 and 2.3.

The sugar derivatives from zones II and III are converted into their per-O-acetates in the conventional way [3], using 100 μl of acetic anhydride–pyridine (1:1, v/v). Excess reagent is decomposed with a few drops of methanol and the reaction mixture is evaporated by centrifugal freeze-drying (see Section 2.3).

N-4-Nitrophenyl-2,3,4,6-tetra-O-acetyl-β-D-glucopyranosylamine (**1**) the compound from zone II is uniform as such and its structure can be determined by ^{1}H NMR spectroscopy. The acetylated compounds from zone III according to TLC in ethyl acetate–cyclohexane (1:1) separate N-4-nitrophenyl-2,3,4,6-tetra-O-acetyl-β-D-galactopyranosylamine (**2**), R_F 0.3, and *N*-4-nitrophenyl-3,4,6-tri-O-acetyl-2-N-acetyl-β-D-glucopyranosylamine (**3**), R_F 0.13, which can be separately eluted.

To elute the hydrophobic acetates from silica gel, ethanol–chloroform (1:1, v/v) is used. The overall yields of the acetates, which are uniform by HPTLC and pure by ^{1}H NMR of a standard, starting from the mixture of free monosaccharides, are **1** = 84%, **2** = 80% and **3** = 73%. Considering the two chemical reactions, these yields are acceptable. The extraction procedures are essentially quantitative, as could be demonstrated with a radioactive sample of [^{14}C]-D-glucose derivative.

Analytical

Six samples of aqueous solutions containing from 2.69 to 0.084 mg of maltose [4] were evaporated by centrifugal freeze-drying. To each sample the reagents DMSO (40 μl), solution b (10 μl) and solution c (20 μl) were added and treated as described in Section 2.4. After diluting the reaction mixtures each with the same amount of methanol (140 μl), aliquots (1 μl) were applied as spots on the concentration zone of HPTLC plates, separated by ca. 2 cm and chromatographed using ethyl acetate–methanol–water (7:2:1). The product N-4-nitrophenylmaltosylamine (R_F 0.39) is clearly visible under UV radiation. The zones containing the derivative are eluted and worked up as described in Sections 2.2 and 2.3. The isolation procedure is quantitative [the yield of isolated compound is 89% (calculated on the basis of the initial amount of maltose and measured by absorption at 375 nm)]. Measuring the UV absorption at 375 nm and plotting it against the initial amount of maltose gives the calibration graph shown in Fig. 3. If the sugar concentrations are significantly lower (ca. ten times lower than the lowest value in Fig. 3), the optical properties of the N-4-nitrophenylglycosylamines are not sensitive enough for reliable determination. In such a case the formation of dansylhydrazones [1] is advisable.

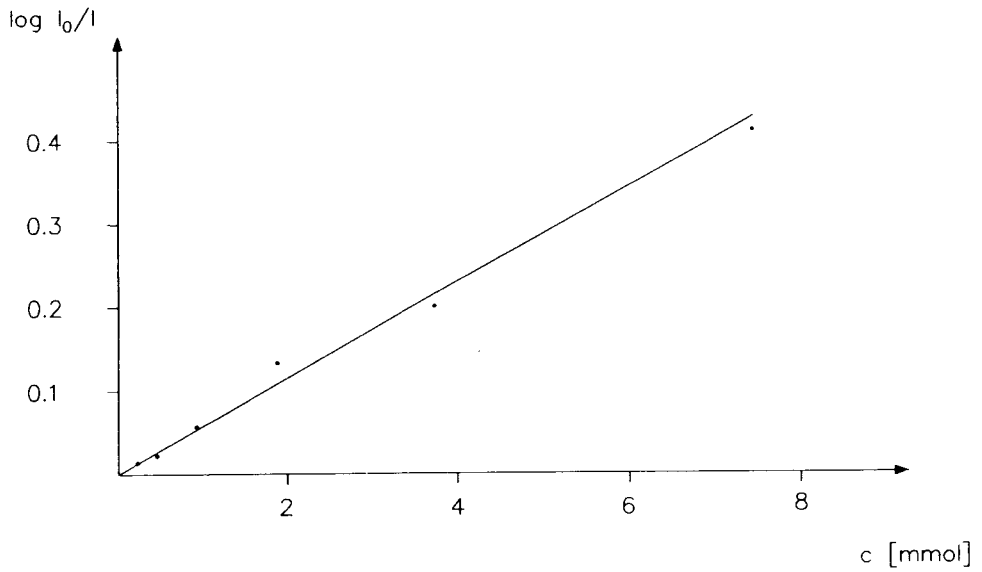

Fig. 3. Calibration graph for N-4-nitrophenylmaltosylamine, measured at 375 nm.

Acknowledgement

We thank the Deutsche Forschungsgemeinschaft for financial support.

References

[1] G. Avigad, *J. Chromatogr.*, 139 (1977) 343–347.
[2] H. Kurth and J. Lehmann, *Biomed. Chromatogr.*, 1 (1986) 58–63.
[3] R.L. Whistler and M.L. Wolfrom, *Methods Carbohydr. Chem.*, 2 (1963) 211–215.
[4] J. Lehmann, St. Petry, M. Scheuring and M. Schmidt-Schuchardt, *Carbohydr. Res.*, in press.

Author Index

Journal of Chromatography A

Request for Manuscripts

Susumu Honda will edit a special, thematic issue of the *Journal of Chromatography A* entitled

Chromatographic and Electrophoretic Analyses of Carbohydrates

Both reviews and research articles will be included.
Topics such as the following will be covered:

- Gas chromatography and gas chromatography–mass spectrometry of carbohydrates
- Supercritical fluid chromatography of carbohydrates
- Thin-layer chromatography of carbohydrates
- Liquid chromatography of carbohydrates
  - Separations based on various modes including adsorption, hydrophilic interaction, hydrophobic interaction, ion exchange, ligand exchange, size exclusion, bioaffinity, etc.
  - Derivatization
  - Preparative liquid chromatography
  - High-performance liquid chromatography–mass spectrometry
- Electrophoresis of carbohydrates
  - Gel electrophoresis
  - Capillary zone electrophoresis
  - Micellar electrokinetic capillary chromatography
  - Ultrasensitive detection
  - Derivatization
  - Capillary electrophoresis–mass spectrometry
- Chromatography and electrophoresis in glycobiology
  - Release of carbohydrates from glycoconjugates
  - Monosaccharide composition analysis
  - Oligosaccharide mapping
  - Oligosaccharide sequencing
  - Automated analysis of carbohydrates

Potential authors of reviews should contact Roger Giese, Editor, prior to any submission. Address: Mugar Building Rm 122, Northeastern University, Boston, MA 02115, USA; tel.: (+1-617) 373-3227; fax: (+1-617) 373-8720.

The deadline for receipt of submissions is **November 15, 1994**. Manuscripts submitted after this date can still be published in the Journal, but then there is no guarantee that an accepted article will appear in this special, thematic issue. Four copies of the manuscript, citing this issue, should be submitted to the Editorial Office, *Journal of Chromatography A*, P.O. Box 681, NL-1000 AR Amsterdam, The Netherlands. All manuscripts will be reviewed and acceptance will be based on the usual criteria for publishing in the *Journal of Chromatography A*.

ANALYTICAL BIOTECHNOLOGY

Proceedings of the 4th International Symposium on Analytical Methods, Systems and Strategies in Biotechnology (ANABIOTEC '92), Noordwijkerhout, The Netherlands, 21-23 September 1992

Edited by **C. van Dijk**

Previously published as part of the 1993 subscription to the journals *Analytica Chimica Acta* and *Journal of Biotechnology*

ANABIOTEC '92 focused on the further integration of biotechnology and analytical chemistry. The results of this symposium clearly demonstrated that a substantial progress could be reported in the application of both conventional and new analytical techniques, the latter essentially based on natural analytical tools such as biomolecules. The main themes covered during this meeting are fermentation monitoring, chromatography, instrumental analysis, biosensors and bioanalysis.

A selection of the contents.
Preface.
Process Control. Monitoring and control of recombinant protein production (K. Schügerl *et al.*). Rapid and quantitative analysis of bioprocesses using pyrolysis mass spectrometry and neural networks: application to indole production (R. Goodacre, D.B. Kell). Characterization of a sampling unit based on tangential flow filtration for on-line bioprocess monitoring (T. Buttler, L. Gorton, G. Marko-Varga). Automated monitoring of biotechnological processes using on-line ultrafiltration and column liquid chromatography (N.C. Van de Merbel *et al.*). On-line monitoring of penicillin V during penicillin fermentations: a comparison of two different methods based on flow-injection analysis (M. Carlsen *et al.*). Development of an on-line method for the monitoring of vicinal diketones and their precursors in beer fermentation (C. Mathis *et al.*). Monitoring of fermentation by infrared spectrometry. Alcoholic and lactic fermentations (D. Picque *et al.*).
Chromatography and other Separation Techniques. Chromatographic analysis of biopolymers distribution in "poly-hemoglobin", an intermolecularly crosslinked hemoglobin solution (J. Simoni, G. Simoni, M. Feola). Application of multivariate mathematical-statistical methods for the comparison of the retention behaviour of porous graphitized carbon and octadecylsilica columns (E. Forgács, T. Cserháti, B. Bordás).
Antibodies. Catalytic antibodies: new developments (R. Hilhorst).
Biosensors. Measurements of nitric oxide in biological materials using a porphyrinic microsensor (T. Malinski *et al.*). Reusable fiber-optic-based immunosensor for rapid detection of imazethapyr herbicide (R.B. Wong, N. Anis, M.E. Eldefrawi). Biosensor monitoring of blood lactate during open-heart surgery (M. Kyröläinen *et al.*).
Instrumental Techniques. Introduction to the dielectric estimation of cellular biomass in real time, with special emphasis on measurements at high volume fractions (C.L. Davey *et al.*). Spectral analysis of interactions between proteins and dye ligands (J. Hubble, A.G. Mayes, R. Eisenthal).
Enzymatic Analysis. Preservation of shelf life of enzyme based analytical systems using a combination of sugars, sugar alcohols and cationic polymers or zinc ions (T.D. Gibson, J.N. Hulbert, J.R. Woodward).
Colloidal Carbon Particles. Colloidal carbon particles as a new label for rapid immunochemical test methods: Quantitative computer image analysis of results (A. van Amerongen *et al.*). Author Index.

ELSEVIER SCIENCE B.V.

© 1993 208 pages Hardbound
Price: Dfl. 265.00 (US $ 151.50)
ISBN 0-444-81640-2

ORDER INFORMATION

For USA and Canada
ELSEVIER SCIENCE INC.
P.O. Box 945
Madison Square Station
New York, NY 10160-0757
Fax: (212) 633 3880

In all other countries
ELSEVIER SCIENCE B.V.
P.O. Box 330
1000 AH Amsterdam
The Netherlands
Fax: (+31-20) 5862 845

US$ prices are valid only for the USA & Canada and are subject to exchange rate fluctuations; in all other countries the Dutch guilder price (Dfl.) is definitive. Customers in the European Union should add the appropriate VAT rate applicable in their country to the price(s). Books are sent postfree if prepaid.

Bioaffinity Chromatography

Second, Completely Revised Edition

By **J. Turková**

Journal of Chromatography Library Volume 55

Bioaffinity chromatography is now the preferred choice for the purification, determination or removal of many biologically active substances. The book includes information on biologically active substances with their affinants, solid supports and methods of coupling, summarized in tables covering classical, high-performance liquid and large-scale bioaffinity chromatography.

Optimization of the preparation and the use of highly active and stable biospecific adsorbents is discussed in several chapters. Following a chapter dealing with the choice of affinity ligands, affinity-sorbent bonding is described in detail. Other chapters give information on solid supports, the most common coupling procedures and a general discussion of sorption and elution. Several applications of bioaffinity chromatography are described, e.g. quantitative evaluation of biospecific complexes and many applications in medicine and in the biotechnology industry.

Contents:

© 1993 818 pages Hardbound
Price: Dfl. 495.00 (US$ 282.75)
ISBN 0-444-89030-0

ORDER INFORMATION

ELSEVIER SCIENCE B.V.
P.O. Box 330
1000 AH Amsterdam
The Netherlands
Fax: (+31-20) 5862 845

For USA and Canada
P.O. Box 945
Madison Square Station
New York, NY 10159-0945
Fax: (212) 633 3680

US$ prices are valid only for the USA & Canada and are subject to exchange rate fluctuations; in all other countries the Dutch guilder price (Dfl.) is definitive. Customers in the European Union should add the appropriate VAT rate applicable in their country to the price(s). Books are sent postfree if prepaid.

ELSEVIER SCIENCE

PUBLICATION SCHEDULE FOR THE 1995 SUBSCRIPTION

Journal of Chromatography A and *Journal of Chromatography B: Biomedical Applications*

MONTH	O 1994	N 1994	D 1994	
Journal of Chromatography A	683/1 683/2 684/1	684/2 685/1 685/2 686/1	686/2 687/1 687/2 688/1 + 2	The publication schedule for further issues will be published later.
Bibliography Section				
Journal of Chromatography B: Biomedical Applications				

INFORMATION FOR AUTHORS

(Detailed *Instructions to Authors* were published in *J. Chromatogr. A*, Vol. 657, pp. 463–469. A free reprint can be obtained by application to the publisher, Elsevier Science B.V., P.O. Box 330, 1000 AH Amsterdam, Netherlands.)

Types of Contributions. The following types of papers are published: Regular research papers (full-length papers), Review articles, Short Communications and Discussions. Short Communications are usually descriptions of short investigations, or they can report minor technical improvements of previously published procedures; they reflect the same quality of research as full-length papers, but should preferably not exceed five printed pages. Discussions (one or two pages) should explain, amplify, correct or otherwise comment substantively upon an article recently published in the journal. For Review articles, see inside front cover under Submission of Papers.

Submission. Every paper must be accompanied by a letter from the senior author, stating that he/she is submitting the paper for publication in the *Journal of Chromatography A* or *B*.

Manuscripts. Manuscripts should be typed in **double spacing** on consecutively numbered pages of uniform size. The manuscript should be preceded by a sheet of manuscript paper carrying the title of the paper and the name and full postal address of the person to whom the proofs are to be sent. As a rule, papers should be divided into sections, headed by a caption (*e.g.*, Abstract, Introduction, Experimental, Results, Discussion, etc.). All illustrations, photographs, tables, etc., should be on separate sheets.

Abstract. All articles should have an abstract of 50–100 words which clearly and briefly indicates what is new, different and significant. No references should be given.

Introduction. Every paper must have a concise introduction mentioning what has been done before on the topic described, and stating clearly what is new in the paper now submitted.

Experimental conditions should preferably be given on a *separate* sheet, headed "Conditions". These conditions will, if appropriate, be printed in a block, directly following the heading "Experimental".

Illustrations. The figures should be submitted in a form suitable for reproduction, drawn in Indian ink on drawing or tracing paper. Each illustration should have a caption, all the *captions* being typed (with double spacing) together on a *separate sheet*. If structures are given in the text, the original drawings should be provided. Coloured illustrations are reproduced at the author's expense, the cost being determined by the number of pages and by the number of colours needed. The written permission of the author and publisher must be obtained for the use of any figure already published. Its source must be indicated in the legend.

References. References should be numbered in the order in which they are cited in the text, and listed in numerical sequence on a separate sheet at the end of the article. Please check a recent issue for the layout of the reference list. Abbreviations for the titles of journals should follow the system used by *Chemical Abstracts*. Articles not yet published should be given as "in press" (journal should be specified), "submitted for publication" (journal should be specified), "in preparation" or "personal communication".

Vols. 1–651 of the *Journal of Chromatography*; *Journal of Chromatography, Biomedical Applications* and *Journal of Chromatography, Symposium Volumes* should be cited as *J. Chromatogr.* From Vol. 652 on, *Journal of Chromatography A* (incl. Symposium Volumes) should be cited as *J. Chromatogr. A* and *Journal of Chromatography B: Biomedical Applications* as *J. Chromatogr. B*.

Dispatch. Before sending the manuscript to the Editor please check that the envelope contains four copies of the paper complete with references, captions and figures. One of the sets of figures must be the originals suitable for direct reproduction. Please also ensure that permission to publish has been obtained from your institute.

Proofs. One set of proofs will be sent to the author to be carefully checked for printer's errors. Corrections must be restricted to instances in which the proof is at variance with the manuscript.

Reprints. Fifty reprints will be supplied free of charge. Additional reprints can be ordered by the authors. An order form containing price quotations will be sent to the authors together with the proofs of their article.

PRINCIPAL COMPONENTS

By **D.L. Massart** and **P.J. Lewi**

This attractively packaged set, comprising 4 videos, a manual and a software package, is an introduction to the use of principal components analysis (PCA) and related methods in chemometrics. Emphasis has been placed on the use of PCA to display graphically the structure of data sets or to extract graphically information from such a set (display methods). However, links are provided to several other important methods, such as evolving factor analysis, principal component regression and partial least squares.

In order to induce students to learn PCA, and convince them of the usefulness of the methods, several real-life examples have been included. These examples have been chosen to illustrate the generality of the data analysis approach. The data pertain to food, industrial and environmental analysis, animal experimentation, medicinal chemistry, virology and epidemiology. In the software section an additional example concerned with food analysis has been added. Section 3 of the manual contains a complete list of figures. This allows the user to look at some of the figures in a more leisurely fashion or to re-read text which has been heard when viewing the videos. Some of the visuals and some of the texts (occasionally shortened) have been included in this section.

Two types of software augment this series. The first is a tutorial version of a commercial software package called SPECTRAMAP, which has been modified for didactical use. SPECTRAMAP is a performant software for methods derived from PCA that gives excellent display quality.

The other type of software is a listing of a MATLAB® program. In order to understand completely a mathematical algorithm or method, the authors recommend the user to program it himself, using MATLAB®. In this way the user can also obtain all the intermediate results, thereby understanding what happens with a data set when analyzed by PCA. This section also contains an additional data set with which the user can experiment with the software. Some hints are given in to teachers and self-learners on how to use the material to optimize results.

Contents: VIDEOS:

Part A: Principal components as display method.

Part B: Display variables and relationships between variables and objects.

Part C: Singular value decomposition, Eigenvalues; Evolving factor analysis; Software and exercises.

Part D: The display of latent variables in tabulated data.

A 25-minute demonstration video, containing a representative selection from all four video tapes is available at cost price.

ELSEVIER

An imprint of Elsevier Science

MANUAL:

1. Introduction.
2. Proposed didactical concepts.
3. List of Visuals.
4. Software Section.

4A. SPECTRAMAP (P.J. Lewi, J. Van Hoof, M. Nijs).

4B. A MATLAB program for principal components analysis (M. Massart).

©1994 Complete set VHS PAL
Price: Dfl. 1750.00 (US$1000.00)
ISBN 0-444-81622-4
Complete set VHS NTSC
Price: Dfl. 1750.00 (US$1000.00)
ISBN 0-444-81655-0
Manual
Price: Dfl. 65.00 (US$37.00)
ISBN 0-444-81653-4
Demonstration copy
VHS PAL Video
Price: Dfl. 50.00 (US$28.50)
ISBN 0-444-81980-0
Demonstration copy
VHS NTSC Video
Price: Dfl. 50.00 (US$28.50)
ISBN 0-444-81979-7

Additional copies of the manual may be ordered separately.

ORDER INFORMATION

ELSEVIER SCIENCE B.V.
P.O. Box 330
1000 AH Amsterdam
The Netherlands
Fax: +31 (20) 5862 845

For USA and Canada
P.O. Box 945
Madison Square Station
New York, NY 10159-0945
Fax: +1 (212) 633 3680

US$ prices are valid only for the USA & Canada and are subject to exchange rate fluctuations; in all other countries the Dutch guilder price (Dfl.) is definitive. Customers in the European Union should add the appropriate VAT rate applicable in their country to the price(s). Books are sent postfree if prepaid.